ZooKeys 1070: 1–12 (2021)
doi: 10.3897/zookeys.1070.69186
https://zookeys.pensoft.net

RESEARCH ARTICLE

A peer-reviewed open-access journal
ZooKeys
Launched to accelerate biodiversity research

Effect of climate change on the potential distribution of *Heloderma alvarezi* (Squamata, Helodermatidae)

Aarón Gómez-Cruz[1,2], Nancy G. Santos-Hernández[1], José Alberto Cruz[3], Daniel Ariano-Sánchez[4], Christian Ruiz-Castillejos[1], Eduardo E. Espinoza-Medinilla[1], José A. De Fuentes-Vicente[1]

1 *Laboratorio de Investigación y Diagnóstico Molecular (LIDiaM), Instituto de Ciencias Biológicas, Universidad de Ciencias y Artes de Chiapas, Tuxtla Gutiérrez, Chiapas, México* **2** *Red Mesoamericana y del Caribe para la Conservación de Anfibios y Reptiles, Tuxtla Gutierrez, Mexico* **3** *Centro Universitario Tenancingo, Universidad Autónoma del Estado de México, México* **4** *Centro de Estudios Ambientales y Biodiversidad, Universidad Del Valle de Guatemala, Guatemala*

Corresponding author: José A. De Fuentes-Vicente (jose.defuentes@unicach.mx), Nancy G. Santos-Hernández (nancy.santos@unicach.mx)

Academic editor: Aaron Bauer | Received 27 May 2021 | Accepted 3 October 2021 | Published 10 November 2021

http://zoobank.org/93C7A758-017E-4C2C-BE1B-B0D52D318B50

Citation: Gómez-Cruz A, Santos-Hernández NG, Cruz JA, Ariano-Sánchez D, Ruiz-Castillejos C, Espinoza-Medinilla EE, De Fuentes-Vicente JA (2021) Effect of climate change on the potential distribution of *Heloderma alvarezi* (Squamata, Helodermatidae). ZooKeys 1070: 1–12. https://doi.org/10.3897/zookeys.1070.69186

Abstract

Climate change represents a real threat to biodiversity conservation worldwide. Although the effects on several species of conservation priority are known, comprehensive information about the impact of climate change on reptile populations is lacking. In the present study, we analyze outcomes on the potential distribution of the black beaded lizard (*Heloderma alvarezi* Bogert & Martin del Campo, 1956) under global warming scenarios. Its potential distribution, at present and in projections for the years 2050 and 2070, under both optimistic and pessimistic climate change forecasts, were computed using current data records and seven bioclimatic variables. General results predict a shift in the future potential distribution of *H. alvarezi* due to temperature increase. The optimistic scenario (4.5 W/m^2) for 2070 suggests an enlargement in the species' distribution as a response to the availability of new areas of suitable habitat. On the contrary, the worst-case scenario (7 W/m^2) shows a distribution decrease by 65%. Moreover, the range distribution of *H. alvarezi* is directly related to the human footprint, which consequently could magnify negative outcomes for this species. Our research elucidates the importance of conservation strategies to prevent the extinction of the black beaded lizard, especially considering that this species is highly threatened by aversive hunting.

Keywords
Climatic change, beaded lizard, conservation, Chiapas, México

Introduction

In the coming years, the impacts of climate change are projected to play a critical role in global biodiversity dynamics. Since 1980, rainfall and runoff levels at a global scale have decreased annually, which causes an overall prolongation of the dry season and affects entire biomes and ecosystems (Chou et al. 2012). The temperature of the planet has increased by approximately 1.1 °C since the pre-industrial period, and it is expected to have increased by 4.1 °C by the end of this century if current emission trends continue unchanged (Hidalgo et al. 2013; IPCC 2014; Masson-Delmote et al. 2018). In addition, deforestation, extractive activities, and the introduction of invasive species might contribute to the increasing negative effects on biodiversity (Durán et al. 2020).

Adaptative and geographic expansion responses of each group of organisms are crucial in determining their preservation or extinction. Accelerated global warming is causing the eradication of a significant proportion of the global reptile diversity (Sinervo et al. 2010; Durán et al. 2020). Due to their high species-richness, lizards constitute a major group of conservation concern (e.g., Sinervo et al. 2010; Diele-Viegas et al. 2020; Rozen-Rechels et al. 2020). In Mexico, research studies focusing on the effects of climate change on reptiles, and specifically on lizards, have been increasing in the last decade (e.g., Sinervo et al. 2017; Lara-Reséndiz et al. 2019, 2021; Domínguez-Guerrero et al. 2020; Gadsden et al. 2020). Nevertheless, studies relating to helodermatids are scarce.

Heloderma alvarezi, commonly known as the black beaded lizard, is one of the least studied Mexican lizards; hence, the impacts of climate change on this species are not well understood. However, the negative outcomes for helodermatids, given their sensitivity to temperature fluctuations, have been documented (Aranda-Coello et al. 2019; Ariano-Sánchez et al. 2020). For example, high temperatures may lead to fatal physiological alterations such as water loss and an elevated heart rate (DeNardo et al. 2004; Labra et al. 2008). In Mexico, the black beaded lizard has been reported in the Isthmus of Tehuantepec in the southern state of Oaxaca, the central lowlands of Chiapas, and on the border with Guatemala. Moreover, its presence was identified in the Nentón River Valley region of western Guatemala (Álvarez del Toro 1972; Ariano 2011). A lack of information makes it difficult to accurately determine the geographic distribution and conservation status of this species.

This study aimed to determine the potential geographical distribution of *H. alvarezi*, and to estimate the projected scenarios for 2050 and 2070 considering predicted climate change. Assessing the distribution of this species and the long-term environmental effects will allow us to understand its spatiotemporal variation, and to design effective conservation strategies for this species.

Materials and methods

Heloderma alvarezi point locality data

Heloderma alvarezi distribution data were collected between January and June 2020 from several bibliographic databases. These included GBIF (GBIF.org), Naturalista (naturalista.mx), VertNet (vertnet.org), and technical publications from the gray literature (Ariano 2011). To remove duplicate record entries and sampling errors, the data were filtered with the Wallace 1.0.6.1 software (Kass et al. 2018). Points were thinned to a distance of 1 km to avoid an overfitting in the modeling (e.g., Borzeé et al. 2019). In this way, a total of 27 records of *H. alvarezi* was obtained (Fig. 1).

Climate modeling and prediction with all *H. alvarezi* distribution data

The Maximum Entropy (Maxent) approach (Philips et al. 2006, 2017) was used to model suitable potential areas for *H. alvarezi* under current and future climatic conditions based on presence-only observations of the species. According to the presence records of *H. alvarezi* used in our analyses, the biogeographical provinces Sierra Madre, Central Plateau, and Central Depression in Chiapas State, Mexico (Morrone 2019) were considered as the species' accessible area (*M*) (Soberón & Peterson 2005). Climate modeling was performed at a 30 arc-second resolution with WorldClim2 climate data for 1950–2000 (Fick and Hijmans 2017). Pearson's correlation coefficient was calculated for the 19 bioclimatic variables to evaluate multicollinearity, and to reduce uncertainty in the species distribution models (Elith et al. 2011; Cruz-Cárdenas et al. 2014). One variable was removed from any pair of variables with greater than 80% correlation, leaving seven bioclimatic variables to be used in the final models (Table 1). Ecological niche models were performed using the Maximum Entropy algorithm implemented in the Maxent v. 3.4.1 software. This software has been demonstrated to generate accurate predictions even when small sample sizes are used (Philips et al. 2006; Pearson et al. 2007; Martínez-Méndez et al. 2016).

Niche models were projected to future scenarios for the years 2041–2060 and 2061–2080 using a GCM MIROC 6 model under different Representative Concentration Pathways (RCPs). Models were evaluated under simulated radiative forcings of 4.5 and 7 W/m^2 to develop optimistic and pessimistic climate change forecasts, respectively (Lara-Reséndiz et al. 2019; Pérez 2020). To determine anthropogenic impact on the distribution of *H. alvarezi*, a carbon footprint estimation layer was overlaid on the niche models generated (Venter et al. 2016, 2018). The carbon footprint was obtained using cumulative emissions for the period 1993–2009, derived from population density, electrical power infrastructure, cultivable land areas, grasslands, roads, and railways (Venter et al. 2016, 2018).

Predictive accuracy was evaluated using the area under the curve (AUC). This can range in value from 0 to 1. A value less than 0.5 signifies that the classifier performs worse than a random classifier (Felicísimo et al. 2011; Mateo et al. 2011; Santillan

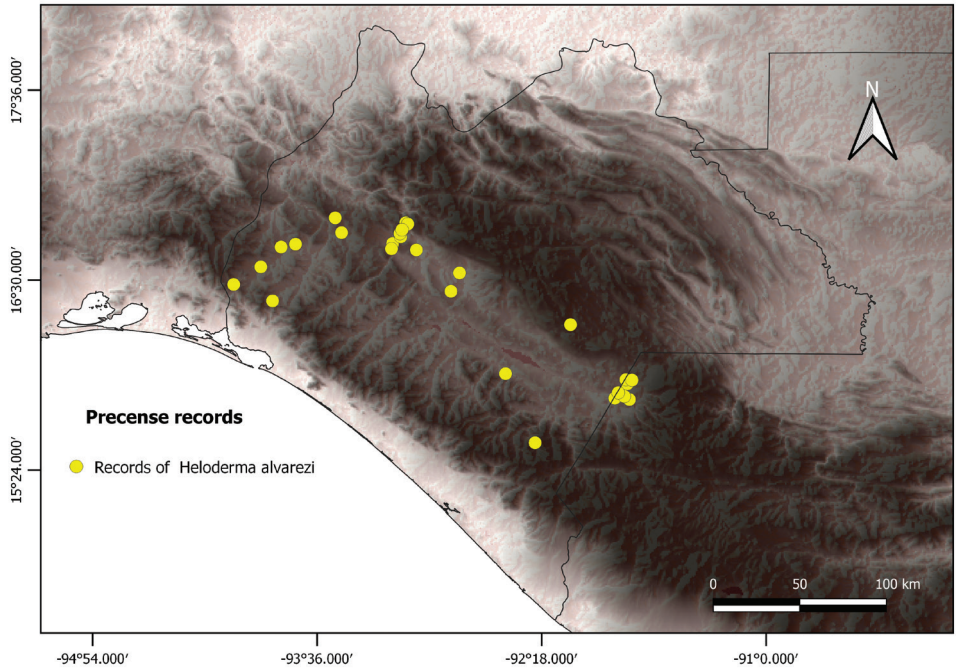

Figure 1. Presence records of *H. alvarezi* (yellow dots). Darker zones on grayscale indicate a higher altitude.

2013). The model with the highest statistical significance (AUC = 0.972) was selected. Model outputs were exported to QGIS 3.6.3 (QGIS.org 2020) and thresholded to 10% (Mejía et al. 2018), creating a binary distribution map where non-suitable areas are represented as zero (0) and suitable areas as one (1).

Results

The current potential distribution model covered a range of 11,218.63 km^2, specifically across the Central Depression of Chiapas and the border with Guatemala (Fig. 2). The area of suitability increased at higher altitudes, from 400 to 1000 m a.s.l. Most of the distribution of the black beaded lizard is delimited by geographical barriers, such as the large mountain ranges that surround the valleys of the Central Depression in Mexico and Guatemala.

Distribution models projected to the future for *H. alvarezi* show variations according to the case scenario and year. The distribution decreases by 12% for the optimistic scenario in 2050, compared with the current distribution. By 2070, the distribution is expected to increase by 61% with a displacement towards altitudes between 800 and 2000 m, mainly in the Sierra Madre de Chiapas. On the other hand, pessimistic scenarios for 2050 exhibit an increased distribution of *H. alvarezi* (32%), although predictions for 2070 reveal a reduction of 65.5% (Fig. 3).

Table 1. Bioclimatic variables and their contribution to model projections.

Acronym	Variable	Percentage contribution	Permutation importance
Bio10	Mean temperature of warmest quarter	31.1	34.2
Bio15	Precipitation seasonality	30	4.7
Bio17	Precipitation of driest quarter	20.9	46.2
Bio2	Mean diurnal range	15.4	12.6
Bio3	Isothermality	1.9	0.2
Bio4	Temperature seasonality	0.7	1.9
Bio18	Precipitation of warmest quarter	0.1	0.3

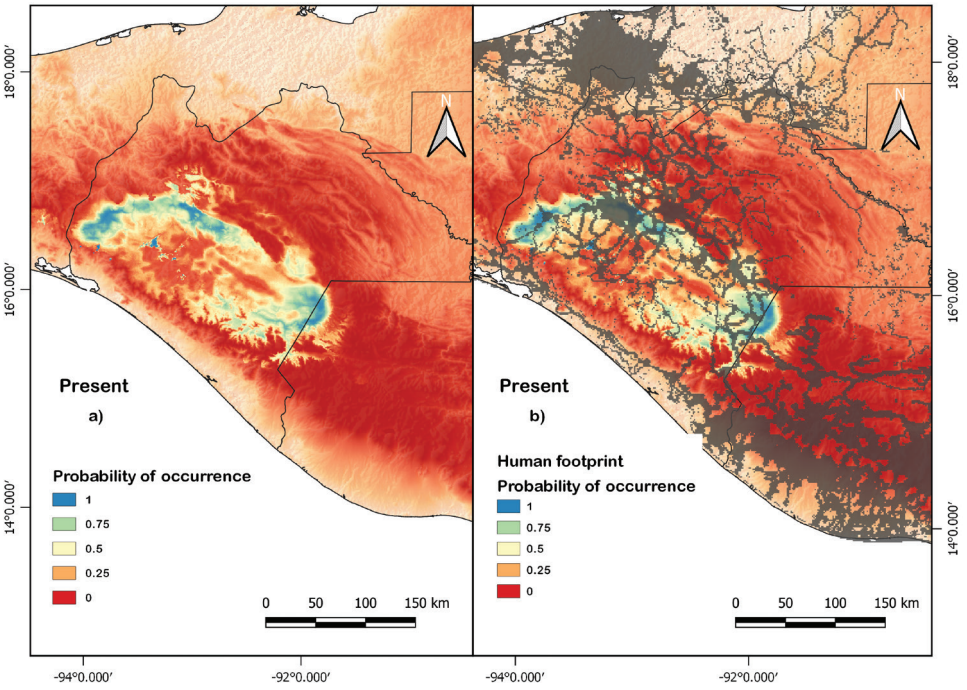

Figure 2. Current potential distribution model of *H. alvarezi* at present (**a**) and overlaid with human footprint (**b**).

Discussion

According to our present-day distribution models, the distribution area of *H. alvarezi* extends over 11,218.63 km^2 in the Central Chiapas Depression in Mexico and the Nentón River Valley in Guatemala. These areas are highly fragmented by human activity, which could induce individuals to settle where the impact of the human footprint is less pronounced, mainly on the borders of the Sierra Madre de Chiapas. This distribution excludes the regions of Socotelnango and La Concordia (Mexico) due to inappropriate environmental conditions (Suppl. material 1). Except for *H. charlesbogerti* (Campbell & Vannini, 1988), the distribution of *H. alvarezi* is the most restricted of any species in the Family Helodermatidae (Ariano 2007). The areas of high elevation in the Isthmus of Tehuantepec may act as a barrier that restricts the distribution of *H. alvrezi* in the direction of Oaxaca (Domínguez-Vega et al. 2012).

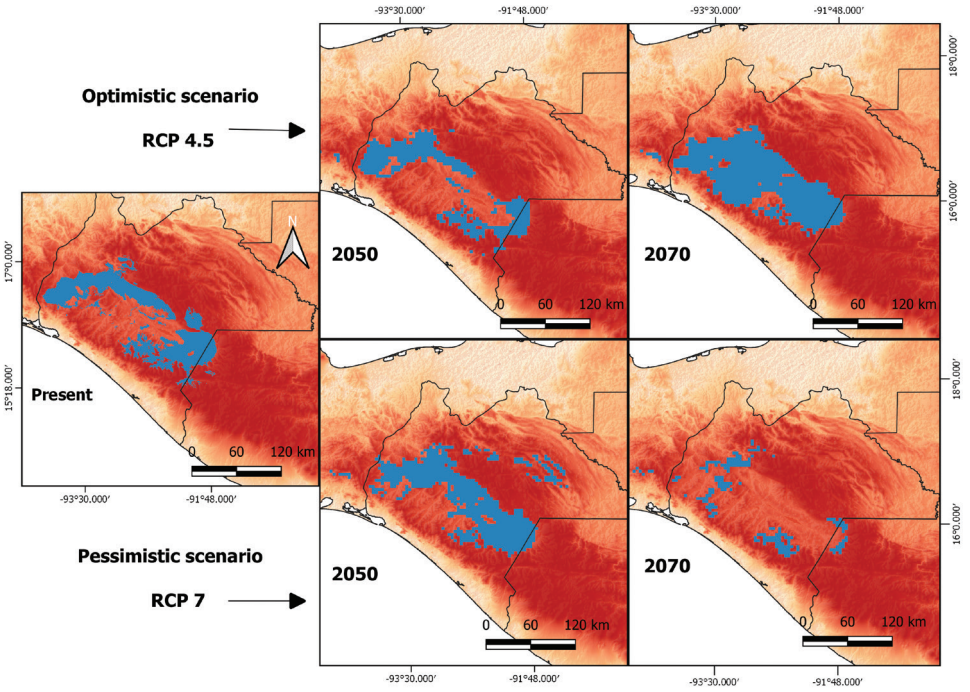

Figure 3. Potential distribution of *H. alvarezi* under different climate change scenarios using different Representative Concentration Pathways (RCP) and the seven bioclimatic variables that best explain the potential distribution of *H. alvarezi.*

Our results suggest that *H. alvarezi* is found principally in seasonally tropical dry forests (SDTF), categorized as a highly threatened ecosystem (Trejo and Dirzo 2000; Trejo 2010). Over 30% of forest loss in Chiapas has been prompted by anthropic activities (Rocha et al. 2010). In addition to deforestation of the ecosystem, the aversive hunting of helodermatids may play an important role in their current distribution. Hunting intensity may be greater where the species distribution overlaps with the human footprint, although data are lacking. Historically, hunting, which threatens their distribution and abundance (Fig. 2a) (Aranda-Coello et al. 2019), has been carried out because of the appearance of these lizards and myths about their venom, as well as for the illegal skin trade.

Because projected distribution maps predict future implications of climate change on a species' conservation status, these climatic forecasts enable us to take forward-thinking actions. The seven highest-contributing bioclimatic variables in the potential distribution modeling of *H. alvarezi*, in order, were: mean temperature of warmest quarter (Bio10), precipitation seasonality (Bio15), precipitation of driest quarter (Bio17) and mean diurnal range (Bio2). These are consistent with the findings of Domínguez-Vega et al. (2012) on the distribution of the genus *Heloderma*. It is important to mention that these models do not consider additional factors, such as aversive hunting (killing by local communities due to fear of their poisonous nature) (Domínguez-Vega et al. 2017). Hence, further research might examine these conditions.

When the human footprint layer was overlaid on the present-day distribution model of *H. alvarezi*, it may be seen that anthropogenic impact could be considerable. It has been observed with other organisms that human population growth, roads, and changes in land use affect an organism's existence, especially by the occupation and transformation of the landscape, the alteration of the habitat and dispersal of physicochemical pollutants (Beck 2005; Colino-Rabanal and Lizana 2012; Pitts et al. 2017). However, not all species will have the same degree of exposure to the human impact, as this depends on taxon-specific ecological requirements (Colino-Rabanal and Lizana 2012).

According to our climate change scenarios, under an optimistic scenario (RCP 4.5) the distribution of the lizard would decrease by 2050, however, a substantial increase in projected distribution range is expected by 2070. This increase in distribution is expected towards the Sierra Madre de Chiapas, where perhaps suitable bioclimatic conditions for *H. alvarezi* are expected. Environmental factors (i.e., temperature and humidity) affect the species' behavior and its habitat selection (Labra et al. 2008; Sinervo et al. 2018; Altamirano-Benavides et al. 2019).

As expected, the most unfavorable conditions to *H. alvarezi* will occur under a pessimistic scenario. This model projects a reduction in the distribution range by 65%; this percentage is higher compared to other *Heloderma*, such as *H. suspectum* (Giermanowsky et al. 2018), but similar to those of other lepidosaurs (see Güizado-Rodríguez et al. 2012). It is proposed that this scenario will lead to a decrease in precipitation and humidity, and would cause alterations in the species' behavior. We know that the prolonged length of the aestivation period of these lizards ends with the arrival of the rainy period (Domínguez-Vega et al. 2012; Aranda-Coello et al. 2019; Ariano-Sánchez et al. 2020).

In addition, the rainy season begins the foraging and reproduction activity of the helodermatids, so a prolonged dry season would cause alterations in the population structure of these lizards (Ariano-Sánchez et al. 2020). Sinervo et al. (2010) suggested a probability of 91% for the extinction of Helodermatidae by 2080; this projection is consistent with our estimations for a pessimistic scenario. For some species, the process of adaptation to environmental changes is mostly slow and the ability to withstand climatic variations is limited (Foden et al. 2007). Rapid environmental changes and anthropogenic effects will be crucial to the survival of this species and could exacerbate the effects of range reduction. Analogously, the lack of knowledge about the thermal ecology of *H. alvarezi* in the wild is an important constraint on understanding its adaptability (Aranda-Coello et al. 2019). Therefore, it could be usefully explored in further research.

The implementation of conservation programs for species highly sensitive to climate change is fundamental. The present study suggests that the future of the black beaded lizard is not encouraging under different climate change scenarios. Promoting structural and functional connectivity among the remaining SDT patches and their associated mesic conditions is the most effective weapon to facilitate the altitudinal and latitudinal migration of the species under a global warming forecast. Additionally, slowing down climate change constitutes a primary focus on conservation status for the organisms living in xeric ecosystems, included *H. alvarezi*.

References

Altamirano-Benavides MA, Domínguez-Guerrero SF, Muñoz-Nolasco FJ, Arenas-Moreno DM, Santos-Bibiano R, Gómez-Trejo R, Lozano-Aguilar LE, Fierro-Estrada N, Gandarrilla-Aizpuro FJ, Woolrich-Piña GA, Martínez-Méndez N, Lara-Reséndiz RA, Méndez-de la Cruz FR (2019) Ecología térmica y riesgo de extinción ante el cambio climático de *Gonatodes concinnatus* (Squamata: Sphaerodactylidae), una lagartija endémica de la Amazonía occidental. Revista Mexicana de Biodiversidad 90: 1–12. https://doi.org/10.22201/ib.20078706e.2019.90.2824

Álvarez A, Raymundo V, Ruiz JA, Santiago-Pérez AL (2020) Efecto del cambio climático a partir de los escenarios RCP 4.5 y 8.5 del año 2050 en el balance hídrico del Área Natural Protegida La Primavera, Jalisco, México. Áreas Naturales Protegidas Scripta 6: 53–74. https://doi.org/10.18242/anpscripta.2020.06.06.01.0004

Álvarez del Toro M (1972) Los reptiles de Chiapas. Publicación del Instituto de Historia Natural, Tuxtla Gutiérrez, Chiapas, México.

Aranda-Coello JM, Gómez A, Mendoza OM, Reyes E (2019) Termorregulación en el comportamiento de *Heloderma alvarezi* (Squamata: Helodermatidae) en cautiverio. Revista Latinoamericana de Herpetología 2: 41–46.

Ariano D (2007) Distribución potencial, ámbitos de hogar y patrones de comportamiento del Lagarto Escorpión *Heloderma horridum charlesbogerti* (Sauria: Helodermatidae) con notas sobre el primer reporte de caso de envenenamiento por esta especie en Guatemala. Tesis de Maestría. Universidad de Costa Rica

Ariano D (2011) Distribución, ecología, evaluación y desarrollo de estrategias para la conservación del Escorpión negro (*Heloderma horridum alvarezi*) en los bosques secos de Guatemala. FONACYT. Accessed 03 March 2020 from: https://fondo.senacyt.gob.gt/portal/index.php/catalogo/15-codigo/568-08-2011-medio-ambiente.

Ariano-Sánchez D, Mohr R, Reinhardt S, Rosell F (2020) Escaping drought: Seasonality effects on home range, movement patterns and habit selection of the Guatemalan Beaded Lizard. Global Ecology and Conservation 23: 1–13. https://doi.org/10.1016/j.gecco.2020.e01178

Borzée A, Choi Y, Kim YE, Jablonski PG, Jang Y (2019) Interspecific variation in seasonal migration and brumation behavior in two closely related species of treefrogs. Frontiers in Ecology and Evolution 7: 1–16. https://doi.org/10.3389/fevo.2019.00055

Ceballos G, Martínez L, García A, Espinoza E, Bezaury J, Dirzo R (2010) Diversidad, amenazas y áreas prioritarias para la conservación de las selvas bajas del Pacífico de México. En CONABIO. Trejo, I. (primera edición) Las selvas secas del Pacífico Mexicano. Ciudad de México, México. pp. 41–51

Chou C, Chen C, Tan P, Chen KT (2012) Mechanisms for global warming impacts on precipitation frequency and intensity. Journal of Climate 25: 3291–3306. https://doi.org/10.1175/JCLI-D-11-00239.1

Colino-Rabanal VJ, Lizana M (2012) Herpetofauna and roads: a review. Basic and Applied Herpetology 25: 5–31. https://ojs.herpetologica.org/index.php/bah/article/view/12

Cruz-Cárdenas G, Villaseñor JL, López-Mata L, Martínez-Meyer E, Ortiz E (2014) Selección de predictores ambientales para el modelado de la distribución de las especies en Maxent.

Revista Chapingo. Serie Ciencias Forestales y del Ambiente 20: 187–201. DOI:10.5154/r.rchscfa.2013.09.034

DeNardo DF, Zubal TE, Hoffman TC (2004). Cloacal evaporative cooling: a previously undescribed means of increasing evaporative water loss at higher temperatures in a desert ectotherm, the Gila monster *Heloderma suspectum*. The Journal of Experimental Biology 207: 945–953. https://doi.org/10.1242/jeb.00861

Diele-Viegas L, Figueroa RT, Viela B, Duarte CF (2020) Are reptiles toast? A worldwide evaluation of Lepidosauria vulnerability to climate change. Climate Change 159: 581–599. https://doi.org/10.1007/s10584-020-02687-5

Domínguez-Guerrero S, Bodensteiner, BL, Pardo-Ramírez A, Aguillón-Gutiérrez AR, Méndez-de la Cruz FR, Muñoz, MM (2020) Thermal physiology responds to interannual temperature shifts in a montane horned lizard, *Phrynosoma orbiculare*. Journal of Experimental Zoology 335: 1–10. https://doi.org/10.1002/jez.2403

Domínguez-Vega H, Monroy-Vilchis O, Balderas-Valdivia CJ, Gienger CM, Ariano-Sánchez D (2012) Predicting the potential distribution of the beaded lizard and identification of priority areas for conservation. Journal for Nature Conservation 20: 247–253. http://dx.doi.org/10.1016/j.jnc.2012.04.003

Domínguez-Vega H, Monroy-Vilchis O, Manjarrez J, Balderas-Valdivia CJ (2017) Aversive hunting and frequency ecology of Beaded lizards (Squamata: Helodermatidae). Perspectives in Ecology and Conservation 15: 47–51. http://dx.doi.org/10.1016/j.pecon.2016.11.003

Durán PN, Loya JL, Ruiz JA, González DR, García JD, Martínez S, Crespo MR (2020). Impacto del cambio climático en la distribución potencial de *Tithonia diversifolia* (Hemsl.) A. Gray en México. Revista Mexicana de Ciencias Pecuarias 11: 93–106. https://doi.org/10.22319/rmcp.v11s2.4705

Elith J, Philips SJ, Hastie T, Dudík M, Chee YE, Yates J (2011) A statistical explanation of Maxent for ecologists. Diversity and Distributions 17: 43–57. https://doi.org/10.1111/j.1472-4642.2010.00725.x

Felicísimo AM, Muñoz J, Villalba CJ, Mateo RG (2011) Impactos del cambio climático sobre la flora española. Conservación Vegetal 15: 6–10.

Fick SE, Hijmans RJ (2017) WorldClim2: new 1-km spatial resolution climate surfaces for global land areas. International Journal of Climatology 37: 4302–4315. https://doi.org/10.1002/joc.5086

Foden W, Midgley GF, Hughes G, Bond WJ, Thuiller W, Hoffman MT, Kaleme P, Underhill LG, Rebelo A, Hannah L (2007) A changing climate is eroding the geographical range of the Namib Desert tree aloe through population declines and dispersal lags. Diversity and Distributions 13: 645–653. https://doi.org/10.1111/j.1472-4642.2007.00391.x

Gadsden H, Lara-Reséndiz RA, Minjarrez-Flores NF, Gatica-Colima A, Smith GR (2020) Thermoregulation in a saxicolous population of the lizard *Urosaurus ornatus* from the northern Chihuahua Desert, Mexico. Amphibia-Reptilia 42:153–166: 1–14. https://doi.org/10.1163/15685381-bja10037

GBIF.org (2021) GBIF Occurrence Download. Accessed 16 August 2019 from: https://doi.org/10.15468/dl.unfegz.

Giermakowski JT, Ryan M, Latella I (2018) Evaluation of the distribution and conservation status of the Gila Monster (*Heloderma suspectum*) in southwestern New Mexico Final Report.. Consulted 16 August 2020 from: https://www.wildlife.state.nm.us/download/conservation/share-with-wildlife/reports/2017/Evaluation-of-the-distribution-and-conservation-status-of-the-Gila-monster-Heloderma-suspectum-in-southwest-New-Mexico-_-Tom-Giermakowski.pdf

Güizado-Rodríguez MA, Ballesteros-Barrera C, Casas-Andreu G, Téllez-Valdés O, Salgado-Ugarte IH (2012) The impact of global warming on the range distribution of different climatic groups of *Aspidocelis costata costata*. Zoological Science 29: 834–843. https://doi.org/10.2108/zsj.29.834

Hidalgo HG, Amador JA, Alfaro EJ, Quesada B (2013) Hydrological climate change projections for Central America. Journal of Hydrology 495: 94–112. 10.1016/j.jhydrol.2013.05.004

Intergovernmental Panel on Climate Change (2014). Climate Change 2014 – Impacts, Adaptation and Vulnerability: Part A: Global and Sectoral Aspects: Working Group II Contribution to the IPCC Fifth Assessment Report. Cambridge: Cambridge University Press. https://doi.org/10.1017/CBO9781107415379

Kass JM, Vilela B, Aiello-Lammens ME, Muscarella R, Merow C, Anderson RP (2018) Wallace: A flexible platform for reproducible modeling of species niches and distributions built for community expansion. Methods in Ecology and Evolution 9: 1151–1156. https://doi.org/10.1111/2041-210X.12945

Labra A, Vidal MA, Solís R, Penna M (2008) Ecofisiología de anfibios y reptiles. In: Vidal MA, Labra A (eds) Herpetología de Chile. Science. Verlag, Santiago de Chile, Chile, pp. 483–516.

Lara-Reséndiz R, Galina-Tessaro P, Pérez-Delgadillo AG, Valdez-Villavicencio JH, Méndez-de la Cruz FR (2019) Efecto del cambio climático en una especie de lagartija termófila de amplia distribución (*Dipsosaurus dorsalis*): un enfoque ecofisiológico. Revista Mexicana de Biodiversidad 90: 1–11. https://doi.org/10.22201/ib.20078706e.2019.90.2888

Lara-Reséndiz R, Galina-Tessaro P, Sinervo B, Miles DB, Valdez-Villavicencio JH, Valle-Jiménez FI, Méndez-de la Cruz FR (2021) How will climate change impact fossorial lizard species? Two examples in the Baja California Peninsula. Journal of Thermal Biology 95. https://doi.org/10.1016/j.jtherbio.2020.102811

Martínez-Mendez N, Aguirre-Planter E, Eguiarte LE, Jaramillo-Correa JP (2016) Modelado de nicho ecológico de las especies (Pinaceae) en México: Algunas implicaciones taxonómicas y para la conservación. Botanical Sciences 9: 5–24. DOI: 10.17129/botsci.5008

Masson-Delmote V, Zhai VP, Pörtner HO (2018) Global Warming of 1.5 °C. An IPCC Special Report on the impacts of global warming of 1.5 °C above pre-industrial levels and related global greenhouse gas emission pathways, in the context of strengthening the global response to the threat of climate change, sustainable development, and efforts to eradicate poverty. IPCC. Accessed 13 April 2020 from: https://www.ipcc.ch/site/assets/uploads/sites/2/2019/06/SR15_Full_Report_Low_Res.pdf.

Mateo RG, Felicísimo AM, Muñoz J (2011) Modelos de distribución de especies: Una revisión sintética. Revista Chilena de Historia Natural 84: 217–240. http://dx.doi.org/10.4067/S0716-078X2011000200008

Mejía D, Tonon MD, Abad L (2018) Distribución potencial del género *Polylepis* en la Cuenca del río Paute bajo un escenario de cambio climático. Revista de la Facultad de Ciencias Químicas 19: 21–37.

Morrone JJ (2019) Regionalización biogeográfica y evolución biótica de México: encrucijada de la biodiversidad del Nuevo Mundo. Revista Mexicana de Biodiversidad 90: 1–68. https://doi.org/10.22201/ib.20078706e.2019.90.2980

Naturalista.mx (2021) CONABIO. Accessed 20 August 2019 from: https://www.naturalista.mx/taxa/35009-Heloderma-horridum-alvarezi

Pearson RG, Raxworthy CJ, Nakamura M, Peterson AT (2007) Predicting species distributions from small numbers of occurrence records: a test case using cryptic geckos in Madagascar. Journal of Biogeography 34: 102–117. DOI: 10.1111/j.1365-2699.2006.01594.x

Phillips SJ, Anderson RP, Schapire RE (2006) Maximum entropy modeling of species geographic distributions. Ecological Modelling 190: 231–259. https://doi.org/10.1016/j.ecolmodel.2005.03.026

Phillips SJ, Anderson RP, DudÍk M, Schapire RE, Blair ME (2017) Opening the black box: An open-source release of MaxEnt. Ecography 40: 887–893. https://doi.org/10.1016/j.ecolmodel.2005.03.026

Pitts S, Hughes BD, Mali I (2017) Rattlesnake nuisance removals and urban expansion in Phoenix, Arizona. Western North American Naturalist 77: 309–316. https://doi.org/10.3398/064.077.0304

QGIS.org, 2021. QGIS Geographic Information System. QGIS Association. Accessed 20 February 2020 from: http://www.qgis.org.

Rocha, AG, Ramírez N, González-Espinoza M (2010) Riqueza y diversidad de árboles del bosque tropical caducifolio en la depresión central de Chiapas. Boletín de la Sociedad Botánica de México 87: 89–103. https://doi.org/10.17129/botsci.313

Rozen-Rechels D, Rutschmann A, Dupoué A, Blaimont P, Chauveau V, Miles DB, Guillon M, Richard M, Badiane A, Meylan S, Clobert J (2020) Interaction of hydric and thermal conditions drive geographic variation in thermoregulation in a widespread lizard. Ecological Monographs, 91: https://doi.org/10.1002/ecm.1440

Santillán V (2013) Aplicación de sistemas de información geográfica (SIG) para la elaboración de modelos zoogeográficos: un estudio de caso. Universidad del Azauy. Accessed 5 April 2020 from: http://dspace.uazuay.edu.ec/bitstream/datos/3324/1/09343.pdf.

Sinervo B, Lara RA, Miles DB (2017) Climate Change and Collapsing Thermal Niches of Mexican Endemic Reptiles. UC Office of the President: UC-Mexico Initiative. Accessed 16 December 2020 from: https://escholarship.org/uc/item/4xk077hp.

Sinervo B, Méndez de la Cruz F, Miles DB, Heulin B, Bastiaans E, Villagrán-Santa Cruz M, Lara-Resendiz R, Martínez-Méndez N, Calderón-Espinosa ML, Meza-Lázaro RN, Gadsden H, Ávila LJ, Morando M, De la Riva IJ, Sepúlveda PV, Duarte-Rocha CF, Ibargüengoytía N, Aguilar-Puntriano C, Massot M, Lepetz V, Oksanen TA, Chapple DG, Bauer AM, Branch WR, Clobert J, Sites Jr JW (2010) Erosion of lizard diversity by climate change and altered thermal niches. Science 328: 894–899. https://doi.org/10.1126/science.1184695

Sinervo B, Miles DB, Wu Y, Méndez-de la Cruz FR, Kirchhof S, Qi Y (2018) Climate change, thermal niches, extinction risk and maternal-effect rescue of toad-headed lizards, *Phryno-*

cephalus, in thermal extremes of the Arabian Peninsula to the Qinghai-Tibetan Plateau. Integrative Zoology 13: 450–470. https://doi.org/10.1111/1749-4877.12315

Soberón J, Peterson AT (2005) Interpretation of models of fundamental ecological niches and species' distributional areas. Biodiversity Informatics 2: 1–10.

Trejo I, Dirzo R (2000) Deforestation of seasonal dry tropical forest a national and local analysis in Mexico. Biological Conservation 94: 133–142. https://doi.org/10.1016/S0006-3207(99)00188-

3Venter O, Sanderson EW, Magrach A, Allan JR, Beher J, Jones KR, Possingham HP, Laurance WF, Wood P, Fekete BM, Levy MA, Watson JE (2018) Last of the Wild Project, Version 3 (LWP-3): 2009 Human Footprint, 2018 Release. Palisades, NY: NASA Socioeconomic Data and Applications Center (SEDAC). https://doi.org/10.7927/H46T0JQ4

Venter O, Sanderson EW, Magrach A, Allan JR, Beher J, Jones KR, Possingham HP, Laurance WF, Wood P, Fekete BM, Levy MA, Watson JE (2016) Global Terrestrial Human Footprint Maps for 1993 and 2009. Scientific Data 3:16006 https://doi.org/10.1038/sdata.2016.67

VertNet.org (2021) VertNet. Accessed 18 August 2019 from: http://portal.vertnet.org/search?q=Heloderma+alvarezi

Supplementary material 1

Supplementary figures and table

Authors: Aarón Gómez-Cruz, Nancy G. Santos-Hernández, José Alberto Cruz, Daniel Ariano-Sánchez, Christian Ruiz-Castillejos1, Eduardo E. Espinoza-Medinilla1, José A. De Fuentes-Vicente

Data type: species data

Explanation note: **Figure S1.** Current potential distribution map of *H. alvarezi* with political boundaries. **Figure S2.** Future potential distribution of *H. alvarezi* with current human footprint projections. **Table S3.** *Heloderma alvarezi* presence records used for potential distribution modeling.

Link: https://doi.org/10.3897/zookeys.1070.69186.suppl1

ZooKeys 1070: 13–30 (2021)
doi: 10.3897/zookeys.1070.72742
https://zookeys.pensoft.net

RESEARCH ARTICLE

A peer-reviewed open-access journal
ZooKeys
Launched to accelerate biodiversity research

Characterization of the complete mitochondrial genome of *Myrmus lateralis* (Heteroptera, Rhopalidae) and its implication for phylogenetic analyses

Wanqing Zhao[1], Dajun Liu[1], Qian Jia[1], Xin Wu[1], Hufang Zhang[1]

1 *Department of Biology, Xinzhou Teachers University, Xinzhou 034000, Shanxi, China*

Corresponding author: Hufang Zhang (zh_hufang@sohu.com)

Academic editor: Laurence Livermore | Received 12 August 2021 | Accepted 25 October 2021 | Published 10 November 2021

http://zoobank.org/9F874E62-5B59-408F-9810-8539A3C5E85A

Citation: Zhao W, Liu D, Jia Q, Wu X, Zhang H (2021) Characterization of the complete mitochondrial genome of Myrmus lateralis (Heteroptera, Rhopalidae) and its implication for phylogenetic analyses. ZooKeys 1070: 13–30. https://doi.org/10.3897/zookeys.1070.72742

Abstract

Mitochondrial genomes (mitogenomes) are widely used in research studies on phylogenetic relationships and evolutionary history. Here, we sequenced and analyzed the mitogenome of the scentless plant bug *Myrmus lateralis* Hsiao, 1964 (Heteroptera, Rhopalidae). The complete 17,309 bp genome encoded 37 genes, including 13 protein-coding genes (PCGs), 22 transfer RNA (tRNA) genes, two ribosomal RNA (rRNA) genes, and a control region. The mitogenome revealed a high A+T content (75.8%), a positive AT-skew (0.092), and a negative GC-skew (–0.165). All 13 PCGs were found to start with ATN codons, except for *cox1*, in which TTG was the start codon. The Ka/Ks ratios of 13 PCGs were all lower than 1, indicating that purifying selection evolved in these genes. All tRNAs could be folded into the typical cloverleaf secondary structure, except for *trnS1* and *trnV*, which lack dihydrouridine arms. Phylogenetic trees were constructed and analyzed based on the PCG+rRNA from 38 mitogenomes, using maximum likelihood and Bayesian inference methods, showed that *M. lateralis* and *Chorosoma macilentum* Stål, 1858 grouped together in the tribe Chorosomatini. In addition, Coreoidea and Pyrrhocoroidea were sister groups among the superfamilies of Trichophora, and Rhopalidae was a sister group to Alydidae + Coreidae.

Keywords

Mitogenome, next-generation sequencing, phylogeny, scentless plant bugs

Introduction

Mitochondria are important cytoplasmic organelles in eukaryotic cells, playing a critical role in cell metabolism, disease, apoptosis, and senescence. Mitochondrial genomes are characterized by a simple structure, stable composition, conserved arrangement, maternal inheritance, and rapid evolutionary rate (Simon et al. 2006; Cameron 2014; Tyagi et al. 2020). Therefore, mitochondrial genomes (mitogenomes) have been widely used in phylogenetic analyses and studies on population genetics (Yuan et al. 2015; Song et al. 2019; Xu et al. 2021). For most insects, the mitogenome is typically a double-stranded circular DNA molecule from 15 to 20 kb in size, including 13 protein-coding genes (PCGs), 22 transfer RNA (tRNA) genes, two ribosomal RNA (rRNA) genes, as well as a long non-coding region, also known as the control or AT-rich region (Wolstenholme 1992; Boore 1999; da Fonseca et al. 2008; Yang et al. 2018). Next-generation sequencing enables large amount of sequence data to be obtained and analyzed in a more economically efficient manner. As a result of advances in this technology, it is now more feasible to obtain the complete mitogenome of large taxa; thus, molecular phylogenetic analysis has been revolutionized (Beckenbach et al. 2009; Kocher et al. 2014).

Rhopalidae, commonly known as scentless plant bugs, is a family of Pentatomomorpha insects in the superfamily Coreoidea (Schaefer and Chopra 1982; Schaefer and Panizzi 2000; Steill and Meyer 2003). The Rhopalidae includes 26 genera and 279 species distributed throughout the biogeographical areas of the world (CoreoideaSF Team 2021); many species are of critical importance as pests of pasture grass (Carroll and Loye 2012). In China, Rhopalidae includes two subfamilies, Serinethinae (containing only one genus) and Rhopalinae (containing 20 genera) (Dolling 2006). Phylogeny for the tribes of Rhopalinae has been hypothesized based on morphology, but several concurrent hypotheses still exist (Schaefer 1993; Li and Zheng 1994; Davidova-Vilimova et al. 2000; Henry 2019). Although there are several published studies examining the relationships among infrafamilial levels of the Coreoidea, a consensus regarding the relationships among different families and subfamily lineages has not been reached (Souza et al. 2009; Ghahari et al. 2012; Forthman et al. 2019). In addition, some studies support Aradoidea as sister group of Trichophora (which includes Pentatomoidea, Lygaeoidea, Pyrrhocoroidea and Coreoidea), but the relationship within Trichophora is still under debate (Li et al. 2005; Xie et al. 2005; Linnavuori 2007; Tian et al. 2011; Weirauch and Schuh 2011).

Myrmus lateralis Hsiao, 1964 is an endemic species of China (Beijing, Hebei, eastern Inner Mongolia), Korea, Mongolia, and Russia (Far East) (Liu et al. 1994; Aukema and Rieger 2006; CoreoideaSF Team 2021). Adults are present in both forests and grasslands during July and August (Nonnaizab 1986). To date, only four complete mitogenomes from the Rhopalidae have been published in GenBank, and all of them belong to Rhopalinae (Table 1). According to the latest classification, five tribes are classified in the Rhopalidae (CoreoideaSF Team 2021). The tribe Chorosomatini Fieber, 1860 contains five genera (*Agraphopus* Stål, 1872; *Chorosoma* Curtis, 1830; *Ithamar* Kirkaldy, 1902; *Leptoceraea* Jakovlev, 1873; *Myrmus* Hahn, 1832 and *Xenogenus* Berg, 1883), of which only *Myrmus* and *Chorosoma* are distributed in China.

Table 1. List of sequences used to reconstruct the phylogenetic tree.

	Family	Species	Accession number
Outgroup	Nabidae	*Himacerus nodipes*	JF927832
Ingroup	Aradidae	*Aradacanthia heissi*	HQ441233
		Aradus compar	NC_030362
		Aneurus similis	NC_030360
	Cydnidae	*Macroscytus gibbulus*	NC_012457
		Adrisa magna	NC_042429
		Scoparipes salvazai	MF614955
	Pentatomidae	*Eurydema dominulus*	NC_044762
		Palomena viridissima	NC_050166
		Eysarcoris guttigerus	MN831205
		Arma custos	MT535604
		Pentatoma semiannulata	MT985377
	Colobathristidae	*Phaenacantha marcida*	EU427342
	Rhyparochromidae	*Panaorus albomaculatus*	NC_031364
	Malcidae	*Malcus inconspicuus*	EU427339
	Lygaeidae	*Kleidocerys resedae*	KJ584365
	Pyrrhocoridae	*Dindymus rubiginosus*	NC_042439
		Euscopus rufipes	NC_042436
		Melamphaus faber	NC_042435
		Dysdercus decussatus	NC_042438
		Antilochus coquebertii	NC_042441
	Rhopalidae	*Stictopleurus subviridis*	EU826088
		Myrmus lateralis	**MN412595**
		Chorosoma macilentum	MN412594
		Aeschyntelus notatus	EU427333
		Corizus sp.	KM983397
	Alydidae	*Riptortus pedestris*	EU427344
		Neomegalotomus parvus	MG253274
	Coreidae	*Hydaropsis longirostris*	EU427337
		Clavigralla tomentosicollis	KY274846
		Acanthocoris sp.	MF497707
		Enoplops potanini	MF497720
		Leptoglossus membranaceus	MF497724
		Anoplocnemis curvipes	KY906099
		Mictis tenebrosa	MF497729
		Pseudomictis brevicornis	MF497732
		Molipteryx lunata	MF497721
		Notopteryx soror	KX505857

In this study, we sequenced and annotated the complete mitogenome of *M. lateralis*. We examined the genomic features, nucleotide composition, codon usage, RNA secondary structure, evolutionary pattern of 13 PCGs and characteristics of the control region. Finally, we evaluated the phylogenetic relationship of the mitochondrial sequence data at different taxonomic levels.

Material and methods

Sampling, DNA extraction and sequencing

Adult specimens of *Myrmus lateralis* were collected from Jincheng City, Shanxi Province, China on 20 July 2014. Specimens were preserved in 100% ethanol and stored at –20 °C. The genomic DNA was extracted from leg muscles using a ONE-4-ALL

Genomic DNA Mini-Prep Kit (BS88504; Sangon, Shanghai, China) according to the manufacturer's protocols. The mitogenome was sequenced using the whole-genome shotgun method on an Illumina Miseq platform (Personalbio, Shanghai, China). After filtering low-quality and adapter contaminated reads, A5-miseq version 20150522 (Coil et al. 2015) was used for contig assembly.

Gene annotation and sequence analysis

Sequence annotation was performed using Geneious 10.1.3 (Kearse et al. 2012) and the MITOS web server (Bernt et al. 2013). Annotations of 13 protein-coding regions were edited manually by predicting open reading frames using the invertebrate mitochondrial code. The secondary structures of the tRNA genes were predicted with tRNAscan-SE web server (http://lowelab.ucsc.edu/tRNAscan-SE/) (Tamura et al. 2013). The identification of rRNA genes was performed based on their putative secondary structures and by comparing nucleotide sequences with those of previously reported mitogenomes. The control region was identified through the boundary of neighboring genes. The number of tandem repeats of control region was investigated with Tandem Repeats Finder (http://tandem.bu.edu/trf/trf.html) (Benson 1999) and the presence of stem-loop was predicted by Mfold Web Server (http://mfold.rna.albany.edu) (Zuker 2003). The annotated mitogenome sequence of *Myrmus lateralis* has been submitted to GenBank under the accession number MN412595.

The base compositions, codon usages, and relative synonymous codon usage (RSCU) values were calculated by MEGA 6.0. AT and GC skew were calculated by the following formulae: AT skew = (A–T)/(A+T) and GC skew=(G–C)/(G+C). To analyse the evolutionary patterns of the 13 PCGs, the rates of nonsynonymous substitution (Ka), the rates of synonymous substitution (Ks), and the ratio of Ka/Ks for each gene were calculated by the software DnaSP 5.0 (Librado and Rozas 2009).

Phylogenetic analyses

In addition to the mitogenome newly sequenced here, 37 other mitogenomes were taken from Genbank for the phylogenetic analyses (Table 1). The nucleic acids of 13 PCGs and two rRNAs were extracted by Geneious 10.1.3 and aligned with the Muscle algorithm in MEGA 6.0. Finally, the individual alignments were concatenated to make the datasets of PCG+rRNA (nucleotide alignment including 13 protein-coding genes and two rRNA genes) with SequenceMatrix (Vaidya et al. 2011).

The dataset was used to reconstruct phylogenetic trees under Bayesian inference (BI) and maximum likelihood (ML) using MrBayes 3.2.6 (Ronquist et al. 2012) and RaxML 8.0.2 (Stamatakis 2015) respectively. BI analysis was performed using a TVM+I+G model selected by jModeltest (Darriba et al. 2012). Two independent runs of four Markov Chains Monte Carlo (MCMC) chains in parallel for 5,000,000 generations were applied and sampled every 1,000 generations. Tracer 1.7 (Rambaut et al. 2018) was used to analyze the trace files from the Bayesian MCMC runs. Stationarity was

considered to be reached when ESS (estimated sample size) value above 100 as MrBayes suggested. The first 25% of sampled trees were discarded as burn-in, and the remaining trees were used to calculate a 50% majority rule consensus tree. The ML tree was constructed using the GTR+I+G model, and nodal support values were evaluated through an ultrafast bootstrap approach, with 10,000 replicates.

Results

Genome organization

The 17,309 bp mitochondrial genome of *Myrmus lateralis* was determined to be a typical circular nucleotide molecule, consisting of 13 PCGs, 22 tRNA genes, two rRNA genes, and a putative control region (Table 2). For the gene arrangement, 23 genes (nine PCGs and 14 tRNAs) were found on the majority strand and 14 genes (four PCGs, eight tRNAs, and two rRNAs) were found on the minority strand. In addition, the mitogenome contains 10 gene overlaps totaling 37 bp and ranging from 1 to 8 bp; the longest overlap is being found between *trnW* and *trnC*. Thirteen intergenic spacers equal to 77 bp were observed, ranging from 1 to 18 bp, the longest being found between *trnS2* and *nad1*.

Nucleotide composition and codon usage

The mitochondrial genome of *M. lateralis* was strongly biased toward A+T (75.8%) in nucleotide composition, with 75.5%, 75.7%, 71.3%, and 74.8% A+T content in PCGs, rRNAs, tRNAs, and control regions, respectively. The nucleotide composition and skewness of the mitogenome is shown in Table 3. The three codon positions of PCGs possessed different A+T content; the third site had the highest value (80.1%), whereas the second site had the lowest (74.3%). The mitogenome had more A and G content than T and C, with a positive AT-skew (0.092) and a negative GC-skew (–0.165). The AT-skew of PCGs and three codon positions were all negative, –0.018 in PCGs, –0.214 in the first, –0.050 in the second, and –0.099 in the third codon positions. The GC-skew of PCGs (0.033) and the second codon position (0.127) was slightly and moderately positive, respectfully, while the first and third codon positions were both negative (–0.018 and –0.020, respectively). AT-skew values for the tRNA and rRNA genes were both negative (–0.057 and –0.001, respectively), while the GC-skew was obviously positive for tRNAs (0.292) and slightly positive for rRNAs (0.019).

Relative synonymous codon usage (RSCU) values of the 13 PCGs were calculated based on 3633 codons (Fig. 1). UUU (F, Phe), UAU (Y, Tyr), UUA (L, Leu2), and AUU (I, Ile) were the most frequently used codons, accounting for 28.24% of all codons. All synonymous codons ending with A or U were more frequent than those ending with C or G, except in three cases: CGG (RSCU = 0.97) was used more than CGU (RSCU = 0.55) for Arg, AGG (RSCU=1.03) was used more than AGA (RSCU = 0.99) for Ser1, and GGG (RSCU=1.27) was used more than GGU (RSCU = 1.12) for Gly.

Table 2. Organization of the mitochondrial genome of *Myrmus lateralis*.

Gene	Strand	Size(bp)	Position		Intergenicnucleotides(IGN)	Antico-don	Codons	
			Start	Stop			Start	Stop
trnI	J	66	1	66	0	GAU	—	—
trnQ	N	69	64	132	2	UUG	—	—
trnM	J	69	137	205	4	CAU	—	—
nad2	J	985	207	1191	1	—	ATG	T
trnW	J	63	1204	1266	12	UCA	—	—
trnC	N	62	1259	1320	–8	GCA	—	—
trnY	N	64	1321	1384	0	GUA	—	—
cox1	J	1539	1387	2925	2	—	TTG	TAA
trnL2^{UUR}	J	66	2921	2986	–5	UAA	—	—
cox2	J	676	2987	3662	0	—	ATT	T
trnK	J	72	3663	3734	0	CUU	—	—
trnD	J	65	3738	3802	3	GUC	—	—
atp8	J	162	3803	3964	0	—	ATA	TAA
atp6	J	669	3958	4626	–7	—	ATG	TAA
cox3	J	790	4626	5415	–1	—	ATG	T
trnG	J	63	5413	5475	–3	UCC	—	—
nad3	J	349	5476	5824	0	—	ATA	T
trnA	J	63	5825	5887	9	UGC	—	—
trnR	J	64	5891	5954	3	UCG	—	—
trnN	J	66	5954	6019	–1	GUU	—	—
trnS1^{AGN}	J	69	6023	6091	3	GCU	—	—
trnE	J	64	6091	6154	–1	UUC	—	—
trnF	N	66	6154	6219	–1	GAA	—	—
nad5	N	1702	6220	7921	0	—	ATA	T
trnH	N	63	7931	7993	9	GUG	—	—
nad4	N	1317	7994	9310	0	—	ATG	TAA
nad4L	N	288	9304	9591	–7	—	ATT	TAA
trnT	J	62	9594	9655	3	UGU	—	—
trnP	N	64	9656	9719	0	UGG	—	—
nad6	J	483	9728	10210	8	—	ATA	TAA
cytB	J	1137	10210	11346	–1	—	ATG	TAG
trnS2^{UCN}	J	69	11345	11413	–2	UGA	—	—
nad1	N	927	11432	12358	18	—	ATT	TAA
trnL1^{CUN}	N	67	12359	12425	0	UAG	—	—
rrnL	N	1261	12426	13686	0	—	—	—
trnV	N	69	13687	13755	0	UAC	—	—
rrnS	N	967	13756	14722	0	—	—	—
Control region		2587	14723	17309	0	—	—	—

Note: J refers to major strand; N refers to minus strand

Table 3. Nucleotide composition and skewness of the *Myrmus lateralis* mitochondrial genome.

Feature	T%	C%	A%	G%	A+T%	AT-skew	GC-skew
Whole genome	34.4	14.1	41.4	10.1	75.8	0.092	–0.165
PCGs	42.2	11.8	33.3	12.6	75.5	–0.118	0.033
PCGs-1st	44	14.1	28.5	13.6	72.5	–0.214	–0.018
PCGs-2nd	39	11	35.3	14.2	74.3	–0.05	0.127
PCGs-3rd	44	10.4	36.1	10	80.1	–0.099	–0.02
tRNAs	40	8.6	35.7	15.7	75.7	–0.057	0.292
rRNAs	35.7	14.1	35.6	14.7	71.3	–0.001	0.019
Control region	35	15.9	39.8	9.4	74.8	0.064	–0.257

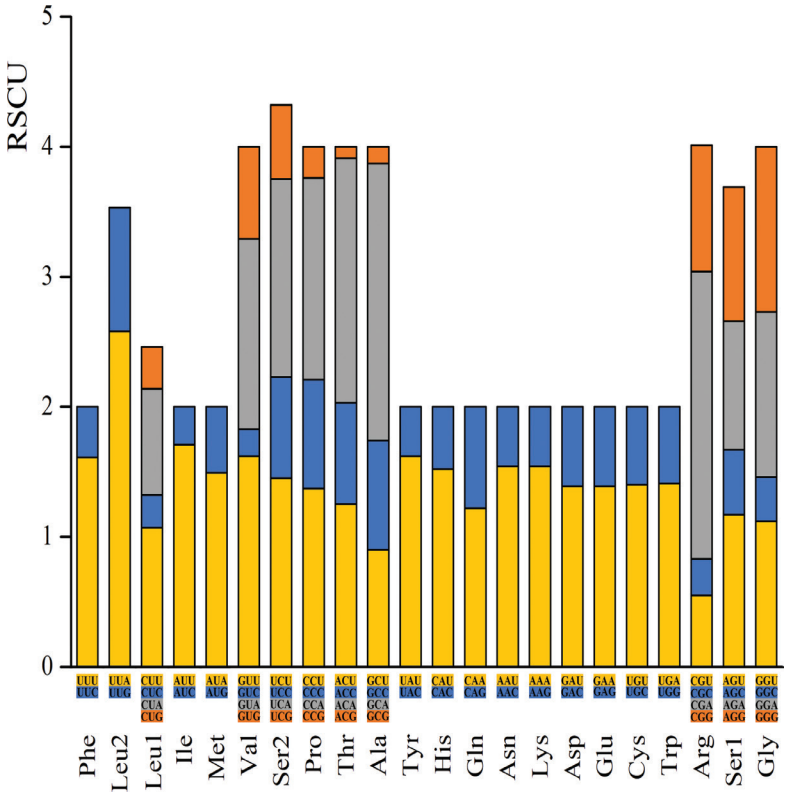

Figure 1. The relative synonymous codon usage (RSCU) in the *Myrmus lateralis* mitogenome.

Protein coding genes

In the *M. lateralis* mitogenome, nine PCGs were located on the J-strand (majority strand) and four PCGs were located on the N-strand (minority strand). The PCGs had a total length of 11,024 bp that accounted for 63.69% of the complete mitogenome. Among the mitochondrial proteins, Leu (16.67%), Phe (11.02%), and Tyr (9.58%) were the most frequent amino acids.

Most PCGs started with a typical ATN codon; five started with ATG (*nad2, atp6, cox3, nad4*, and *cytb*), four with ATA (*atp8, nad3, nad5*, and *nad6*), and three with ATT (*cox2, nad4L, and nad1*). The only unusual initiation codon was TTG in *cox1*. Among the 13 PCGs, seven genes ended with the complete stop codon TAA (*cox1, atp8, atp6, nad1, nad4*, and *nad4L*) or TAG (*cytb*), whereas five genes ended with the partial termination codon T (*nad2, cox2, cox3, nad3*, and *nad5*).

The evolutionary patterns of the 13 PCGs were analyzed and shown in Figure 2. The highest values for both Ka and Ks were observed for *atp8 and cytb*. *atp8* exhibited the highest Ka/Ks value, whereas *cox1* exhibited the lowest. The Ka/Ks values for all 13 PCGs were below 0.29.

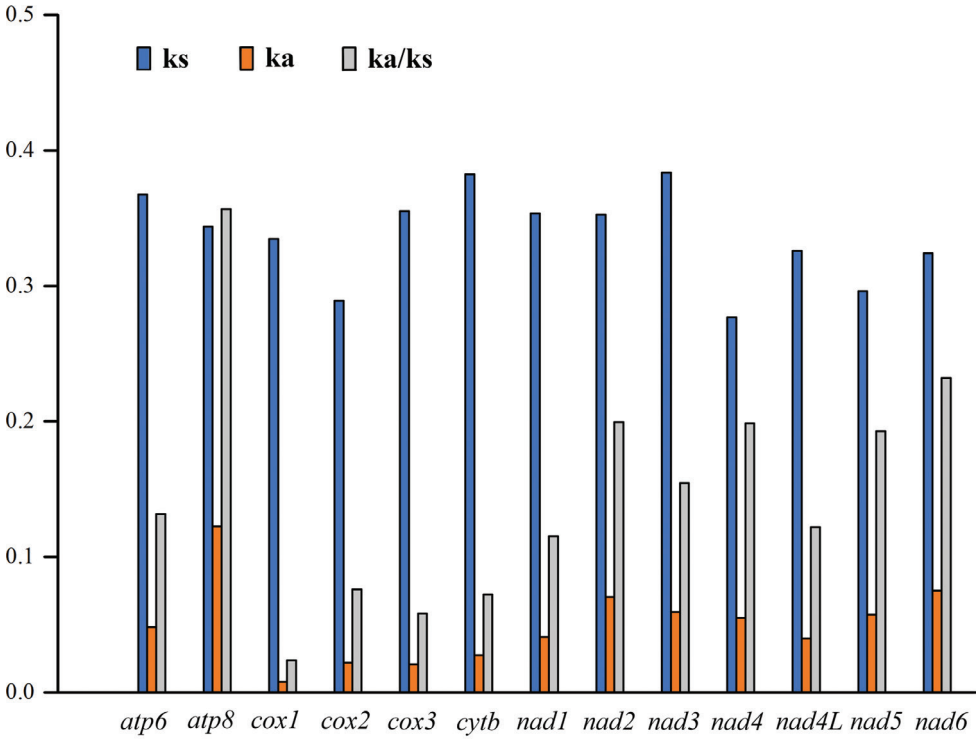

Figure 2. The rates of nonsynonymous substitution (Ka), the rates of synonymous substitution (Ks), and the ratio of Ka/Ks for each PCGs of *Myrmus lateralis* mitogenome

Transfer RNAs and ribosomal RNAs

A total of 22 tRNA genes were encoded by the *M. lateralis* mitogenome, ranging from 62 bp (*trnC* and *trnT*) to 72 bp (*trnK*) in length (Table 2). Eight tRNA genes (*trnQ, trnC, trnY, trnF, trnH, trnP, trnL1*$^{(CUN)}$ and *trnV*) were encoded on the N-strand; the remaining 14 genes were encoded on the J-strand. The 22 tRNA genes had a total length of 1,445 bp, accounting for 8.34% of the complete mitogenome. The predicted secondary structures are shown in Figure 3. All tRNA genes could be folded into typical cloverleaf secondary structures, except for *trnS1* and *trnV*, in which the necessary dihydrouridine (DHU) arms were replaced with a simple loop. A total of 16 wobbled G-U pairs were found (six in acceptor stems, eight in DHU stems, one anticodon stems, and one in TΨC stems) that formed weak bonds in the tRNAs.

The large 1,261 bp *rrnL* gene was located between *trnL1* $^{(CUN)}$ and *trnV*, and the small 967 bp *rrnS* gene was located between *trnV* and the control region. The secondary structures of both the *rrnL* and *rrnS* genes are shown in Figures 4, 5. The secondary structure of the *rrnL* gene contained five domains (I, II, IV, V, VI); domain III was absent, whereas the *rrnS* gene consisted of three domains (I, II, III). Both rRNAs included many mismatched base pairs, most of which were G-U.

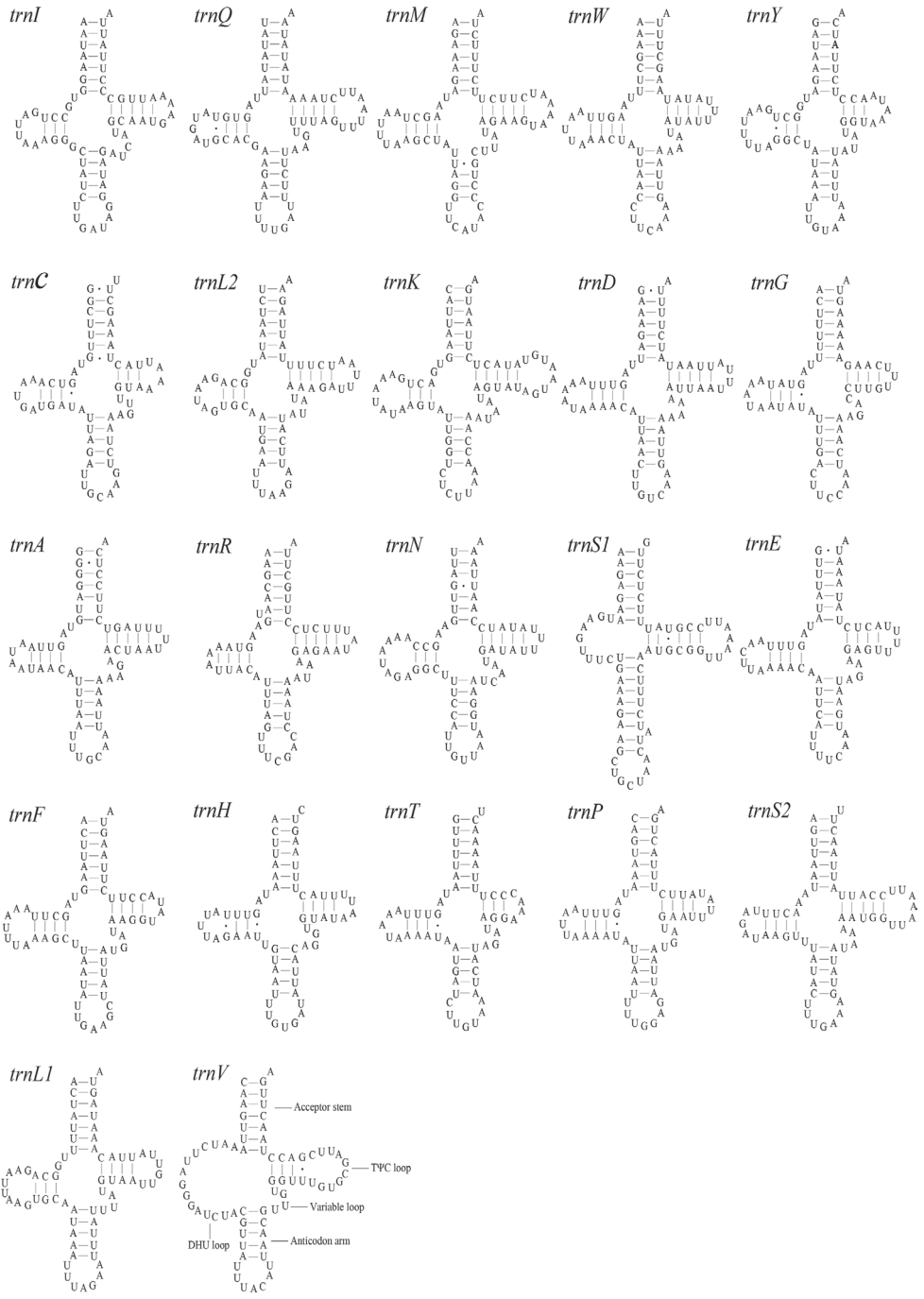

Figure 3. Predicted secondary structure of tRNA genes in the *Myrmus lateralis* mitogenome.

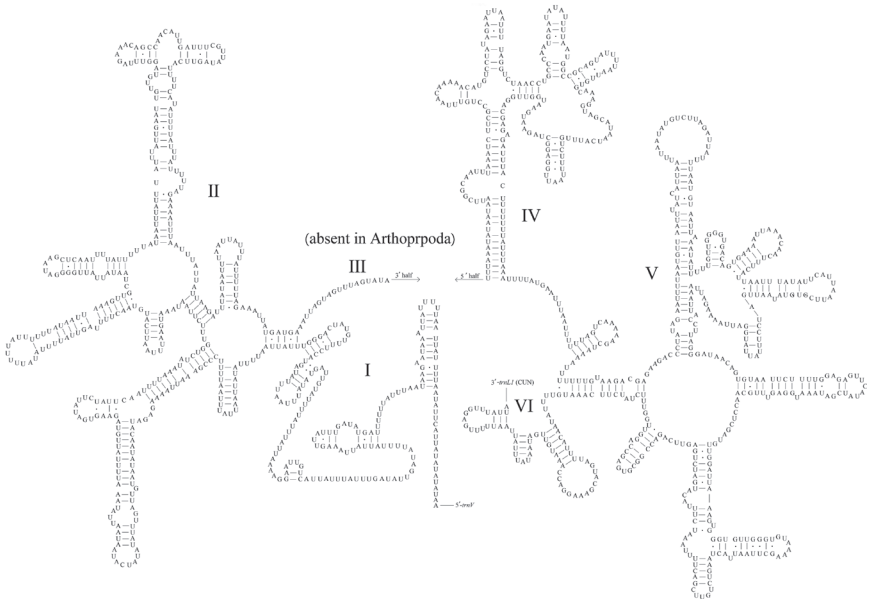

Figure 4. Predicted secondary structure of the *rrnL* in the *Myrmus lateralis* mitogenome.

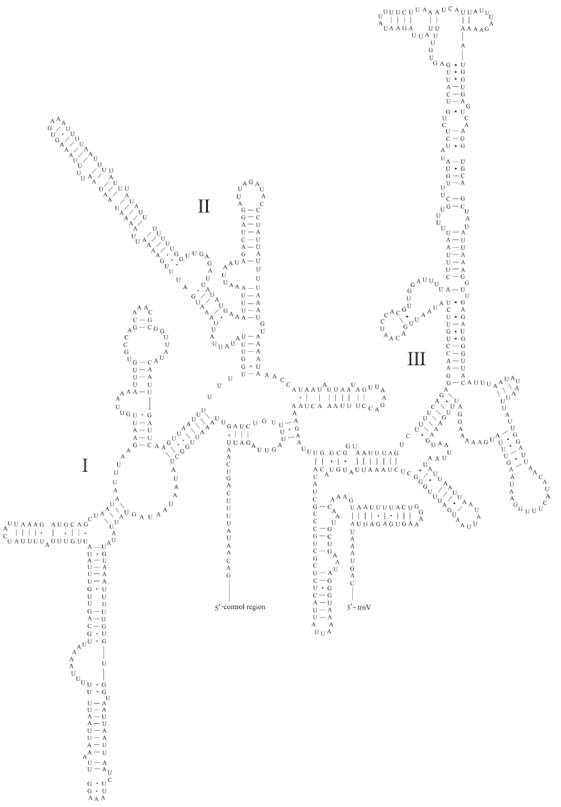

Figure 5. Predicted secondary structure of the *rrnS* in the *Myrmus lateralis* mitogenome.

Control region

The 2587 bp mitochondrial control region of *M. lateralis* was located between the *rrnS* gene and *trnI*. The A+T content (74.76%) was higher than the G+C content (25.24%), with a positive AT-skew and a negative GC-skew. In the control region, tandem repeat sequences, polyT stretch, polyA stretch, stem-loop structure, tandem repeats, and $G(A)_n$ motif were commonly found. Based on these features, we identified the following important elements: a 13 bp polyT stretch, a $G(A)_9T$ sequence, an ATAGA motif, and a 9 bp polyA stretch. In addition, a stem-loop structure was observed at the end of the control region (Fig. 6). Although no longer tandem repeat sequences were identified, stretches of $T(A)_4$ occurred many times.

Phylogenetic analyses

We conducted phylogenetic analyses based on the nucleotide sequences of the PCG+rRNA from eleven families within five superfamilies; one species from the Nabidae (damsel bugs) was used as an outgroup. The dataset contained 14,128 nucleotide sites from these 38 taxa. The BI and ML analyses generated identical phylogenetic results with most posterior probabilities (PP) of one and bootstrap pseudoreplicates (BP) of 100 (Fig. 7). Pentatomoidea, Lygaeoidea, Pyrrhocoroidea, and Coreoidea, the trichophorans, were all monophyletic and highly supported in both analyses (PP > 0.85 and BP > 92). A sister relationship between Coreoidea and Pyrrhocoroidea was recovered, and Pentatomoidea formed a sister group with the other superfamilies of the remaining Trichophora. Both analyses provided robust support (PP > 0.95 and BP > 85) for three families within Coreoidea: Alydidae was closer to Coreidae than Rhopalidae. Sub-

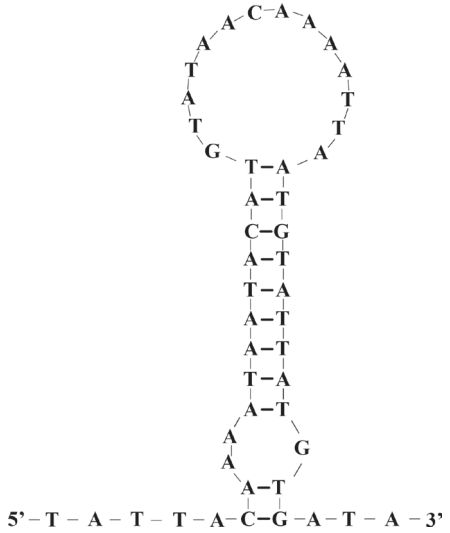

Figure 6. The stem-loop of control region in the *Myrmus lateralis* mitogenome.

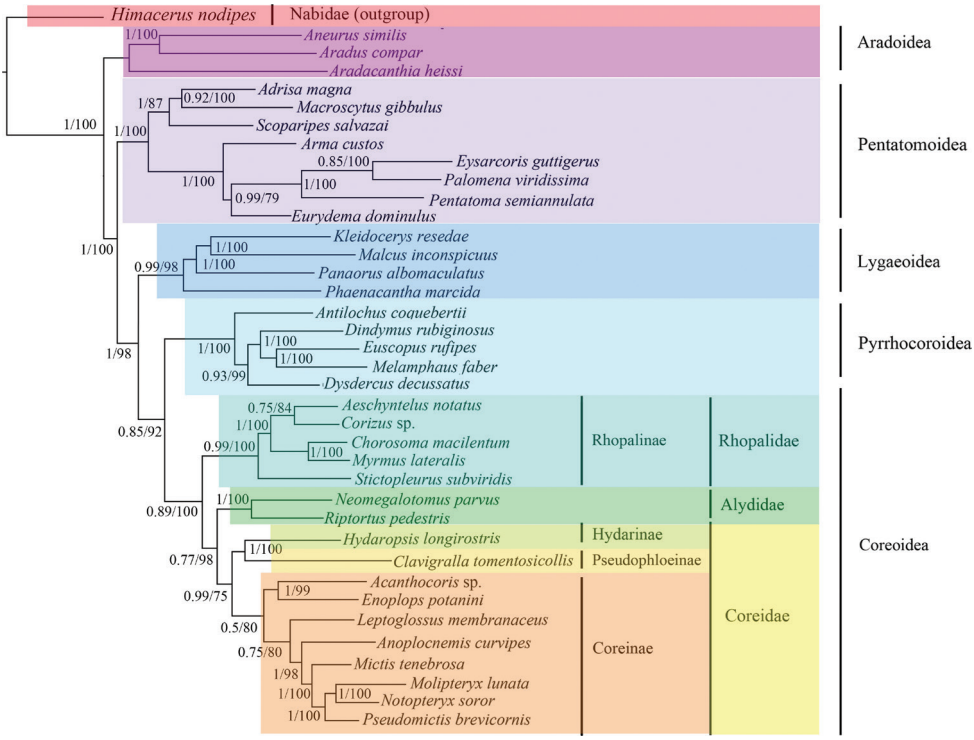

Figure 7. The phylogenetic relationships of PCG+rRNA using BI and ML methods. Numbers above each node indicate Bayesian posterior probabilities values and ML bootstrap values.

families of Coreidae were also supported with an internal relationship of ((Hydarinae + Pseudophloeinae) + Coreinae) (PP > 0.77 and BP > 75). Among Rhopalinae species, *Stictopleurus subviridis* Hsiao, 1977 was identified as sister to a group of other Rhopalinae species (PP = 0.99 and BP = 100). *M. lateralis* was close to *Chorosoma macilentum* Stål, 1858 (PP = 1 and BP = 100) and they both belonged to the tribe Chorosomatini.

Discussion

In this study, we sequenced the mitogenome of *Myrmus lateralis* and built the molecular phylogenetic relationships with 37 other heteropteran taxa. The mitogenome was found to be 17,309 bp long, with 37 genes arranged consistent with other species of Hemiptera (Song et al. 2012; Li et al. 2017; Zhao et al. 2021). The control region represented the largest reported non-coding region for insect mitogenomes owing to its various motifs and tandem repeats (Cook et al. 1999; Li et al. 2015). Although the 2587 bp long control region possessed several elements, such as a polyT stretch, a $G(A)_nT$ sequence, an ATAGA motif, a stem-loop, and a polyA stretch, tandem repeats were not observed.

The present study analyzed the initiation and termination codons of the 13 PCGs. The majority of PCGs used common start codons (ATN), except for *cox1*, which was initiated with TTG, a frequently used start codon in heteropteran mitogenomes (Quek et al. 2021; Zhao et al. 2021). The partial termination codon T was found in *nad2, cox2, cox3, nad3* and *nad5*. Some researchers have proposed that the incomplete termination codon could be completed via post-transcriptional polyadenylation (Ojala et al. 1981). Among the synonymous codons, codons ending with an A or U were more frequent than those ending in a G or C and were also observed in other heteropteran species (Zhao et al. 2019; Li et al. 2021). In this study, the lowest evolutionary rate was observed in *cox1*, indicating that this gene can be effectively used as a DNA barcoding marker. The Ka/Ks values for all 13 PCGs were far less than one, indicating that all of the PCGs evolved under purifying selection, thus, they can be used to investigate phylogenetic relationships.

Although many studies have reconstructed phylogenetic relationships among members of Pentatomomorpha, the relationships of different levels are still ambiguous (Li et al. 2005; Liu et al. 2019; Souza-Firmino et al. 2020; Kaur and Singh 2021). The results from previous research were congruent with the result that Trichophora includes four superfamilies of Pentatomomorpha except Aradoidea, and with the monophyly of four superfamilies of Trichophora (Henry 1997; Hua et al. 2008; Yuan et al. 2015; Song et al. 2019). Hua et al. (2008) and Liu et al. (2019) supported Pentatomoidea as the basal group of Trichophora and Coreoidea as a sister group to Lygaeoidea based on mitochondrial genomes. The superfamilies Coreoidea and Pyrrhocoroidea were supported as sister taxa based on cladistic analysis (Henry 1997), as well as 37 mitochondrial genes analysis (Yuan et al. 2015). Whereas our mitogenomic data showed that Coreoidea and Pyrrhocoroidea were sister groups based on ML and BI analyses using the PCG+rRNA dataset. This result from our study was consistent with that from the study of Song et al. (2019) based on relationship analysis of Pentatomomorpha PCGs.

At the family level, Rhopalidae was found to be a sister group to Alydidae + Coreidae. This relationship, based on mitogenomes, was consistent with that based on cladistic analysis by Li (1996) and Henry (1997). Despite the availability of numerous species, the classification patterns for the family Coreidae were weak in terms of both morphology and molecular data (Bressa et al. 2008; Forthman et al. 2019; Froeschner 2019). In this study, Hydarinae and Pseudophloeinae grouped the sister cluster. However, due to the limited samples, the relationships among Coreidae needs more studies in the future.

Previous studies on the classification of Rhopalinae came to a variety of conclusions and the positions of some species were not clear (Schaefer and Chopra 1982; Liu 1994; Aukema and Rieger 2006). The hypothesis that the genus *Stictopleurus* belongs to the Rhopalini tribe was corroborated based on morphological studies by Aukema and Rieger (2006). However, it did not group together with other Rhopalini species in this study. The monophyly of Rhopalini should be explored in the future studies with additional specimens.

Conclusions

The complete mitogenome of the scentless plant bug *Myrmus lateralis* was sequenced using next-generation sequencing technologies, providing the fifth mitogenome sequence from approximately 230 species of Rhopalidae. The nucleotide composition, codon usage, RNA structures, and protein-coding genes evolution were analyzed in our paper. The mitogenome of *M. lateralis* revealed the phylogenetic position of *Myrmus*. However, more mitogenomes should be sequenced to investigate the mitogenomic evolution and phylogenetic relationships of Rhopalidae.

Acknowledgments

This project was supported by the National Science Foundation Project of China (no. 31501876, 31872272) and supported by Scientific Research Project of Xinzhou Teachers University (2018KY04).

Reference

Dolling WR (2006) Family Rhopolidae Amyot & Serville, 1843. In: Catalog of the Heteroptera of the Palaearctic Region. The Netherlands Entomological Society, Amsterdam, 8–27.

Beckenbach AT, Stewart JB (2009) Insect mitochondrial genomics 3: the complete mitochondrial genome sequences of representatives from two neuropteroid orders: a dobsonfly (order Megaloptera) and a giant lacewing and an owlfly (order Neuroptera). Genome 52(1): 31–38. https://doi.org/10.1139/G08-098

Benson G (1999) Tandem repeats finder: a program to analyze DNA sequences. Nucleic Acids Research 27(2): 573–580. https://doi.org/10.1093/nar/27.2.573

Bernt M, Donath A, Jühling F, Externbrink F, Florentz C, Fritzsch G, Pütz J, Middendorf M, Stadler PF (2013) MITOS: improved de novo metazoan mitochondrial genome annotation. Molecular Phylogenetics and Evolution 69(2): 313–319. https://doi.org/10.1016/j.ympev.2012.08.023

Boore JL (1999) Animal mitochondrial genomes. Nucleic Acids Research 27(8): 1767–1780. https://doi.org/10.1093/nar/27.8.1767

Bressa MJ, Franco MJ, Toscani MA, Papeschi AG (2008) Heterochromatin heteromorphism in *Holhymenia rubiginosa* (Heteroptera: Coreidae). European Journal of Entomology 105(1): 65–72. https://doi.org/10.14411/eje.2008.009

Cameron SL (2014) Insect mitochondrial genomics: implications for evolution and phylogeny. Annual Review of Entomology 59: 95–117. https://doi.org/10.1146/annurev-ento-011613-162007

Carroll SP, Loye JE (2012) Soapberry bug (Hemiptera: Rhopalidae: Serinethinae) native and introduced host plants: biogeographic background of anthropogenic evolution. Annals of the Entomological Society of America 105(5): 671-684. https://doi.org/10.1603/AN11173

Coil D, Jospin G, Darling AE (2014) A5-miseq: an updated pipeline to assemble microbial genomes from Illumina MiSeq data. Bioinformatics 31(4): 587–589. https://doi.org/10.1093/bioinformatics/btu661

Cook CE, Wang Y, Sensabaugh G (1999) A mitochondrial control region and cytochromebphylogeny of sika deer (*Cervus nippon*) and report of tandem repeats in the control region. Molecular Phylogenetics and Evolution 12(1): 47–56. https://doi.org/10.1006/mpev.1998.0593

CoreoideaSF Team (2021) Coreoidea species file online. Version 5.0/5.0. http://Coreoidea.SpeciesFile.org. [Accessed on: 2021-10-26]

da Fonseca RR, Johnson WE, O'Brien SJ, Ramos MJ, Antunes A (2008) The adaptive evolution of the mammalian mitochondrial genome. BMC Genomics 9(1): 1–22. https://doi.org/10.1186/1471-2164-9-119

Darriba D, Taboada GL, Doallo R, Posada D (2012) jModelTest 2: more models, new heuristics and parallel computing. Nature methods 9(8): 772–772. https://doi.org/10.1038/nmeth.2109

Davidova-Vilimova J, Nejedla M, Schaefer CW (2000) Dorso-abdominal scent glands and metathoracic evaporatoria in adults of central European Rhopalidae (Hemiptera: Heteroptera), with a discussion of phylogeny and higher systematics. European Journal of Entomology 97(2): 213–222. https://doi.org/10.14411/eje.2000.039

Forthman M, Miller CW, Kimball RT (2019) Phylogenomic analysis suggests Coreidae and Alydidae (Hemiptera: Heteroptera) are not monophyletic. Zoologica Scripta 48(4): 520–534. https://doi.org/10.1111/zsc.12353

Froeschner RC (1988) Family Coreidae Leach, 1815: the coreid bugs. In: Catalog of the Heteroptera, or true bugs, of Canada and the continental United States. CRC Press, Boca Raton, 69–92. https://doi.org/10.1201/9781351070447-9

Ghahari H, Moulet P, Linnavuori R, Ostovan H (2012) An annotated catalog of the Iranian Coreidae, Rhopalidae, and Stenocephalidae (Hemiptera: Heteroptera: Pentatomomorpha: Coreoidea). Zootaxa 3519(1): 1–31. https://doi.org/10.11646/zootaxa.3519.1.1

Henry TJ (1997) Phylogenetic analysis of family groups within the infraorder Pentatomomorpha (Hemiptera: Heteroptera), with emphasis on the Lygaeoidea. Annals of the Entomological Society of America 90(3): 275–301. https://doi.org/10.1093/aesa/90.3.275

Henry TJ (1988) Family Rhopalidae Amyot and Serville, 1843 (= Corizidae Douglas and Scott, 1865): the scentless plant bugs. In: Catalog of the Heteroptera, or True Bugs, of Canada and the Continental United States. CRC Press, Boca Raton, 652–664. https://doi.org/10.1201/9781351070447-37

Hua J, Li M, Dong P, Cui Y, Xie Q, Bu W (2008) Comparative and phylogenomic studies on the mitochondrial genomes of Pentatomomorpha (Insecta: Hemiptera: Heteroptera). BMC genomics 9(1): 1–15. https://doi.org/10.1186/1471-2164-9-610

Kaur R, Singh D (2021) Cytochrome b sequence divergence and phylogenetic relationships among different species of family Pentatomidae (Hemiptera: Heteroptera). International Journal of Tropical Insect Science 41(2): 1177–1183. https://doi.org/10.1007/s42690-020-00303-8

Kearse M, Moir R, Wilson A, Stones-Havas S, Cheung M, Sturrock S, Buxton S, Cooper A, Markowitz S, Duran C (2012) Geneious Basic: an integrated and extendable desktop software platform for the organization and analysis of sequence data. Bioinformatics 28: 1647–1649. https://doi.org/10.1093/bioinformatics/bts199

Kocher A, Kamilari M, Lhuillier E, Coissac E, Péneau J, Chave J, Murienne J (2014) Shotgun assembly of the assassin bug Brontostoma colossus mitochondrial genome (Heteroptera, Reduviidae). Gene 552(1): 184–194. https://doi.org/10.1016/j.gene.2014.09.033

Librado P, Rozas J (2009) DnaSP v5: a software for comprehensive analysis of DNA polymorphism data. Bioinformatics 25(11): 1451–1452. https://doi.org/10.1093/bioinformatics/btp187

Linnavuori RE (2007) Studies on the Piesmatidae, Berytidae, Pyrrhocoridae, Stenocephalidae, Coreidae, Rhopalidae, Alydidae, Cydnidae, and Plataspidae (Heteroptera) of Gilan and the adjacent provinces in northern Iran. Acta Entomologica Musei Nationalis Pragae 47: 77–91. https://www.aemnp.eu/data/article-1138/1119-47_0_77.pdf

Li H, Leavengood JM, Chapman EG, Burkhardt D, Song F, Jiang P, Liu J, Zhou X, Cai W (2017) Mitochondrial phylogenomics of Hemiptera reveals adaptive innovations driving the diversification of true bugs. Proceedings of the Royal Society B: Biological Sciences 284(1862): e20171223. https://doi.org/10.1098/rspb.2017.1223

Li HM, Deng RQ, Wang JW, Chen ZY, Jia FL, Wang XZ (2005) A preliminary phylogeny of the Pentatomomorpha (Hemiptera: Heteroptera) based on nuclear 18S rDNA and mitochondrial DNA sequences. Molecular Phylogenetics and Evolution 37(2): 313–326. https://doi.org/10.1016/j.ympev.2005.07.013

Li R, Li M, Yan J, Bai M, Zhang H (2021) Five Mitochondrial Genomes of the Genus *Eysarcoris* Hahn, 1834 with Phylogenetic Implications for the Pentatominae (Hemiptera: Pentatomidae). Insects 12(7): 597. https://doi.org/10.3390/insects12070597

Li Y, Kocot KM, Schander C, Santos SR, Thornhill DJ, Halanych KM (2015) Mitogenomics reveals phylogeny and repeated motifs in control regions of the deep-sea family Siboglinidae (Annelida). Molecular Phylogenetics and Evolution 85: 221–229. https://doi.org/10.1016/j.ympev.2015.02.008

Liu Y, Li H, Song F, Zhao Y, Wilson JJ, Cai W (2019) Higher-level phylogeny and evolutionary history of Pentatomomorpha (Hemiptera: Heteroptera) inferred from mitochondrial genome sequences. Systematic Entomology 44(4): 810–819. https://doi.org/10.1111/syen.12357

Liu Q, Zheng LY, Nonnajzab (1994) The classification and faunal analyses of Rhopalidae (Hemiptera) in China. Journal of Arid Land Resources and Environment 8(3): 102–115.

Li XZ (1996) Cladistic analysis and higher classification of Coreoidea (Heteroptera). Entomologia Sinica 3(4): 283–292. https://doi.org/10.1111/j.1744-7917.1996.tb00277.x

Nonnaizab (1986) Fauna of Inner Mongolia (Hemiptera: Heteroptera). Inner Mongolia People's Publishing House, Hohhot, 298 pp.

Ojala D, Montoya J, Attardi G (1981) tRNA punctuation model of RNA processing in human mitochondria. Nature 290(5806): 470–474. https://doi.org/10.1038/290470a0

Quek ZBR, Chang JJM, Ip YCA, Chan YKS, Huang D (2021) Mitogenomes reveal alternative initiation codons and lineage-specific gene order conservation in echinoderms. Molecular Biology and Evolution 38(3): 981–985. https://doi.org/10.1093/molbev/msaa262

Rambaut A, Drummond AJ, Xie D, Baele G, Suchard MA (2018) Posterior summarization in Bayesian phylogenetics using Tracer 1.7. Systematic Biology 67(5): 901. https://doi.org/10.1093/sysbio/syy032

Ronquist F, Teslenko M, Van Der Mark P, Ayres DL, Darling A, Höhna S, Larget B, Liu L, Suchard MA, Huelsenbeck JP (2012) MrBayes 3.2: efficient Bayesian phylogenetic infer-

ence and model choice across a large model space. Systematic Biology 61(3): 539–542. https://doi.org/10.1093/sysbio/sys029

Schaefer CW (1993) Origins of the New World Rhopalinae (Hemiptera: Rhopalidae). Annals of the Entomological Society of America 86(2): 127–133. https://doi.org/10.1093/aesa/86.2.127

Schaefer CW, Chopra NP (1982) Cladistic analysis of the Rhopalidae, with a list of food plants. Annals of the Entomological Society of America 75(3): 224–233. https://doi.org/10.1093/aesa/75.3.224

Schaefer CW, Panizzi AR (2000) Scentless plant bugs (Rhopalidae). In: Schaefer CW, Panizzi AR (Eds) Heteroptera of Economic Importance. CRC Press, Boca Raton, 331–342. https://doi.org/10.1201/9781420041859

Simon C, Buckley TR, Frati F, Stewart JB, Beckenbach AT (2006) Incorporating molecular evolution into phylogenetic analysis and a new compilation of conserved polymerase chain reaction primers for animal mitochondrial DNA. Annual Review of Ecology, Evolution and Systematics 37: 545–579. https://doi.org/10.1146/annurev.ecolsys.37.091305.110018

Song N, Zhang H, Zhao T (2019) Insights into the phylogeny of Hemiptera from increased mitogenomic taxon sampling. Molecular phylogenetics and evolution 137: 236–249. https://doi.org/10.1016/j.ympev.2019.05.009

Song N, Liang AP, Bu CP (2012) A molecular phylogeny of Hemiptera inferred from mitochondrial genome sequences. PloS ONE 7(11): e48778. https://doi.org/10.1371/journal.pone.0048778

Souza HV, Souza FB, Maruyama SRC, Castanhole MMU, Itoyama MM (2009) Meiosis, spermatogenesis and nucleolar behavior in the seminiferous tubules of Alydidae, Coreidae and Rhopalidae (Heteroptera) species. Genetics and Molecular Research 8(4): 1383–1396 https://doi.org/10.4238/vol8-4gmr672

Souza-Firmino TSD, Alevi KCC, Itoyama MM (2020) Chromosomal divergence and evolutionary inferences in Pentatomomorpha infraorder (Hemiptera, Heteroptera) based on the chromosomal location of ribosomal genes. Plos ONE 15(2): e0228631. https://doi.org/10.1590/S0074-02762013000300017

Stamatakis A (2015) Using RAxML to infer phylogenies. Current Protocols in Bioinformatics 51(1): 6–14. https://doi.org/10.1002/0471250953.bi0614s51

Steill J, Meyer J (2003) The Rhopalidae of Florida. Insect Classification Project 4 (30): 1–23. http://entnemdept.ufl.edu/choate/rhopalidae.pdf

Tamura K, Stecher G, Peterson D, Filipski A, Kumar S (2013) MEGA6: molecular evolutionary genetics analysis version 6.0. Molecular Biology and Evolution, 30(12): 2725–2729. https://doi.org/10.1093/molbev/mst197

Tian XX, Xie Q, Li M, Gao CQ, Cui Y, Xi L, Bu W (2011) Phylogeny of pentatomomorphan bugs (Hemiptera-Heteroptera: Pentatomomorpha) based on six Hox gene fragments. Zootaxa 2888: 57–68. https://doi.org/10.11646/zootaxa.2888.1.5

Tyagi K, Chakraborty R, Cameron SL, Sweet AD, Chandra K, Kumar V (2020) Rearrangement and evolution of mitochondrial genomes in Thysanoptera (Insecta). Scientific reports 10(1): 1–16. https://doi.org/10.1038/s41598-020-57705-4

Vaidya G, Lohman DJ, Meier R (2011) SequenceMatrix: concatenation software for the fast assembly of multi-gene datasets with character set and codon information. Cladistics 27(2): 171–180. https://doi.org/10.1111/j.1096-0031.2010.00329.x

Wolstenholme DR (1992) Animal mitochondrial DNA: structure and evolution. International Review of Cytology 141: 173–216. https://doi.org/10.1016/S0074-7696(08)62066-5

Weirauch C, Schuh RT (2011) Systematics and evolution of Heteroptera: 25 years of progress. Annual Review of Entomology 56: 487–510. https://doi.org/10.1146/annurev-ento-120709-144833

Xu N, Ding J, Que Z, Xu W, Ye W, Liu H (2021) The mitochondrial genome and phylogenetic characteristics of the Thick-billed Green-Pigeon, *Treron curvirostra*: the first sequence for the genus. ZooKeys 1041: 167–182. https://doi.org/10.3897/zookeys.1041.60150

Xie Q, Bu W, Zheng L (2005) The Bayesian phylogenetic analysis of the 18S rRNA sequences from the main lineages of Trichophora (Insecta: Heteroptera: Pentatomomorpha). Molecular Phylogenetics and Evolution 34: 448–451. https://doi.org/10.1016/j.ympev.2004.10.015

Yang QQ, Liu SW, Song F, Liu GF, Yu XP (2018) Comparative mitogenome analysis on species of four apple snails (Ampullariidae: Pomacea). International Journal of Biological Macromolecules 118: 525–533. https://doi.org/10.1016/j.ijbiomac.2018.06.092

Yuan ML, Zhang QL, Guo ZL, Wang J, Shen YY (2015) The complete mitochondrial genome of Corizus tetraspilus (Hemiptera: Rhopalidae) and phylogenetic analysis of Pentatomomorpha. PLoS ONE 10(6): e0129003. https://doi.org/10.1371/journal.pone.0129003

Zhao L, Wei J, Zhao W, Chen C, Gao X, Zhao Q (2021) The complete mitochondrial genome of *Pentatoma rufipes* (Hemiptera, Pentatomidae) and its phylogenetic implications. ZooKeys 1042: 51–72. https://doi.org/10.3897/zookeys.1042.62302

Zhao W, Zhao Q, Li M, Wei J, Zhang X, Zhang H (2019) Comparative mitogenomic analysis of the *Eurydema* genus in the context of representative Pentatomidae (Hemiptera: Heteroptera) taxa. Journal of Insect Science 19(6): 20. https://doi.org/10.1093/jisesa/iez122

Zuker M (2003) Mfold web server for nucleic acid folding and hybridization prediction. Nucleic Acids Research 31(13): 3406–3415. https://doi.org/10.1093/nar/gkg595

ZooKeys 1070: 31–40 (2021)
doi: 10.3897/zookeys.1070.73377
https://zookeys.pensoft.net

RESEARCH ARTICLE

A peer-reviewed open-access journal
ZooKeys
Launched to accelerate biodiversity research

A new species of the genus *Hylcalosia* Fischer (Hymenoptera: Braconidae: Alysiinae) from South Korea, with a key to the Korean species

Ju-Hyeong Sohn[1*], Cornelis van Achterberg[2*], Yunjong Han[1], Hyojoong Kim[1]

1 *Animal Systematics Lab., Department of Biology, Kunsan National University, Gunsan, 54150, Republic of Korea* **2** *State Key Laboratory of Rice Biology and Ministry of Agriculture / Key Lab of Agricultural Entomology, Institute of Insect Science, Zhejiang University, Hangzhou, 310058, China*

Corresponding author: Hyojoong Kim (hkim@kunsan.ac.kr)

Academic editor: Xue-xin Chen | Received 23 August 2021 | Accepted 16 October 2021 | Published 10 November 2021

http://zoobank.org/9D7BA9C7-A572-4700-9324-11D0E05EB3F5

Citation: Sohn J, van Achterberg C, Han Y, Kim H (2021) A new species of the genus *Hylcalosia* Fischer (Hymenoptera: Braconidae: Alysiinae) from South Korea, with a key to the Korean species. ZooKeys 1070: 31–40. https://doi.org/10.3897/zookeys.1070.73377

Abstract

The species of the genus *Hylcalosia* Fischer, 1967 (Braconidae: Alysiinae) from South Korea are revised. One species, *Hylcalosia bicolor* **sp. nov.**, is new to science. They are described and illustrated herein and an identification key to the Korean species is added. In addition, the DNA barcode region of the mitochondrial cytochrome c oxidase subunit I (COI) has been analysed for the new species and *H. sutchanica* is used for genetic comparison.

Keywords

COI barcode, cyclostome, koinobiont, natural enemy, parasitoid wasp, systematics, taxonomy

* These authors contributed equally.

Introduction

The subfamily Alysiinae, which is one of the large taxa in the family Braconidae, occurs worldwide and contains over 2,440 valid species (Yu et al. 2016). In Korea, 180 species in 21 genera are listed in the National Species List of South Korea (NIBR 2019). This group can be discriminated from other subfamilies by having non-overlapping mandibles and is subdivided into two tribes, Alysiini and Dacnusini, which are distinguished from each other by the presence or absence of fore wing vein r-m, respectively (Shaw and Huddleston 1991). Alysiinae are known as koinobiont endoparasitoids of dipteran larvae, characteristically using their mandible (with three or four teeth, rarely more or less) to break open the puparium of the host.

Hylcalosia Fischer, 1967 is a small genus of Alysiinae, which includes 18 species (Yu et al. 2016, Yao et al. 2020). This genus is easily diagnosed by the rugose or granulated second and third metasomal tergites combined by the acutely protruding clypeus and enlarged upper valve of the ovipositor (van Achterberg 1983). Fischer (1967) re-described the type species from Myanmar *Holcalysia ruficeps* Cameron, 1910. Van Achterberg (1983) revised the genus *Hylcalosia* and described two new species: *H. maetoi* and *H. hemiflava* from Japan and Indonesia, respectively. Belokobylskij (1992) added two new species from Russia: *H. hymaenei* and *H. sutchanica*. Papp (1994) described *H. adsimilis* from North Korea and Chen & Wu (1994) *H. complexa* from China. Fischer (2008) added *H. laosensis* as a new species from Laos and Zheng et al. (2012) *H. ventisulcata* as a new species in China. Belokobylskij (2015) revised the Russian *Hylcalosia* species and synonymised *H. adsimilis* with *H. sutchanica*, reported *H. maetoi* from South Korea and described a new species, *H. livadiae*. Finally, four new species (*H. carinata*, *H. melasaraia*, *H. poricrenulata* and *H. verticalis*) were described from China by Zhu et al. (2018) and five new species (*H. bothynis*, *H. dichromata*, *H. eurykephale*, *H. leura* and *H. perkna*) from Thailand by Yao et al. (2020).

In this study, we present new morphological characters and the barcoding sequences of the COI region of *H. bicolor* sp. nov. and one previously-recorded species, *H. sutchanica*. Descriptions, diagnoses, an identification key and photographs of the diagnostic characters are provided.

Materials and methods

Samples used in this study were collected with Malaise traps in South Korea at the DMZ Botanical Garden, Mandae-ri, Haean-myeon, Yanggu-gun, Gangwon-do. Sorting and preparation were done at the Animal Systematics Lab. (ASL), Department of Biology, Kunsan National University (KSNU) at Gunsan. For morphological identification, Zhu et al. (2017, 2018) and Yao et al. (2020) were used. Morphological characters were observed with a Leica M205C stereomicroscope. The Taxapad database (Yu et al. 2016) was used for references. We followed the terminology of Wharton (2002)

and van Achterberg (1993). The type specimens are deposited in Korea National Arboretum (KNA).

A LEICA DMC2900 digital camera and a LEICA M205C stereomicroscope (Leica Geosystems AG) were used for photography and several pictures were taken for each height using multi-focusing technology. LAS V4.11 (Leica Geosystems AG, Wetzlar, Germany) and HeliconFocus 7 (Helicon Soft, Kharkiv, Ukraine) software were used for stacking work. After stacking work, illustrations were created using Adobe Photoshop CS6.

Extraction of DNA was done in ASL, KSNU. Whole genomic DNA was extracted from the specimens by using a DNeasy Blood & Tissue kit (QIAGEN Inc., Dusseldorf, Germany) following the manufacturer's protocol. In order to conserve morphologically-complete voucher specimens, the DNA extraction method was used slightly modified from the 'non-destructive method' by Favret (2005) and 'freezing method' by Yaakop et al. (2009). In the original protocol, the sample was crushed or wounded and then soaked with 180 µl of buffer ATL + 20 µl of proteinase, followed by three hours incubation at 55°C. In slightly modified DNA extraction methods, samples were soaked with 180 µl of buffer ATL + 20 µl of proteinase K without destroying the sample, followed by 20 minutes incubation at 55°C and then kept in a freezer at -21°C overnight. After that, the general protocol was used for the remaining steps. The primer-set of LCO-1490 (5'-GGTCAACAAATCATAAAGATATTGG-3') and HCO-2198 (5'-TAAACTTCAGGGTGACCAAAAAATCA-3') was used to amplify approximately 658 bp as the partial front region of the COI. The polymerase chain reaction (PCR) products were amplified by using AccuPowerH PCR PreMix (BIONEER, Corp., Daejeon, Korea) in 20 µl reaction mixtures containing 0.4 µM of each primer, 20 µM of dNTPs, 20 µM of $MgCl_2$ and 0.05 µg of the genomic DNA template. PCR amplification was performed using a GS1 thermo-cycler (Gene Technologies, Ltd., Essex, UK) according to the following procedure: initial denaturation at 95°C for 5 min, followed by 34 cycles at 94°C for 35 sec; an annealing temperature of 48°C for 25 sec; an extension at 72°C for 45 sec and a final extension at 72°C for 5 min. The PCR products were visualised by electrophoresis on a 1.5% agarose gel. A single band was observed, purified using a QIAquick PCR purification kit (QIAGEN, Inc., Milan, Italy) and then sequenced directly using an automated sequencer (ABI Prism 3730 XL DNA Analyzer) at Macrogen Inc. (Seoul, South Korea).

Sequence alignments were performed in MEGA version 7 (Kumar et al. 2016) with the ClustalW tool. To estimate the pairwise genetic distances, the *P*-distance model was conducted using MEGA version 7.

Table 1. COI pairwise genetic distances between two *Hylcalosia* species from South Korea.

	Hylcalosia sutchanica	***Hylcalosia bicolor***
Hylcalosia sutchanica	0.00	
Hylcalosia bicolor	0.091	0.00

Results

A total of 563 bp of the COI barcode region were sequenced from *H. bicolor* sp. nov. and *H. sutchanica* which were deposited in GenBank (accession numbers MZ717196, MZ717194). Pairwise distances were estimated by using the *P*-distance model with the option for pairwise deletion. As a result, *H. bicolor* sp. nov. showed a fairly large genetic difference of 6% from *H. sutchanica*.

Hylcalosia Fischer, 1967

Holcalysia Cameron, 1910: 6 [nec Cameron, 1905]; Shenefelt, 1974: 993. Type species: *Holcalysia ruficeps* Cameron, 1910.

Hylcalosia Fischer, 1967: 125; Shenefelt, 1974: 993; Chen & Wu, 1994: 85; Belokobylskij, 1998: 297; Zheng, Chen & Yang, 2012: 454; Belokobylskij, 2015: 530. Type species: *Holcalysia ruficeps* Cameron, 1910.

Diagnosis. First flagellomere distinctly shorter than second (Figs 1B, 2B), eye slightly oval and glabrous, clypeus triangularly protruding anteriorly (Figs 1E, 2E), labrum small triangular shape, mandible with 3–4 teeth or lobes (Figs 1J, 2J), maxillary palp with 6 segments; notauli partially or completely present, scutellar sulcus distinct, precoxal sulcus complete (Figs 1G, 2G); fore wing (Figs 1C, 2C) vein 2-SR slightly bent, vein 2-SR shorter than vein 3-SR; hind wing vein 1-M longer than vein 1r-m; propodeum largely rugose (Figs 1F, 2F); second and third tergites rugose or granulated (Figs 1H, 2H); tarsal claws rather slender (Figs 1K,L; 2K,L).

Biology. Unknown.

Distribution. Palaearctic (East) and Oriental Regions.

Key to species of *Hylcalosia* Fischer from Korea

1. Second metasomal tergite 1.4–1.5 times longer than third tergite (Fig. 3B); mesoscutum largely blackish or dark brown; medio-posterior depression of mesoscutum short (Fig. 2F); [vein r of fore wing comparatively long (Fig. 2C)] .... ***H. sutchanica* Belokobylskij, 1992**
– Second metasomal tergite 1.1–1.2 times as long as third tergite (Fig. 3A); mesoscutum largely red or reddish-brown; medio-posterior depression of mesoscutum long (Fig. 1F) **2**
2. Head entirely black; vein r of fore wing comparatively short (Fig. 1C), 0.4 times as long as maximum width of pterostigma (Fig. 1C); metasoma largely reddish-brown; first metasomal tergite largely subparallel-sided (Fig. 1H); eye in dorsal view about 1.7 times longer than temple (Fig. 1D) ..... ***H. bicolor* sp. nov.**
– Head (except stemmaticum) brownish-yellow; vein r of fore wing medium-sized, 0.9 times as long as maximum width of pterostigma; metasoma black; first tergite

gradually widened posteriorly; eye in dorsal view about as long as temple.....
..... ***H. maetoi* van Achterberg, 1983**

***Hylcalosia bicolor* Sohn & van Achterberg, sp. nov.**
http://zoobank.org/CBFECB61-CB8E-4847-9F08-9B360554BEDE
Figures 1A–L

Type material. ***Holotype***. ♀ (KNA), South Korea, DMZ Botanical Garden, Mandae-ri, Haean-myeon, Yanggu-gun, Gangwon-do, 38°15'09.3"N, 128°06'40.6"E, 27 May–20 Jun 2017, Shin & Kim leg. GenBank accession no. MZ717196.

Comparative diagnosis. This species is similar to *H. verticalis* Zhu, van Achterberg & Chen, 2018 from China because of the vertical vein r-m of fore wing, deep and coarsely crenulate notauli, eye much longer than temple in dorsal view and second tergite about as long as third tergite or slightly longer, but differs by having the hind tibia yellowish-brown (largely blackish in *H. verticalis*), the third metasomal tergite (except basally) largely smooth and, in lateral view, truncated apically (coarsely rugose and rounded apically in *H. verticalis*), vein 1-r-m of hind wing shorter than vein 1-M (about of equal length in *H. verticalis*), the pterostigma subparallel-sided apically (slightly widened in *H. verticalis*), vein 3-CU1 of fore wing comparatively short (long in *H. verticalis*) and the precoxal sulcus wide medially (comparatively narrow in *H. verticalis*).

Description. ♀. Length of body in lateral view 2.6 mm, length of antenna 4.7 mm and length of fore wing 2.9 mm.

***Colour*.** Body (Fig. 1A) mainly reddish-brown; head black; antenna brown basally; mandible reddish-brown. ***Head*.** Head (Fig. 1D) width 1.6 times median length in dorsal view. Antenna (Fig. 1B) 1.8 times longer than body in female, 43-segmented. First flagellomere 0.7 times longer than second. Eye slightly oval, 1.1 times as long as wide in lateral view. Width of face (Fig. 1E) 2.1 times its height from ventral rim of antennal sockets to upper margin of clypeus; face with long setae. Eye in dorsal view 1.7 times as long as temple. Ocello-ocular line (OOL) 4.5 times longer than diameter of anterior ocellus; OOL:antero-posterior ocellar line (AOL):postero-ocellar line (POL) = 18:6:7. Stemmaticum concave. Vertex smooth and shiny with groove. Mandible with four teeth or lobes (Fig. 1J); dorsal tooth large and lobe-shaped; ventral tooth lobe-shaped, middle of tooth curved. Medial length of mandible 1.7 times longer than maximum width. Labrum small, 1.4 times longer than wide. Maxillary palp 0.5 times longer than mesosoma.

***Mesosoma*.** Mesosoma (Fig. 1F) 2.0 times longer than wide in dorsal view: with medio-posterior depression; notauli coarsely crenulate anteriorly and deeply impressed, up to anterior level of medio-posterior depression (Fig. 1F); scutellar sulcus indistinct, with two carinae and sparse setae; small basal bump on hind coxa. Propodeum (Fig. 1F) largely reticulate, 1.7 times longer than wide in dorsal view. Metapleuron anteriorly crenulate and with setae; precoxal sulcus (Fig. 1G) crenulated, with about nine carinae. Fore wing (Fig. 1C) 2.4 times as long as wide; pterostigma long and robust, 3.4 times longer than wide; vein r of fore wing 2.6 times longer than wide and 0.4

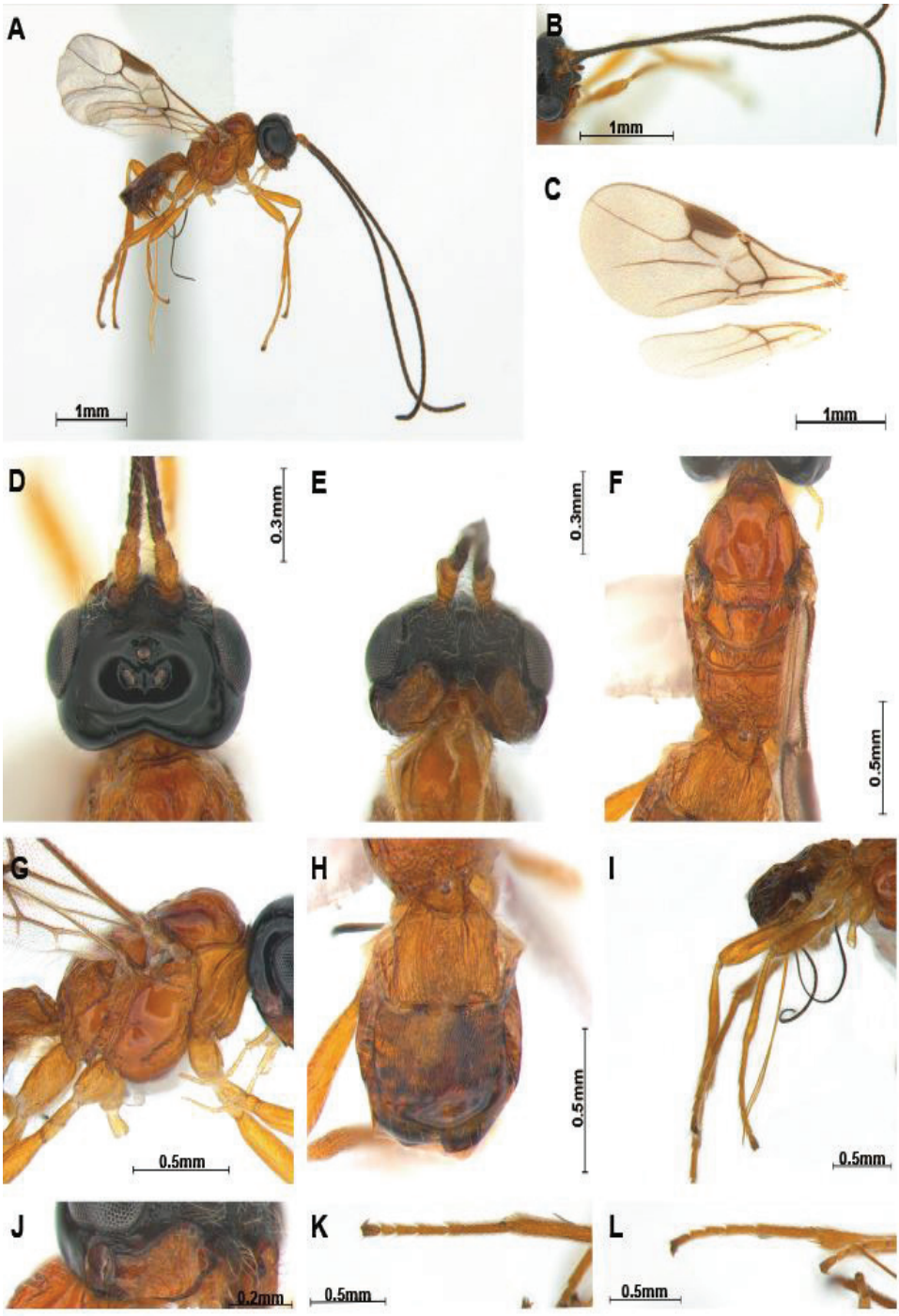

Figure 1. *Hylcalosia bicolor* sp. nov., ♀, holotype **A** body, lateral view **B** antennae **C** wings **D** head, dorsal view **E** head, ventral view **F** mesosoma, dorsal view **G** mesosoma, lateral view **H** propodeum and first metasomal tergite, dorsal view **I** ovipositor and hind leg, lateral view **J** mandible, lateral view **K** hind tarsus, dorsal view **L** hind tarsus, lateral view.

times as long as maximum width of pterostigma; vein 1-M slightly bent; 2-SR+M not sclerotised; veins 1-SR+M:2-SR = 9:12; veins 2-SR: r: 3-SR = 12:3:7; first subdiscal cell of fore wing 2.8 times longer than wide. Hind wing veins M+CU:1-M:1r-m = 10:6:4.

Leg. Hind coxa compressed, 1.5 times longer than hind trochanter; hind femur 0.7 times longer than hind tibia and 8.0 times longer than wide; hind tibia 1.1 times longer than hind tarsus, tarsal claws slender (Fig. 1L).

Metasoma. First tergite parallel-sided posteriorly, striate and 1.1 times longer than its apical width (Fig. 3A); first tergite 0.9 times as long as second. Second tergite distinctly rugose and 1.2 times as long as third tergite, third tergite (except basally) largely smooth (Fig. 3A). Setose part of ovipositor sheath (Fig. 1I) 1.3 times longer than mesosoma, 1.3 times metasoma, 1.3 times as long as hind tibia, with long setae.

Male. Unknown.

Distribution. South Korea.

Hylcalosia sutchanica Belokobylskij, 1992

Figures 2A–L

Hylcalosia sutchanica Belokobylskij, 1992: 148; 1998: 298; 2015: 538; Fischer, 2008: 722; Zheng et al., 2012: 455.

Hylcalosia adsimilis Papp, 1994: 139; Belokobylskij, 1998: 298; Fischer, 2008: 722; Yu et al., 2012; Zheng et al., 2012: 455. Synonymized by Belokobylskij (2015).

Material. 2♀ (KNA), South Korea, DMZ Botanical Garden, Mandae-ri, Haeanmyeon, Yanggu-gun, Gangwon-do, 38°15'09.3"N, 128°06'40.6"E, 20 Jun–4 Jul 2017, Shin & Kim leg. GenBank accession no. MZ717194.

Re-description. ♀, length of body in lateral view 2.6–2.7 mm, length of antenna 4.1–4.3 mm and length of fore wing 2.7–2.9 mm.

Colour. Body largely blackish; head entirely black dorsally and anteriorly brown, antenna reddish-brown and apically dark brown, mandible pale brown and apically dark brown; first tergite reddish-brown and mesonotum entirely blackish or dark brown.

Head. Head (Fig. 2D) width 1.6 times median length in dorsal view. Antenna (Fig. 2B) 1.6 times longer than body, 40 or 42 segmented. First flagellomere 0.7 times as long as second, second flagellomere 1.1 times longer than third. Eye slightly oval, 1.1 times as long as wide in lateral view. Width of face (Fig. 2E) 2.0 times its height from ventral rim of antennal sockets to upper margin of clypeus; face with long setae. Eye in dorsal view 2.4 times as long as temple. Ocello-ocular line (OOL) 4.0 times longer than diameter of anterior ocellus; OOL:antero-posterior ocellar line (AOL):postero-ocellar line (POL) = 12:5:5. Vertex smooth and shiny with groove. Mandible (Fig. 2J) with four teeth and setae; dorsal tooth large and lobe-shaped and distinctly surpassing apex of first tooth, ventral tooth lobe-shaped, middle of tooth curved; second tooth narrow and sharp with dark brown tip and separated from first tooth by incision in lateral view. Medial length of mandible 1.7 times longer than maximum width. Labrum small, 1.3 times longer than wide. Maxillary palp 0.7 times as long as mesosoma.

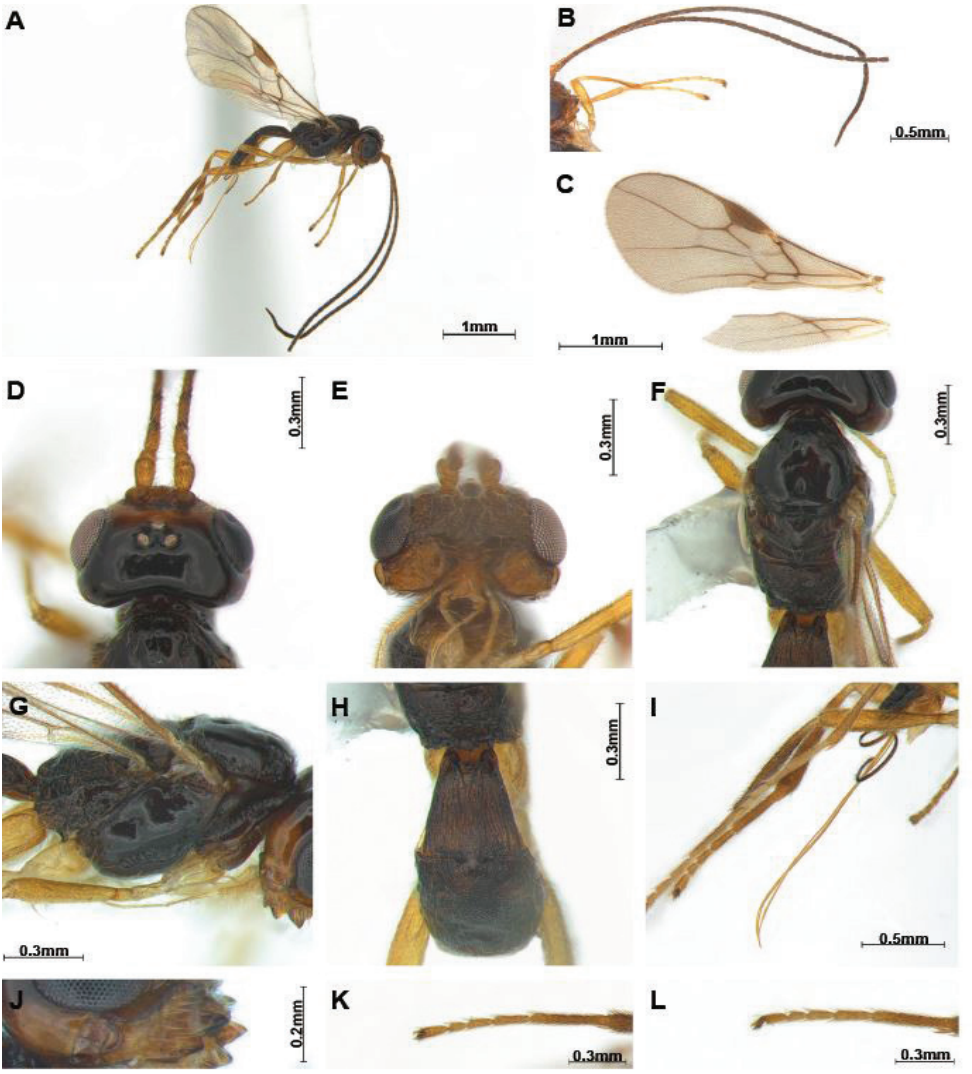

Figure 2. *Hylcalosia sutchanica* Belokobylskij, 1992 ♀ **A** body, lateral view **B** antennae **C** wings **D** head, dorsal view **E** head, ventral view **F** mesosoma, dorsal view **G** mesosoma, lateral view **H** propodeum and first metasomal tergite, dorsal view **I** ovipositor and hind leg, lateral view **J** mandible, lateral view **K** hind tarsus, dorsal view **L** hind tarsus, lateral view.

Mesosoma. Mesosoma (Fig. 2G) 2.1 times longer than wide in dorsal view; notauli moderately crenulated, but situated far from comparatively small medio-posterior depression (Fig. 2F); scutellar sulcus with four carinae; laterally mesopleuron and metapleuron with long setae, metapleuron distinctly rugose. Anterior half of propodeum smooth, posterior of median carina reticulate-rugose (Fig. 2H), lateral view of propodeum not curved dorsally; precoxal sulcus (Fig. 2F) shallow and with 14 crenulae. Fore wing (Fig. 2C) 2.4 times longer than wide; pterostigma long and thick, 3.4 times longer than wide; vein r of fore wing 2.9 times longer than wide; vein 2-SR slightly bent;

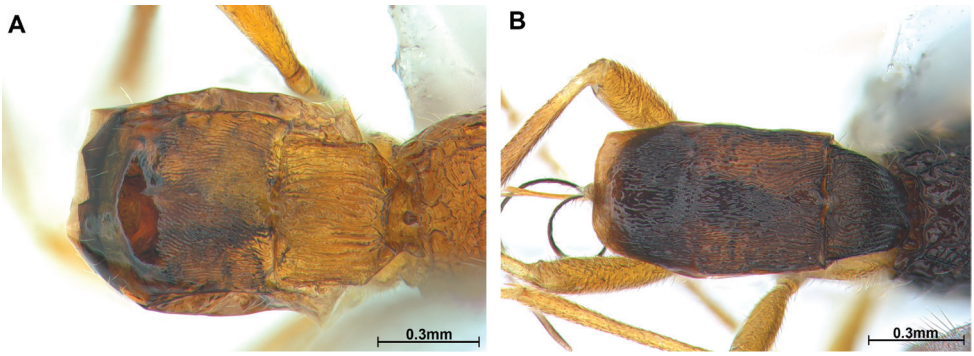

Figure 3. Metasoma, dorsal view **A** *Hylcalosia bicolor* sp. nov. **B** *Hylcalosia sutchanica* Belokobylskij, 1992

vein 2-SR+M and r-m not sclerotised; veins 2-SR: r: 3-SR = 11:2:7; first subdiscal cell of fore wing 1.5 times longer than wide. Hind wing veins M+CU:1-M:1r-m = 11:7:5.

Leg. Hind coxa smooth and 1.2 times longer than hind trochanter; hind femur 0.9 times as long as hind tibia and 8.5 times longer than wide; hind tibia 0.9 times longer than hind tarsus, tarsal claws slender (Fig. 2L).

Metasoma. First tergite gradually widened posteriorly (Fig. 3B), striate and comparatively narrow, 1.1 times longer than its apical width; first tergite 0.8 times as long as second tergite, second tergite 1.4–1.5 times longer than third and largely rugose and third tergite largely rugose (Fig. 3B). Setose part of ovipositor sheath (Fig. 2I) 1.5 times longer than mesosoma, 1.7 times longer than hind tibia and with medium-sized setae.

Distribution. Russia, China, Korea.

Acknowledgements

This work was supported by the Korean National Arboretum (KNA1-1-20) and a grant from the National Institute of Biological Resources (NIBR), funded by the Ministry of Environment (MOE) of the Republic of Korea (NIBR202130203).

References

Belokobylskij SA (1992) Finding of the genus *Hylcalosia* (Hymenoptera, Braconidae, Alysiinae) of the USSR and descriptions of two new species from the south of the Far East. Zoologicheskiy Zhurnal 71(5): 143–149. [Entomological Review. 71(9): 142–147.]

Belokobylskij SA (1998) Tribe Alysiini. In: Ler PA (Ed.) Key to Insects of the Russian Far East. Dal'nauka, Vladivostok, 163–298. [In Russian]

Belokobylskij SA (2015) The genus *Hylcalosia* Fischer, 1967 (Hymenoptera: Braconidae: Alysiinae) of the Russian Far East. Zootaxa 4040 (5): 530–542. https://doi.org/10.11646/zootaxa.4040.5.2

Cameron P (1910) On some Asiatic species of the Braconid subfamilies Rhogadinae, Agathinae, and Macrocentrinae and of the Alysiidae. Wiener Entomologische Zeitschrift 29: 1–10. https://doi.org/10.5962/bhl.part.23337

Chen JH, Wu ZS (1994) The Alysiini of China: (Hymenoptera: Braconidae: Alysiinae). China Agricultural Press, Fuzhou, 1–218. [In Chinese, with summary in English]

Favret C (2005) New non-destructive DNA extraction and specimen clearing technique for aphids (Hemiptera). Proceedings of the Entomological Society of Washington 107: 469–470.

Fischer M (1967) Seltene Alysiinae aus verschiedenen Erdteilen. Annalen des Naturhistorischen Museums in Wien 70: 109–138.

Fischer M (2008) Über die Gattungen *Idiasta* Foerster, *Aphaereta* Foerster und *Hylcalosia* Fischer (Hyme-noptera, Braconidae, Alysiinae). Linzer Biologische Beiträge 40 (1): 703–734

Kumar S, Stecher G, Tamura K (2016) MEGA7: Molecular evolutionary genetics analysis version 7.0 for bigger datasets. Molecular, Biology and Evolution. 33: 1870–1874. https://doi.org/10.1093/molbev/msw054

NIBR (2019) National List of Species of Korea. National Institute of Biological Resources. http://kbr.go.kr [accessed on 20/08/21].

Papp J (1994) Braconidae (Hymenoptera) from Korea, XV. Acta Zoologica Academiae Scientiarum Hungaricae 40(2): 133–156.

Shenefelt RD (1974) Braconidae 7. Alysiinae. Hymenopterorum Catalogus. Pars 11: 985-1113.

Shaw MR, Huddleston T (1991) Classification and biology of Braconid wasps (Hymenoptera: Braconidae). Handbooks for the Identification of British Insects 7(11): 1–126.

van Achterberg C (1983) A revision of the genus *Hylcalosia* Fischer (Hymenoptera: Braconidae, Alysiinae). Zoologische Mededelingen Leiden 57 (8): 81–90.

van Achterberg C (1993) Illustrated key to the subfamilies of the Braconidae (Hymenoptera: Ichneumonoidea). Zoologische Verhandelingen Leiden 283: 1–189.

Wharton RA (2002) Revision of the Australian Alysiini (Hymenoptera:Braconidae). Invertebrate Systematics 16: 7–105. https://doi.org/10.1071/IT01012

Yaakop S, van Achterberg C, Idris AB (2009) *Heratemis* Walker (Hymenoptera: Braconidae: Alysiinae: Alysiini): revision and reconstruction of the phylogeny combining molecular data and morphology. Tijdschrift voor Entomologie 152: 1–64. https://doi.org/10.1163/22119434-900000268

Yao J-L, van Achterberg C, Sharkey MJ, Chapman EG, Chen J-H (2020) Five species and a genus new for Thailand, with description of five new species of *Hylcalosia* Fischer (Hymenoptera: Braconidae: Alysiinae). Insect Systematics and Evolution 51: 610–636 https://doi.org/10.1163/1876312X-00002303

Yu DSK, van Achterberg C, Horstmann K (2016) Taxapad 2016, Ichneumonoidea 2015. Database on flash-drive. www.taxapad.com, Nepean, Ontario, Canada.

Zheng M-L, Chen J-H, Yang J-Q (2012) A new species in the genus *Hylcalosia* (Hymenoptera: Braconidae) from China. Entomotaxonomia 34(2): 453–458.

Zhu J-C, van Achterberg C, Chen X-X (2017) An illustrated key to the genera and subgenera of the Alysiini (Hymenoptera, Braconidae, Alysiinae), with three genera new for China. ZooKeys 722: 37–79. https://doi.org/10.3897/zookeys.722.14799

Zhu J-C, van Achterberg C, Chen X-X (2018) Review of the genus *Hylcalosia* Fischer (Hymenoptera, Braconidae, Alysiinae), with description of four new species from China. Zootaxa 4462(4):547–565. https://doi.org/10.11646/zootaxa.4462.4.7

ZooKeys 1070: 41–50 (2021)
doi: 10.3897/zookeys.1070.73484
https://zookeys.pensoft.net

RESEARCH ARTICLE

A peer-reviewed open-access journal
ZooKeys
Launched to accelerate biodiversity research

A new species of *Neohagenulus* Traver, 1938 from Hispaniola (Ephemeroptera, Leptophlebiidae, Hagenulinae, Hagenulini)

Michel Sartori[1,2]

1 *Museum of Zoology, Palais de Rumine, Place Riponne 6, CH-1014, Lausanne, Switzerland* **2** *Department of Ecology and Evolution, Biophore, University of Lausanne, CH-1015, Lausanne, Switzerland*

Corresponding author: Michel Sartori (michel.sartori@vd.ch)

Academic editor: L. Pereira-da-Conceicoa | Received 25 August 2021 | Accepted 23 October 2021 | Published 10 November 2021

http://zoobank.org/C6532DEC-44A2-4150-BBA3-11BF711C068B

Citation: Sartori M (2021) A new species of *Neohagenulus* Traver, 1938 from Hispaniola (Ephemeroptera, Leptophlebiidae, Hagenulinae, Hagenulini). ZooKeys 1070: 41–50. https://doi.org/10.3897/zookeys.1070.73484

Abstract

Here, I report a new species of the genus *Neohagenulus* Traver, 1938 from the Dominican Republic. The genus was believed to be endemic to Puerto Rico until now. *Neohagenulus hodeceki* **sp. nov.** is described at the nymphal stage. Some discussion on the tribe Hagenulini is also provided.

Keywords

Borinquena, *Careospina*, *Hagenulus*, morphology, new species, nymph, sexual dimorphism

Introduction

Nine genera of the family Leptophlebiidae have been found on four islands of the Greater Antilles, Cuba, Hispaniola, Jamaica and Puerto Rico (Naranjo Lopez and Peters 2016) and some of them are sometimes considered to be subgenera (Kluge 1994). Except for *Farrodes* Peters, 1971, *Hagenulopsis* Ulmer, 1920 and *Hagenulus* Eaton, 1882, which include species distributed in the continental Americas, all other genera are endemic to the Greater Antilles. These are *Borinquena* Traver, 1938 with two species in Puerto Rico and one in Cuba, *Careospina* Peters, 1971 with four species in Cuba and one in Hispaniola, *Neohagenulus* Traver, 1938 with three species in Puerto Rico and *Poecilophlebia*

Kluge, 1994, *Traverina* Peters, 1971 and *Turquinophlebia* Kluge, 1994, each with one, two and one species endemic to Cuba, respectively (Naranjo Lopez et al. 2019).

Hispaniola is one of the less-studied for mayflies of the four islands. Two leptophlebiid species are currently known, *Hagenulus eatoni* Banks, 1924 and *Careospina annulata* Peters, 1971. The former is only known by the type series, which consists of 11 pinned females collected in 1912 at Diquini, Haiti and the latter is known only by the holotype, a pinned male imago collected in 1934 from Mont La Hotte, Haiti. Kluge (1994) considered the systematic position of *C. annulata* as unclear, pending the description of the nymph to fix its status.

Here, I report the presence of the genus *Neohagenulus* on Hispaniola, from the Dominican Republic, based on nymphs which are described as a new species. This is the first species of this genus known outside of Puerto Rico.

Material and methods

The specimens have been collected in the Dominican Republic during a field trip in summer 2021.

Nymphs were preserved in 100% ethanol. Nymphal habitus were photographed using a Canon EOS 6D camera and the Visionary Digital Passport imaging system (formerly available and distributed by Dun Inc., Virginia) and processed with Adobe Photoshop Lightroom and Helicon Focus version 5.3.

Two nymphs were dissected in Cellosolve (2-Ethoxyethanol) with subsequent embedding in Euparal medium and mounting on slides. Fore- and hind wingpads of a submature female nymph were dissected and subimaginal wings examined. Microscopic pictures were taken using an Olympus BX51 microscope coupled with an Olympus SC50 camera; photographs were enhanced with Olympus Stream Basic 2.3.2 stacking software and Adobe Photoshop version 21.2.2.

The material is deposited in the collections of the Museum of zoology, Lausanne (MZL) and the Museo National de Historia Natural "Prof. Eugenio de Jesús Marcano", Santo Domingo, Dominican Republic (MNHNSD).

Results

***Neohagenulus hodeceki* sp. nov.**
http://zoobank.org/FDBF727E-87FD-4120-9E62-BDBCECBA8659

Material. ***Holotype***. Dominican Republic male nymph in ethanol, La Vega Province, Valle Nuevo National Park, 18°52'01"N, 70°34'44"W, 12 Jul. 2021, ca 900 m a.s.l., J. Hodeček leg. (GBIFCH00834690) [MZL] ***Paratypes***. 5 nymphs in ethanol [MNHNSD] (MNHNSD 11.05 – MNHNSD 11.09), 12 nymphs in ethanol (GBIF-

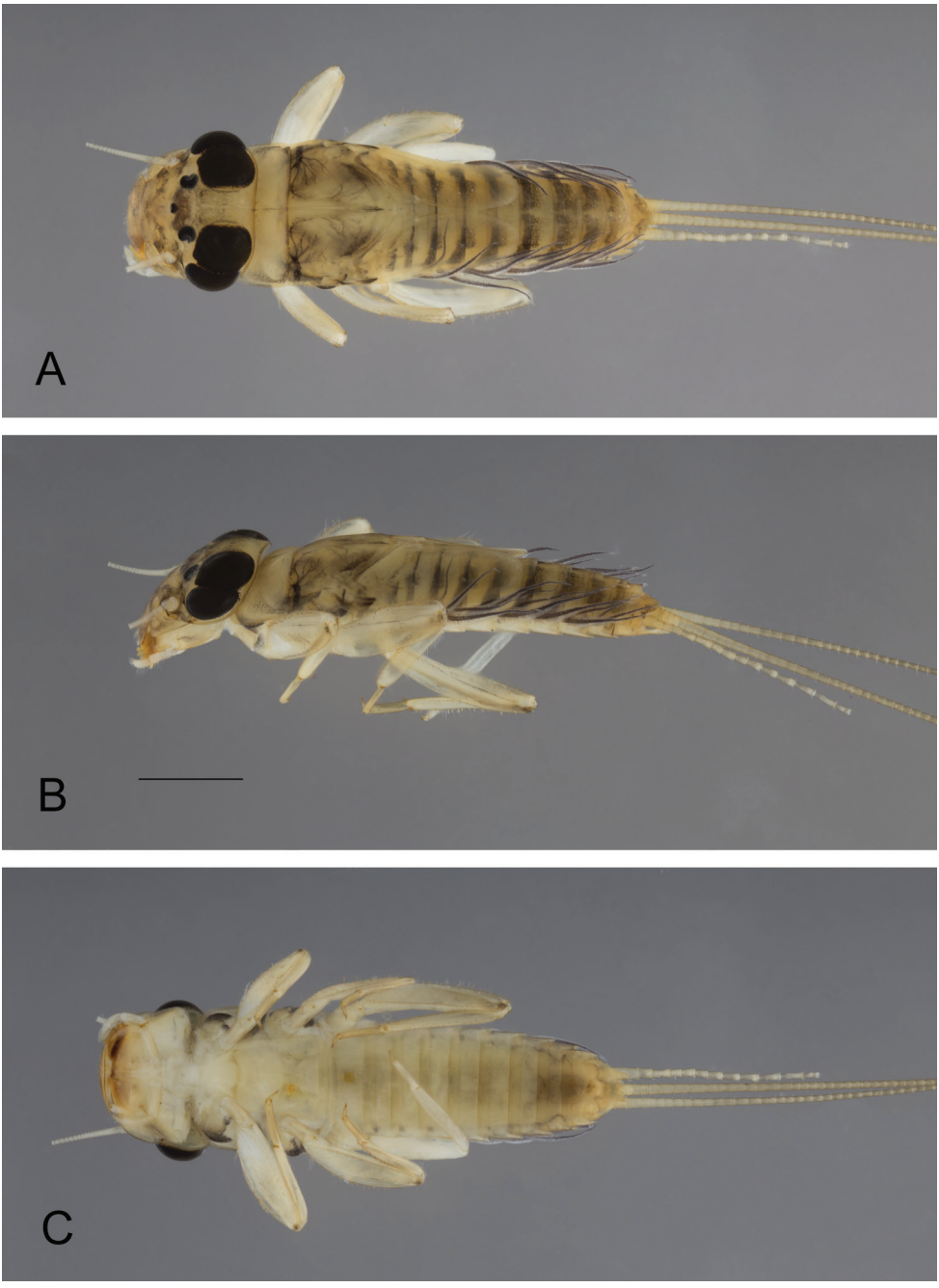

Figure 1. *Neohagenulus hodeceki* sp. nov., nymphal habitus **A** dorsal view **B** lateral view **C** ventral view. Scale bar: 1 mm.

CH00834691), 2 female nymphs on slide (GBIFCH00604114-GBIFCH00604115), same data as holotype. [MZL]

Other material. Dominican Republic 1 nymph, La Vega Province, Armando Bermúdez National Park, 19°04'02"N 70°51'50.7"W, ca 1100 m a.s.l., 15 Jul. 2021, J. Hodeček leg. (GBIFCH00834694) [MZL]

Etymology. The new species is named after its collector, Dr Jiří Hodeček (CHUV, Lausanne), forensic entomologist.

Description. ***Nymph*** (not mature): body length up to 7 mm, cerci slightly longer than body length, paracercus longer than cerci.

Coloration. Cuticular coloration evenly light brown on whole body; hypodermal coloration as in Fig 1: head washed with grey, darker between ocelli, convex band between antennae, upper portion of male eyes black; prothorax greyish laterally and on posterior margin, mesothorax with blackish tracheation laterally, with maculae posteriorly; legs light brown, apex of femora with blackish dots, tarsi darker than tibiae; abdominal tergites I–V light brown with posterior black band larger laterally and with two antero-submedian maculae, tergites VI–VIII greyish brown, posterior margin and sagittal line light brown, tergite IX paler than previous ones, tergite X medium brown; sternites uniformly light brown, last two darker; cerci uniformly light brown.

Mouthparts. Labrum (Fig 2A) larger than clypeus, about two times broader than long, dorsally with two rows of long and thin setae, proximal row very close to distal margin, tuft of long setae laterally, more abundant at anterolateral corner, ventrally with two submedian fields of long and stout setae, antero-median emargination smooth, with four equally sized denticles (Fig 2B). Mandibles outer margin regularly convex, with tuft of small and thin setae in middle, with outer and inner incisors composed of three teeth, outer margins slightly serrated, prostheca with stout and long process and well-developed tuft of thin setae (Fig 2C). Maxillary palp three-segmented (Fig 2D), second segment ca 1.25× length of segment 1, segment 3 conical, outer margin concave near apex, ca 1.5× longer than wide and 0.50−0.60× length of segment two, crown of the galea-lacinia with subapical setae arranged in two rows of 8−9 laterally and 11−12 centrally. Hypopharynx with lingua convex, with deep incision distally, lateral processes well developed, but shorter than lingua, slightly curved inwards; superlinguae laterally expanded, distal margin covered with long setae up to the tip (Fig 3B). Labium (Fig 3A) with narrow glossae, with stout setae at apex, paraglossae rhomboid, outer margin almost straight, with numerous long setae laterally and apically; labial palp three-segmented, first and second segments subequal in length, or segment two slightly longer, third segment ca 0.35−0.40× length of segment two, 2.5−2.6× longer than wide.

Thorax. Forelegs with femora ca 2.5× longer than wide, outer margin with row of very long and thin setae, together with apical and subapical rows of long, stout and pointed setae, inner margin with subapical row of long and stout setae (shorter than those on the outer margin), with small stout setae in proximal part, dorsal surface with scattered small to medium-sized stout setae; tibiae shorter than femora, with long and thin setae on outer margin, inner margin with several rows of stout small to medium-sized setae; tarsi only with thin setae, claw moderately hooked, with a row of 12−14 teeth, increasing in size distally (Fig 3C). Midlegs similar to forelegs, except

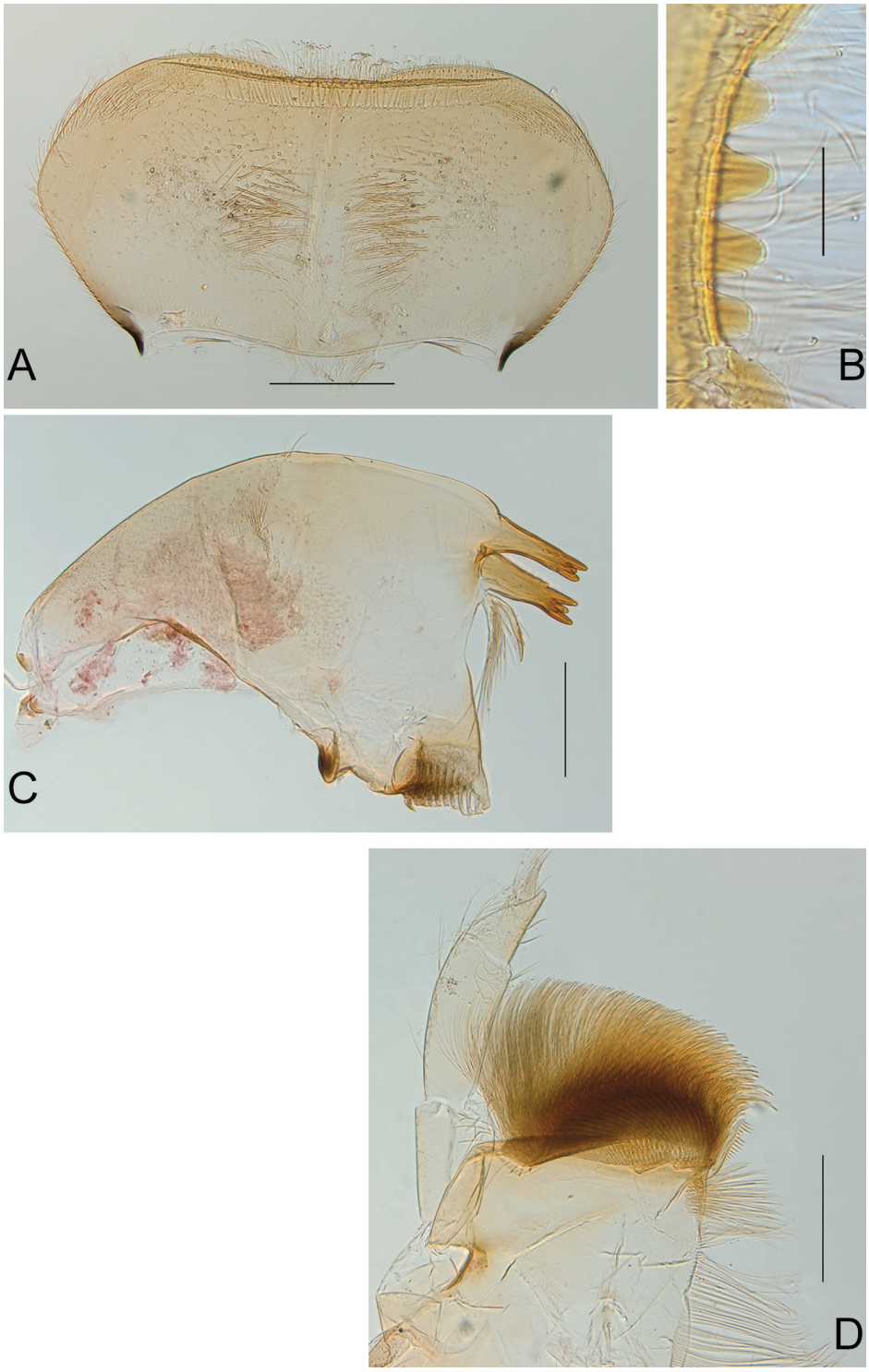

Figure 2. *Neohagenulus hodeceki* sp. nov. mouthparts **A** labrum in dorsal view **B** antero-median emargination of the labrum **C** left mandible **D** maxilla. Scale bars: 0.2 mm (**A**, **C**, **D**); 0.05 mm (**B**).

inner margin of tibiae with fewer stout setae. Hindlegs with femora almost 3× longer than wide, similar to forelegs in ornamentation except outer margin with shorter and less numerous thin setae; hind tibia shorter than femora, with outer margin covered with long and thin setae, together with short and medium-sized stout and pointed setae, inner margin with marginal row of short and submarginal row of longer stout setae (Fig 3D). Fore wingpad markedly different between male and female nymphs: in males, evenly brown with veins hardly visible (Fig 1A), in females with longitudinal veins well marked, crossveins flanked with dark brown bands (Fig 4A); in both sexes, base of wingpads tinted with brown in costal, subcostal and anal fields. Hind wingpad very small, tinted with greyish brown at base, with costal process large and slightly pointed, almost as long as the rounded apex of wing (Fig 4B).

Abdomen. Posterior margin of tergites I–III smooth, of segments IV–VIII with small needle-like denticles, slightly increasing in size posteriorly, tergites IX and X with triangular denticles; posterior margin of sternite IX concave in the middle (Fig. 4C); posterolateral projections on abdominal segments II–IX, increasing in size posteriorly (Fig. 4C); gills present on segments I–VII alike, each gill deeply forked almost at base (Fig. 4D) with purplish longitudinal and lateral tracheations, size of gills in decreasing order: II=V>III>IV=VI>I>VII. Cerci with whorls of small setae at the end of each segment.

Male imago, female imago, eggs unknown.

Discussion

The new species is attributed to the genus *Neohagenulus* mainly based on the posterolateral projections present on abdominal segments II–IX. In the redescription proposed by Peters (1971), these projections are present on segments III–IX for Puerto Rican species; this is the main character to separate nymphs of *Neohagenulus* from those of *Careospina*, where these projections are located on segments (V) VI–IX. Another closely related (sub)genus is *Borinquena*, as defined by Kluge (1994), which possesses an elongated third segment of labial palp, longer than half the length of second segment, which is not the case in *N. hodeceki* (about one-third the length of second segment).

Another consideration for placement of the new species in the genus *Neohagenulus* is the size of the costal projection on the hind wingpad, suggesting that the hind wing of this species possesses a well-developed and long process. In *Careospina*, the costal process is present and normally developed (Peters 1971: fig 29), whereas it is hypertrophied in *Neohagenulus* (Peters 1971: figs 34–42), reaching the apex of the wing. This character can also be found in *Borinquena* (Kluge 1994: fig 53). All in all, morphological differences between nymphs of *Borinquena*, *Careospina* and *Neohagenulus* are tiny; in *N. hodeceki*, the length of the second segment of the maxillary palp is about 1.25× the length of the first segment, a character which matches the diagnosis of *Careospina* rather than that of *Neohagenulus*, where both segments are of equal size. These three genera seem easier to separate at the male imaginal stage, based on the shape of the hind wing, forceps and penes (Peters 1971; Kluge 1994).

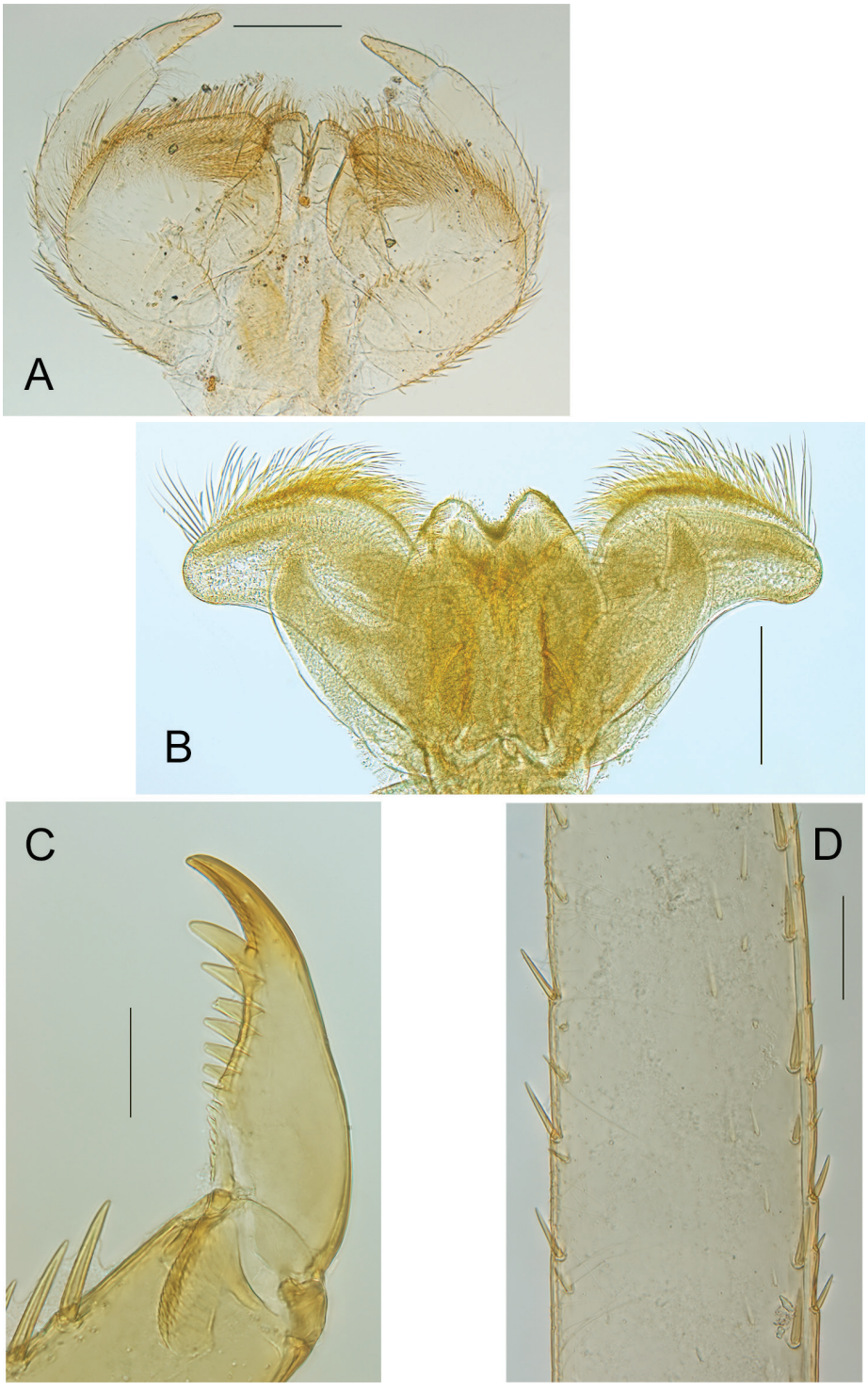

Figure 3. *Neohagenulus hodeceki* sp. nov. mouthparts and legs **A** labium **B** hypopharynx **C** claw **D** detail of hind tibia. Scale bars: 0.2 mm (**A–C**); 0.1 mm (**D**)

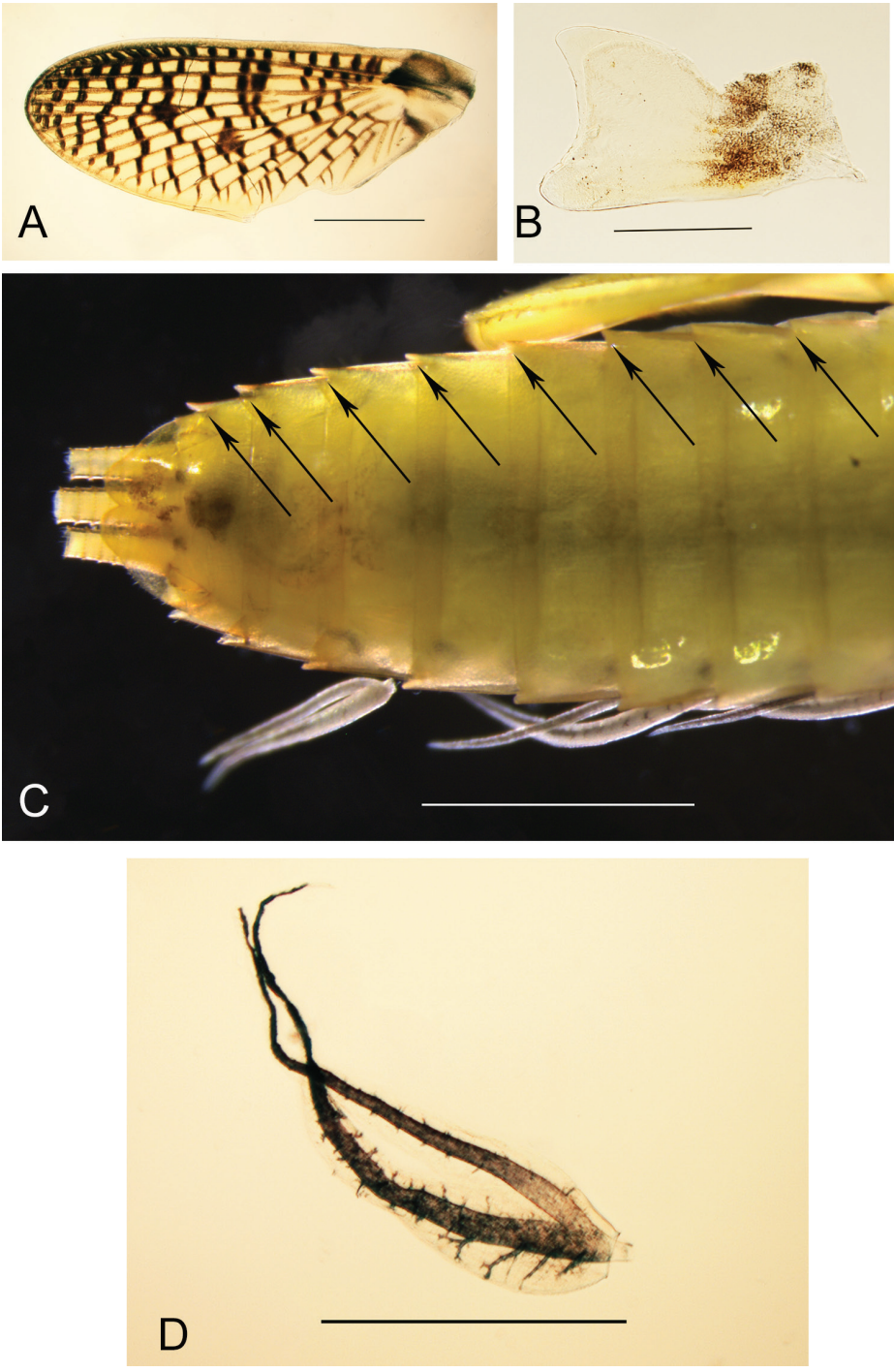

Figure 4. *Neohagenulus hodeceki* sp. nov. thorax and abdomen. **A** female fore wingpad **B** female hind wingpad (same specimen) **C** abdomen in ventral view (arrows indicate posterolateral projections on segments II–IX) **D** gill IV. Scale bars: 0.5 mm (**A**, **D**), 0.2 mm (**B**), 1 mm (**C**).

Despite of this, *N. hodeceki* can be separated from species of *Careospina* (all known from Cuba) and *Borinquena* (Puerto Rico and Cuba) at the nymphal stage by the number of posterolateral projections on the abdomen and from species of *Neohagenulus* (all known from Puerto Rico), by the size of the second segment of the maxillary palp.

A remarkable character is the difference in the fore wingpad coloration between male and female nymphs; this dimorphism is not reported within *Neohagenulus* or *Careospina* species, although females often have costal and subcostal fields of forewing more tinted than in males. This difference is nevertheless testified for the species *Hagenulus jamaicensis* Peters, 1971 where male forewing is hyaline except some crossveins "surrounded with brown clouds" at the tip of the wing, whereas the female forewing exhibits almost all crossveins "surrounded with dark brown clouds" (Peters 1971: figs 58, 61).

Among the tribe Hagenulini (sensu Monjardim et al. 2020) and according to Kluge (1994), *Hagenulus* sensu lato, or Hagenulus/fg2, is composed of the following taxa: *Borinquena*, *Careospina*, *Hagenulopsis*, *Hagenulus s.s.*, *Neohagenulus*, *Poecilophlebia* and *Turquinophlebia*, which form a monophyletic lineage. The genus *Borinquena* is reported from Hispaniola only by fossil records from Dominican amber, together with the extinct genus *Hagenulites* Staniczek, 2003 (Staniczek 2003; Staniczek et al. 2017).

The fact that the genus *Borinquena* is known from Puerto Rico and Cuba by five extant species and from Hispaniola by four extinct species indicates a larger distribution of the genus in the Miocene. Due to the lack of prospection on Hispaniola, it is therefore possible that the genus is still present but overlooked. In any case, a better understanding of the diversity of the tribe Hagenulini on Hispaniola is required before any biogeographical or phylogeographic attempt.

Neohagenulus hodeceki is the third extant leptophlebiid species reported from Hispaniola, the first one for almost a century and the first one known at the nymphal stage. Although I fully agree that the knowledge of the imaginal stages is of prime importance, I think it is noteworthy to formally mention and describe this taxon due to the scarcity of data on the leptophlebiids of Hispaniola. Considering the diversity reported for fishes (Rodriguez-Silva and Schlupp 2021) and caddisflies (Flint and Sikora 2004) for instance, we might deduct that mayfly diversity in Hispaniola is greatly underestimated.

Acknowledgements

My sincere thanks to Jiří Hodeček (CHUV, Lausanne) and Jiří Pirkl for collecting these interesting specimens. Dr Hodeček's fieldwork was made possible by a collecting permit and an export permit (VAPB-08862) issued by the Ministry of Environment and Natural resources, Santo Domingo, which is greatly acknowledged. Gabriel de los Santos (MNHNSD) is thanked for his logistic support. I appreciated the careful review and suggestions made by Arnold Staniczek (SMNS, Stuttgart) and Luke M. Jacobus (IUPC, Columbus).

References

Flint Jr OS, Sykora JL (2004) Caddisflies of Hispaniola, with special reference to the Dominican Republic (Insecta: Trichoptera). Annals of Carnegie Museum 73(1): 1–60.

Kluge NJ (1994) A revision of Leptophlebiidae of Cuba (Ephemeroptera). Zoosystematica Rossica 2[1993]: 247–285.

Monjardim M, Paresque R, Salles FF (2020) Phylogeny and classification of Leptophlebiidae (Ephemeroptera) with an emphasis on Neotropical fauna. Systematic Entomology 45: 415–429. https://doi.org/10.1111/syen.12402

Naranjo López C, Peters JG (2016) New records of Ephemeroptera (Insecta) from Jamaica and the Dominican Republic. In: Yoshimura M, Takemon Y (Eds) International Progress in Ephemeroptera and Plecoptera Research (13th International Conference on Ephemeroptera and 17th International Symposium on Plecoptera). Biology of Inland Waters Supplement 3: 83–91.

Naranjo López C, Peters JG, López del Castillo P (2019) Ephemeroptera (Insecta) in Cuba. Insecta Mundi 736: 1–52.

Peters WL (1971) A revision of the Leptophlebiidae of West Indies (Ephemeroptera). Smithsonian Contributions to Zoology 62: 1–46. https://doi.org/10.5479/si.00810282.62

Rodriguez-Silva R, Schlupp I (2021) Biogeography of the West Indies: a complex scenario for species radiations in terrestrial and aquatic habitats. Ecology and Evolution 11: 2416–2430. https://doi.org/10.1002/ece3.7236

Staniczek AH (2003) New fossil mayflies from Dominican amber (Insecta: Ephemeroptera: Leptophlebiidae: Atalophlebiinae). Stuttgarter Beiträge zur Naturkunde, Serie B (Geologie und Paläontologie) 341: 1–22.

Staniczek AH, Godunko RJ, Krzeminski W (2017) A new fossil mayfly species of the genus *Borinquena* Traver, 1938 (Ephemeroptera: Leptophlebiidae: Atalophlebiinae) from Miocene Dominican Amber. Annales Zoologici 67: 113–119. https://doi.org/10.3161/00034541ANZ2017.67.1.013

ZooKeys 1070: 51–72 (2021)
doi: 10.3897/zookeys.1070.70531
https://zookeys.pensoft.net

RESEARCH ARTICLE

A peer-reviewed open-access journal
ZooKeys
Launched to accelerate biodiversity research

Two new species of *Byrrhinus* Motschulsky, 1858 (Coleoptera, Limnichidae, Limnichinae) from Negros, Philippines

Emmanuel D. Delocado[1], Hendrik Freitag[1]

1 *Ateneo Biodiversity Research Laboratory, Department of Biology, School of Science and Engineering, Ateneo de Manila University, Quezon City, 1108 Philippines*

Corresponding author: Emmanuel D. Delocado (edelocado@ateneo.edu)

Academic editor: Christopher Majka | Received 23 June 2021 | Accepted 22 September 2021 | Published 10 November 2021

http://zoobank.org/F8729B74-D604-41C2-8173-6634E4330CF6

Citation: Delocado ED, Freitag H (2021) Two new species of *Byrrhinus* Motschulsky, 1858 (Coleoptera, Limnichidae, Limnichinae) from Negros, Philippines. ZooKeys 1070: 51–72. https://doi.org/10.3897/zookeys.1070.70531

Abstract

Two new species of Limnichidae beetles, *Byrrhinus negrosensis* **sp. nov.** and *Byrrhinus villarini* **sp. nov.**, are described from the Island of Negros in the Philippines. The adult specimens of the new species can be differentiated by patterns of body punctation, colour and orientation of elytral pubescence, posterolateral angle of pronotum, tarsomere length ratio and aedeagal form. Two clades, representing the two new species, were retrieved in the Maximum Likelihood gene tree using the 3'-end of the *COI* gene. Maximum genetic divergence within *B. negrosensis* sp. nov. and *B. villarini* sp. nov. were recorded to be 2.3% and 1.3%, respectively, while the mean interspecific divergence between the two new species was 19.7%. Morphological descriptions, digital photographs and *COI* sequences were provided for the two species. The state of knowledge of *Byrrhinus* is reviewed and an updated Philippine checklist is provided. By coupling morphological and molecular data, this paper provides the first additional new species of Philippine *Byrrhinus* in the last 28 years.

Keywords

Biodiversity assessment, COI, integrative taxonomy, minute marsh-loving beetle, Negros Island, new species

Introduction

Byrrhinus Motschulsky, 1858 is the most speciose limnichid genus with currently at least 87 species (Yoshitomi, unpublished data). Approximately 20% of known limnichid species belong to the genus *Byrrhinus*. The distribution of the genus is pantropical, but it is lacking or not yet recorded in some regions (Hernando and Ribera 2016). Currently, *Byrrhinus* is one of the two genera recorded in both the Old and New Worlds, although notably absent in the Nearctic and Palearctic (Wooldridge 1987).

The distinguishing features of *Byrrhinus* include its elongate oval habitus and deeply bisinuate pronotum and elytral base (Wooldridge 1987), as well as having a spiculum which can be dismantled from the male aedeagus (Hernando and Ribera 2014b). Additionally, *Byrrhinus* species generally possess a long yellowish pubescence and a densely punctured pronotum and metasternum. Like most members of Limnichidae, larval and pupal stages of *Byrrhinus* are undescribed. The internal anatomy was documented by Hinton (1939).

The genus was originally erected in 1858 to contain *Byrrhinus latus* Motschulsky, 1858 from India. Later on, Blackburn (1896), Sharp (1902) and Pic (1922, 1923) described species from Australia, Africa and America and classified them in different genera, including *Eulimnichus* Casey, 1889, "*Notiocyphon* Blackburn, 1896", "*Cyphonichus* Sharp, 1902", "*Byrrhininus* Pic, 1922" and *"Pelocherops* Pic, 1923" with the last four being synonymised with *Byrrhinus*. Some of the species originally described as "*Cyphonichus*", however, belong instead to genus *Paralimnichus* Deléve, 1973. Valuable taxonomic revisions on the genus were undertaken by Champion (1923), Deléve (1973) and Wooldridge (1987) who provided re-descriptions and a key to New World species. Subgenera and species groupings were erected by Satô (1965) and Deléve (1968), respectively, though these were not widely used in more recent publications. The most recent contribution to the genus was a new species from Angola (Matsumoto 2021).

Currently, five *Byrrhinus* species have been recorded in the Philippines (Deléve 1973; Wooldridge 1993; Freitag et al. 2016), namely, *B. convexus* (Blackburn, 1896), *B. ferax* Wooldridge, 1993, *B. punctatus* (Pic, 1922), *B. subtestaceus* Pic, 1923 and *B. tarawakanus* Deléve, 1973. A key to Philippine species for *Byrrhinus* was provided by Wooldridge (1993). Of the five species, two are not endemic to the country, namely *B. convexus* which was recorded also from Australia and *B. ferax* which was also recorded from Malaysia. Currently, the known distribution of *Byrrhinus* in the Philippines is confined to the Islands of Luzon, Mindoro, Mindanao, Palawan and Tawi-Tawi with many islands being under-surveyed. In fact, Freitag et al. (2016) note that the currently known diversity of aquatic and riparian Coleoptera in the Philippines is less than half of the totally expected number of species which is partly due to very uneven sampling efforts throughout the Archipelago.

Species identification in limnichid beetles is challenging due to their cryptic nature and subtle interspecific phenetic differences. Congeneric species are typically differentiated through details in genitalia, pubescence and punctation. Thus, to accelerate species discovery of the almost cryptic *Byrrhinus* fauna in a megadiverse locality, this study uses DNA

sequences to complement morphological descriptions. This approach, referred to as integrative taxonomy (Dayrat 2005; Will et al. 2005), has been performed in several aquatic and riparian insect groups to fast-track biodiversity documentation (Tänzler et al. 2014; Riedel and Tänzler 2016; Garces et al. 2020; Kodada et al. 2020; Sabordo et al. 2020).

This contribution presents two new species, *Byrrhinus negrosensis* sp. nov. and *Byrrhinus villarini* sp. nov., as supported by morphological and genetic data. Both species were collected from the Island of Negros in the central Philippine island group of Visayas. Recent extensive and collaborative sampling by the Ateneo Biodiversity Research Laboratory on this Island has led to the discovery of new aquatic insect species (Garces et al. 2020; Kaltenbach et al. 2020a, 2020b; Komarek and Freitag 2020; Sabordo et al. 2020).

Materials and methods

Taxon sampling

The organismic material used in this study was primarily retrieved in the scope of the School of Science and Engineering Industry 4.0 Research Fund (SI4-013) project on the freshwater macroinvertebrate diversity inventory by the Ateneo Biodiversity Research Laboratory of the Ateneo de Manila University, Quezon City, Philippines (AdMU). A light trap was set on riverbanks between 6:00 pm to 8:00 pm. Insects attracted to the black light were manually collected and stored in vials with 95% ethanol. Specimens were stored in a freezer (–20 °C) prior to their examination. Collections of the Ateneo Biodiversity Research Laboratory from previous field works of the second author were also examined and used for the molecular analysis of this study.

DNA extraction and sequencing

Isolation of DNA was performed using the Qiagen DNeasy kit (Qiagen, Hilden, Germany) following the instructions of the manufacturer for animal tissues (Qiagen 2006). For all successful extractions, amplification of the 3'-end of cytochrome *c* oxidase subunit I (*COI-3'*) gene by polymerase chain reaction (PCR) was done using the primer pair Jerry (5'-CAACATTTATTTTGATTTTTTGG-3') and Pat (5'-TCCAATGCACTAATCTGCCATATTA-3') (Simon et al. 1994). The PCR temperature progression was set as 180 s at 94 °C; 35 cycles of 30 s at 94 °C, 60 s at 50 °C, 90 s at 72 °C; 300 s at 72 °C. Cleaning and sequencing of successful PCR products was done by Macrogen Europe.

Phylogenetic analysis

The sequences of both complementary strands were traced manually using CHROMAS (Goodstadt and Ponting 2001) and their consensus sequences were generated using the software BioEdit v.7.2.5 (Hall 1999). Their ends were trimmed to generate

Table 1. GenBank and BOLD accession numbers of *COI-3'* mtDNA sequences of specimens used in this analysis.

Species	Specimen code	Locality	Sex	GenBank	BOLD	GenSeq nomenclature
Byrrhinus negrosensis sp. nov.	EDD116	Negros	female	OK316812	COLPH052-21	genseq-2 COI
	EDD119	Negros	male	OK316811	COLPH053-21	genseq-2 COI
	EDD122	Negros	male	OK316808	COLPH054-21	genseq-1 COI
	EDD123	Negros	male	OK316803	COLPH055-21	genseq-2 COI
	EDD127	Negros	male	OK316809	COLPH056-21	genseq-2 COI
	EDD270	Negros	male	OK316807	COLPH057-21	genseq-2 COI
Byrrhinus villarini sp. nov.	EDD113	Negros	female	OK316817	COLPH058-21	genseq-2 COI
	EDD114	Negros	male	OK316815	COLPH059-21	genseq-2 COI
	EDD115	Negros	male	OK316804	COLPH060-21	genseq-2 COI
	EDD121	Negros	male	OK316813	COLPH061-21	genseq-1 COI
	EDD124	Negros	male	OK316818	COLPH062-21	genseq-2 COI
	EDD126	Negros	male	OK316805	COLPH063-21	genseq-2 COI
Byrrhinus ferax Wooldridge, 1993	EDD067	Mindoro	male	OK316810	COLPH064-21	genseq-4 COI
Byrrhinus sp. A	EDD057	Palawan	male	OK316816	COLPH065-21	genseq-4 COI
Byrrhinus sp. B	EDD105	Luzon	male	OK316806	COLPH066-21	genseq-4 COI
Byrrhinus sp. C	EDD112	Mindanao	female	OK316814	COLPH067-21	genseq-4 COI
Byrrhinus sp.	UPOL RK0663	Cameroon		KX092882	GBCL40978-19	
Byrrhinus sp.	UPOL RK0664	Indonesia		KX092889	GBCL40979-19	
Byrrhinus sp.	UPOL RK0727	Malaysia		KX092888	GBCL40980-19	
Limnichus sp. (outgroup)	UPOL RK0666	Indonesia		KX092883	GBCL40986-19	
Limnichus sp. (outgroup)	UPOL RK0725	Malaysia		KX092886	GBCL40987-19	

a complete matrix of all sequences used. All publicly available *COI-3'* sequences (Kundrata et al. 2017) for *Byrrhinus*, namely from Indonesia, Malaysia and Cameroon, as well as for *Limnichus* spp., were downloaded from NCBI BLAST (Altschul et al. 1990). *Limnichus*, also a member of subfamily Limnichinae, was chosen to serve as outgroup of the phylogenetic analysis (Table 1). All new and reference sequences were aligned using MUSCLE 3.7 (Edgar 2004). Sequences generated from this study were labelled as EDD### and were submitted to the Barcode of Life Database (BOLD; https://www.doi.org/10.5883/DS-BYRRHNEG). Table 1 provides the BOLD and NCBI GenBank accession numbers.

Generation of a Maximum Likelihood (ML) tree with bootstrap analysis for 1000 replicates, as well as genetic distance computation using Kimura-2-paramter (K2P) model (Kimura 1980), was performed in MEGA 7 (Kumar et al. 2016). The ML tree was constructed using the best-fitted substitution model which was GTR+G+I (lnL = -3885.57). Visualisation of relationships amongst less divergent sequences for new species was done by constructing a TCS haplotype network (Clement et al. 2000) through statistical parsimony analysis as implemented in PopArt (Leigh and Bryant 2015).

Morphological analysis

External morphology was examined by using an OLYMPUS SZ61 stereomicroscope (Olympus, Tokyo, Japan). The terminal abdominal portion of the specimens was dissected and treated overnight with lactic acid. The male aedeagi were then observed

under an OLYMPUS CX21 compound microscope (Olympus, Tokyo, Japan). The specimen and its genitalia were glued on to entomologic paper for vouchering purposes. Photographs of vouchers were taken using a Canon EOS 6D with a macro lens and were stacked in Helicon Focus Pro v.7.6.1 (Helicon Soft, Kharkiv, Ukraine) and further processed using Adobe Photoshop CS6 (Adobe, San Jose, CA, USA). The aedeagi were digitally drawn over microscopic photograph underlays using Inkscape (GNU GPL, Boston, MA, USA).

Congeneric vouchers and type material at the Natural History Museum, Vienna, Austria (**NMW**) and Institute of Evolutionary Biology, Barcelona, Spain (**IBE**) were also examined.

Terminologies of the species' descriptions follow the Limnichidae chapter of the Handbook of Zoology/Coloeptera (Hernando and Ribera 2016). Type specimens of the new species were deposited at the Philippine National Museum of Natural History, Manila, Philippines (**PNM**), Ateneo de Manila University, Quezon City, Philippines (**AdMU**) and Museum für Naturkunde Berlin, Germany (**ZMB**). Holotype labels were quoted verbatim from specimen labels with backslashes (\) indicating line break.

The following abbreviations were used:

a.s.l.	above sea level;	**EW**	elytra width;	**TL**	total length.
BS	bootstrap value;	**PL**	pronotum length;		
EL	elytra length;	**PW**	pronotum width;		

Results

DNA sequence analysis

The alignment of *COI-3'* sequences is composed of 723 bases with 221 parsimony-informative sites and 281 variable sites. No sequence in the matrix contains gaps, insertion, deletions or ambiguous sites. Sequences of *Byrrhinus* have low G-C concentration (16.5–20.2% C, 15.6–16.2% G).

Two clades were retrieved from the *Byrrhinus* specimens from Negros (Fig. 1), with each reciprocally monophyletic clade having representative specimens from two rivers about 200 km apart. The first clade, described here as *Byrrhinus negrosensis* sp. nov., is strongly supported (BS = 100, Fig. 1) with an intraspecific distance ranging from 0 to 2.3% with an average of 1.3% (Table 2; Suppl. material 1: Table S1). Meanwhile, the second clade, described here as *Byrrhinus villarini* sp. nov., is also strongly supported (BS = 100), but the maximum intraspecific distance (1.3%) is smaller than that in *B. negrosensis* sp. nov. The clade formed by *B. villarini* sp. nov. and *Byrrhinus* sp. from Malaysia appears to be strongly supported (BS = 100), but the genetic distance between the two populations averages at 5.9% (Table 2). The interspecific distance between the two Negros species ranges from 19.0 to 20.7%

Table 2. Mean genetic distance of *Byrrhinus* specimens, based on partial *COI-3'* sequences (in %).

#	Identity	*n*	1	2	3	4	5	6	7	8	9
1	*Byrrhinus negrosensis* sp. nov.	6	1.3								
2	*Byrrhinus villarini* sp. nov.	6	19.7	0.4							
3	*Byrrhinus ferax* Wooldridge, 1993	1	13.2	13.8	–						
4	*Byrrhinus* sp. A	1	19.8	16.2	19.5	–					
5	*Byrrhinus* sp. B	1	16.6	15.6	19.4	17.7	–				
6	*Byrrhinus* sp. C	1	18.2	17.5	21.4	10.6	19.6	–			
7	*Byrrhinus* sp. (Malaysia)	1	20.0	5.8	17.0	16.4	17.0	13.7	–		
8	*Byrrhinus* sp. (Indonesia)	1	21.6	20.0	21.7	22.2	22.4	17.9	20.2	–	
9	*Byrrhinus* sp. (Cameroon)	1	25.16	28.2	28.6	24.7	25.0	26.5	28.9	23.4	–

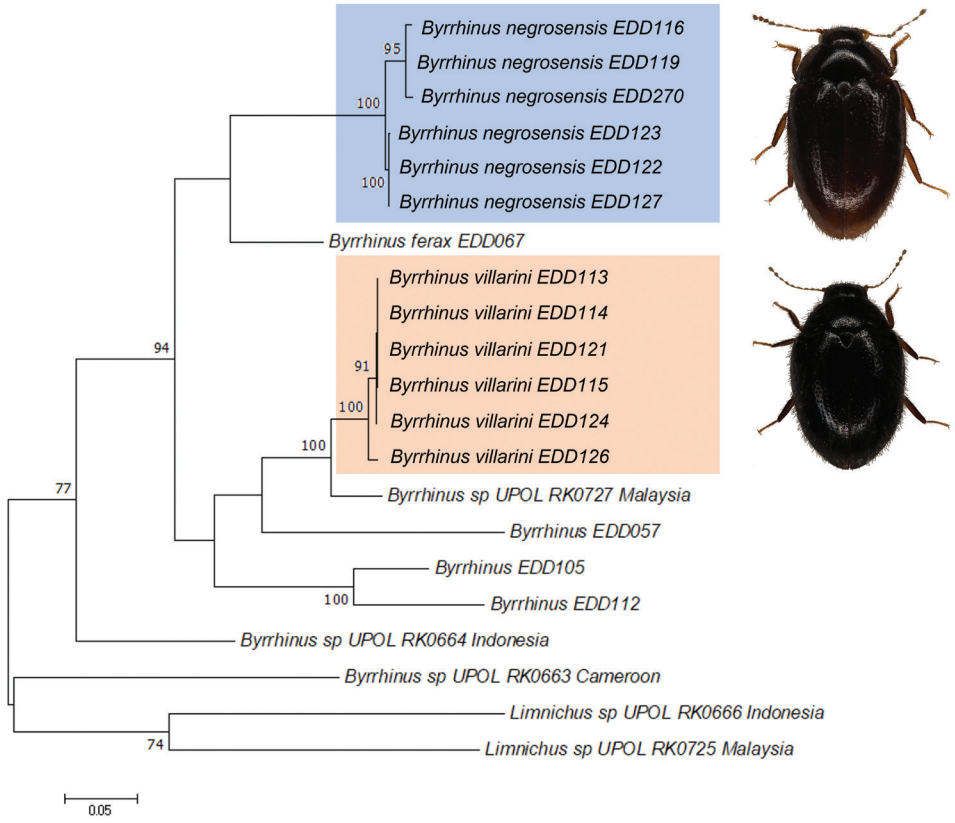

Figure 1. Maximum Likelihood gene tree using partial *COI-3',* based on GTR+G+I parameter, 1000 bootstraps. Only bootstrap support values > 70% are indicated.

(mean = 19.7; Suppl. material 1: Table S1). With the exception of *B. villarini* sp. nov. and the sequence from Malaysia, the interspecific distance of the two new species from Negros with other Philippine *Byrrhinus* (12.8–20.0%) and publicly available sequences of non-Philippine *Byrrhinus* (19.5–29.0%) ranges from moderately high to high.

Taxonomy

Family Limnichidae Erichson, 1847
Subfamily Limnichinae Erichson, 1847
Genus *Byrrhinus* Motschulsky, 1858

***Byrrhinus negrosensis* sp. nov.**
http://zoobank.org/95FDB6E9-6691-44BA-895A-D42954CA7086
Figures 2, 4, 5

Type locality. Philippines • Negros Island, Negros Oriental, Valencia, Casaroro River, in secondary vegetation; ca. 09°18'N, 123°14'E; ca.150 m a.s.l.

Type material. ***Holotype*:** Philippines • ♂ (PNM: EDD122), "PHIL: Negros Or., Valencia, \ Casaroro River, downstr., sec.veg.; \ ca. 09°18'N; 123°14'E; ca.150 m a.s.l.; \ 01 Sep. 2019, leg. Garces & Pelingen (655)L"; GenBank: OK316808; BOLD: COLPH054-21; EDD122, habitus and terminal parts of abdomen including genitalia glued separately on to entomological card. ***Paratypes*:** Philippines • 3♂♂ (ADMU: EDD123, EDD127): same data as holotype; GenBank: OK316803, OK316809; BOLD: COLPH055-21, COLPH056-21 • 3♂♂, 3♀♀: (ADMU: EDD116, EDD119, EDD270; PNM; ZMB) "PHIL: Negros Occ., Murcia, \ Pandanon River, sec.veg.; \ ca. 10°34'54"N; 123°10'30"E; ca. 440 m a.s.l.; \ 01 May 2019, leg. Freitag

Figures 2, 3. Habitus of new *Byrrhinus* species **2** *Byrrhinus negrosensis* sp. nov. **3** *Byrrhinus villarini* sp. nov. Scale bar: 1 mm.

et al. (650)L"; GenBank: OK316807, OK316811, OK316812; BOLD: COLPH052-21, COLPH053-21, COLPH057-21.

Description. ***Body*****:** (Fig. 2) elongate-oval, TL = 3.2 mm (2.9–4.1 mm), EW = 2.1 mm (1.8–2.3 mm), widest behind mid-leg; dorsal surface brown to dark brown; body appendages slightly paler than body, moderately densely and evenly covered with yellow–brown to brown, fine, quite long, mostly erect pubescence; antennae yellow-brown to brown; femora and tibiae brown; tarsi brown.

Head**:** obscurely rugulose; broadly laminate over eyes; margins of frons grooved over eyes; sides of frons with deep and well–marked pit-like depressions. Punctation minute, sparse, slightly coarser near epistomal suture. Pubescence dense and erect in anterior regions, sparse and recumbent posteriad. Eyes slightly convex, visible from above; upper margin of eyes strongly bordered, margin anteriorly almost reaching insertion of antennae, extending posterior of eyes although weaker. Surface of head posterior to eyes flat, without depressions or fossae; surface with fine and sparse punctation, denser and coarser on clypeus; surface between punctures smooth and shiny. Antennae moniliform, strongly pubescent; pedicel oblong, brown, slightly darker than adjacent antennomeres; antennomeres longer than wide, brown, darker distally, terminal antennomeres asymmetrical and darker than pedicel; pubescence brown, of two series: first series composed of one to two pairs of long and erect pubescence per antennomere, about as long as antennomere and second series composed of denser, shorter, paler, recumbent pubescence.

Pronotum**:** transverse, slightly paler on sides than on disc, distinctly wider at base; anterior margin of pronotum slightly concave, but almost straight between eyes, without crenulations, bordered; lateral margins only slightly arched, posterolateral angle 75–80°, with prominent borders; posterior margin with a distinct double sinuation; PL/PW = 0.42 (0.40–0.43); PW/PL = 2.40 (2.30–2.51). Punctation dense, minute and shallowly impressed; punctures larger than that of the head, denser at median line and posterior margins, sparse near suture and anteriad; surface between punctures rugose. Pubescence similar to the erect series of the head, denser on the anterior one-third of the lateral margin, evenly spaced on the rest of the margin, very sparse to almost obsolete and slightly decumbent proximally. Hypomeron flat, without depressions or fossae.

Elytra**:** EL/EW = 1.36 (1.30–1.43); EL/PL = 3.63 (3.63–3.85); EW/PW = 1.23 (1.16–1.27); TL/EW = 1.78 (1.66–1.78), slightly less than 4.0 times longer than the pronotum, widest at anterior 0.25; anterior margin of elytra bordered, bi-sinuately articulated with pronotum; lateral margins slightly explanate in anterior half; apices jointly rounded; humeral callus weak. Elytra with two series of punctation; first series with nine or more perceptible and irregular rows of large, deeply impressed punctures; punctures of medial five rows denser and more strongly impressed in anterior half; increasingly scattered, finer and more shallowly impressed laterally and posteriorly; intervals and interstices distinctly broader than punctures; second series of punctures much smaller, densely and evenly distributed over entire elytra. Pubescence long, yellowish-brown to brown, of two distinct types (erect and recumbent): erect series on sides, slightly recumbent series on disc; erect series longer and denser; recumbent series shorter, very sparse. Scutellum subtriangular, with irregular and densely punc-

tured surface; with two series of punctation, few large and deeply impressed punctures, numerous finer and shallowly impressed ones; pubescence erect, sparse. Metathoracic wings well developed. Epipleura almost flat.

***Ventral surface*:** punctation dense and almost uniform; pubescence brown, minute, long, finer than on dorsal side, recumbent, dense and evenly distributed. Prosternum slightly impressed at the process; process narrow, punctation more distinct at tip. Mesosternal ridge along posterior margins of mesosternum distinct. Metasternum perforate at sides, with raised triangular, rugulose area behind mesocoxal cavities; raised area comprising nearly half of surface; metasternal ridge along posterior margin of metasternum faint laterally, well-developed medially. Abdominal punctation finer at mid-line than at sides; surface between punctation with polygonal network, with median pore. Intermetacoxal plate on ventrite I triangular, strongly acuminate. Abdominal ventrite I with depressions for reception of metafemora and metatibiae; ventrites I–III connate, fused; ventrites IV–V without polygonal network; ventrite V distinctly emarginate.

***Legs*:** less than half of body length. Tibia brown, lateral margins darker, distal margin with comb of long spines; protibia very short, a little longer than half of either mesotibia and metatibia, lateral margin slightly concave, setae denser than on mesotibia and metatibia; mesotibia with lateral margin curved more prominently in interior margins, setae evenly distributed; metatibia almost twice as long as protibia, slightly longer than mesotibia, lateral margins almost parallel, setae sparse and almost recumbent; apex of mesotibia and metatibia smoothly and broadly curved. Tarsi 5-5-5, brown, paler towards the apex, almost half as long as mesotibia; tarsomere length ratio ca. 1.0:1.0:1.0:1.0:4.0 (0.9–1.1: 0.9–1.1: 0.9–1.1: 0.9–1.1: 3.5–4.7); tarsomere 1 widest towards the apex, distal margin almost double the width of proximal margin, with dense comb of setae; tarsomeres 2–4 similar to tarsomere 1, but outer edge with long yellow spiny setae on both sides, remaining portions with sparse minute setae; tarsomere 5 widest towards the apex, almost triangular, with long robust spiny setae. Tarsal claws long, narrow, symmetrical.

***Male genitalia*:** (Figs 4, 5) length 0.67 mm (0.65–0.71 mm), width 0.11 mm (0.10–0.14 mm), very slender, strongly sclerotised; median lobe more exposed in ventral view than dorsal view. Median lobe of aedeagus almost as long as parameres, symmetrical; apex flat, broad, most slender subapically, with pair of rows of short denticles subapically (ventral view), convexly widened basally; basal portion wider than apical portion. Parameres symmetrical; apices slender and moderately separated dorsally, broader and converged ventrally, inner margin of parameres subparallel near tips, distinctly concave in the middle converging basally in V-shape; with tubular lobes protruding medio-apically in apical third below the denticles of the median lobe, median gap wider dorsally and exposing the full width of median lobe. Basal lobe asymmetrical, with strongly sclerotised basal margins. Ventrite VIII U–shaped, with narrow apical membranous lamina. Spiculum prominent.

***Female genitalia*:** ovipositor relatively short (0.58–0.62 mm long), straight.

Differential diagnosis. In the elongate oval shape, the new species resembles several species, including *B. ferax* and *B. tarawakanus*. Amongst the Philippine species, the

range of size overlaps with *B. subtestaceus* and *B. ferax*. The protibia of *B. negrosensis* sp. nov. is notably smaller than the mesotibia and metatibia. The male genitalia of *B. negrosensis* sp. nov. resembles that of *B. ferax* due to the medially parallel paramere apices, which is quite uncommon in the Oriental members of the genus. Despite numerous similarities, *B. negrosensis* sp. nov. differs from *B. ferax* in the dorsally V-shaped basal fusion point of the parameres (Fig. 4), while the latter possesses a U-shape parameral fusion. *B. negrosensis* sp. nov. varies by 13.2% mean genetic distance (723 bp *COI-3'* mtDNA barcode) from the most similar *B. ferax* and by at least 16.1% from any other Philippine congener with available barcode (Suppl. material 1: Table S1).

Distribution. This species is only recorded from the Island of Negros in the Philippines.

Remarks. No external sexual dimorphism is observed. Teneral specimens are significantly paler brown.

Etymology. The species is named after the Island of Negros from where the specimens were collected.

***Byrrhinus villarini* sp. nov.**

http://zoobank.org/45EC216F-0B75-4550-B9DF-123B9672A7FA

Figures 3, 6, 7

Type locality. Philippines • Negros Island, Occidental Mindoro, Murcia, Pandanon River in secondary vegetation; ca. 10°34'54"N, 123°10'30"E; ca. 440 m a.s.l.

Type material. ***Holotype*:** Philippines • ♂ (PNM: EDD121), "PHIL: Negros Occ., Murcia, \ Pandanon River, sec.veg.; \ ca. 10°34'54"N; 123°10'30"E; ca. 440 m a.s.l.; \ 01 May 2019, leg. Freitag et al. (650)L"; GenBank: OK316813; BOLD: COLPH061-21; EDD121, habitus and terminal parts of abdomen including aedeagus glued separately on to entomological card. ***Paratypes*:** Philippines • 3♂♂, 4♀♀ (AdMU: EDD113, EDD114; PNM; ZMB: EDD115): same locality data as holotype; GenBank: OK316804, OK316815, OK316817; BOLD: COLPH058-21, COLPH059-21, COLPH060-21 • 3♂♂ (AdMU: EDD124, EDD126): "PHIL: Negros Or., Valencia, \ Casaroro River, downstr., sec.veg.; \ ca. 09°18'N; 123°14'E; ca. 150 m a.s.l.; \ 01 Sep. 2019, leg. Garces & Pelingen (655)L"; GenBank: OK316805, OK316818; BOLD: COLPH062-21, COLPH063-21.

Description. ***Body*:** (Fig. 3) ovoid, TL = 2.8 mm (2.2–2.9 mm), EW = 1.9 mm (1.4–1.9 mm), widest behind mid-leg; dorsal surface very dark–brown to black; body appendages slightly paler than body, moderately densely and evenly covered with brown, fine, quite long, mostly erect pubescence; antennae yellow–brown; femora and tibiae brown; tarsi dark yellowish, but darker on terminal ends of segments.

***Head*:** obscurely rugulose; broadly laminate over eyes; margins of frons grooved over eyes; sides of frons with deep and well–marked pit-like depressions. Punctation minute, slightly coarser near epistomal suture. Pubescence brown, fine, quite long, erect, more numerous and denser on the anterior region. Eyes slightly convex, visible

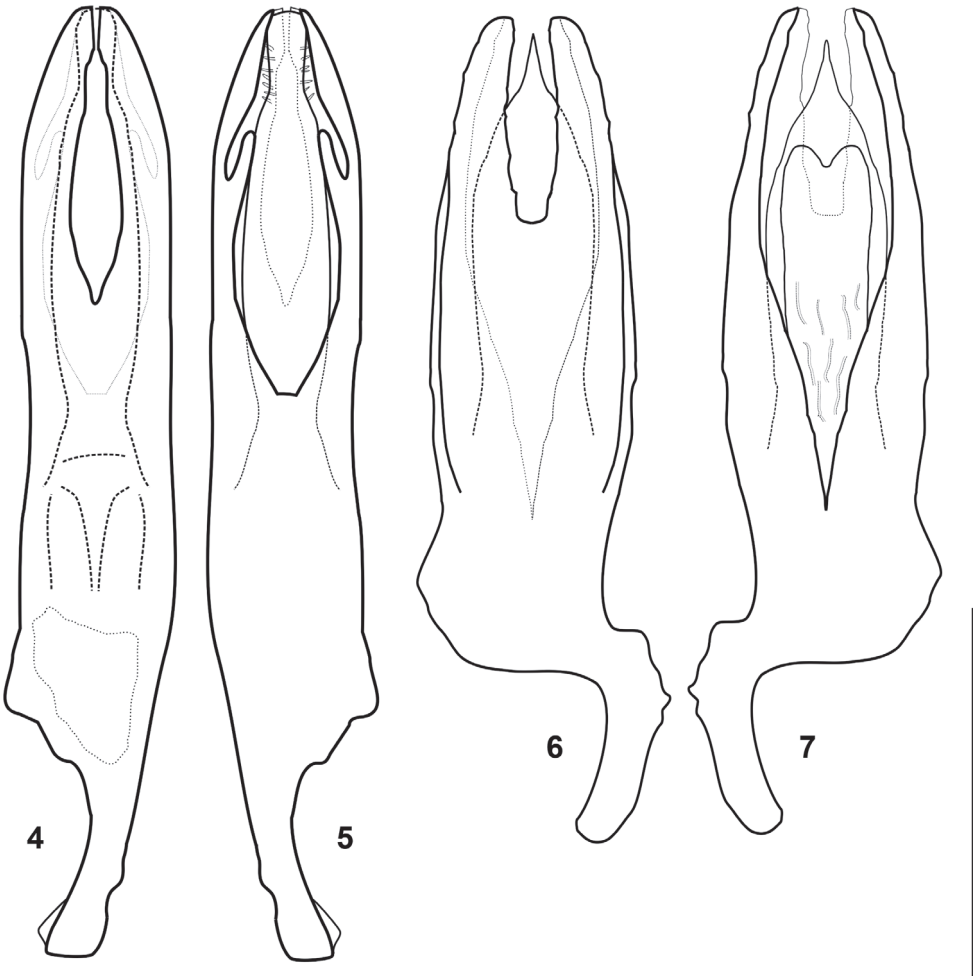

Figures 4–7. Male aedeagi of **4, 5** *Byrrhinus negrosensis* sp. nov. (EDD122) and **6, 7** *Byrrhinus villarini* sp. nov. (EDD121) in (**4, 6**) dorsal and (**5, 7**) ventral views. Scale bar: 0.25 mm.

from above; upper margin of eyes bordered; anterior margin almost reaching insertion of antennae, extending posterior of eyes although weaker. Surface of head posterior to eyes flat, without depressions or fossae; surface with fine and sparse punctation, denser and coarser on clypeus; surface between punctures smooth and shiny. Antennae moniliform, strongly pubescent; pedicel globular, brown, darker than adjacent antennomeres; antennomeres longer than wide, yellow-brown; pubescence brown, uniform, erect, mostly as long as antennomere.

***Pronotum*:** transverse, black, with dark brown colouration on the sides, distinctly narrower at base; anterior margin of pronotum straight, without crenulations, bordered; lateral margins strongly arched, posterolateral angle ca. 50°, with prominent borders; posterior margin with distinct double sinuation; PL/PW = 0.42 (0.40–0.44); PW/PL = 2.40 (2.28–2.50). Punctation strong and deeply impressed, but sparse;

punctures stronger than that of the head, larger at posterior margins, sparse near suture and anteriad, surface very depressed at projections along posterior margin. Pubescence similar to that on the head, slightly decumbent near the median line, denser at sides. Hypomeron flat, without depressions or fossae.

***Elytra*:** EL/EW = 1.41 (1.30–1.41); EL/PL = 4.14 (4.11–4.14); EW/PW = 1.20 (1.20–1.21); TL/EW = 1.75 (1.68–1.78); elytra slightly more than 4.0 times longer than the pronotum; widest at anterior 0.2; anterior margin of elytra bordered, strongly bisinuately articulated with the pronotum; lateral margins pronounced, finer towards apex; apices jointly rounded; humeral callus weak. Elytra punctation of two series; first series with nine or ten distinct and almost regular rows of large deeply impressed punctures; increasingly scattered, finer, not as strongly impressed as in rows laterally and posteriorly; intervals and interstices distinctly broader than punctures; second series of small punctures moderately dense only and less conspicuous than in previous species. Pubescence long, brown, with yellowish shade depending on illumination, of two distinct types: erect series on sides, slightly recumbent series on disc; erect series longer and denser; disc series shorter, sparse. Scutellum subtriangular, with few punctures and pubescence similar to surrounding area of elytra. Metathoracic wings well developed. Epipleura almost flat.

***Ventral surface*:** punctation dense and uniform; pubescence brown, minute, long, finer than on dorsal side, recumbent, dense and evenly distributed. Prosternum slightly impressed at the process; process narrow, punctation more distinct at tip. Mesosternal ridge along posterior margins distinct. Metasternum minutely perforate at sides, with raised triangular, rugulose area behind cavities; raised area comprising nearly half of surface; metasternal ridge along posterior margin of metasternum faint laterally, well-developed medially. Abdominal punctation finer at mid-line than at sides; surface between punctation with polygonal network, with median pore. Intermetacoxal plate on ventrite I triangular, strongly acuminate. Abdominal ventrite I with depressions for reception of metafemora and metatibiae; ventrites I–III connate, fused; ventrites IV–V without polygonal network; ventrite V distinctly emarginate apically.

***Legs*:** length less than half of body length. Tibia brown, lateral margins darker, curved, with pre-apical comb of spines; metatibia slightly longer than protibia and mesotibia; apex of mesotibia and metatibia slightly curved. Tarsi 5-5-5, dark yellow to light brown, paler towards the apex, about two-thirds of length of tibia; tarsomere length ratio ca. 1.2:1.0:1.0:1.0:2.9 (1.0–1.5: 0.8–1.0: 0.8–1.0: 0.8–1.0: 2.7–3.3); tarsomere 1 brown, with parallel margins, widest towards the apex, with dense comb of setae; tarsomeres 2–4 almost globular, outer edge with long yellow spiny setae on both sides, remaining portions with sparse minute setae; tarsomere 5 more yellow than brown, widest towards the apex, with at least three pairs of long robust spiny setae. Tarsal claws long, narrow, symmetrical.

***Male genitalia*:** (Figs 6, 7) length 0.58 mm (0.57–0.59 mm), width 0.14 mm (0.12–0.17 mm), stout, strongly sclerotised; median lobe more exposed in ventral view than dorsal view. Median lobe of aedeagus a bit shorter than parameres, symmetrical, broad, non-planar, varying in dorsal and ventral views; on dorsal view, apex acuminate, significantly and abruptly convexly widened mediad, middle portion wide;

on ventral view, median lobe with an additional, slightly more slender, subcordiform lobe, reaching apical 0.3 where it terminates deeply emarginate. Parameres symmetrical, with outer face irregularly outlined and uneven texture near apex; apices dorsally broad; apices obliquely rounded; inner margins dorsally very slightly concave, almost unevenly sub-parallel; not distinctly convergent basally, forming a U–shape extending one-fourth the length of genitalia; ventrally only half as wide as in dorsal view, opening wider and exposing the entire width of median lobe, converging basally to form a deep "V". Basal lobe asymmetrical, with strongly sclerotised basal margins. Ventrite VIII U–shaped, with narrow apical membranous lamina. Spiculum prominent.

***Female genitalia*:** ovipositor relatively short (0.50–0.56 mm long), straight.

Differential diagnosis. In the ovoid shape, the new species resembles *B. vestitus* (Sharp, 1902), *B. maculatus* Wooldridge, 1987 and *B. magnus* Wooldridge, 1987. Compared to other Philippine species, the range of size overlaps with *B. punctatus* and *B. tarawakanus*. The new species is remarkably different from these two in the smaller posterolateral angle (ca. 50°) of the pronotum in *B. villarini* sp. nov. compared to *B. punctatus* and *B. tarawakanus*, as well as *B. negrosensis* sp. nov. (75–80°). In addition to the posterolateral angle measure of pronotum, *B. villarini* sp. nov. is notably different from *B. negrosensis* sp. nov. in the length of tarsomere 5. Tarsomere 5 of *B. villarini* sp. nov. is as long as tarsomeres 2–4, while tarsomere 5 of *B. negrosensis* sp. nov. is almost as long as tarsomeres 1–4. Additionally, erect series of elytral pubescence is present on the posterior end of both species, but covers the distal one-third only of elytra in *B. villarini* sp. nov., while covering the distal one-half in *B. negrosensis* sp. nov.

Males of *B. villarini* sp. nov. are easily recognisable because the parameres are dorsally fused forming a rather shallow "U" (Fig. 6), not a "V" as in *B. negrosensis* sp. nov. (Fig. 4). This U–shaped opening separating the parameres extends only one-fourth the length of the aedeagus, while the opening spans at least half of the aedeagus for other Philippine species, such as *B. ferax*, *B. punctatus* and *B. tarawakanus*. The median lobe of the aedeagus resembles that of *B. tarawakanus* in terms of shape and height of the parameres. However, the median lobe of *B. villarini* sp. nov. is stouter and wider towards the middle portion.

B. villarini sp. nov. varies by 5.8% mean genetic distance (723 bp *COI-3'* mtDNA barcode) from an unidentified, but presumably closely-related Malaysian species and by at least 13.4% from any other Philippine congeners with available barcodes (Suppl. material 1: Table S1).

Distribution. This species is only recorded from the Island of Negros in the Philippines.

Remarks. No external sexual dimorphism is observed.

Etymology. The new species is named and dedicated to the immediate past president of the Ateneo de Manila University, Fr Jose Ramon T. Villarin, SJ, PhD, who finished his term last year. During his reign for the past decade, Fr Villarin showed ardent support for research activities on the environment and sustainability. He is also a member of the Intergovernmental Panel on Climate Change which was conferred the 2007 Nobel Peace Prize for their study and recommendations on counteracting the global climate crisis.

Byrrhinus ferax Wooldridge, 1993

Byrrhinus ferax Wooldridge, 1993: 359–360 (orig. descr.).

Additional material examined. Philippines • ♂ (AdMU), Occ. Mindoro, Sablayan, small limestone river; rootpacks, dist. primary forest; ca. 12°47'49"N, 120°54'33"E; ca. 100 m a.s.l.; 01 Jan. 1995, leg. Mendoza "(365)M"; GenBank: OK316810; BOLD: COLPH064-21.

Remarks. Assignment of the specimen to this taxon was based primarily on genital characters. No remarkable difference was noted compared to the original description. The material used for the molecular analysis in this study was collected 90 km south of one of the localities of the paratypes, but on the same island. Known distribution of *B. ferax* includes the Philippine Islands of Mindoro and Mindanao.

Additional *Byrrhinus* specimens examined

The three specimens listed below have an interspecific divergence of 10.6 to 19.6% (Table 2). Given the single-specimen samples that are currently available only, they will not receive further treatment in this study.

***Byrrhinus* sp. A:** Philippines • 1 ♂, Palawan, P. Princesa, Irawan River, 6 km NW of PPC, 0.5 km upstream of water plant ca. 9°49'50"N, 118°39'46"E; 105 m a.s.l.; 06 Aug. 2019, leg. H. Freitag "(60b)M"; GenBank: OK316816; BOLD: COLPH065-21.

***Byrrhinus* sp. B:** Philippines • 1 ♂, Camarines Sur, Lupi, Brgy. Sooc, Sooc River, Bicol National Park; ca. 13°52'28"N, 122°56'38"E; 90 m a.s.l.; 09 Aug. 1996; leg. Mendoza "(M585)L"; GenBank: OK316806; BOLD: COLPH066-21.

***Byrrhinus* sp. C:** Philippines • 1 ♂, Mindanao, Agusan N, R.T.R, Panaytayon, paddy field, ca.10 m a.s.l. 9°02'53"N, 125°35'03"E; leg. Freitag & Pangantihon 05. Jul. 2018 "(890)L"; GenBank: OK316814; BOLD: COLPH067-21.

Checklist and distribution of the species of *Byrrhinus* in the Philippines

Byrrhinus convexus (Blackburn, 1896): Luzon, Australia
Byrrhinus ferax Wooldridge, 1993: Mindoro, Mindanao (Cotabato, Davao); Borneo (Malaysia: Sabah)
Byrrhinus negrosensis sp. nov.: Negros
Byrrhinus punctatus (Pic, 1922): Luzon, Mindoro
Byrrhinus villarini sp. nov.: Negros
Byrrhinus subtestaceus Pic, 1923: Luzon
Byrrhinus tarawakanus Deléve, 1973: Palawan, Tawi-Tawi

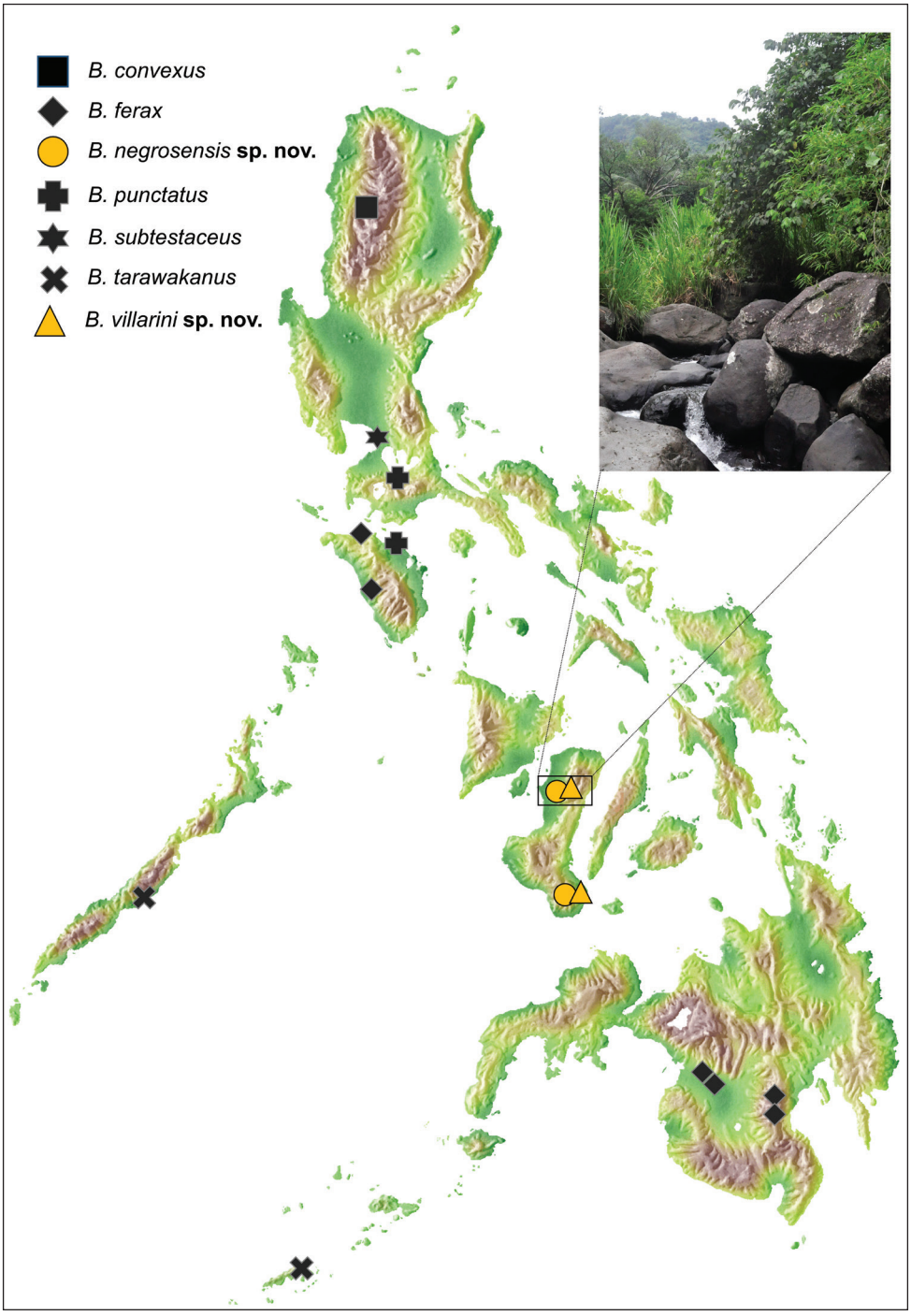

Figure 8. Updated distribution of known *Byrrhinus* in the Philippines; inset shows Pandanon River in Murcia "(650)L", which is the type locality of *B. villarini* sp. nov.

Discussion

The two new *Byrrhinus* species described here, *B. negrosensis* sp. nov. and *B. villarini* sp. nov., increase the total number of Philippine *Byrrhinus* from five to seven. This contribution using the integrative taxonomic approach provides the first additional record on Philippine *Byrrhinus* species in the last 28 years and provides the first records from the Visayas (Fig. 8; see updated checklist). This study demonstrates that sampling in one of the several islands of Visayas reveals previously undocumented entomofauna.

Characters used to differentiate limnichid species, such as pubescence and punctation patterns and aedeagal structure (Hernando and Ribera 2014a, 2014b), were notably different for the two Negros *Byrrhinus* species as described above. From the materials studied, *B. villarini* sp. nov. is smaller (2.1–2.9 mm) than *B. negrosensis* sp. nov. (2.9–4.1 mm) though these size ranges are not unique compared other *Byrrhinus* species. While the usual body ratios (PL/PW, EL/EW, EL/PL, EW/PW, TL/EW) applied to Limnichidae (Yoshitomi 2019) did not substantially help discriminating the two new species, the length ratios of the tarsomeres and the posterolateral angle of the pronotum appear to be distinct. Female specimens show no distinct differences from the male external morphology.

Phylogenetic analysis retrieved strongly supported clades (BS = 100) corresponding to the two newly-described species (Fig. 1). Each species was poorly clustered (BS < 70) with *Byrrhinus* from other islands. The sequences of *B. negrosensis* sp. nov. clustered with the first *COI-3'* sequence for *B. ferax*. Moreover, the sequences for *B. villarini* sp. nov. clustered with *Byrrhinus* sp. from Malaysia in a well-supported clade. While the genetic distance is low at 5.9% (Table 2), it is beyond the recognised 3% rule-of-thumb for intraspecific divergence limit for insects (Hebert et al. 2003; Astrin et al. 2012). The said sequence, together with the other reference sequences used in this analysis, was generated in a study on resolving superfamily phylogeny (Kundrata et al. 2017). As the sequence was not accompanied by a proper species-level identification or informative photographs on BOLD, no further discussion can be provided on this clade of presumably closely-related species.

The clustering of conspecific sequences in the gene tree is also reflected in the statistical parsimony network generated for the two new species (Fig. 9). Conspecific sequences from different localities are less divergent than sequences of syntopic, but non-conspecific specimens. The gene tree (Fig. 1) also shows that the two new Negros species are genetically closer to some other *Byrrhinus* species which are not (yet) recorded from Negros than with each other.

Entomofaunal diversity has been experiencing a tremendous decline in both local (Hallmann et al. 2021; Warren et al. 2021) and global scales (Sánchez-Bayo and Wyckhuys 2019), with catastrophic impacts on the current ecosystem services (Faridah-Hanum et al. 2018; Wagner et al. 2021). Especially in time of accelerated biodiversity decline, coupling morphological and molecular data is essential in fast-tracking species discovery particularly in highly cryptic and highly diverse taxa (Tänzler et al. 2014; Platania et al. 2020; Maasri et al. 2021). In such cases, proper taxonomic identification

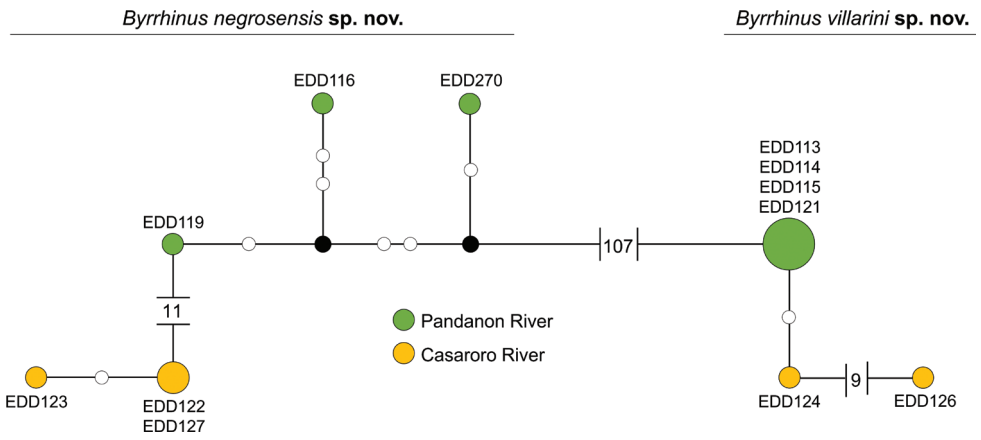

Figure 9. Statistical parsimony network of sequenced *B. negrosensis* sp. nov. and *B. villarini* sp. nov. specimens using *COI-3'* (723 bp).

of cryptic taxa using an integrative approach has been shown to be essential in mapping appropriate conservation measures (Arribas et al. 2013). These discoveries came at a time of increased anthropogenic activities in the protected areas and highly pristine localities in the Island.

Acknowledgements

We would like to thank the Bureau of Fisheries and Aquatic Resources (BFAR) for their continuous assistance in issuing Gratuitous Permit (GP 0133-17 and renewals) which allows sampling and collecting specimens from aquatic habitats. We also would like to thank local government units of Murcia and Valencia and their Environment and Natural Resources Office for their Prior Informed Consents and thus granting permission to conduct sampling in their locality and for providing logistical assistance in the field.

We also thank the members of the Biodiversity Laboratory, Marc Sabordo, Dr Jhoana Garces, Clister Pangantihon and Arthien Pelingen, for their valuable contribution in sampling, sorting and safekeeping the specimens.

Additionally, we thank Dr Thomas von Rintelen and Mr Robert Scheiber at Museum für Naturkunde, Berlin, Germany (MfN) for supervising the molecular laboratory work training during the internship of the first author under the Biodiversity Teaching in a Philippine-Cambodian-German Network (BIO-PHIL) project. We would like to express our sincerest gratitude to Dr Manfred A. Jäch (NMW) for allowing access to the museum's extensive type collections. We also thank in a very special way the late Dr Ignacio Ribera (IBE) who provided valuable guidance on morphological differentiation of the specimens. We also thank Dr Bill Shepard and an anonymous reviewer, as well as subject editor Dr Christopher Majka, for their helpful feedback on improving this manuscript.

The study was partly funded by the School of Science and Engineering Industry 4.0 Research Fund (SI4-013) of the Ateneo de Manila University. Inspection of type specimens at European collections and taxonomy training of the first author were made possible through the Biodiversity Teaching in a Philippine-Cambodian-German Network (BIO-PHIL) project funded by the German Academic Exchange Service (DAAD project BIO-PHIL 57393541).

References

Altschul SF, Gish W, Miller W, Myers EW, Lipman DJ (1990) Basic local alignment search tool. Journal of Molecular Biology 215: 403–410. https://doi.org/10.1016/S0022-2836(05)80360-2

Arribas P, Andújar C, Sánchez-Fernández D, Abellán P, Millán A (2013) Integrative taxonomy and conservation of cryptic beetles in the Mediterranean region (Hydrophilidae). Zoologica Scripta 42: 182–200. https://doi.org/10.1111/zsc.12000

Astrin JJ, Stüben PE, Misof B, Wägele JW, Gimnich F, Raupach MJ, Ahrens D (2012) Exploring diversity in cryptorhynchine weevils (Coleoptera) using distance-, character- and tree-based species delineation. Molecular Phylogenetics and Evolution 63: 1–14. https://doi.org/10.1016/j.ympev.2011.11.018

Blackburn T (1896) Further notes on Australian Coleoptera, with descriptions of new genera and species. Transactions of the Royal Society of South Australia 14: 35–109. https://doi.org/10.1080/18324460.1912.10439228

Casey TL (1889) Coleopterological notices. I. (with an appendix on the termitophilous Staphylinidae of Panama). Annals of the New York Academy of Sciences 5: 39–198. https://doi.org/10.1111/j.1749-6632.1890.tb57003.x

Champion GC (1923) Some Indian Coleoptera (12). Entomologist's Monthly Magazine 59: 219–224.

Clement M, Posada D, Crandall KA (2000) TCS: a computer program to estimate gene genealogies. Molecular Ecology 9: 1657–1659. https://doi.org/10.1046/j.1365-294x.2000.01020.x

Dayrat B (2005) Towards integrative taxonomy. Biological Journal of the Linnean Society 85: 407–415. https://doi.org/10.1111/j.1095-8312.2005.00503.x

Deléve J (1968) Contribution a l'etude des "Dryopoidea". Les Limnichinae d'Afrique (Coeloptera Limnichidae). Bulletin et Annales de la Société Royale d'Entomologie de Belgique 104: 212–274.

Deléve J (1973) Limnichidae, Dryopidae et Elminthidae des iles Philippines et de l'Archipel Bismarck (Insecta, Coleoptera, Dryopoidea) [Noon a Dan Papers No. 122]. Steenstrupia 3: 17–30.

Edgar RC (2004) MUSCLE: Multiple sequence alignment with high accuracy and high throughput. Nucleic Acids Research 32: 1792–1797. https://doi.org/10.1093/nar/gkh340

Erichson WF (1847) Naturgeschichte der Insecten Deutschlands. Coleoptera, vol III. Berlin, Germany, Verlag der Nicolaischen Buchhandlung, 481–800. https://doi.org/10.5962/bhl.title.50882

Faridah-Hanum I, Rawat G, Yahara T, Sheppard A, Mohapatra A, Murphy B, Hewitt C, Raghunathan C, Courchamp F, Maheswaran G, Freitag H, Piggott J, Kumar M, Abi-Said M, Takamura N, Rawal R, Corlett R, Dai R, Thwin S, Miyashita T, Yamakita T, Kadoya T, Hussain T, Nakashizuka T, Haryoko T, Shirayama Y, Son Y, Niamir A, Febria C, Jia L, Leong J-A, Wesche K, Opgenoorth L, Perkin S, Katayama N, Zhang Y, Sirin A, Minayeva T, Dugardzhav C, Dejid N, Tucker M, ʻOhukaniʻōhiʻa Gon S, Ghosh S (2018) Status, trends and future dynamics of biodiversity and ecosystems underpinning nature's contributions to people. In: Karki M, Senaratna Sellamuttu S, Okayasu S, Suzuki W (Eds) The IPBES regional assessment report on biodiversity and ecosystem services for Asia and the Pacific. IPBES Secretariat of the Intergovernmental Science-Policy Platform on Biodiversity and Ecosystem Services, Bonn, 220–336. [citeulike-article-id:14587842]

Freitag H, Jäch MA, Wewalka G (2016) Diversity of aquatic and riparian Coleoptera of the Philippines: checklist, state of knowledge, priorities for future research and conservation. Aquatic Insects 37: 177–213. https://doi.org/10.1080/01650424.2016.1210814

Garces JM, Sartori M, Freitag H (2020) Integrative taxonomy of the genus *Dudgeodes* Sartori, 2008 (Insecta, Ephemeroptera, Teloganodidae) from the Philippines with description of new species and supplementary descriptions of Southeast Asian species. ZooKeys 2020: 93–129. https://doi.org/10.3897/zookeys.910.48659

Goodstadt L, Ponting CP (2001) CHROMA: Consensus-based colouring of multiple alignments for publication. Bioinformatics 17: 845–846. https://doi.org/10.1093/bioinformatics/17.9.845

Hall TA (1999) BioEdit: a user-friendly biological sequence alignment editor and analysis program for Windows 95/98/NT. Nucleic Acids Symposium Series 41: 95–98.

Hallmann CA, Ssymank A, Sorg M, De Kroon H, Jongejans E (2021) Insect biomass decline scaled to species diversity: general patterns derived from a hoverfly community. Proceedings of the National Academy of Sciences 118: e2002554117. https://doi.org/10.1073/pnas.2002554117

Hebert PDN, Cywinska A, Ball SL, DeWaard JR (2003) Biological identifications through DNA barcodes. Proceedings of the Royal Society B: Biological Sciences 270: 313–321. https://doi.org/10.1098/rspb.2002.2218

Hernando C, Ribera I (2014a) Taxonomic revision of the genus *Caccothryptus* Sharp (Coleoptera: Limnichidae). Koleopterologische Rundschau 84: 281–304.

Hernando C, Ribera I (2014b) The Limnichidae (Coleoptera) of the Arabian Peninsula and the Island of Socotra. Acta Entomologica Musei Nationalis Pragae 54: 173–189.

Hernando C, Ribera I (2016) 19.5 Limnichidae Erichson, 1846. In: Beutel RG, Leschen RAB (Eds) Handbook of Zoology, Vol. IV (Part 38), Coleoptera, Beetles, Volume I: Morphology and Systematics (Archostemata, Adephaga, Myxophaga, Polyphaga partim). Walter de Gruyter, Berlin & New York, 605–612.

Hinton HE (1939) An inquiry into the natural classification of the Dryopoidea, based partly on a study of their internal anatomy (Coleoptera). Transactions of the Royal Entomological Society of London 89: 133–184. https://doi.org/10.1111/j.1365-2311.1939.tb00739.x

Kaltenbach T, Garces JM, Gattolliat J-L (2020a) A new genus of Baetidae (Insecta, Ephemeroptera) from Southeast Asia. European Journal of Taxonomy 612: 1–32. https://doi.org/10.5852/ejt.2020.612

Kaltenbach T, Garces JM, Gattolliat J-L (2020b) The success story of *Labiobaetis* Novikova & Kluge in the Philippines (Ephemeroptera, Baetidae), with description of 18 new species. ZooKeys 1002: 1–114. https://doi.org/10.3897/zookeys.1002.58017

Kimura M (1980) A simple method for estimating evolutionary rates of base substitutions through comparative studies of nucleotide sequences. Journal of Molecular Evolution 16(2): 111–120. https://doi.org/10.1007/BF01731581

Kodada J, Jäch MA, Freitag H, Čiamporová-Zaťovičová Z, Goffová K, Selnekovič D, Čiampor F (2020) *Ancyronyx clisteri*, a new spider riffle beetle species from Borneo, redescription of *A. sarawacensis* Jäch including a description of the larva and new distribution data for *A. procerus* Jäch using DNA barcodes (Coleoptera, Elmidae). ZooKeys 2020: 25–64. https://doi.org/10.3897/zookeys.912.47796

Komarek A, Freitag H (2020) Taxonomic revision of *Agraphydrus* Regimbart, 1903 V. Philippine species and their first DNA barcodes (Coleoptera: Hydrophilidae: Acidocerinae). Koleopterologische Rundschau 90: 201–242.

Kumar S, Stecher G, Tamura K (2016) MEGA7: Molecular Evolutionary Genetics Analysis version 7.0 for bigger datasets. Molecular Biology and Evolution 33: 1870–1874. https://doi.org/10.1093/molbev/msw054

Kundrata R, Jäch MA, Bocak L (2017) Molecular phylogeny of the Byrrhoidea–Buprestoidea complex (Coleoptera, Elateriformia). Zoologica Scripta 46: 150–164. https://doi.org/10.1111/zsc.12196

Leigh JW, Bryant D (2015) POPART: full-Feature Software for Haplotype Network Construction. Methods in Ecology and Evolution 6: 1110–1116. https://doi.org/10.1111/2041-210X.12410

Maasri A, Jähnig S, Adamescu M, Adrian R, Baigun C, Baird D, Matista-Morales A, Bonada N, Brown L, Cai Q, Campos-Silva J, Clausnitzer V, Contreras-MacBeath T, Cooke S, Datry T, Delacamara G, Dijkstra K-D, Do VT, Domisch A, Dudgeon D, Eros T, Freitag H, Freyhof J, Friedrich J, Friedrichs-Manthey M, Geist J, Gessner M, Goethals P, Gollock M, Gordon C, Grossart H-P, Culemvuga G, Gutiérrez-Fonseca P, Haase P, Hering D, Hahn HJ, Hawkins C, He F, Heino J, Hermoso V, Hogan Z, Hoelker F, Jeschke J, Jiang M, Johnson R, Kalinkat G, Karimov B, Kasangaki A, Kimieri I, Kohlmann B, Kummerlen M, Kuiper J, Kupilas B, Langhans S, Lansdown R, Leese F, De Meester L, Magbanua F, Matsuzaki S, Monaghan M, Mumladze L, Muzon J, Ndongo PM, Nejstgaard J, Nikitina O, Ochs C, Odume ON, Opperman J, Patricio H, Pauls S, Raghavan R, Ramirez A, Rashni B, Ross-Gillespie V, Samways M, Scharfer R, Schmidt-Kloiber A, Seehausen O, Shah DN, Sharma R, Soininen J, Sommerwerk N, Stockwell J, Suhling F, Shah RDT, Tharme R, Thorp J, Tickner D, Tockner K, Tonkin J, Valle M, Vitule J, Volk M, Wang D, Wolter C, Worischka S (2021) A global agenda for advancing freshwater biodiversity research. Authorea. https://doi.org/10.22541/au.161640764.49902060/v1

Matsumoto K (2021) New species and records of Angolan Limnichidae (Coleoptera: Limnichidae). Zootaxa 4985(1): 111–117. https://doi.org/10.11646/zootaxa.4985.1.7

Motschulsky Vde (1858) Entomologie speciale. Insectes des Indes orientales. Etudes Entomologique 7: 20–122.

Pic M (1922) Nouveautés diverses. Melanges Exotico-Entomologiques 36: 1–32.

Pic M (1923) Nouveautés diverses. Melanges Exotico-Entomologiques 40: 1–32.

Platania L, Vodă R, Dincă V, Talavera G, Vila R, Dapporto L (2020) Integrative analyses on Western Palearctic Lasiommata reveal a mosaic of nascent butterfly species. Journal of Zoological Systematics and Evolutionary Research: 1–14. https://doi.org/10.1111/jzs.12356

Qiagen (2006) DNeasy Blood & Tissue Handbook. https://doi.org/10.1111/ele.12937

Riedel A, Tänzler R (2016) Revision of the Australian species of the weevil genus *Trigonopterus* fauvel. ZooKeys 2016: 97–162. https://doi.org/10.3897/zookeys.556.6126

Sabordo MR, Delocado E, Freitag H (2020) Two new species of the genus *Ancyronyx* Erichson, 1847 from the Island of Negros, Philippines (Insecta, Coleoptera, Elmidae). Tijdschrift voor Entomologie: 1–18. https://doi.org/10.1163/22119434-20192087

Sánchez-Bayo F, Wyckhuys KAG (2019) Worldwide decline of the entomofauna: A review of its drivers. Biological Conservation 232: 8–27. https://doi.org/10.1016/j.biocon.2019.01.020

Satô M (1965) The Limnichid-beetles of Formosa. Special Bulletin of the Lepidopteran Society of Japan 30: 121–125.

Sharp D (1902) Descriptions of Oriental Limnichini (Coleoptera, Fam. Byrrhidae). Entomologist's Monthly Magazine 38: 61–64.

Simon C, Frati F, Beckenbach A, Crespi B, Liu H, Flook P (1994) Evolution, weighting, and phylogenetic utility of mitochondrial gene sequences and a compilation of conserved polymerase chain reaction primers. Annals of the Entomological Society of America 87: 651–701. https://doi.org/10.1093/aesa/87.6.651

Tänzler R, Toussaint EFA, Suhardjono YR, Balke M, Riedel A (2014) Multiple transgressions of Wallace's Line explain diversity of flightless *Trigonopterus* weevils on Bali. Proceedings of the Royal Society B: Biological Sciences 281(1782): e20132528. https://doi.org/10.1098/rspb.2013.2528

Wagner DL, Grames EM, Forister ML, Berenbaum MR, Stopak D (2021) Insect decline in the Anthropocene: Death by a thousand cuts. Proceedings of the National Academy of Sciences of the United States of America 118: e2023989118. https://doi.org/10.1073/pnas.2023989118

Warren MS, Maes D, van Swaay CAM, Goffart P, Van Dyck H, Bourn NAD, Wynhoff I, Hoare D, Ellis S (2021) The decline of butterflies in Europe: problems, significance, and possible solutions. Proceedings of the National Academy of Science of the United States of America 118: e20002551117. https://doi.org/10.1073/pnas.2002551117

Will KW, Mishler BD, Wheeler QD (2005) The perils of DNA barcoding and the need for integrative taxonomy. Systematic Biology 54: 844–851. https://doi.org/10.1080/10635150500354878

Wooldridge DP (1987) New World Limnichinae IX: A Revision of Neotropical *Byrrhinus* Motschulsky (Coleoptera: Dryopoidea: Limnichidae). The Coleopterists Society 41: 303–314.

Wooldridge DP (1993) A new species of *Byrrhinus* Motschulsky from the Philippine Islands and Borneo (Coleoptera: Limnichidae). The Coleopterists Society 47: 359–361.

Yoshitomi H (2019) Review of the Asian Thaumastodinae (Coleoptera, Byrrhoidea, Limnichidae), with a phylogeny of the genera. European Journal of Taxonomy 2019: 1–45. https://doi.org/10.5852/ejt.2019.583

Supplementary material 1

Table S1

Authors: Emmanuel D. Delocado, Hendrik Freitag

Data type: Genetic distance

Explanation note: **Table S1.** Kimura 2-parameter (K2P) genetic distance of the samples of *Byrrhinus* specimens, based on their aligned partial *COI-3'* sequences of 723 bp length (in %).

Link: https://doi.org/10.3897/zookeys.1070.70531.suppl1

ZooKeys 1070: 73–86 (2021)
doi: 10.3897/zookeys.1070.58859
https://zookeys.pensoft.net

RESEARCH ARTICLE

A peer-reviewed open-access journal
ZooKeys
Launched to accelerate biodiversity research

Two new species of the genus *Ptychoptera* Meigen, 1803 (Diptera, Ptychopteridae) from Yunnan, China with remarks on the distribution of Chinese species

Xiao Zhang[1], Zehui Kang[1]

1 *Key Lab of Integrated Crop Pest Management of Shandong Province, College of Plant Health and Medicine, Qingdao Agricultural University, Qingdao 266109, China*

Corresponding author: Zehui Kang (kangzehui1987@163.com)

Academic editor: Gunnar Kvifte | Received 21 September 2020 | Accepted 15 October 2021 | Published 11 November 2021

http://zoobank.org/DC161AAB-E0B1-46DF-B38D-2E27AE6B324F

Citation: Zhang X, Kang Z (2021) Two new species of the genus *Ptychoptera* Meigen, 1803 (Diptera, Ptychopteridae) from Yunnan, China with remarks on the distribution of Chinese species. ZooKeys 1070: 73–86. https://doi.org/10.3897/zookeys.1070.58859

Abstract

Sixteen known species of the genus *Ptychoptera* Meigen, 1803 have been recorded from China, of which three occur in Yunnan Province. Herein, two new species from Yunnan, *P. cordata* **sp. nov.** and *P. yunnanica* **sp. nov.**, are described from China. An updated key to *Ptychoptera* is presented for all Chinese species.

Keywords

Chinese fauna, new taxa, phantom crane flies, Ptychopterinae, taxonomy

Introduction

The genus *Ptychoptera* Meigen, 1803 is the largest of the three extant genera in the family Ptychopteridae, with nearly 80 known species (Kang et al. 2019; Boardman 2020). Sixteen *Ptychoptera* species have been previously recorded from China, of which ten species were published recently by Kang et al. (2013) and Kang et al. (2019). The genus *Ptychoptera* can be diagnosed from the other two genera by the following characters: larvae metapneustic and eucephalous, body segments with serially arranged hairs arising from small papillae, and terminal of abdomen with a long retractable respiratory siphon; adults with 13–14 flagellomeres, wing mostly with infuscation, 3 branches of medial vein reaching wing margin, and gonopod with a simple gonocoxite and a varied gonostylus (Rozkošný 1997; Nakamura and Saigusa 2009; Fasbender 2014).

Adults of *Ptychoptera* are often found in sediments rich in organic matter at the margins of streams and reservoirs, or wet forests on the mountains (Wolf et al. 1997; Wolf and Zwick 2001). The adults usually have a long emergence from early spring to late autumn. For example, adults of *P. circinans* Kang, Xue & Zhang, 2019 were collected from March to August, *P. bannaensis* Kang, Yao & Yang, 2013 from April to June and *P. yankovskiana* Alexander, 1945 from June to September (Kang et al. 2013; Kang et al. 2019).

Yunnan Province is situated at the junction of the eastern Asia monsoon region, the tropical monsoon region of southern Asia, the Indo-China and the Tibetan Plateau region (Yang et al. 2004). As one of 25 global biodiversity conservation hotspots, Yunnan is rich in biotic resources (Myers et al. 2000; Myers 2003). Three species of *Ptychoptera* from Yunnan, *P. bannaensis*, *P. lushuiensis* Kang, Yao & Yang, 2013 and *P. wangae* Kang, Yao & Yang, 2013, were first found and described by Kang et al. (2013). Since then, further new materials of the genus from Yunnan became available. In this paper, two new species from Yunnan are described and illustrated. An updated key to *Ptychoptera* species from China is also presented.

Materials and methods

Specimens were collected by net or by Malaise trap and kept in 75% alcohol. Photographs were taken by a Canon EOS-77D and EF 100 mm f/2.8L IS USM. Genitalia were prepared by boiling the apical portion of the abdomen in lactic acid for 0.5–1.0 hours; then they were examined, and illustrations prepared, using a ZEISS Stemi 2000-C stereomicroscope. After examination, the removed abdomen was transferred to fresh glycerine and stored in a microvial pinned to the respective specimen. Type specimens are deposited in the Entomological Museum of Qingdao Agricultural University, Qingdao, China (QAU) and the Entomological Museum of China Agricultural University, Beijing, China (CAU). Morphological terminology is based primarily on McAlpine (1981) and Fasbender (2014).

Taxonomy

Key to *Ptychoptera* from China

1 Wing with r-m arise from R_{4+5}, Rs not longer than r-m (Figs 1c, 3c) **2**
– Wing with r-m arise from Rs before or at fork, Rs at least 1.5 times length of r-m **9**
2 Mesopleuron mostly brown; epandrial clasper brown ..... ***P. circinans* Kang, Xue & Zhang, 2019 (Fujian)**
– Mesopleuron uniformly yellow; epandrial clasper uniformly yellow **3**
3 Gonostylus long and slender, about 1.5 times length of gonocoxite ..... ***P. bannaensis* Kang, Yao & Yang, 2013 (Yunnan)**
– Gonostylus short, as long as gonocoxite (Figs 2c, 4c) **4**
4 Postnotum dark brown with a big yellow spot (Figs 1b, 3b) **5**
– Postnotum uniformly black **6**
5 Wing with spots at forks of R_{1+2}, R_{4+5} and M_{1+2} forming a band (Fig. 1c); abdomen with first tergum yellow with caudal 1/5 light brown (Fig. 1a); subapical spine of epandrium absent (Fig. 2b); anterior lobe of basal lobe of gonostylus not bilobate, medial lobe of basal lobe of gonostylus not bilobate (Fig. 2c); apical process of paramere semilunar, apex expanding outward (Fig. 2c) ..... ***P. cordata* sp. nov. (Yunnan)**
– Wing with spots at forks of R_{1+2}, R_{4+5} and M_{1+2} separated (Fig. 3c); abdomen with first tergum dark brown with basal 1/5 yellow (Fig. 3a); subapical spine of epandrium transverse conical (Fig. 4b); anterior lobe of basal lobe of gonostylus bilobate, medial lobe of basal lobe of gonostylus bilobate (Fig. 4c); apical process of paramere hook-shaped, apex incurvated (Fig. 4c) ..... ***P. yunnanica* sp. nov. (Yunnan)**
6 Wing with a distinct spot at fork of R_{4+5}, spots at forks of R_{1+2} and M_{1+2} weak and nearly invisible ..... ***P. lii* Kang, Yao & Yang, 2013 (Guizhou)**
– Wing with three distinct spots at forks of R_{1+2}, R_{4+5} and M_{1+2} separated or forming a band **7**
7 Second tergum anterior margin yellow with a median brown spot; medial lobe of basal lobe of gonostylus slender, finger-shaped ..... ***P. lushuiensis* Kang, Yao & Yang, 2013 (Yunnan)**
– Second tergum anterior margin yellow brown; medial lobe of basal lobe of gonostylus board, tongue-shaped **8**
8 Abdomen with 5th and 6th terga dark brown, 6th and 7th sterna mostly brown; apical stylus of gonostylus hook-shaped ..... ***P. emeica* Kang, Xue & Zhang, 2019 (Sichuan)**
– Abdomen with 5th and 6th terga mostly yellow, 6th and 7th sterna yellow; apical stylus of gonostylus finger-shaped (Nakamura and Saigusa 2009) ..... ***P. formosensis* Alexander, 1924 (Taiwan; Japan)**

9 Mesopleuron yellow **10**
– Mesopleuron black **12**
10 Wing with bands and clouds **11**
– Wing without band or cloud..... ***P. wangae*** **Kang, Yao & Yang, 2013 (Yunnan)**
11 Base of Rs with an elliptic cloud; abdomen with sterna yellow .....
..... ***P. qinggouensis*** **Kang, Yao & Yang, 2013 (Neimenggu)**
– Base of Rs without cloud; abdomen with sterna black.....
..... ***P. clitellaria*** **Alexander, 1935 (Sichuan)**
12 Epandrial lobes merged with epandrial claspers **13**
– Epandrial lobes not merged with epandrial claspers..... **17**
13 Wing with r-m its own length before fork of Rs; epandrial claspers short and blunt..... ***P. separata*** **Kang, Xue & Zhang, 2019 (Xizang)**
– Wing with r-m close to fork of Rs; epandrial claspers slender..... **14**
14 Wing with an elliptic cloud at middle of CuA_1 ..... **15**
– Wing without an elliptic cloud at middle of CuA_1 ..... **16**
15 Epandrial claspers curved downward, tip bifurcated .....
..... ***P. gutianshana*** **Yang & Chen, 1995 (Zhejiang)**
– Epandrial claspers straight, tip not bifurcated.....
..... ***P. bellula*** **Alexander, 1937 (Jiangxi)**
16 Gonostylus much longer than gonocoxite .....
..... ***P. xinglongshana*** **Yang, 1996 (Gansu)**
– Gonostylus not longer than gonocoxite.....
..... ***P. longwangshana*** **Yang & Chen, 1998 (Zhejiang)**
17 Abdomen with 2nd and 3rd terga brownish black; epandrial claspers finger-shaped and broad basally, curved inwards at middle.....
..... ***P. lucida*** **Kang, Xue & Zhang, 2019 (Xinjiang)**
– Abdomen with 2nd and 3rd terga mostly yellow; epandrial claspers flat and acinaciform, middle of inner edge slightly swollen (Kang et al. 2019).....
..... ***P. yankovskiana*** **Alexander, 1945 (Neimenggu; Korea)**

Ptychoptera cordata **sp. nov.**
http://zoobank.org/6568C6B6-5683-4597-9544-7EEECE70DE88
Figs 1, 2

Material examined. China•1♂, ***holotype*** Yunnan Province, Menghai District, Mengbang Reservoir; 21°54'50"N, 100°17'36"E; 1272 m; 6 Jun. 2019; Z. Kang leg.; QAU•1♂, ***paratype*** same collection data as for preceding; QAU.

Diagnosis. Postnotum dark brown, mediotergite with a cordiform yellow spot; wing marked with two brown bands; apical process of paramere semilunar, apex expanding outward; lateral extension of terminal division of hypandrium triangular with a pair of semicircular lobes medially, terminal division of hypandrium umbelliform.

Description. Male. Body length 7.5–8.0 mm, wing length 7.0–7.5 mm.

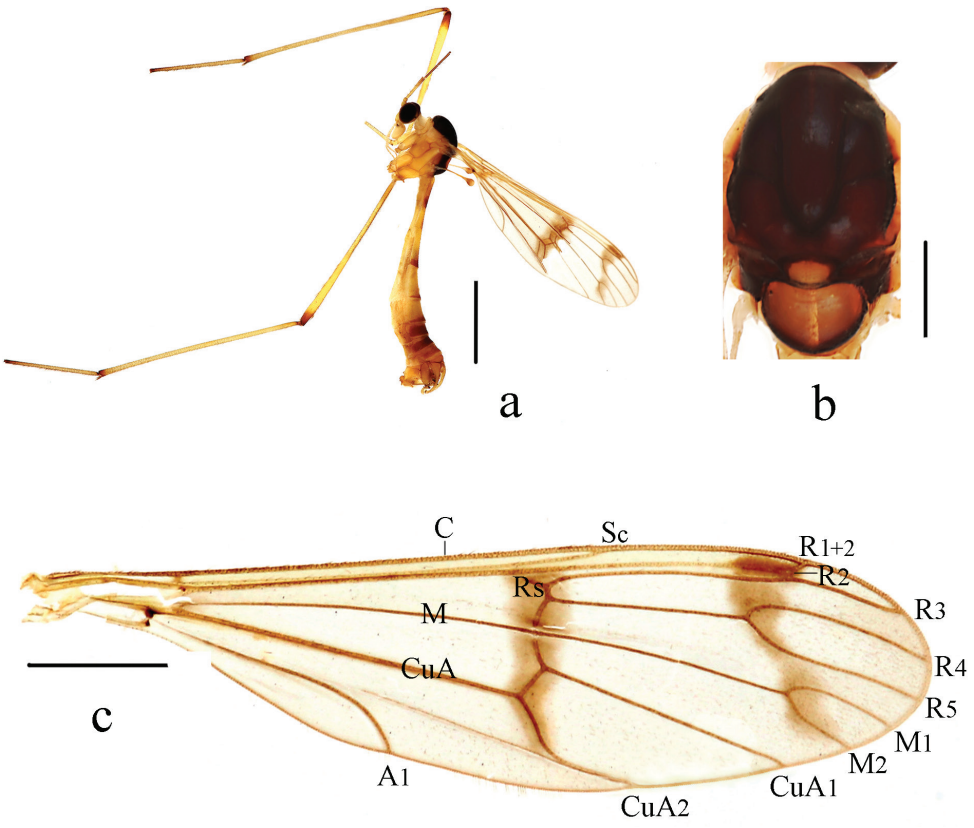

Figure 1. *Ptychoptera cordata* sp. nov. **a** habitus of male, lateral view **b** thorax, dorsal view, **c** wing. Scale bars: 2.0 mm (**a**); 0.5 mm (**b**); 1.0 mm (**c**).

Vertex and frons brown; face and clypeus yellow with light brown hairs; gena yellow with a black elliptical spot medially, hairs on gena brown; occiput yellow. Compound eyes black without pubescence. Scape, pedicel and basal 2/3 of 1st flagellomere yellow, remaining flagellomeres brown, setae dark brown. Proboscis light yellow with light brown hairs. Palpus yellow with last segment gradually darked apically, hairs brown.

Thorax (Fig. 1a, b). Pronotum and propleuron light yellow. Prescutum, scutum and paratergite uniformly black. Scutellum mostly dark brown, middle area yellow with a patch of dense brown hairs. Mediotergite of postnotum dark brown, middle area with a cordiform yellow spot. Laterotergite half brown, outer half yellow with dense dark brown hairs, in dorsal view. Mesopleuron and metapleuron uniformly yellow. Coxae and trochanters yellow; femora yellow with brown ring apically; tibiae yellow with brown ring apically; 1st tarsomere of fore and hind legs yellow brown with brown ring apically. Hairs on legs brown. Wing (Fig. 1c) 3.7 times as long as wide, subhyaline, marked with two brown bands as follows: median band extending from basa of Rs to middle section of CuA_2; subapical band extending from tip of R_1, cover-

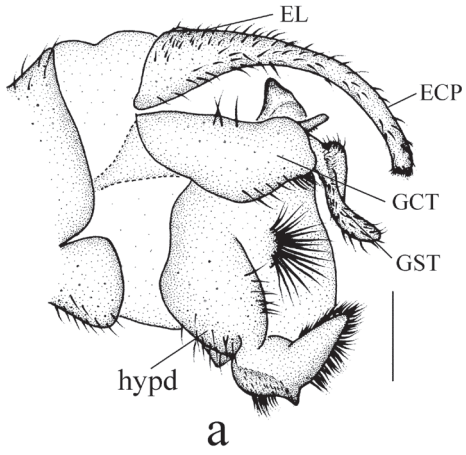
EL
ECP
GCT
GST
hypd

a

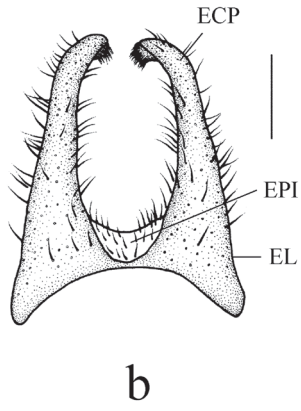
ECP
EPI
EL

b

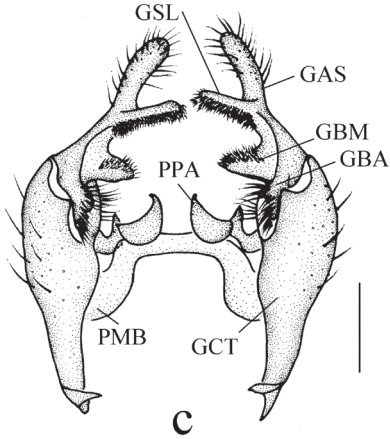
GSL
GAS
GBM
GBA
PPA
PMB
GCT

c

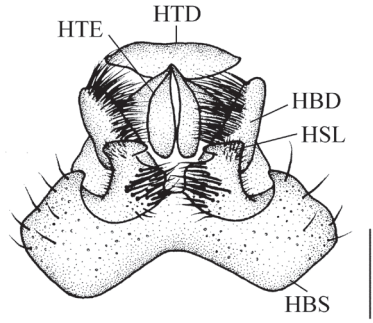
HTE
HTD
HBD
HSL
HBS

d

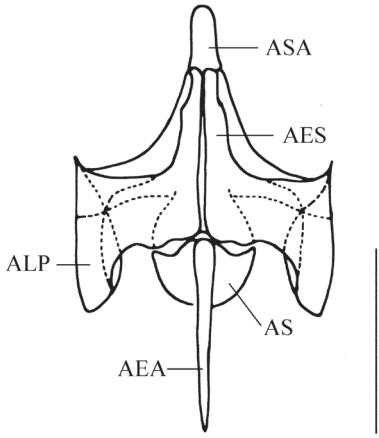
ASA
AES
ALP
AS
AEA

e

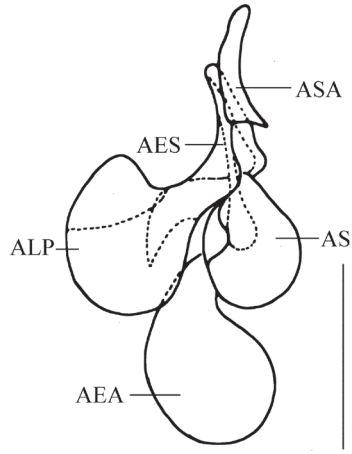
ASA
AES
ALP
AS
AEA

f

ing pterostigma and extending to tip of M_2. Veins brown; Sc ending in C at level of basal 1/3 of R_{2+3}; Rs straight, slightly shorter than r-m; r-m arise from R_{4+5}. Halter and prehaltere pale yellow with brown hairs.

Abdomen (Fig. 1a). First tergum yellow with caudal 1/5 light brown, 2nd tergum yellow with middle area and caudal 1/6 brown, 3rd and 4th terga yellow with posterior margin brown, 5th tergum yellow with caudal 1/2 brown, 6th and 7th terga brown with posterior margin yellow. Sterna yellow. Hairs on abdomen brown.

Male genitalia (Fig. 2) yellow. Epandrium (Fig. 2b) bilobed, epandrial lobe broad, epandrial clasper tapering and curved ventrally to the middle, slender apically, with brown hairs; epiproct with short hairs. Gonocoxite (Fig. 2c) long and stout, 3.3 times as long as wide, basal apodeme small; apical process of paramere semilunar, apex expanding outward. Gonostylus (Fig. 2c): anterior lobe of basal lobe of gonostylus on inner side with dense long hairs; medial lobe of basal lobe of gonostylus tongue-shaped with dense short hairs on posterior margin; secondary lobe of apical stylus of gonostylus finger-shaped with dense short hairs; apical stylus of gonostylus finger-shaped with short hairs. Hypandrium (Fig. 2d): basal scale of hypandrium dumbbell-shaped basally with several hairs; spathate lobe of hypandrium broad at base with dense long hairs on inner side, hook-shaped apically with short hairs on posterior margin; basal division of hypandrium finger-shaped with dense long hairs on inner side; lateral extension of terminal division of hypandrium triangular with a pair of semicircular lobes medially; terminal division of hypandrium umbelliform. Aedeagus (Fig. 2e, f): subapical sclerite tongue-shaped, apex of subapical sclerite round; aedeagal sclerites with apex laterally compressed, with dorsal corner extended anterodorsally, straight sided and convergent, base broad; lateral ejaculatory processes with base straight, narrow, extended straight anterolaterally; discoid apodemes with elongate ovoid dorsal extension; sperm sac subspherical; ejaculatory apodeme flag-like, closely associated with aedeagal sclerites, larger than sperm sac, paralleling anterior margin of sperm sac.

Female. Unknown.

Distribution. China (Yunnan).

Etymology. Specific name from Latin, *cordata* (adjective, feminine, meaning "cordate"), referring to the postnotum with a cordiform spot.

Remarks. This new species is similar to *P. formosensis* from China and Japan but can be separated from the latter by the postnotum dark brown with a cordiform yel-

Figure 2. *Ptychoptera cordata* sp. nov. **a** male genitalia, lateral view **b** epandrium, dorsal view **c** gonocoxite and gonostylus, dorsal view **d** hypandrium, ventral view **e** aedeagus, anterior view **f** aedeagus, lateral view. Scale bars = 0.2 mm. (AEA = Ejaculatory Apodeme, AES = Aedeagal Sclerite, ALP = Lateral Ejaculatory Process, AS = Sperm Sac, ASA = Subapical Sclerite of Aedeagus, ECP = Epandrial Clasper, EL = Epandrial Lobe, EPI = Epiproct, GAS = Apical stylus of gonostylus, GBA = Anterior lobe of basal lobe of gonostylus, GBM = Medial lobe of basal lobe of gonostylus, GCT = Gonocoxite, GSL = Secondary lobe of Apical Stylus of Gonostylus, GST = Gonostylus, HBD = Basal Division of Hypandrium, HBS = Basal scale of Hypandrium, HSL = Spathate Lobe of Hypandrium, HTD = Terminal Division of Hypandrium, HTE = Lateral Extension of Terminal Division, hypd = hypandrium, PMB = Paramere Base, PPA = Apical Process of Paramere).

low spot, the apical stylus of the gonostylus finger-shaped, and the apical process of paramere semilunar with apex expanding outward. In *P. formosensis*, the postnotum is uniformly black, the apical stylus of the gonostylus is flat tongue-like, and the apical process of the paramere is bilobed (Nakamura and Saigusa 2009). This new species is also similar to *P. annandalei* Brunetti, 1918 from Burma, but can be separated from the latter by the apical process of paramere semilunar with apex expanding outward, the apical stylus of the gonostylus and the secondary lobe of the apical stylus of the gonostylus finger-shaped, not crossing. In *P. annandalei*, the apical lobes of the paramere are dorsoventrally flattened and semicircular with the spine curved anteriorly, apices of the apical stylus and secondary lobe of the gonostylus are crossing (Fasbender 2014). This new species is also similar to *P. perbona* Alexander, 1946 from Burma, but can be separated from the latter by the mediotergite with a cordiform yellow spot, the apical stylus of the gonostylus finger-shaped, the apex of the terminal division of the hypandrium with an umbelliform lobe. In *P. perbona*, the mediotergite is uniformly black, the apical stylus of the gonostylus is stylate, the apex of the terminal division of the hypandrium has a pair of needle-like lateral lobes (Alexander 1946; Fasbender 2014).

***Ptychoptera yunnanica* sp. nov.**

http://zoobank.org/A8B3BF32-C722-423F-9FBB-641D0A78B1BB

Figs 3, 4

Material examined. China•1♂, ***holotype*** of *P. yunnanica*; Yunnan Province, Binchuan District, Mt. Jizu; 25°56'38"N, 100°23'58"E; 1875 m; 1 Jun. 2019; Z. Kang leg.; QAU•1♀, ***paratype*** of *P. yunnanica*; same collection data as for preceding; QAU•1♀, ***paratype*** of *P. yunnanica*; Yunnan Province, Panlong District, Yunnan Agricultural University; 25°8'4"N, 102°45'2"E; 1953 m; 28 Apr.–3 Jun. 2016.; L. Wang leg.; Malaise trap; CAU•1♀, ***paratype*** of *P. yunnanica*; Yunnan Province, Panlong District, Yunnan Agricultural University; 25°8'9"N, 102°45'8"E; 1958 m; 28 Apr.–3 Jun. 2016; L. Wang leg.; Malaise trap; CAU•1♂, ***paratype*** of *P. yunnanica*; Yunnan Province, Panlong District, Yunnan Agricultural University; 25°8'22"N, 102°45'14"E; 1965 m; 28 Sep.–24 Nov. 2016; L. Wang leg.; Malaise trap; CAU.

Diagnosis. Postnotum dark brown, mediotergite with a big yellow spot; wing marked with three weak brown clouds at tip of R_1, fork of R_{4+5} and fork of M_{1+2} and a brown band extending from basal of R_{2+3} to middle section of CuA; subapical spine of epandrium transverse conical; basal scale of hypandrium rectangular, anterior margin strongly concaved medially, basal division of hypandrium finger-shaped with dense long hairs basally and medially; terminal division of hypandrium cordiform.

Description. Male. Body length 6.5–8.0 mm, wing length 7–7.5 mm.

Vertex and frons dark brown with brown hairs; face and clypeus yellow with light brown hairs; gena yellow with a black elliptical spot medially, hairs dark brown; occiput yellow. Compound eyes black without pubescence. Scape, pedicel and basal 1/2 of 1st flagellomere yellow, remaining flagellomeres brown, setae on antenna dark

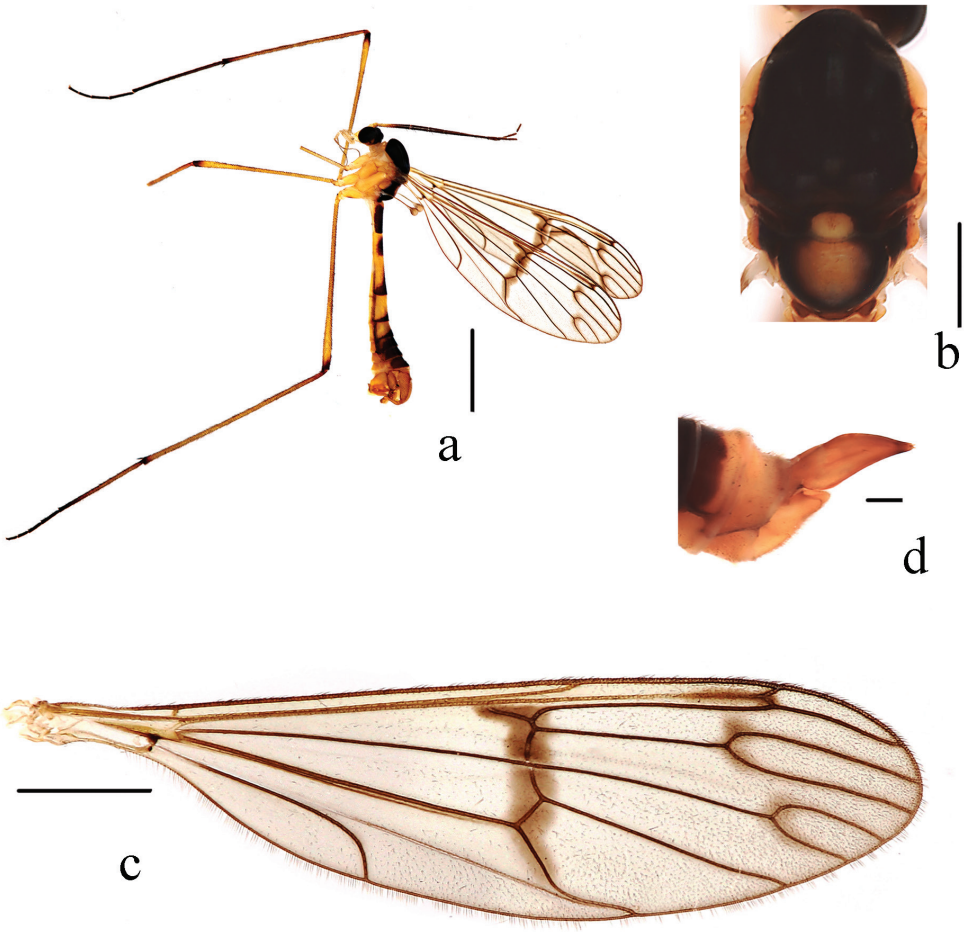

Figure 3. *Ptychoptera yunnanica* sp. nov. **a** habitus of male, lateral view **b** thorax, dorsal view **c** wing **d** female terminalia, lateral view. Scale bars: 2,0 mm (**a**); 0,5 mm (**b**); 1,0 mm (**c**); 0,2 mm (**d**).

brown. Proboscis light yellow with brown hairs. Palpus yellow with terminal of last segment brown, hairs brown.

Thorax (Fig. 3a, b). Pronotum and propleuron light yellow. Prescutum, scutum and paratergite uniformly black. Scutellum mostly brown, middle area yellow with a patch of dense dark brown hairs. Mediotergite of postnotum dark brown, middle area with a big yellow spot. Upper half of laterotergite dark brown, lower half of laterotergite yellow, with brown hairs, in dorsal view. Mesopleuron and metapleuron uniformly yellow. Coxae and trochanters yellow; fore femur yellow and gradually darkened apically; mid and hind femora yellow with brown ring apically; tibiae yellowish brown with brown ring apically; 1st tarsomere of fore and mid legs brown, 1st tarsomere of hind leg yellow with a narrow dark brown ring apically, other tarsomeres dark brown. Hairs on legs dark brown. Relative length of 1st to 5th tarsomeres in hind leg as 7: 2: 1.2: 1: 1.

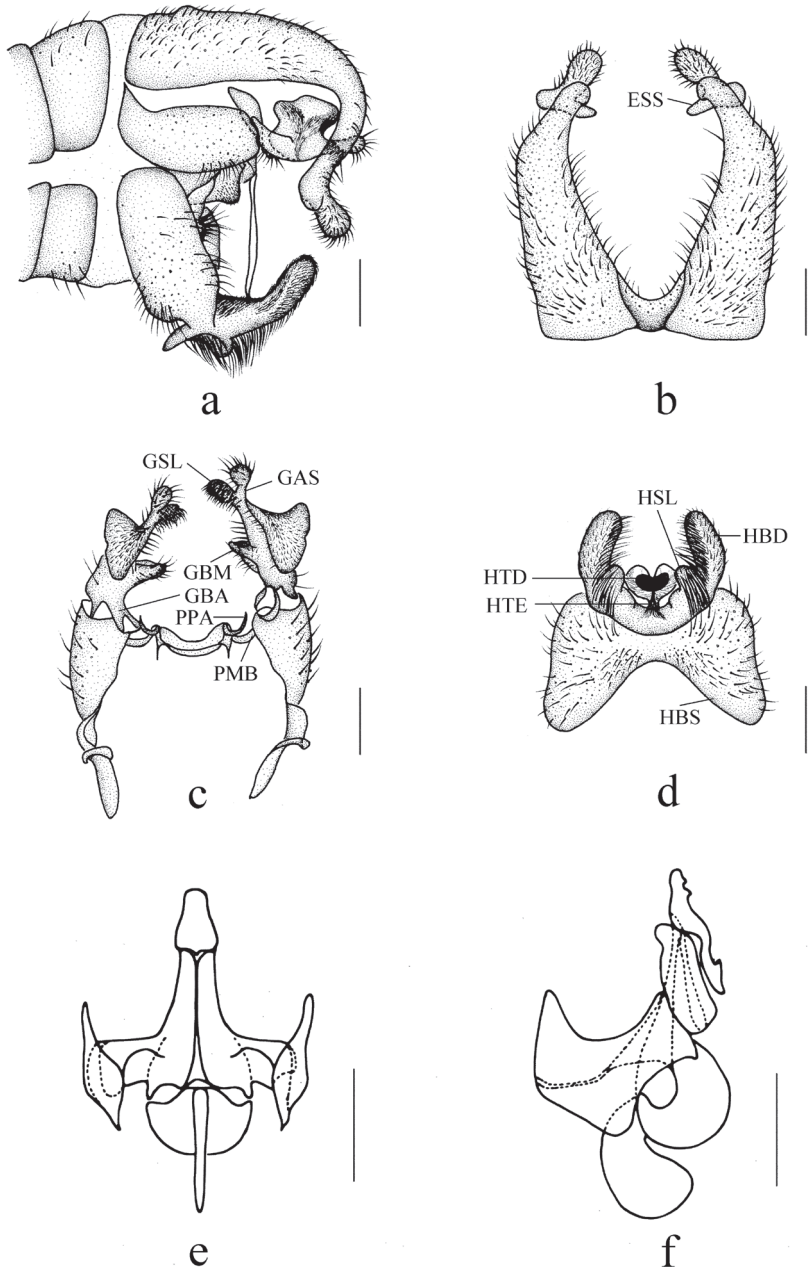

Figure 4. *Ptychoptera yunnanica* sp. nov. **a** male genitalia, lateral view **b** epandrium, dorsal view **c** gonocoxite and gonostylus, dorsal view **d** hypandrium, ventral view **e** aedeagus, anterior view **f** aedeagus, lateral view. Scale bars: 0.2 mm. (ESS = Subapical Spine of Epandrium, GAS = Apical stylus of gonostylus, GBA = Anterior lobe of basal lobe of gonostylus, GBM = Medial lobe of basal lobe of gonostylus, GSL = Secondary lobe of Apical Stylus of Gonostylus, HBS = Basal scale of Hypandrium, HSL = Spathate Lobe of Hypandrium, HTD = Terminal Division of Hypandrium, HTE = Lateral Extension of Terminal Division, hypd = hypandrium, PMB = Paramere Base, PPA = Apical Process of Paramere).

Wing (Fig. 3c) 3.8 times as long as wide, subhyaline, marked with three brown clouds and a brown band as follows: three weak brown clouds at tip of R_1, fork of R_{4+5} and fork of M_{1+2}; median band extending from basa of Rs to middle section of CuA_2. Veins brown; Sc ending in C not at level of basal 1/3 of R_{2+3}; Rs straight, slightly longer than r-m; r-m arise from R_{4+5}. Halter and prehaltere pale yellow with brown hairs.

Abdomen (Fig. 3a). First tergum dark brown with basal 1/5 yellow, 2nd tergum yellow with middle area and caudal 1/6 dark brown, 3rd tergum yellow with caudal 1/5 dark brown, 4th tergum yellow with caudal 1/4 dark brown, 5th to 7th terga dark brown. Sterna yellow. Hairs on abdomen brown.

Male genitalia (Fig. 4) yellow. Epandrium (Fig. 4b) bilobed, epandrial lobe broad, epandrial clasper tapering distally and curved downward, slightly swollen apically; subapical spine of epandrium transverse conical, with brown hairs; epiproct with short hairs. Gonocoxite (Fig. 4c) short and slender, 2 times as long as wide, basal apodeme 3/4 as long as gonocoxite; apical process of paramere hook-shaped, apex incurvated. Gonostylus (Fig. 4c): anterior lobe of basal lobe of gonostylus bilobate without hairs; medial lobe of basal lobe of gonostylus finger-shaped on middle of inner side with short hairs; secondary lobe of apical stylus of gonostylus fan-shaped basally without hairs, finger-shaped apically with dense short setae; apical stylus of gonostylus finger-shaped with dense short hairs. Hypandrium (Fig. 4d): basal scale of hypandrium rectangular, anterior margin strongly concaved medially; spathate lobe of hypandrium papillary without hairs; basal division of hypandrium finger-shaped with dense long hairs basally and medially; lateral extension of terminal division thin; terminal division of hypandrium cordiform. Aedeagus (Fig. 4e, f): subapical sclerite tongue-shaped, slightly caved bilaterally, apex of subapical sclerite round; aedeagal sclerites with apex laterally compressed, with dorsal corner extended anterodorsally, straight sided and convergent, base broad; lateral ejaculatory processes with base straight, narrow, extended straight anterolaterally; apodemes with elongate quadrangular dorsal extension; sperm sac subspherical; ejaculatory apodeme flag-like, closely associated with aedeagal sclerites, subequal to sperm sac, paralleling anterior margin of sperm sac.

Female. Body length 8.5–9.0 mm, wing length 9.0–9.5 mm. Similar to male. Third tergum yellow with caudal 1/3 brown, 4th and 5th terga brown, 6th tergum brown with caudal 1/3 yellow, 7th and 8th terga yellow. Terminalia (Fig. 3d): 8th sternum yellow, 2.8 times as long as 7th sternum; cercus yellow with brown end, blade-shaped, 10th tergum + cercus 1.8 times as long as 8th sternum.

Distribution. China (Yunnan).

Etymology. Specific name *yunnanica* (adjective, feminine) referring to the type locality, Yunnan.

Remarks. This new species is similar to *P. persimilis* Alexander, 1947 from Burma, but can be separated from it by have a mediotergite with a big yellow spot, the subapical spine of the epandrium transverse conical, the apical process of the paramere hook-shaped with the apex incurvated. In *P. persimilis*, the mediotergite does not have a big yellow spot, only the adjoining portion of the scutellum is yellow; the epandrium is nematoform, the apex is expanded and slipper-like, the paramere has elongate, ribbon-

like spines directed posterior, crossing medially (Alexander 1947; Fasbender 2014). This new species is also similar to *P. praescutellaris* Alexander, 1946 from Burma, but can be separated from it by having the subapical spine of the epandrium transverse conical, and the secondary lobe of the apical stylus finger-shaped. In *P. praescutellaris*, the apex of the epandrial clasper is bulbous and without a conical projection, and the secondary lobe of the apical stylus is subtrapezoidal (Alexander 1946; Fasbender 2014). This new species resembles somewhat *P. emeica* from China but can be easily separated from the latter by the postnotum dark brown with a big yellow spot, the basal 1/3 of the yellow second abdomen tergum with a median brown spot, the subapical spine of the epandrium transverse conical, and the medial lobe of the basal lobe of the gonostylus finger-shaped. In *P. emeica*, the postnotum is uniformly black, the basal 1/3 of the second tergum of the abdomen is uniformly brown, the epandrium has no transverse conical subapical spine, and the medial lobe of the basal lobe of the gonostylus is broad and tongue-shaped (Kang et al. 2019). Finally, the new species can be separated from *P. lushuiensis* from China by the postnotum dark brown with a big yellow spot, the subapical spine of the epandrium transverse conical, the apical process of the paramere hook-shaped with the apex incurvated, and the terminal division of the hypandrium cordiform. In *P. lushuiensis*, the postnotum is uniformly black, the surstylus of the epandrium does not have a transverse conical subapical spine, the apical process of paramere is sclerotized triangular, and the terminal division of hypandrium cordiform is X-shaped (Kang et al. 2013).

Distribution of *Ptychoptera* species in China

In total, 18 species of *Ptychoptera* are recorded from China. According to Fasbender (2014), the *Ptychoptera* fauna of China is a complex of the *P. tibialis* group, the *P. contaminata* group, the Southeast Asian *Ptychoptera* and unplaced species. One species, *P. separata*, is endemic to Tibet, China and belongs to the *P. tibialis* group, which otherwise is mainly distributed in the Indian Subcontinent. Two species, *P. lucida* and *P. yankovskiana*, can clearly be characterized as species of the *P. contaminata* group and are distributed in the East Palaearctic region. Twelve Southeast Asian *Ptychoptera* species, namely *P. bannaensis*, *P. bellula*, *P. circinans*, *P. cordata*, *P. emeica*, *P. formosensis*, *P. gutianshana*, *P. lii*, *P. longwangshana*, *P. lushuiensis*, *P. wangae*, *P. yunnanica* are widely distributed in Southwest and East China. *Ptychoptera qinggouensis* has the same characteristics as species of Southeast Asian *Ptychoptera* and is distributed in Inner Mongolia. Two species with insufficient material or illustrations for placement, *P. clitellaria* and *P. xinglongshana*, are distributed in Gansu and Sichuan, respectively (Fig. 5).

Acknowledgements

We express our sincere thanks to Ding Yang (Beijing) for his great help during the study. We are grateful to Liang Wang (Beijing) for collecting specimens. This work was funded by the National Natural Science Foundation of China [41901061], the

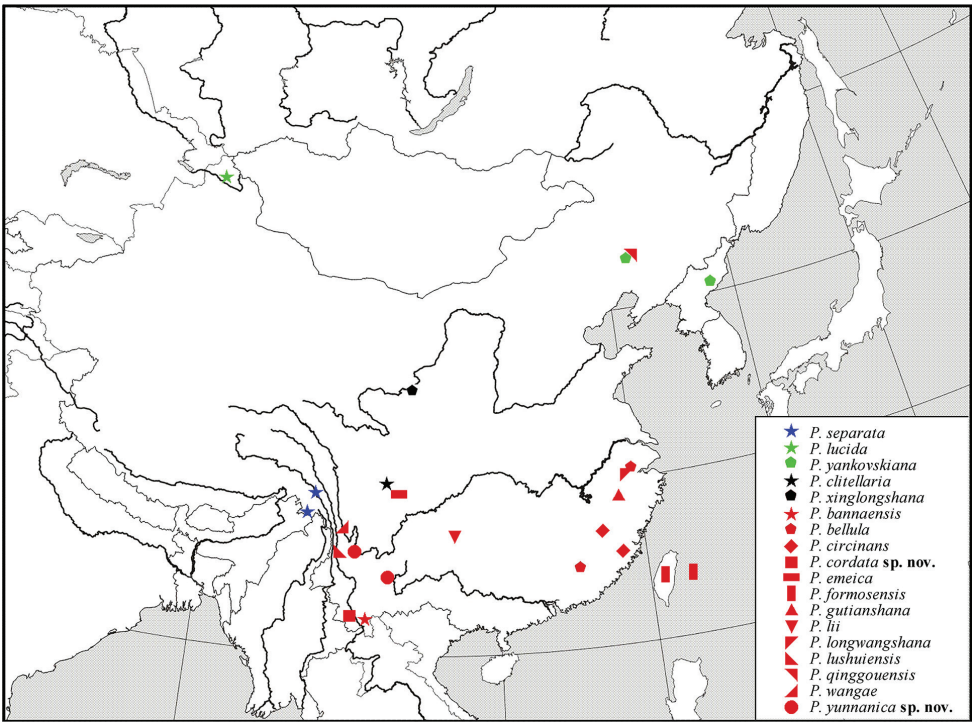

Figure 5. Distribution map of *Ptychoptera* from China.

Shandong Provincial Natural Science Foundation, China [ZR2019BC034] and the High-level Talents Funds of Qingdao Agricultural University, China [663-1119008].

References

Alexander CP (1924) Undescribed species of Japanese Ptychopteridae (Diptera). Insecutor Inscitiae Menstruus 9: 80–83.

Alexander CP (1935) New or little-known Tipulidae from eastern Asia (Diptera). XXIII-XXVII. The Philippine Journal of Science 56: 339–372.

Alexander CP (1937) New species of Ptychopteridae (Diptera). Bulletin of the Brooklyn Entomological Society 32: 140–143.

Alexander CP (1945) Undescribed species of crane-flies from northern Korea (Diptera, Tipuloidea). Transactions of the Royal Entomological Society of London 95: 227–246. https://doi.org/10.1111/j.1365-2311.1945.tb00261.x

Alexander CP (1946) Entomological results from the Swedish expedition 1934 to Burma and British India. Diptera: Ptychopteridae. Collected by René Malaise. Arkiv for Zoologi 38A(2): 1–10.

Alexander CP (1947) New species of Ptychopteridae. Part III. Bulletin of the Brooklyn Entomological Society 42: 19–24.

Boardman P (2020) Twenty-one new species of craneflies (Diptera: Tipulidae and Limoniidae), and a new fold-wing cranefly (Diptera: Ptychopteridae) from Mount Kupe, Cameroon, with notes on eighteen other species new to the country from the same location. Entomologists Monthly Magazine 156: 163–206. https://doi.org/10.31184/M00138908.1563.4042

Fasbender A (2014) Phylogeny and diversity of the phantom crane flies (Diptera: Ptychopteridae). PhD Dissertation, Iowa State University, Ames, 855 pp.

Kang ZH, Xue ZX, Zhang X (2019) New species and record of *Ptychoptera* Meigen, 1803 (Diptera: Ptychopteridae) from China. Zootaxa 4648(3): 455–4723. https://doi.org/10.11646/zootaxa.4648.3.3

Kang ZH, Yao G, Yang D (2013) Five new species of *Ptychoptera* Meigen with a key to species from China (Diptera: Ptychopteridae). Zootaxa 3682(4): 541–555. https://doi.org/10.11646/zootaxa.3682.4.5

McAlpine JF (1981) Morphology and terminology: Adults. In: McAlpine JF, Peterson BV, Shewell GE, Teskey HJ,Vockeroth JR, Wood DM (Eds) Manual of Nearctic Diptera Vol. 1. Agriculture Canada monograph 27. Agriculture Canada, Ottawa, pp. 9–63.

Meigen JW (1803) Versuch einer neuen Gattungs-Eintheilung der europaischen zweiflugligen Insekten. Magazin für Insektenkunde (Illiger) 2: 259–281.

Myers N (2003) Biodiversity hotspots revisited. BioScience 53: 916–917. https://doi.org/10.1641/0006-3568(2003)053[0916:BHR]2.0.CO;2

Myers N, Mittermeier RA, Mittermeier CG, da Fonseca GAB, Kent J (2000) Biodiversity hotspots for conservation priorities. Nature 403: 853–858. https://doi.org/10.1038/35002501

Nakamura T, Saigusa T (2009) Taxonomic study of the family Ptychopteridae of Japan (Diptera). Zoosymposia 3: 273–303. https://doi.org/10.11646/zoosymposia.3.1.23

Rozkošný R (1997) Family Ptychopteridae. Contributions to a manual of Palaearctic Diptera (with special reference to flies of economic importance), Volume 2: Nematocera and lower Brachycera: 291–297.

Wolf B, Zwick P, Marxsen J (1997) Feeding ecology of the freshwater detritivore *Ptychoptera paludosa* (Diptera, Nematocera). Freshwater Biology 38: 375–386. https://doi.org/10.1046/j.1365-2427.1997.00250.x

Wolf B, Zwick P (2001) Life cycle, production, and survival rates of *Ptychoptera paludosa* (Diptera: Ptychopteridae). International Review of Hydrobiology 86: 661–674. https://doi.org/10.1002/1522-2632(200110)86:6<661::AID-IROH661>3.0.CO;2-0

Yang JK, Chen HY (1995) Diptera: Ptychopteridae. In: Zhu, T. (Ed.). Insects and Macrofungi of Gutianshan, Zhejiang. Zhejiang Scientech Press, Hangzhou, pp. 180–182.

Yang JK, Chen HY (1998) Diptera: Ptychopteridae. In: Wu, H. (Ed.). Insects of Longwangshan Nature Reserve. China Forestry Publishing House, Beijing, pp. 240–241.

Yang JK (1996) New record of family Ptychopteridae in Xinglongshan (Diptera: Ptychopteridae). In: Wang X (Ed.) Resources Background Investigation of Gansu Xinglongshan National Nature Reserve. Gansu Minorities Press, Gansu, pp. 288–289.

Yang YM, Tian K, Hao JM, Pei SJ, Yang YX (2004) Biodiversity and biodiversity conservation in Yunnan, China. Biodiversity and Conservation 13(4): 813–826. https://doi.org/10.1023/b:bioc.0000011728.46362.3c

ZooKeys 1070: 87–99 (2021)
doi: 10.3897/zookeys.1070.67779
https://zookeys.pensoft.net

RESEARCH ARTICLE

A peer-reviewed open-access journal
ZooKeys
Launched to accelerate biodiversity research

New species of the genus *Ptychoptera* Meigen, 1803 (Diptera, Ptychopteridae) from Zhejiang, China with an updated key to Chinese species

Jiaqi Shao[1], Zehui Kang[1]

1 *Key Lab of Integrated Crop Pest Management of Shandong Province, College of Plant Health and Medicine, Qingdao Agricultural University, Qingdao 266109, China*

Corresponding author: Zehui Kang (kangzehui1987@163.com)

Academic editor: Gunnar Kvifte | Received 23 April 2021 | Accepted 15 October 2021 | Published 11 November 2021

http://zoobank.org/87CD8309-552D-43BC-B870-4184B09311A1

Citation: Shao J, Kang Z (2021) New species of the genus *Ptychoptera* Meigen, 1803 (Diptera, Ptychopteridae) from Zhejiang, China with an updated key to Chinese species. ZooKeys 1070: 87–99. https://doi.org/10.3897/zookeys.1070.67779

Abstract

We revise the taxonomy of the genus *Ptychoptera* Meigen, 1803 from Zhejiang, East China. One new species from Zhejiang, *P. tianmushana* **sp. nov.**, is described and illustrated. Morphologically, the new species is most similar to *P. emeica* Kang, Xue & Zhang, 2019 and *P. formosensis* Alexander, 1924, but it can be distinguished by the coloration of the abdomen and the details of the male genitalia. In addition, *P. bellula* Alexander, 1937 is recorded from Zhejiang for the first time. Two known species from Zhejiang, *P. longwangshana* Yang & Chen, 1998 and *P. gutianshana* Yang & Chen, 1995, are redescribed and illustrated. A key to Chinese species of *Ptychoptera* is provided.

Keywords

Classification, distribution, phantom crane flies, Ptychopterinae, taxonomic revision

Introduction

The genus *Ptychoptera* Meigen, 1803 is the most species-rich groups worldwide in the family Ptychopteridae, with a total number of nearly 80 known species (Rozkošný 1997; Zwick and Starý 2003; Hancock et al. 2006; Nakamura and Saigusa 2009; Ujvárosi et al. 2011; Kang et al. 2019). It is characterized by the following characters: larvae eucephalic or metapneustic, body segments with serially arranged hairs; abdominal segments 1–3 with a pair of prolegs ventrally; prolegs each with a single hook-like spine; posterior end of abdomen produced into a fairly long retractile respiratory siphon; flagellum in adults 13-segmented; wing with M_{1+2} forked; gonopod with a simple gonocoxite and a gonostylus of variable shape (Alexander 1981; Rozkošný 1997; Nakamura and Saigusa 2009).

Sixteen *Ptychoptera* species were known to occur in China, of which 10 species were published by Kang et al. (2013, 2019). Since these publications, additional new materials of the genus from Zhejiang, China have become available. Zhejiang Province is located on the southeast coast of China. As it is in the middle of subtropical zone with monsoon humid climate and superior natural conditions, Zhejiang is rich in biotic resources. One area, Mount Tianmushan is one of the biodiversity hotspots in China (Zhao et al. 2016).

Two species of *Ptychoptera* were previously recorded from Zhejiang: *P. longwangshana* Yang & Chen, 1998 and *P. gutianshana* Yang & Chen, 1995. In this paper, two *Ptychoptera* species are added to the fauna of Zhejiang, of which *P. tianmushana* sp. nov. is described and illustrated as new to science, and *P. bellula* Alexander, 1937, known previously only from Jiangxi, China, is newly recorded from Zhejiang. In addition, the two known species from Zhejiang are redescribed and illustrated based on the type specimens. A key to Chinese species of *Ptychoptera* based on the type and non-type specimens and literature is provided, and we provide an updated distribution map of *Ptychoptera* species from China (Fig. 1).

Material and methods

Type specimen of the new species in this study was collected from Mount Tianmushan, Zhejiang, China, in June 2019 and deposited in the Entomological Museum of Qingdao Agricultural University, Shandong, China (QAU). Type and determined specimens of *P. bellula* were deposited in the National Museum of Natural History, Smithsonian Institution, Washington, DC, USA (USNM). The determined specimen of *P. bellula* was previously identified by Alexander in 1939 and the identification label is provided (Fig. 4f). Type specimens of *P. longwangshana* and *P. gutianshana* were deposited in the Entomological Museum of China Agricultural University, Beijing, China (CAU). Photographs were captured by a Canon EOS 90D digital camera through a macro lens. Genitalia were prepared by boiling the apical portion of the abdomen in lactic acid for 0.5–1 h and then were examined and illustrations prepared by using a ZEISS Stemi 2000-C stereomicroscope. After examination, the removed abdomen was transferred to fresh glycerine and stored in a microvial on the pin with the specimen.

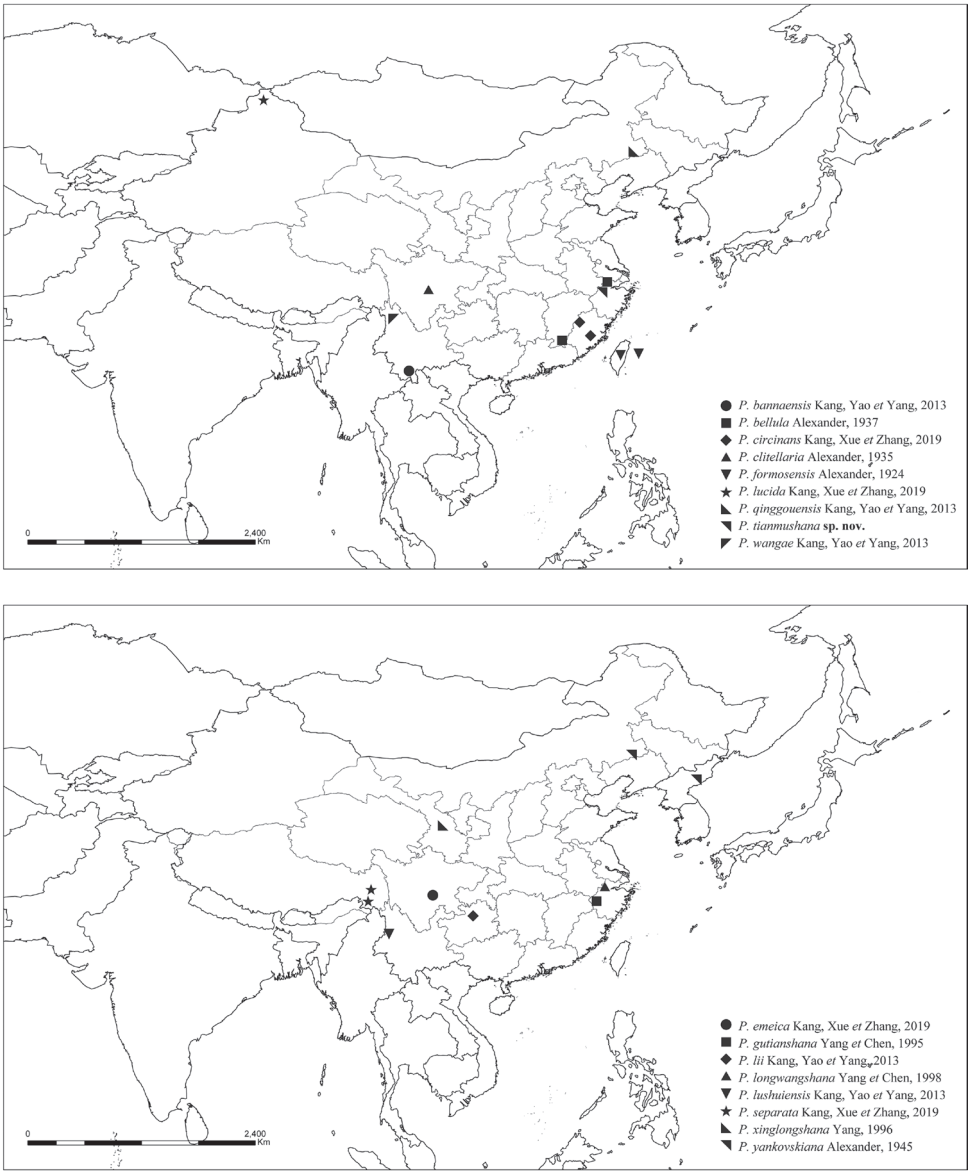

Figure 1. Distribution map of *Ptychoptera* from China.

The present key is an emendation of the identification key of Kang et al. (2019) based on their comprehensive morphology data. Morphological terminology is based primarily on McAlpine (1981) and Fasbender (2014). The following abbreviations in figures are used: aea = ejaculatory apodeme, aes = aedeagal sclerite, alp = lateral ejaculatory process, as = sperm sac, asa = subapical sclerite of aedeagus, epand = epandrium, gas = apical stylus of gonostylus, gbl = basal lobe of gonostylus, goncx = gonocoxite, gonst = gonostylus, hypd = hypandrium, pm = paramere, prct = proctiger, sur = surstylus.

Taxonomy

Key to Chinese species of *Ptychoptera*

1 Wing with r-m beyond fork of Rs, Rs not longer than r-m (Fig. 2c) **2**
– Wing with r-m before or at fork of Rs, Rs at least 1.5 times length of r-m (Figs 4e, 5a, b) **8**
2 Mesopleuron mostly brown, epandrium yellow with caudal 1/2 brown..... ..... ***P. circinans*** **Kang, Xue & Zhang, 2019 (Fujian)**
– Mesopleuron uniformly yellow, epandrium uniformly yellow (Fig. 2a) **3**
3 Gonostylus long and slender, about 1.5 times length of gonocoxite .... ***P. bannaensis*** **Kang, Yao & Yang, 2013 (Yunnan)**
– Gonostylus short, as long as gonocoxite (Figs 3c, 5e) **4**
4 Wing with a distinct spot at fork of R_{4+5}, two spots at forks of R_{1+2} and M_{1+2} weak and nearly invisible ..... ***P. lii*** **Kang, Yao & Yang, 2013 (Guizhou)**
– Wing with three distinct spots at forks of R_{1+2}, R_{4+5} and M_{1+2} separated (Fig. 2c) or forming a band (Figs 4e, 5a, b) **5**
5 Basal 1/3 of second tergum of abdomen yellow with a median brown spot; lobe on middle area of gonostylus digitiform, slender .... ***P. lushuiensis*** **Kang, Yao & Yang, 2013 (Yunnan)**
– Basal 1/3 of second tergum of abdomen uniformly brown (Fig. 2a); lobe on middle area of gonostylus broad, tongue-shaped (Fig. 3c) **6**
6 Abdomen with 5th and 6th terga dark brown (Fig. 2a), tip of gonostylus with a hook-shaped ventral lobe (Fig. 3c) 7
– Abdomen with 5th and 6th terga mostly yellow, tip of gonostylus with a digitiform ventral lobe (Nakamura and Saigusa 2009) .... ***P. formosensis*** **Alexander, 1924 (Taiwan; Japan)**
7 Sixth and 7th sterna yellow, tip of surstylus curved up when viewed from the lateral side (Fig. 3a), retrose basal projection on inner side with tip bilobate (Fig. 3c), paramere with a pair of hook-shaped projections and a pair of conical projections (Fig. 3c), subapical sclerite of aedeagus serrated with five teeth (Fig. 3f)..... ..... ***P. tianmushana*** **Shao & Kang, sp. nov. (Zhejiang)**
– Sixth and 7th sterna mostly brown, tip of surstylus not curved up when viewed from the lateral side, retrose basal projection on inner side not bilobate at tip, paramere with a pair of slender L-shaped projections, subapical sclerite of aedeagus serrated with two teeth..... ***P. emeica*** **Kang, Xue & Zhang, 2019 (Sichuan)**
8 Mesopleuron yellow (Fig. 2a) **9**
– Mesopleuron black (Fig. 4a–c) **12**
9 Wing with bands and marks (Figs 2c, 4e, 5a, b) **10**
– Wing without band or mark **11**
10 Base of Rs with an elliptic mark, abdomen with sterna yellow..... ..... ***P. qinggouensis*** **Kang, Yao & Yang, 2013 (Neimenggu)**
– Base of Rs without mark, abdomen with sterna black .... ***P. clitellaria*** **Alexander, 1935 (Sichuan)**

11 Wing with r-m its own length before fork of Rs, epandrium without long surstylus ..... ***P. separata*** **Kang, Xue & Zhang, 2019 (Xizang)**
– Wing with r-m close to fork of Rs, epandrium with a pair of long surstylus ..... ***P. wangae*** **Kang, Yao & Yang, 2013 (Yunnan)**
12 Epandrium with surstylus curved downward (Figs 3a, 5c) **13**
– Epandrium with surstylus not curved downward **14**
13 Wing with an elliptic mark at middle of CuA_1 (Fig. 5b), tip of surstylus bifurcated (Fig. 5c) ..... ***P. gutianshana*** **Yang & Chen, 1995 (Zhejiang)**
– Wing without mark at middle of CuA_1 (Fig. 5a), tip of surstylus not bifurcated ..... ***P. longwangshana*** **Yang & Chen, 1998 (Zhejiang)**
14 Gonostylus much longer than gonocoxite.... ***P. xinglongshana*** **Yang, 1996 (Gansu)**
– Gonostylus not longer than gonocoxite (Figs 3c, 5e) **15**
15 Wing with an elliptic mark at middle of CuA_1 (Fig. 4a, b, e) ..... ***P. bellula*** **Alexander, 1937 (Jiangxi, Zhejiang)**
– Wing without mark at middle of CuA_1 (Figs 2c, 5a) **16**
16 Abdomen with 2nd and 3rd terga brownish black; surstylus digitiform and broad basally, curved inwards at middle ..... ***P. lucida*** **Kang, Xue & Zhang, 2019 (Xinjiang)**
– Abdomen with 2nd and 3rd terga mostly yellow; surstylus flat and acinaciform, middle of inner edge slightly swollen (Kang et al. 2019) ..... ***P. yankovskiana*** **Alexander, 1945 (Neimenggu; Korea)**

Ptychoptera tianmushana **Shao & Kang, sp. nov.**
http://zoobank.org/85E310AB-B6CC-4C07-841A-4E2BED7ED0C5
Figures 2, 3

Type material. ***Holotype*** male (QAU), China, Zhejiang Province, Lin'an District, Mount Tianmushan, 2019.V.15, Xiao Zhang.

Diagnosis. Wing marked with two brown bands. Epandrium bilobed, each lobe strongly elongated and forming a long surstylus, surstylus broadest at base, tapering and curved downward distally to middle, curving up at tip. Gonostylus with four projections and lobes. Hypandrium rectangular, posterior margin with a V-shaped projection bearing dense long hairs posteriorly, a triangular projection bearing dense short hairs laterally and a pair of elliptic projections bearing dense long hairs posteriorly.

Description. Male. Body length 7.0 mm, wing length 8.0 mm.

Head mostly dark brown, except gena yellow with a black elliptical spot intermediately; clypeus yellow; hairs on head dark brown. Compound eyes black without pubescence. Antenna with scape, pedicel and basal half of 1st flagellomere yellow, other flagellomeres light brown, hairs on antenna brown. Proboscis yellow with brown hairs. Palpus yellow with last segment light brown, hairs brown.

Thorax (Fig. 2b). Pronotum yellow. Propleuron yellow. Mesonotum mostly dark brown with middle area of scutellum yellow and lower half of laterotergite yellow.

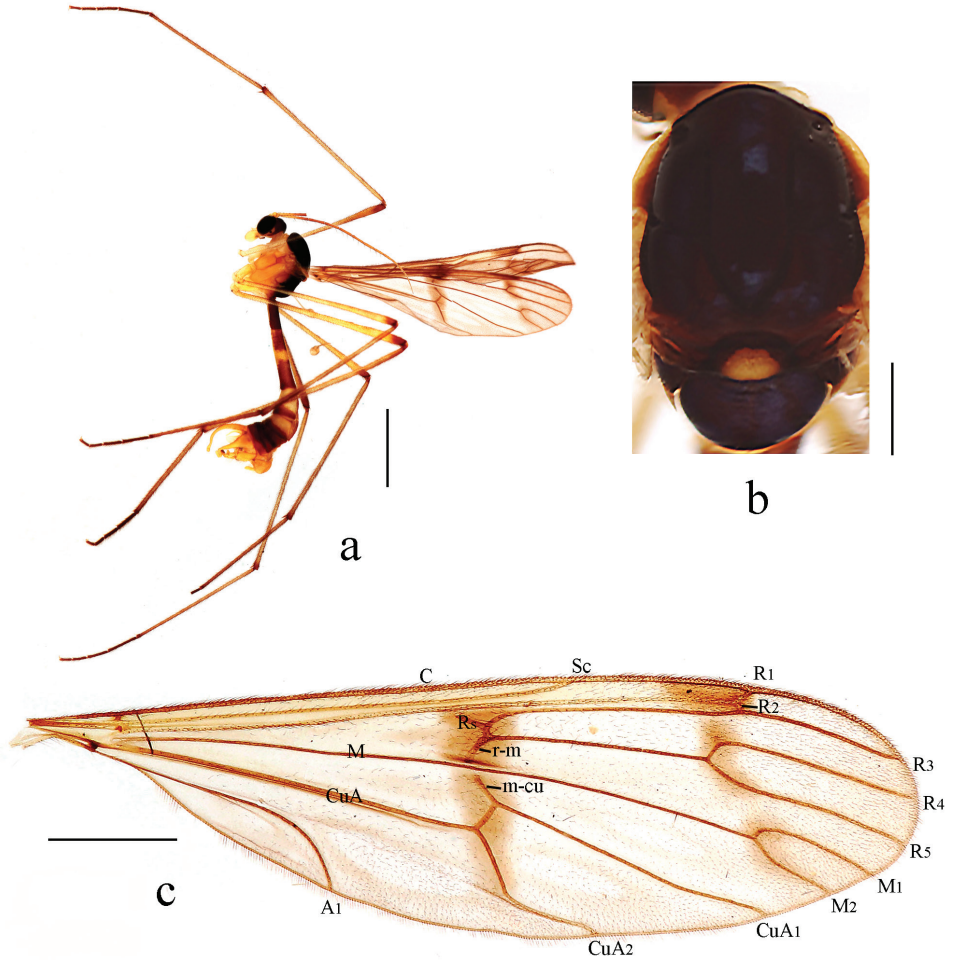

Figure 2. *Ptychoptera tianmushana* sp. nov. **a** habitus of male, lateral view **b** thorax, dorsal view **c** wing. Scale bars: 2.0 mm (**a**); 0.5 mm (**b**); 1.0 mm (**c**).

Mesopleuron uniformly yellow. Coxae and trochanters yellow; fore femur yellow and gradually darkened apically; mid and hind femora yellow with brown ring apically; tibiae yellow with brown ring apically; 1st tarsomere yellow brown and gradually darkened apically, 2nd to 5th tarsomeres uniformly dark brown. Hairs on legs brown. Relative length of 1st to 5th tarsomeres in hind leg as 11.2 : 2.8 : 1.6 : 1 : 1. Wing (Fig. 2c) 3.4 times as long as wide, subhyaline, marked with two brown bands as follows: median band broad and distinct, extending from basal part of cell r_{2+3} to fork of CuA; subapical band extending from anterior margin of wing, covering tip of R_1 and R_2, fork of R_{4+5}, and extending to fork of M_{1+2}, slightly separated into three marks. Veins brown; Sc ending in C not at level of basal third of R_{2+3}; Rs straight, as long as r-m. Haltere and prehaltere pale yellow with brown hairs.

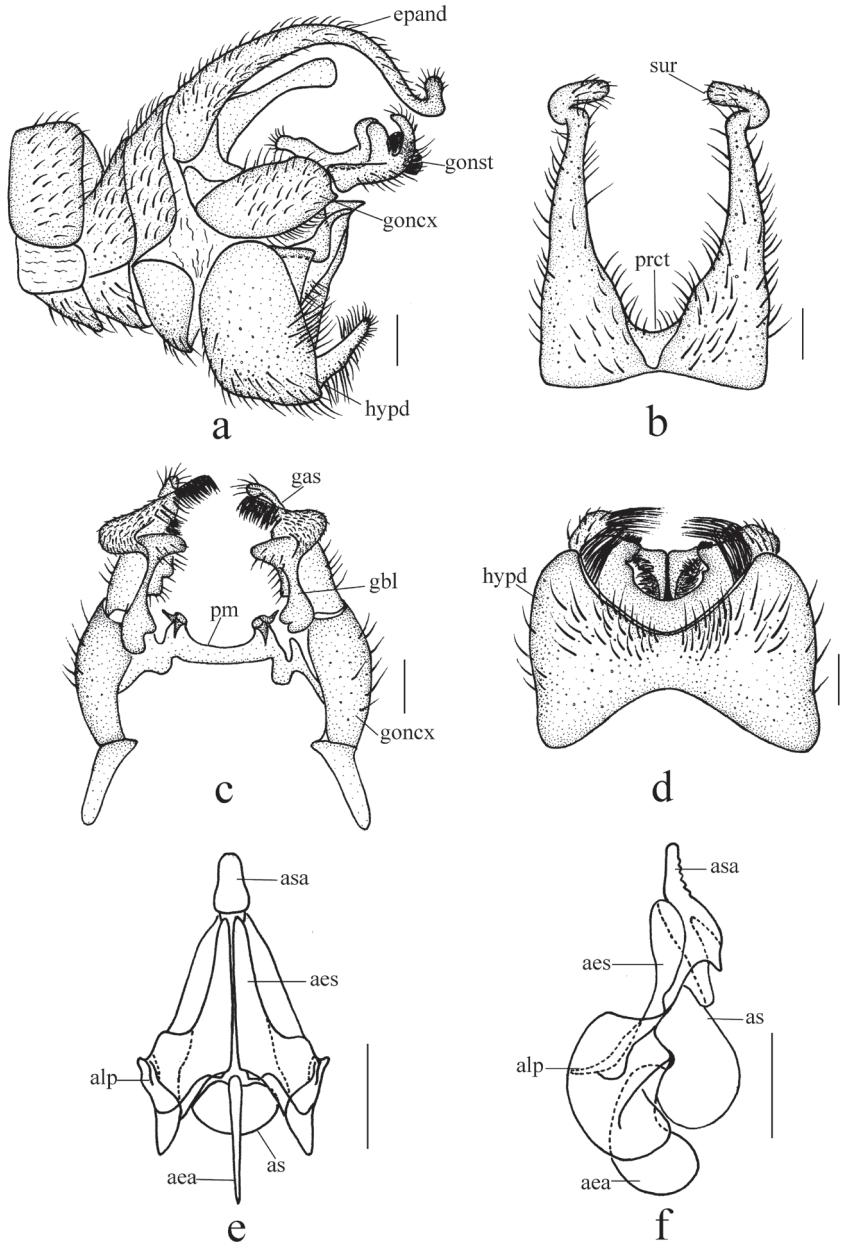

Figure 3. *Ptychoptera tianmushana* sp. nov. **a** male genitalia, lateral view **b** epandrium, dorsal view **c** gonocoxite and gonostylus, dorsal view **d** hypandrium, ventral view **e** aedeagus, anterior view **f** aedeagus, lateral view. Scale bars: 0.2 mm.

Abdomen. First tergum brown, 2nd tergum brown with middle quarter area yellow, 3rd and 4th terga pale yellow with caudal third brown, 5th to 7th terga uniformly brown. Sterna pale yellow. Hairs on abdomen brown.

Male genitalia yellow. Epandrium (Fig. 3b) bilobed, each lobe strongly elongated and forming a long surstylus, surstylus broadest at base, tapering and curved downward distally to middle, curving up at tip, with brown hairs; proctiger with short hairs. Gonocoxite (Fig. 3c) long and stout, 3 times as long as wide, basal apodeme two-thirds as long as gonocoxite; paramere with a pair of hook-shaped projections and a pair of conical projections. Gonostylus (Fig. 3c) with four projections and lobes: a strong retrose basal projection on inner side with tip bilobate; a broad tongue-shaped lobe on middle area with several long hairs apically; a dumbbell-shaped apical lobe broad basally with uniformly short hairs, apical with dense short setae; an apical hooked projection with several long hairs. Hypandrium (Fig. 3d) rectangular, anterior margin concaved medially, posterior margin with a V-shaped projection bearing dense long hairs posteriorly, a triangular projection bearing dense short hairs laterally and a pair of elliptic projections bearing dense long hairs posteriorly. Aedeagus (Fig. 3e, f): subapical sclerite tongue-shaped, slightly caved bilaterally, apex of subapical sclerite round; subapical sclerite serrated with five teeth when viewed from lateral side.

Female. Unknown.

Distribution. China (Zhejiang).

Etymology. The species is named after the type locality Mount Tianmushan.

Remarks. This new species is very similar to *P. emeica* from China but can be separated from it by the 6th and 7th sterna of abdomen being yellow, the tip of the surstylus being curved up when viewed from the lateral side, the tip of the retrose basal projection on inner side being bilobate, the paramere having a pair of hook-shaped projections and a pair of conical projections, and the subapical sclerite of aedeagus being serrated with five teeth. In *P. emeica*, the 6th and 7th sterna of abdomen are mostly brown, the tip of the surstylus is not curved up when viewed from the lateral side, the tip of the retrose basal projection on inner side is not bilobate, the paramere have a pair of slender L-shaped projections, and the subapical sclerite of aedeagus is serrated with two teeth (Kang et al. 2019). In ecology, they live together with similar habitat. The adult of *P. tianmushana* was collected on the plants in close to streams and adults of *P. emeica* often found at the margins of streams or in wet forests. This new species is also similar to *P. formosensis* from China and Japan but can be separated from it by the 5th and 6th terga of abdomen being dark brown, the tip of the surstylus being curved up, the tip of the retrose basal projection on inner side being bilobate, the tip of gonostylus having a hook-shaped ventral lobe. In *P. formosensis*, the 5th and 6th terga of abdomen are mostly yellow, the tip of the surstylus is not curved up, the tip of the retrose basal projection on inner side is not bilobate, the tip of gonostylus have a digitiform ventral lobe (Alexander 1924; Nakamura and Saigusa 2009).

Ptychoptera bellula Alexander, 1937

Figure 4

Ptychoptera bellula Alexander, 1937: 367. Type locality: Hong San, Jiangxi (China).

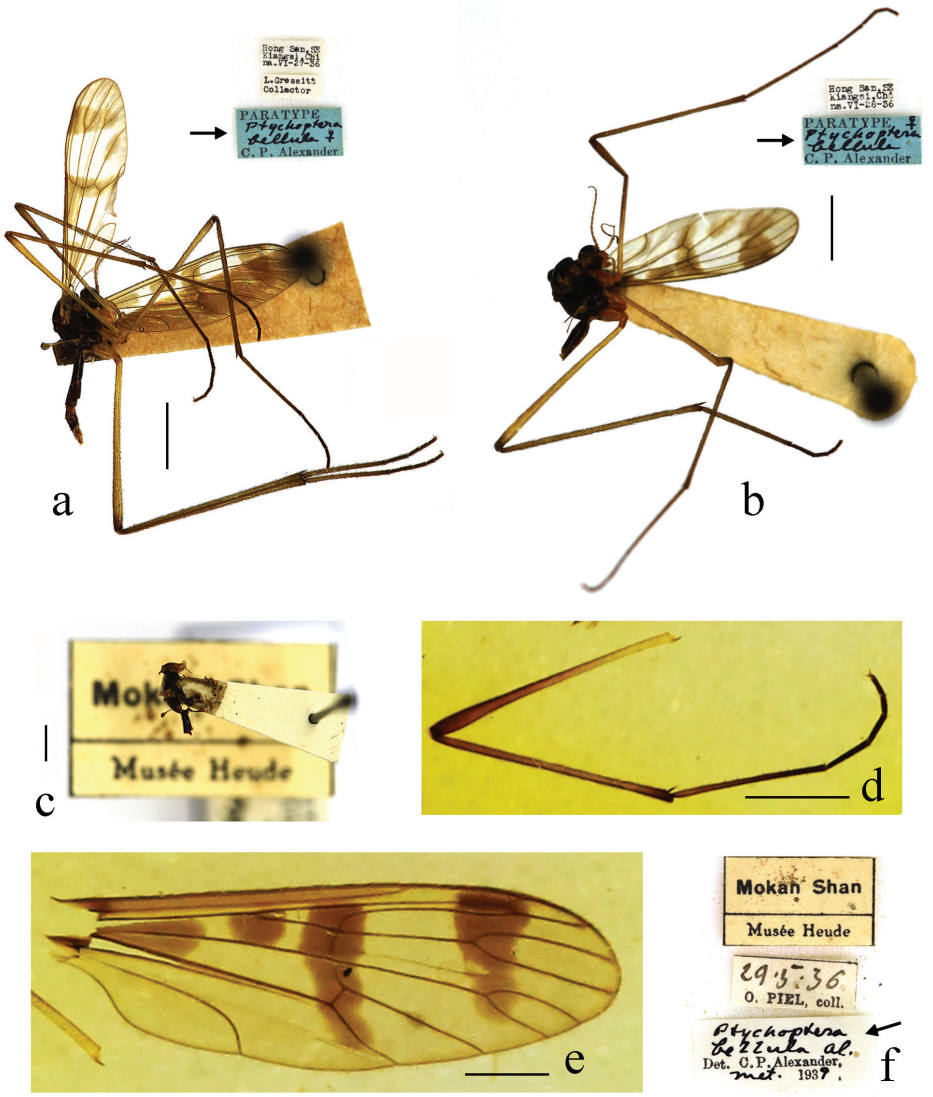

Figure 4. *Ptychoptera bellula* Alexander, 1937 **a** habitus of one paratype, lateral view **b** habitus of the other paratype, lateral view **c–f** one female identified by Alexander (**c** habitus of female, lateral view **d** one leg **e** wing **f** collection and identification labels). Scale bars: 2.0 mm (**a–d**); 1.0 mm (**e**).

Specimens examined. ***Paratypes*:** 2 females (USNM), China: Jiangxi Province, Xunwu District, Hong San (1000–1053 m), 1936.VI.27–28, Judson Linsley Gressitt. **Other material:** 1 female (USNM), China: Zhejiang Province, Deqing District, Mount Moganshan, 1936.V.29, Père Octave Piel.

Diagnosis. General coloration black. Haltere black with base of stem yellow. Wing with heavily brown bands and marks as follows: a large triangular brown mark in base of cells R and M; a irregular quadrate brown mark at origin of Rs; an elliptic brown

mark at midlength of CuA_1; a small oval brown mark at tip of A; median band extending from R to the bend in distal section of CuA_2; subapical band extending from anterior margin of wing, covering tip of R_1 and R_2, to tip of M_2; Rs about three-fifths the length of R_{4+5}, 4 times the length of r-m.

Distribution (new record in bold). China (Jiangxi, **Zhejiang**).

Remarks. The determined specimen of this species collected from Zhejiang was identified by Alexander in 1939, but was not officially published to record. We redetermined it during the study and now record this species from Zhejiang for the first time. For descriptions and illustrations of this species, see Alexander (1937) and Krzeminski and Zwick (1993).

Ptychoptera longwangshana Yang & Chen, 1998

Figure 5a

Ptychoptera longwangshana Yang & Chen, 1998: 240. Type locality: Mount Longwangshan, Anji, Zhejiang (China).

Specimens examined. ***Holotype*** male (CAU), China: Zhejiang Province, Anji District, Mount Longwangshan, 1996.VI.12, Chikun Yang.

Diagnosis. Thorax mostly black. Wing marked with two brown marks and two brown bands. Surstylus of epandrium tapering and curved downward distally, curving up at tip. Gonocoxite wide and gonostylus short and small. Apical part of hypandrium with a pair of curved up and trough-shaped projections.

Description. Wing length 8.0 mm. Wing (Fig. 5a) 3.2 times as long as wide, subhyaline, marked with two brown marks and two brown bands as follows: an oval brown mark at base of R, a triangular brown mark at base of Rs; median band extending from anterior margin of wing, covering base of R_{2+3} and r-m, to middle section of CuA; subapical band extending from anterior margin of wing, covering tip of R_1 and R_2, to M_{1+2} fork, slightly separated into two marks. Veins brown; Sc ending in C at level of basal third of R_{2+3}; Rs straight, 3 times the length of r-m.

Distribution. China (Zhejiang).

Remarks. Only one wing of the holotype was available during the study, while the rest of the holotype was not found in CAU. For a description and illustration of this species, also see Yang and Chen (1998).

Ptychoptera gutianshana Yang & Chen, 1995

Figure 5b–f

Ptychoptera gutianshana Yang & Chen, 1995: 180. Type locality: Mount Gutianshan, Kaihua, Zhejiang (China).

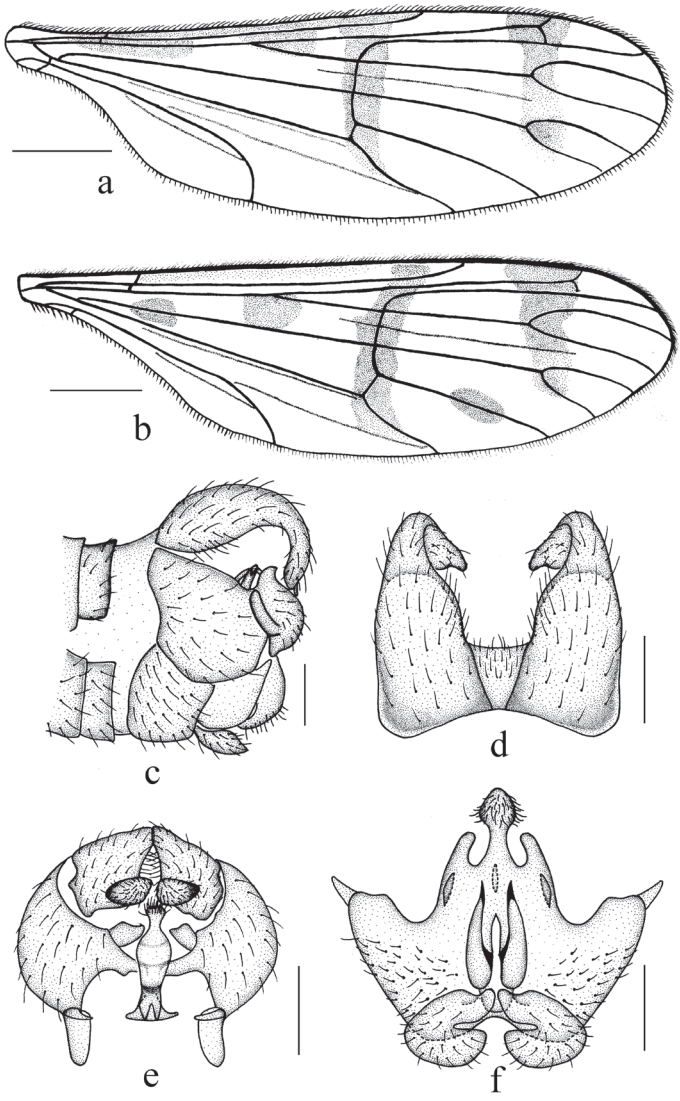

Figure 5. *Ptychoptera longwangshana* Yang & Chen, 1998 and *Ptychoptera gutianshana* Yang & Chen, 1995 **a** wing of *P. longwangshana* **b–f** *P. gutianshana* (**b** wing **c** male genitalia, lateral view **d** epandrium, dorsal view **e** gonocoxite and gonostylus, dorsal view **f** hypandrium, ventral view). Scale bars: 1.0 mm (**a, b**); 0.2 mm (**c–f**).

Specimens examined. ***Holotype*** male (CAU), China: Zhejiang Province, Kaihua District, Mount Gutianshan (350 m), 1993.IV.15, Hong Wu (light trap).

Diagnosis. Wing marked with three brown marks and two brown bands. Surstylus of epandrium broadest at base, tapering and curved downward distally, forked at tip. Paramere with a pair of flaky projections and a vase-shaped projection. Gonostylus irregular rectangular with an elliptic basal projection on inner side with short hairs.

Hypandrium trapeziform, anterior margin with a pair of C-shaped projections, middle area with a pair of digitiform projections, posterior margin with a pair of digitiform projections and a papillary projection.

Description. Wing length 7.5 mm. Wing (Fig. 5b) 3.6 times as long as wide, subhyaline, marked with three brown marks and two brown bands as follows: three elliptic brown marks at base of Rs, at base of M and at midlength of CuA_1; median band extending from anterior margin of wing, covering base of R_{2+3} and r-m, to the bend in distal section of CuA_2; subapical band extending from anterior margin of wing, covering tip of R_1, R_2 and fork of R_{4+5}, to fork of M_{1+2}. Veins brown; Sc ending in C at level of basal half of R_{2+3}; Rs straight, 3 times the length of r-m.

Male genitalia black. Epandrium (Fig. 5d) bilobed, each lobe strongly elongated and forming a long surstylus, surstylus broadest at base, tapering and curved downward distally, forked at tip, with brown hairs; proctiger with short hairs. Gonocoxite (Fig. 5e) short and swollen, 2 times as long as wide, basal apodeme three-eighths as long as gonocoxite; paramere with a pairs of flaky projections and a vase-shaped projection. Gonostylus (Fig. 5e) irregular rectangular with an elliptic basal projection on inner side with dense short hairs. Hypandrium (Fig. 5f) trapeziform, anterior margin with a pair of C-shaped projections, middle area with a pair of digitiform projections, posterior margin with a pair of digitiform projections and a papillary projection, papillary projection with dense short hairs.

Distribution. China (Zhejiang).

Remarks. Only two wings and male genitalia of the holotype were available during the study, while the paratype and the rest of the holotype were not found in CAU. For description and illustration of this species, also see Yang and Chen (1995).

Acknowledgements

We express our sincere thanks to Ding Yang (Beijing) for his great help during the study. We are also very grateful to Yan Li (Shenyang) for great help during the study of the specimens in USNM. This work was supported by the National Natural Science Foundation of China [41901061], the Shandong Provincial Natural Science Foundation, China [ZR2019BC034], the High-level Talents Funds of Qingdao Agricultural University, China [663-1119008], and the National Animal Collection Resource Center, China.

References

Alexander CP (1924) Undescribed species of Japanese Ptychopteridae (Diptera). Insecutor Inscitiae Menstruus 9: 80–83.

Alexander CP (1935) New or little-known Tipulidae from eastern Asia (Diptera). XXIII–XXVII. The Philippine Journal of Science 56: 339–372.

Alexander CP (1937) New species of Ptychopteridae (Diptera). Bulletin of the Brooklyn Entomological Society 32: 140–143.

Alexander CP (1945) Undescribed species of crane-flies from northern Korea (Diptera, Tipuloidea). Transactions of the Royal Entomological Society of London 95: 227–246. https://doi.org/10.1111/j.1365-2311.1945.tb00261.x

Alexander CP (1981) Ptychopteridae. In: McAlpine JF, Peterson BV, Shewell GE, Teskey HJ,Vockeroth JR, Wood DM (Eds) Manual of Nearctic Diptera (Vol. I). Agriculture Canada Monograph 27. Agriculture Canada, Ottawa, 325–328.

Fasbender A (2014) Phylogeny and diversity of the phantom crane flies (Diptera: Ptychopteridae). PhD Dissertation, Iowa State University, Ames, 855 pp.

Hancock EG, Marcos-Garcia MA, Rotheray GE (2006) Ptychopteridae – a family of flies (Diptera) new to the Neotropical Region and description of a new species. Zootaxa 1351: 61–68. https://doi.org/10.11646/zootaxa.1351.1.7

Kang Z, Xue Z, Zhang X (2019) New species and record of *Ptychoptera* Meigen, 1803 (Diptera: Ptychopteridae) from China. Zootaxa 4648(3): 455–472. https://doi.org/10.11646/zootaxa.4648.3.3

Kang Z, Yao G, Yang D (2013) Five new species of *Ptychoptera* Meigen with a key to species from China (Diptera: Ptychopteridae). Zootaxa 3682(4): 541–555. https://doi.org/10.11646/zootaxa.3682.4.5

Krzeminski W, Zwick P (1993) New and little known Ptychopteridae (Diptera) from the Palaearctic region. Aquatic Insects 15: 65–87. https://doi.org/10.1080/01650429309361504

McAlpine JF (1981) Morphology and terminology: Adults. In: McAlpine JF, Peterson BV, Shewell GE, Teskey HJ,Vockeroth JR, Wood DM (Eds) Manual of Nearctic Diptera (Vol. I). Agriculture Canada Monograph 27. Agriculture Canada, Ottawa, 9–63.

Meigen JW (1803) Versuch einer neuen Gattungs-Eintheilung der europaischen zweiflugligen Insekten. Magazin für Insektenkunde (Illiger) 2: 259–281.

Nakamura T, Saigusa T (2009) Taxonomic study of the family Ptychopteridae of Japan (Diptera). Zoosymposia 3: 273–303. https://doi.org/10.11646/zoosymposia.3.1.23

Rozkošný R (1997) Family Ptychopteridae. In: Papp L, Darvas B (Eds). Contributions to a Manual of Palaearctic Diptera (with Special Reference to Flies of Economic Importance), Volume 2: Nematocera and Lower Brachycera. Science Herald, Budapest, 291–297.

Ujvárosi L, Kolcsár PL, Török E (2011) An annotated list of Ptychopteridae (Insecta, Diptera) from Romania, with notes on the individual variability of *Ptychoptera albimana* (Fabricius, 1787). Entomologica Romanica 16: 39–45.

Yang J (1996) New record of family Ptychopteridae in Xinglongshan (Diptera: Ptychopteridae). In: Wang X (Ed.). Resources Background Investigation of Gansu Xinglongshan National Nature Reserve. Gansu Minorities Press, Gansu, 288–289.

Yang J, Chen H (1995) Diptera: Ptychopteridae. In: Zhu T (Ed.). Insects and Macrofungi of Gutianshan, Zhejiang. Zhejiang Scientech Press, Hangzhou, 180–182.

Yang J, Chen H (1998) Diptera: Ptychopteridae. In: Wu H (Ed.). Insects of Longwangshan Nature Reserve. China Forestry Publishing House, Beijing, 240–241.

Zhao L, Li J, Liu H, Qin H (2016) Distribution, congruence, and hotspots of higher plants in China. Scientific Reports 6(1): e19080. https://doi.org/10.1038/srep19080

Zwick P, Starý J (2003) *Ptychoptera delmastroi* sp. n. (Diptera: Ptychopteridae) from Italy. Aquatic Insects 25: 241–246. https://doi.org/10.1076/aqin.25.3.241.15262

ZooKeys 1070: 101–134 (2021)
doi: 10.3897/zookeys.1070.73659
https://zookeys.pensoft.net

RESEARCH ARTICLE

A peer-reviewed open-access journal
ZooKeys
Launched to accelerate biodiversity research

A new insular species of the *Cyrtodactylus pulchellus* group (Reptilia, Gekkonidae) from Tarutao Island, southern Thailand revealed by morphological and genetic evidence

Korkhwan Termprayoon[1], Attapol Rujirawan[1], Natee Ampai[2], Perry L. Wood Jr[3,4], Anchalee Aowphol[1]

1 *Department of Zoology, Faculty of Science, Kasetsart University, Bangkok, 10900 Thailand* **2** *Department of Biology, Faculty of Science, Srinakharinwirot University, Bangkok, 10110 Thailand* **3** *Department of Biological Sciences and Museum of Natural History, Auburn University, Auburn, AL, USA* **4** *Department of Ecology and Evolutionary Biology, University of Michigan, Ann Arbor, MI 48109-1085, USA*

Corresponding author: Anchalee Aowphol (fsciacl@ku.ac.th)

Academic editor: Thomas Ziegler | Received 29 August 2021 | Accepted 4 October 2021 | Published 12 November 2021

http://zoobank.org/FDBBD099-29F0-4521-9B18-AF841BC88F41

Citation: Termprayoon K, Rujirawan A, Ampai N, Wood Jr PL, Aowphol A (2021) A new insular species of the *Cyrtodactylus pulchellus* group (Reptilia, Gekkonidae) from Tarutao Island, southern Thailand revealed by morphological and genetic evidence. ZooKeys 1070: 101–134. https://doi.org/10.3897/zookeys.1070.73659

Abstract

The bent-toed geckos of the *Cyrtodactylus pulchellus* group are widely distributed along the Thai-Malay Peninsula. Although taxonomic and phylogenetic studies of this species group have been continuously conducted, only some populations from Thailand have been included, resulting in hidden diversity within this group. In this study, we used morphological and molecular data to clarify the taxonomic status and describe a new population from Tarutao Island, Satun Province, southern Thailand. *Cyrtodactylus stellatus* **sp. nov.** can be distinguished from its congeners by the combination of the following morphological characters: body size; tuberculation; number of dark body bands, ventral scales, and femoroprecloacal pores in males; presence of precloacal pores in females; and scattered pattern on dorsum. Phylogenetic analyses of the mitochondrial ND2 gene recovered the new species as the sister species to *C. astrum*, with an uncorrected pairwise divergence of 9.78–12.37%. *Cyrtodactylus stellatus* **sp. nov.** is currently only known from Tarutao Island, Thailand. The discovery of this species suggests that the diversity within the *C. pulchellus* group remains underestimated and future exploration of unsurveyed areas are needed to further the understanding of this group and its geographic range.

Keywords
Cyrtodactylus astrum, *Cyrtodactylus stellatus* sp. nov., karst, morphology, phylogeny, taxonomy

Introduction

Bent-toed geckos in the genus *Cyrtodactylus* Gray, 1827 are geographically widespread and inhabit lowland (e.g., peat swamps, karst formations, and limestone forests) to mountainous regions (> 1,500 m a.s.l) of South Asia to Melanesia, ranging from India, Myanmar, Thailand, Vietnam, Cambodia, Malaysia, Java, Papua New Guinea to northern Australia (Wood et al. 2012; Nielsen and Oliver 2017; Pauwels et al. 2018; Purkayastha et al. 2020; Riyanto et al. 2020; Grismer et al. 2020a, 2021a, 2021b). This genus is the most diverse group of gekkotans, comprising 314 nominal species (Uetz et al. 2021). During the last two decades, the number of new species described in this genus has significantly increased with the exploration of unsurveyed karst formations (Luu et al. 2016; Nazarov et al. 2018; Davis et al. 2019; Grismer et al. 2018, 2020b). Moreover, genetic data has become a useful tool for taxonomic studies, revealing hidden diversity within the genus (Murdoch et al. 2019; Chomdej et al. 2020; Neang et al. 2020; Riyanto et al. 2020; Kamei and Mahony 2021; Liu and Rao 2021). Recent molecular studies have further supported the monophyly of this genus based on the most complete phylogenetic analysis to date, and have recognized 31 species groups (Grismer et al. 2021b).

One clade of particular interest is the *Cyrtodactylus pulchellus* group. This relatively diverse group is distributed along the Thai-Malay Peninsula and has high morphological and molecular variation. *Cyrtodactylus pulchellus* Gray, 1827 was thought to be a single wide-ranging species across their distributional range, but following an integrative approach many new species have been described (e.g., *C. bintangrendah* Grismer et al., 2012, *C. langkawiensis* Grismer et al., 2012, and *C. sharkari* Grismer et al., 2014). This species group has been recovered as monophyletic and currently contains 16 recognized species, based on multiple phylogenetic studies (Grismer et al. 2012, 2014, 2016; Quah et al. 2019; Wood et al. 2020; Termprayoon et al. 2021). This group is distributed from the south of the Isthmus of Kra, southern Thailand to southern Peninsular Malaysia and some of its offshore islands (Grismer and Ahmad 2008; Sumontha et al. 2012; Grismer et al. 2012, 2014, 2016; Quah et al. 2019; Wood et al. 2020; Termprayoon et al. 2021). During field surveys, specimens of the *C. pulchellus* group were collected from Tarutao Island, Satun Province, southern Thailand. Initially, these specimens were recognized as an insular population of *C. astrum* Grismer et al., 2012 due to their superficial resemblance in coloration pattern and dorsal tuberculation. A re-examination of these specimens showed morphological differences from its other congeners and mitochondrial DNA sequence data revealed corroborative evidence that the new population of *Cyrtodactylus* from Tarutao Island represents a distinct monophyletic lineage and is the sister species to *C. astrum* from the adjacent mainland. Based on integrative analyses, we considered this new *Cyrtodactylus* population from Tarutao Island as distinct and described it as a new species below.

Materials and methods

Sampling

Field surveys were conducted on Tarutao Island, Mueang Satun District, Satun Province, southern Thailand from November 2017 to November 2019 (Fig. 1). Specimens of the *C. pulchellus* group were collected from karst forest at night (1900–2200 h). Ecological data (air temperature and relative humidity) were recorded using a Kestrel 4000 Weather Meter, and habitat use of each specimen was noted. Geographical coordinates and elevation were recorded using a Garmin GPSMAP 64s. For molecular studies, liver tissue was taken from each euthanized specimen, individually preserved in 95% ethyl alcohol, and stored at -20 °C. Specimens were initially fixed in 10% formalin and later transferred into 70% ethyl alcohol for permanent storage. Voucher specimens were deposited in the herpetological collections of the Zoological Museum, Kasetsart University, Thailand (ZMKU). Additional preserved specimens were examined in the holdings of the Thailand Natural History Museum (THNHM), Thailand, and the La Sierra University Herpetological Collection (LSUHC), La Sierra University, Riverside, California, USA.

DNA extraction and PCR amplification

Total genomic DNA was extracted from ethanol-preserved liver tissue of five *Cyrtodactylus* specimens from Tarutao Island (Table 1) using a NucleoSpin Tissue Kit (Macherey-Nagel GmbH & Co. KG, Germany). A fragment of mitochondrial NADH dehydrogenase subunit 2 (ND2) gene and its flanking tRNAs was amplified using a double-stand Polymerase Chain Reaction (PCR) under the following conditions: initial denaturation at 94 °C for 4 min, followed by 35 cycles of denaturation at 94 °C for 30 sec, annealing at 48–52 °C for 30 sec, extension at 72 °C for 1 min 30 sec, and final extension at 72 °C for 7 min using the primers Metf6 (5' AAGCTTTCGGGCCCATACC 3'; Macey et al. 1997), and COIH (5' AGRGTGCCAATGTCTTTGTGRTT 3'; Macey et al. 1997). PCR products were purified using NucleoSpin Gel and PCR Clean-Up kit (Macherey-Nagel GmbH & Co. KG, Germany). Purified products were sequenced for both strands using the same amplifying primers on an ABI 3730XL DNA Sequencer (Applied Biosystems, CA, USA). Sequences were visually checked and aligned in Geneious R11 (Biomatters, Ltd, Auckland, New Zealand). The protein-coding region of ND2 was translated to amino acids and checked to confirm the lack of premature stop codons. All sequences were deposited in GenBank under the accession numbers OK094494–OK094503 (Table 1).

Phylogenetic analyses

Phylogenetic trees were reconstructed using two different methods, Maximum Likelihood (ML) and Bayesian Inference (BI). The best substitution model for each partition was determined using the Bayesian Information Criterion (BIC) under the

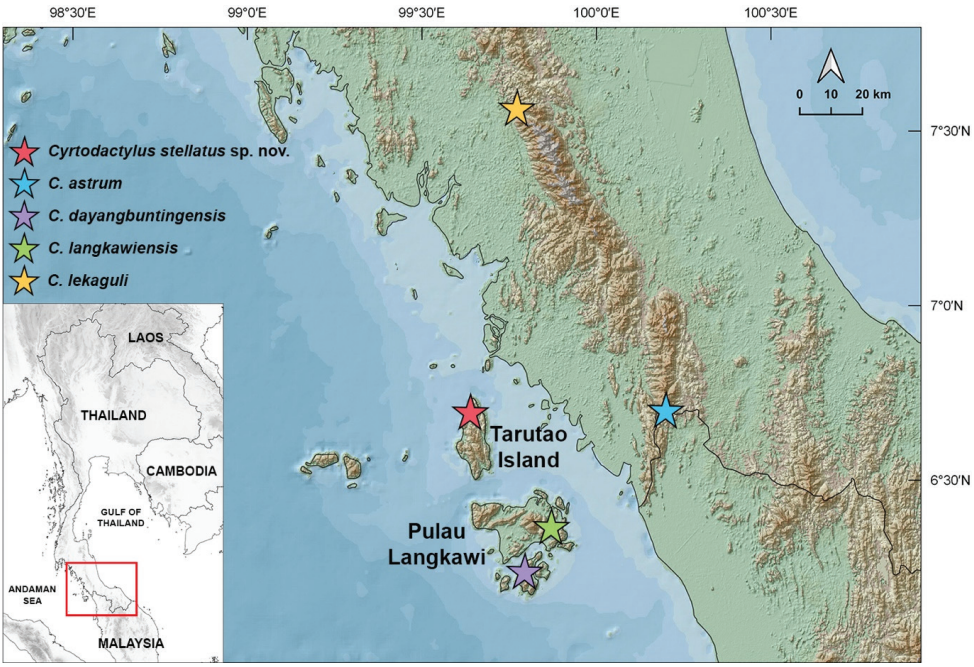

Figure 1. Map showing the type locality of *Cyrtodactylus stellatus* sp. nov. from Tarutao Island, Mueang Satun District, Satun Province, Thailand and the type localities of closely related species, *C. astrum, C. dayangbuntingensis, C. langkawiensis,* and *C. lekaguli*.

greedy search algorithm as implemented in PartitionFinder2 on XSEDE (Lanfear et al. 2016). The selected models for ML and BI were TIM+G for 1st and 2nd codon positions of ND2, TVM+I+G for 3rd codon position of ND2 and TRN+I+G for tRNAs. The ML analysis was performed in IQ-TREE web server v1.6.12 (Trifinopoulos et al. 2016) with 1,000 bootstrap replicates using ultrafast bootstrap approximation (Minh et al. 2013). The BI analysis was performed in MrBayes 3.2.6 on XSEDE (Ronquist et al. 2012) using the CIPRES Science Gateway v3.3 (Miller et al. 2010). Two simultaneous runs were performed with four chains per run, three hot and one cold under the default settings. The analysis was run for 10,000,000 generations and sampled every 1,000 generations from the Markov chain Monte Carlo (MCMC), with the first 25% of each run discarded as burn-in. Stationarity and the effective sample sizes (ESS) for all parameters were assessed in Tracer v1.7.1. (Rambaut et al. 2018). Nodes with ultrafast bootstrap support (UFB) of ≥ 95 and Bayesian posterior probabilities (BPP) of ≥ 0.95 were considered to be strongly supported (Huelsenbeck and Ronquist 2001; Wilcox et al. 2002; Minh et al. 2013). Intraspecific and interspecific uncorrected pairwise genetic divergences (*p*-distance) were calculated in MEGA X 10.0.5 using the pairwise deletion option for the treatment of gaps and missing data in the dataset (Kumar et al. 2018).

Table 1. Samples used in the molecular analyses, including their GenBank accession number (ND2), voucher number and locality. WM = West Malaysia; TH = Thailand.

Species	Locality	Museum No.	GenBank Accession No.	Reference
Outgroup				
Agamura persica	Pakistan, Baluchistan Province, Makran District, Gwadar division	FMNH 247474	JX440515	Wood et al. (2012)
Hemidactylus frenatus	Unknow	NC 00155	JX519468	Grismer et al. (2012)
Tropiocolotes steudneri	captive	JB 28	JX440520	Wood et al. (2012)
C. elok	WM, Pahang, Fraser's Hill, The Gap	LSUHC 6471	JQ889180	Wood et al. (2012)
C. hontreensis	Vietnam, Kien Giang Province, Kien Hai District, Hon Tre Island	LSUHC 8583	JX440539	Wood et al. (2012)
C. intermedius	TH, Chantaburi Province, Khao Khitchakut District	LSUHC 9513	JX519469	Grismer et al. (2012)
	TH, Chantaburi Province, Khao Khitchakut District	LSUHC 9514	JX519470	Grismer et al. (2012)
C. interdigitalis	Lao, Khammouan Province, Nakai District	FMNH 255454	JQ889181	Wood et al. (2012)
Cyrtodactylus sp.	TH, Loei, Phu Rua	FMNH 265806	JX519471	Grismer et al. (2012)
Ingroup				
C. astrum	WM, Perlis, Gua Kelam	LSUHC 8806	JX519481	Grismer et al. (2012)
	WM, Perlis, Gua Kelam	LSUHC 8807	JX519478	Grismer et al. (2012)
	WM, Perlis, Gua Kelam	LSUHC 8808	JX519479	Grismer et al. (2012)
	WM, Perlis, Gua Kelam	LSUHC 8809	JX519480	Grismer et al. (2012)
	WM, Perlis, Kuala Perlis	LSUHC 8815	JX519482	Grismer et al. (2012)
	WM, Perlis, Kuala Perlis	LSUHC 8816 (paratype)	JX519483	Grismer et al. (2012)
	WM, Perlis, Perlis State Park	LSUHC 9215	JX519473	Grismer et al. (2012)
	WM, Perlis, Perlis State Park, Gua Wang Burma	LSUHC 9962	JX519475	Grismer et al. (2012)
	WM, Perlis, Perlis State Park, Gua Wang Burma	LSUHC 9986	JX519476	Grismer et al. (2012)
	WM, Perlis, Perlis State Park, Gua Wang Burma	LSUHC 9987	JX519477	Grismer et al. (2012)
	WM, Perlis, Wang Kelian	LSUHC 10023	JX519474	Grismer et al. (2012)
	WM, Perlis, Wang Kelian	LSUHC 10024	JX519472	Grismer et al. (2012)
C. australotitiwangsaensis	WM, Pahang, Fraser's Hill	LSUHC 8086	JX519486	Grismer et al. (2012)
	WM, Pahang, Fraser's Hill	LSUHC 8087	JX519485	Grismer et al. (2012)
	WM, Pahang, Genting Highlands	LSUHC 6637 (holotype)	JX519484	Grismer et al. (2012)
C. bintangrendah	WM, Kedah, Bukit Mertajam	LSUHC 10331 (paratype)	MN125076	Quah et al. (2019)
	WM, Kedah, Bukit Mertajam	LSUHC 10519	MN125077	Quah et al. (2019)
	WM, Kedah, Bukit Mertajam	LSUHC 10520 (paratype)	MN125078	Quah et al. (2019)
	WM, Kedah, Bukit Palang	LSUHC 9984	JX519487	Grismer et al. (2012)
C. bintangtinggi	WM, Perak, Bukit Larut	LSUHC 8862	JX519493	Grismer et al. (2012)
	WM, Perak, Bukit Larut	LSUHC 9006 (paratype)	JX519494	Grismer et al. (2012)
C. dayangbuntingensis	WM, Kedah, Dayang Bunting Island	LSUHC 14353	MN125090	Quah et al. (2019)
	WM, Kedah, Dayang Bunting Island	LSUHC 14354	MN125091	Quah et al. (2019)
	WM, Kedah, Dayang Bunting Island	LSUHC 14355	MN125092	Quah et al. (2019)
C. evanquahi	WM, Kedah, Gunung Baling	BYU 53435 (holotype)	MN586889	Wood et al. (2020)
	WM, Kedah, Gunung Baling	BYU 53436 (paratype)	MN586890	Wood et al. (2020)
	WM, Kedah, Gunung Baling	BYU 53437 (paratype)	MN586891	Wood et al. (2020)
C. hidupselamanya	WM, Kelantan, Felda Chiku 7	LSUHC 12161 (paratype)	KX011415	Grismer et al. (2016)
	WM, Kelantan, Felda Chiku 7	LSUHC 12162 (paratype)	KX011416	Grismer et al. (2016)
	WM, Kelantan, Felda Chiku 7	LSUHC 12163 (holotype)	KX011417	Grismer et al. (2016)
	WM, Kelantan, Felda Chiku 7	LSUHC 12173 (paratype)	KX011420	Grismer et al. (2016)

Species	Locality	Museum No.	GenBank Accession No.	Reference
C. jelawangensis	WM, Gunung Stong, Kelantan	LSUHC 11060 (paratype)	KJ659850	Grismer et al. (2014)
	WM, Gunung Stong, Kelantan	LSUHC 11062 (holotype)	KJ659852	Grismer et al. (2014)
	WM, Kelantan, Gunung Stong	LSUHC 11061 (paratype)	KJ659851	Grismer et al. (2014)
C. langkawiensis	WM, Kedah, Pulau Langkawi, Wat Wanaram	LSUHC 9120	JX519502	Grismer et al. (2012)
	WM, Kedah, Pulau Langkawi, Wat Wanaram	LSUHC 9122	JX519501	Grismer et al. (2012)
	WM, Kedah, Pulau Langkawi, Wat Wanaram	LSUHC 9123	JX519500	Grismer et al. (2012)
	WM, Kedah, Pulau Langkawi, Wat Wanaram	LSUHC 9124 (paratype)	JX519499	Grismer et al. (2012)
	WM, Kedah, Pulau Langkawi, Wat Wanaram	LSUHC 9125	JX519496	Grismer et al. (2012)
	WM, Kedah, Pulau Langkawi, Wat Wanaram	LSUHC 9434	JX519498	Grismer et al. (2012)
	WM, Kedah, Pulau Langkawi, Wat Wanaram	LSUHC 9435	JX519495	Grismer et al. (2012)
	WM, Kedah, Pulau Langkawi, Wat Wanaram	LSUHC 9437	JX519497	Grismer et al. (2012)
	WM, Kedah, Pulau Langkawi, Wat Wanaram	LSUHC 14347	MN125093	Quah et al. (2019)
	WM, Kedah, Pulau Langkawi, Wat Wanaram	LSUHC 14348	MN125094	Quah et al. (2019)
C. lekaguli	TH, Phang-nga Province, Mueang Phang-nga District	ZMKU R 00720	KX011425	Grismer et al. (2016)
	TH, Phang-nga Province, Mueang Phang-nga District	ZMKU R 00721	KX011426	Grismer et al. (2016)
	TH, Phang-nga Province, Mueang Phang-nga District	ZMKU R 00722	KX011427	Grismer et al. (2016)
	TH, Phang-nga Province, Mueang Phang-nga District	ZMKU R 00723	KX011428	Grismer et al. (2016)
	TH, Trang Province, Na Yong District	ZMKU R 00918	OK094494	This study
	TH, Trang Province, Na Yong District	ZMKU R 00919	OK094495	This study
	TH, Trang Province, Na Yong District	ZMKU R 00920	OK094496	This study
	TH, Trang Province, Na Yong District	ZMKU R 00921	OK094497	This study
	TH, Trang Province, Na Yong District	ZMKU R 00922	OK094498	This study
C. lenggongensis	WM, Perak, Lenggong Valley	LSUHC 9974 (holotype)	JX519490	Grismer et al. (2012)
	WM, Perak, Lenggong Valley	LSUHC 9975 (paratype)	JX519488	Grismer et al. (2012)
	WM, Perak, Lenggong Valley	LSUHC 9976 (paratype)	JX519489	Grismer et al. (2012)
	WM, Perak, Lenggong Valley	LSUHC 9977 (paratype)	JX519491	Grismer et al. (2012)
C. macrotuberculatus	TH, Phuket Province, Kathu District, Kathu Waterfall	ZMKU R 00890	MW809301	Termprayoon et al. (2021)
	TH, Phuket Province, Kathu District, Kathu Waterfall	ZMKU R 00891	MW809302	Termprayoon et al. (2021)
	TH, Phuket Province, Thalang District, Thep Krasatti	ZMKU R 00894	MW809305	Termprayoon et al. (2021)
	TH, Phuket Province, Thalang District, Thep Krasatti	ZMKU R 00895	MW809306	Termprayoon et al. (2021)
	TH, Phuket Province, Thalang District, Thep Krasatti	ZMKU R 00896	MW809307	Termprayoon et al. (2021)
	TH, Satun Province, Mueang Satun District, Adang Island	ZMKU R 00875	MW809295	Termprayoon et al. (2021)
	TH, Satun Province, Mueang Satun District, Rawi Island	ZMKU R 00883	MW809299	Termprayoon et al. (2021)
	TH, Satun Province, Mueang Satun District, Rawi Island	ZMKU R 00887	MW809300	Termprayoon et al. (2021)
	TH, Songkhla Province, Hat Yai District, Thung Tam Sao	ZMKU R 00876	MW809296	Termprayoon et al. (2021)
	TH, Songkhla Province, Hat Yai District, Thung Tam Sao	ZMKU R 00877	MW809297	Termprayoon et al. (2021)
	TH, Songkhla Province, Hat Yai District, Thung Tam Sao	ZMKU R 00878	MW809298	Termprayoon et al. (2021)
	WM, Kedah, Hutan Lipur Sungai Tupah	LSUHC 9671	JX519510	Grismer et al. (2012)
	WM, Kedah, Hutan Lipur Sungai Tupah	LSUHC 9672	JX519511	Grismer et al. (2012)
	WM, Kedah, Hutan Lipur Sungai Tupah	LSUHC 9693	JX519517	Grismer et al. (2012)
	WM, Kedah, Pulau Langkawi, Gunung Machinchang	LSUHC 9448	JX519507	Grismer et al. (2012)

Species	Locality	Museum No.	GenBank Accession No.	Reference
C. macrotuberculatus	WM, Kedah, Pulau Langkawi, Gunung Raya	LSUHC 9428	JX519506	Grismer et al. (2012)
	WM, Kedah, Pulau Langkawi, Lubuk Sembilang	LSUHC 6829	JX519505	Grismer et al. (2012)
	WM, Perlis, Bukit Chabang	LSUHC 10037	JX519519	Grismer et al. (2012)
	WM, Perlis, Bukit Chabang	LSUHC 10038	JX519518	Grismer et al. (2012)
C. pulchellus	WM, Penang, Pulau Pinang, Empangan Air Itam	LSUHC 6668	JX519523	Grismer et al. (2012)
	WM, Penang, Pulau Pinang, Moongate Trail	LSUHC 6727	JX519526	Grismer et al. (2012)
	WM, Penang, Pulau Pinang, Moongate Trail	LSUHC 6728	JX519525	Grismer et al. (2012)
	WM, Penang, Pulau Pinang, Moongate Trail	LSUHC 6729	JX519528	Grismer et al. (2012)
C. sharkari	WM, Pahang, Merapoh, Gua Gunting	LSUHC 11022 (holotype)	KJ659853	Grismer et al. (2014)
Cyrtodactylus stellatus sp. nov.	TH, Satun Province, Mueang Satun District, Tarutao Island	ZMKU R 00903 (paratype)	OK094499	This study
	TH, Satun Province, Mueang Satun District, Tarutao Island	ZMKU R 00905 (holotype)	OK094500	This study
	TH, Satun Province, Mueang Satun District, Tarutao Island	ZMKU R 00906 (paratype)	OK094501	This study
	TH, Satun Province, Mueang Satun District, Tarutao Island	ZMKU R 00907 (paratype)	OK094502	This study
	TH, Satun Province, Mueang Satun District, Tarutao Island	ZMKU R 00908 (paratype)	OK094503	This study
C. timur	WM, Gunung Tebu, Terengganu	LSUHC 10886	KJ659854	Grismer et al. (2014)
	WM, Gunung Tebu, Terengganu	LSUHC 11183 (paratype)	KJ659855	Grismer et al. (2014)
	WM, Gunung Tebu, Terengganu	LSUHC 11184 (paratype)	KJ659856	Grismer et al. (2014)
	WM, Gunung Tebu, Terengganu	LSUHC 11185 (paratype)	KJ659857	Grismer et al. (2014)
C. trilatofasciatus	WM, Pahang, Cameron Highlands	LSUHC 10064	JX519529	Grismer et al. (2012)
	WM, Pahang, Cameron Highlands	LSUHC 10065	JX519530	Grismer et al. (2012)
	WM, Pahang, Cameron Highlands	LSUHC 10066	JX519531	Grismer et al. (2012)

Morphology

The morphological characters and their definition used in this study were modified from previous studies of the *C. pulchellus* group (Grismer and Ahmad 2008; Grismer et al. 2012, 2014, 2016; Quah et al. 2019; Wood et al. 2020), and abbreviations are derived from Grismer et al. (2018, 2020c). All mensural characters were taken with digital calipers to the nearest 0.01 mm on the left side, while scale counts were made on both sides when possible. Scalation and external morphology were evaluated under a Nikon SMZ745 dissecting microscope. Measurement and meristic characters are shown in Table 2, and external morphological characters evaluated are described below.

External morphological characters examined in the *C. pulchellus* group were the degree of body tuberculation, weak tuberculation referring to dorsal body tubercles that are low and rounded whereas prominent tuberculation refer to tubercles that are raise and keeled; the presence or absence of tubercles on the dorsal and ventral surface of the forearms; the presence or absence of tubercles in the gular region, throat, and ventrolateral body folds; the width of the dark body bands relative to the width of the interspace between the bands; the presence or absence of dark pigmentation infused in the white caudal bands of adults; the presence or absence of a precloacal depression or groove; the presence or absence of scattered white/yellow tubercles on the dorsum; and

Table 2. Measurement and meristic characters used in this study, with abbreviations and explanations.

Abbreviations	Characters
Measurement	
SVL	Snout–vent length, taken from the tip of snout to the vent
TW	Tail width, taken at the base of the tail immediately posterior to the postcloacal swelling
TL	Tail length, taken from vent to the tip of the tail, original or regenerated
FL	Forearm length, taken from the posterior margin of the elbow while flexed 90° to the inflection of the flexed wrist
TBL	Tibia length, taken from the posterior surface of the knee while flexed 90° to the base of the heel
AG	Axilla to groin length, taken from the posterior margin of the forelimb at its insertion point on the body to the anterior margin of the hind limb at its insertion point on the body
HL	Head length, the distance from the posterior margin of the retroarticular process of the lower jaw to the tip of the snout
HW	Head width, measured at the angle of the jaws
HD	Head depth, the maximum height of head from the occiput to the throat
ED	Eye diameter, the greatest horizontal diameter of the eyeball
EE	Eye to ear distance, measured from the anterior edge of the ear opening to the posterior edge of the eyeball
ES	Eye to snout distance, measured from anterior most margin of the eyeball to the tip of snout
EN	Eye to nostril distance, measured from the anterior margin of the eyeball to the posterior margin of the external nares
IO	Inter orbital distance, measured between the anterior edges of the orbit
EL	Ear length, the greatest vertical distance of the ear opening
IN	Internarial distance, measured between the nares across the rostrum
Meristic	
SL	Supralabial scales, counted from the largest scale immediately posterior to the dorsal inflection of the posterior portion of the upper jaw to the rostral scale
IL	Infralabial scales, counted from the largest scale immediately posterior to the dorsal inflection of the posterior portion of the upper jaw to the mental scale
PVT	The number of paravertebral tubercles between limb insertions, counted in a straight line immediately left or right of the vertebral column
LRT	The number of longitudinal rows of body tubercles, counted transversely across the center of the dorsum from one ventrolateral fold to the other
VS	The number of longitudinal rows of ventral scales, counted transversely across the center of the abdomen from one ventrolateral fold to the other
4TL	The number of subdigital lamellae beneath the fourth toe, counted from the base of the first phalanx to the claw
FPP	The total number of precloacal and femoral pores in male (i.e., the sum of the number of femoral and precloacal scales bearing pores combined as a single meristic referred to as the femoroprecloacal pores)
PP	The number of precloacal pores in female
BB	The number of dark body bands between limb insertions
DCB	The number of dark caudal bands on the original tail

the presence or absence of white tail tip on the posterior portion of the original tail in hatchlings and juveniles. Color pattern characteristics were taken from digital images of live specimens in both sexes and of all possible age classes prior to preservation.

Statistical analyses

All analyses were performed using the base statistical software in R v3.6.1 (R Core Team 2019). To eliminate bias of sexual dimorphism, adult males and females were analyzed separately. Morphological analyses were run on 15 mensural characters. Tail length (TL) was not included due to their different condition (e.g., original, regenerated, and broken). All measurements of each species were size-adjusted in order to remove potential effects of allometry using the following allometric equation: $X_{adj} = \log[X \pm \beta(SVL \pm SVL_{mean})]$, where X_{adj} = adjusted value; X = measured value; β = unstandardized regression coefficient for each OTU; SVL = measured snout–vent length; SVL_{mean}

= overall average SVL of each OTU (Thorpe 1975, 1983; Turan 1999; Lleonart et al. 2000)—implemented through the R package GroupStruct (Chan and Grismer 2021). Morphological measurements of *C. astrum, C. dayangbuntingensis* Quah et al., 2019, *C. langkawiensis* and *C. lekaguli* Grismer et al., 2012 were obtained from their original descriptions (Grismer et al. 2012; Quah et al. 2019). Additional preserved specimens of *C. astrum* (from Malaysia) and *C. lekaguli* (topotypes) were examined and included in the analyses (Appendix I). Morphometric adjustments were conducted separately on each species and then concatenated into a single data frame to ensure there was no interspecific conflation of variation (Reist 1985; McCoy et al. 2006). Specimens were assigned into five groups (= species) based on phylogenetic analyses which are *Cyrtodactylus* Tarutao Island samples (N = 5 males, 5 females), *C. astrum* (N = 5 males, 3 females), *C. dayangbuntingensis* (N = 2 males), *C. langkawiensis* (N = 2 males, 4 females), and *C. lekaguli* (N = 7 males, 9 females).

Principal components analysis (PCA) was performed on size-adjusted data for each sex using FactoMineR package (Lê et al. 2008) and were visualized with the R package ggplot2 (Wickham 2016). For univariate analysis, Shapiro-Wilk test was used to evaluate data to meet normality assumptions ($p \geq 0.05$) and Levene's test for testing for equality of variance ($p \geq 0.05$). Morphological differences were compared using Analysis of variance (ANOVA) or Kruskal-Wallis test. ANOVA was conducted on normally distributed data with homogeneous variances and were subjected to Tukey HSD post hoc tests (Tukey's test) to determine which characters had statistically different mean values for which pairs of species if ANOVA had a p-value of less than 0.05. Kruskal-Wallis test was performed on non-normally distributed data and followed by a post hoc Dunn's multiple comparison (Dunn's test). Due to limited sample sizes, *C. dayangbuntingensis* (N = 2 males) and males of *C. langkawiensis* (N = 2 males) were excluded from the univariate analysis.

Results

Phylogenetic relationships

The aligned matrix contained 1,429 mtDNA characters from 93 individuals of the *C. pulchellus* group and nine individuals of outgroup species (Table 1). The standard deviation of split frequencies among the two simultaneous BI runs was 0.002676, and the ESS values of all parameters were greater than or equal to 2,494.4. The maximum likelihood value of the best ML tree was lnL = -15,115.412.

The topologies of ML and BI analyses were largely concordant. The ML and BI analyses recovered the *C. pulchellus* group as monophyletic with strong support (≥ 95 UFB, ≥ 0.95 BPP) which is comprised of two major clades referred to as Clades A and B (Figs 2, 3). The *Cyrtodactylus* specimens from Tarutao Island represented a strongly supported monophyletic group (≥ 95 UFB, ≥ 0.95 BPP) within Clade A containing

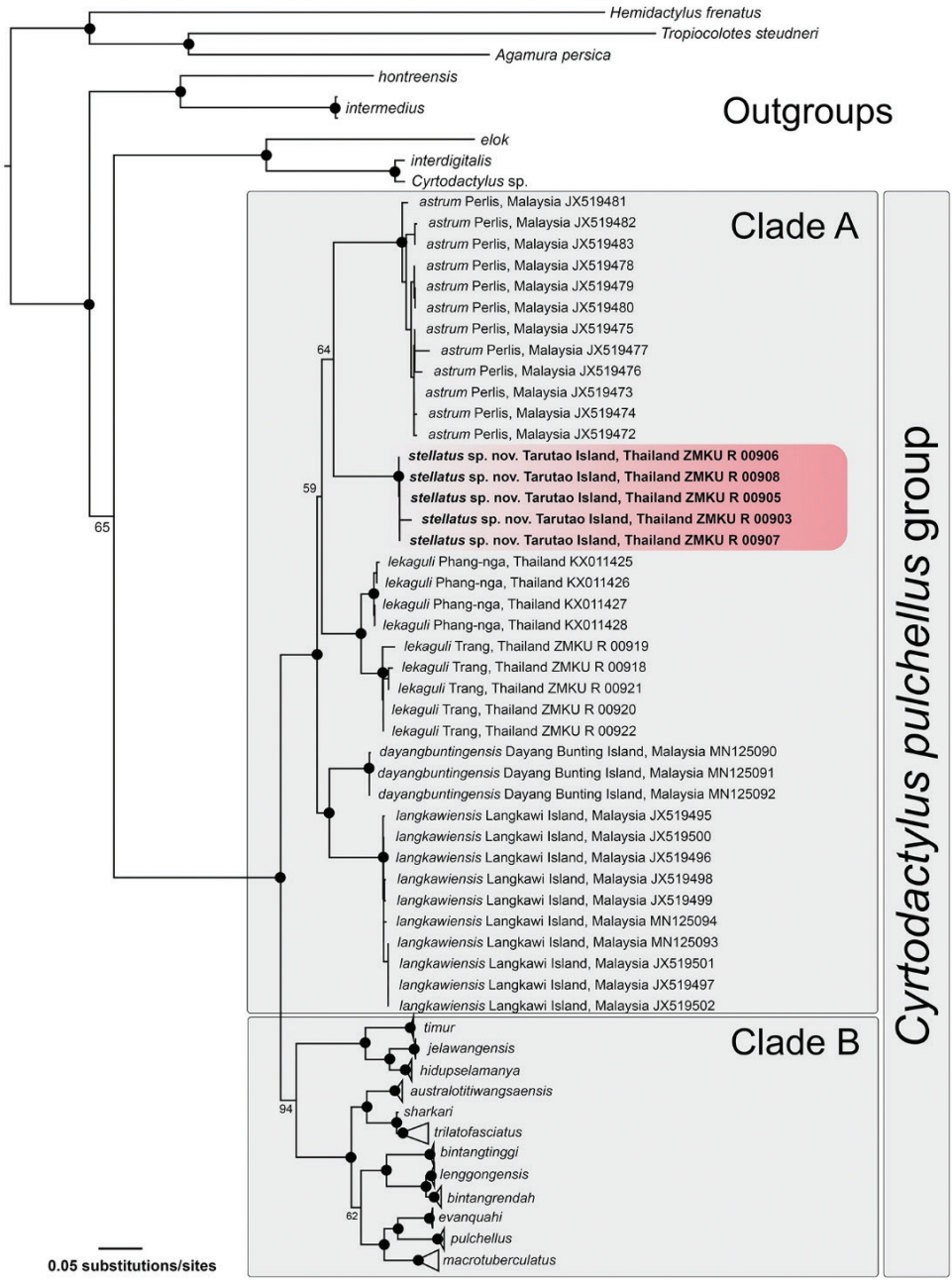

Figure 2. The Maximum Likelihood tree of the *Cyrtodactylus pulchellus* group based on 1,429 bp of the ND2 gene and flanking tRNAs. Support values on branches are ultrafast bootstrap (UFB). Black circles represent nodes strongly supported (UFB ≥ 95).

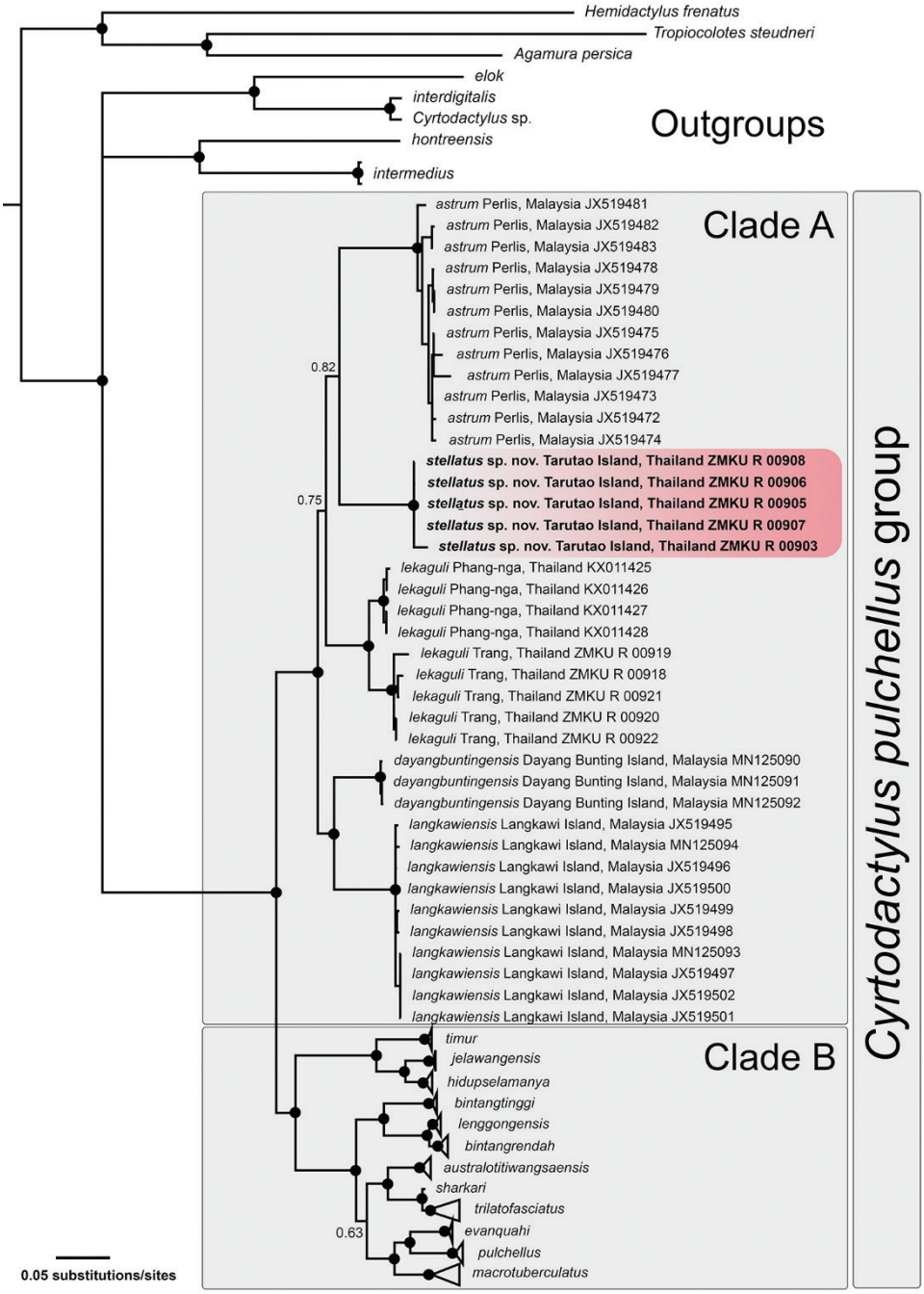

Figure 3. The Bayesian consensus tree of the *Cyrtodactylus pulchellus* group based on 1,429 bp of the ND2 gene and flanking tRNAs. Support values on branches are Bayesian posterior probabilities (BPP). Black circles represent nodes strongly supported (BPP ≥ 0.95).

C. astrum, *C. dayangbuntingensis*, *C. langkawiensis*, and *C. lekaguli*. The Tarutao Island samples were weakly recovered as a sister species to *C. astrum* from the adjacent Peninsular Malaysian mainland (64 UFB, 0.82 BPP). Clade B is composed of all other species including *C. australotitiwangsaensis* Grismer et al., 2012, *C. bintangrendah, C. bintangtinggi* Grismer et al., 2012, *C. evanquahi* Wood et al., 2020, *C. hidupselamanya* Grismer et al., 2016, *C. jelawangensis* Grismer et al., 2014, *C. lenggongensis* Grismer et al., 2016, *C. macrotuberculatus* Grismer and Ahmad, 2008, *C. pulchellus, C. sharkari, C. timur* Grismer et al., 2014 and *C. trilatofasciatus* Grismer et al., 2012. Uncorrected pairwise genetic divergences (*p*-distance) range from 0.00–1.17% within the Tarutao Island specimens and 8.46–12.37% between the Tarutao Island specimens and other species in Clade A (Table 3).

Morphology

The PCA was conducted on members from Clade A. The plots on the first two PC axes showed that the Tarutao Island specimens are clustered separately from other species in both sexes (Fig. 4). In male, the first two principal components explained 66.95% of the morphological variation (Table 4). The first principal component (PC1) accounted for 45.88% of the variation and was heavily loaded on FL_{adj}, TBL_{adj}, HW_{adj}, HD_{adj}, EE_{adj}, ES_{adj}, and EN_{adj}; and the PC2 accounted for 21.07% of the variation and was heavily loaded on TW_{adj}, AG_{adj}, IO_{adj}, and EL_{adj}. PC analysis of females accounted for 56.74% of the variation in first two components. The PC1 accounted for 34.81% of the variation and was heavily loaded on TBL_{adj}, HW_{adj}, EE_{adj}, ES_{adj}, and EN_{adj}; and the PC2 accounted for 21.93% of the variation and was heavily loaded on TW_{adj}, IO_{adj} and IN_{adj}.

The univariate analyses (ANOVA or Kruskal-Wallis test) were significantly different ($p < 0.05$) in most morphological characters among the members of Clade A (except *C. dayangbuntingensis*). In the comparison of adult males, the Tarutao Island population was significantly different from *C. astrum* and *C. lekaguli* in twelve morphological characters (ANOVA or Kruskal-Wallis test, $p < 0.001$–0.006) except AG_{adj}, ED_{adj} and IN_{adj} (ANOVA or Kruskal-Wallis test, $p = 0.051$–0.122). Subsequent Tukey's test or Dunn's test demonstrated that Tarutao Island population was significantly different from *C. astrum* in SVL_{adj}, FL_{adj}, TBL_{adj}, HL_{adj}, HW_{adj}, HD_{adj}, EE_{adj}, ES_{adj}, and EN_{adj}; and *C. lekaguli* in SVL_{adj}, TW_{adj}, FL_{adj}, HL_{adj}, HW_{adj}, HD_{adj}, EE_{adj}, ES_{adj}, IO_{adj}, and EL_{adj}. In adult females, the Tarutao Island population was significantly different

Table 3. Percentage uncorrected pairwise genetic divergence (*p*-distances) of *Cyrtodactylus stellatus* sp. nov. and closely related species (Clade A) calculated from 1,429 base pairs of mitochondrial ND2 gene and flanking tRNAs.

Species	*N*	1	2	3	4	5
1 *Cyrtodactylus stellatus* sp. nov.	5	**0.48 (0.00–1.17)**				
2 *C. astrum*	12	10.50 (9.78–12.37)	**1.37 (0.00–2.97)**			
3 *C. dayangbuntingensis*	3	9.90 (9.56–10.88)	9.86 (9.51–11.21)	**0.14 (0.07–0.22)**		
4 *C. langkawiensis*	10	10.49 (9.86–11.69)	10.19 (9.71–11.59)	7.62 (7.39–7.83)	**0.42 (0.00–0.69)**	
5 *C. lekaguli*	9	9.33 (8.46–10.80)	9.94 (8.98–11.77)	8.58 (8.00–9.59)	9.39 (8.42–10.54)	**2.30 (0.00–4.27)**

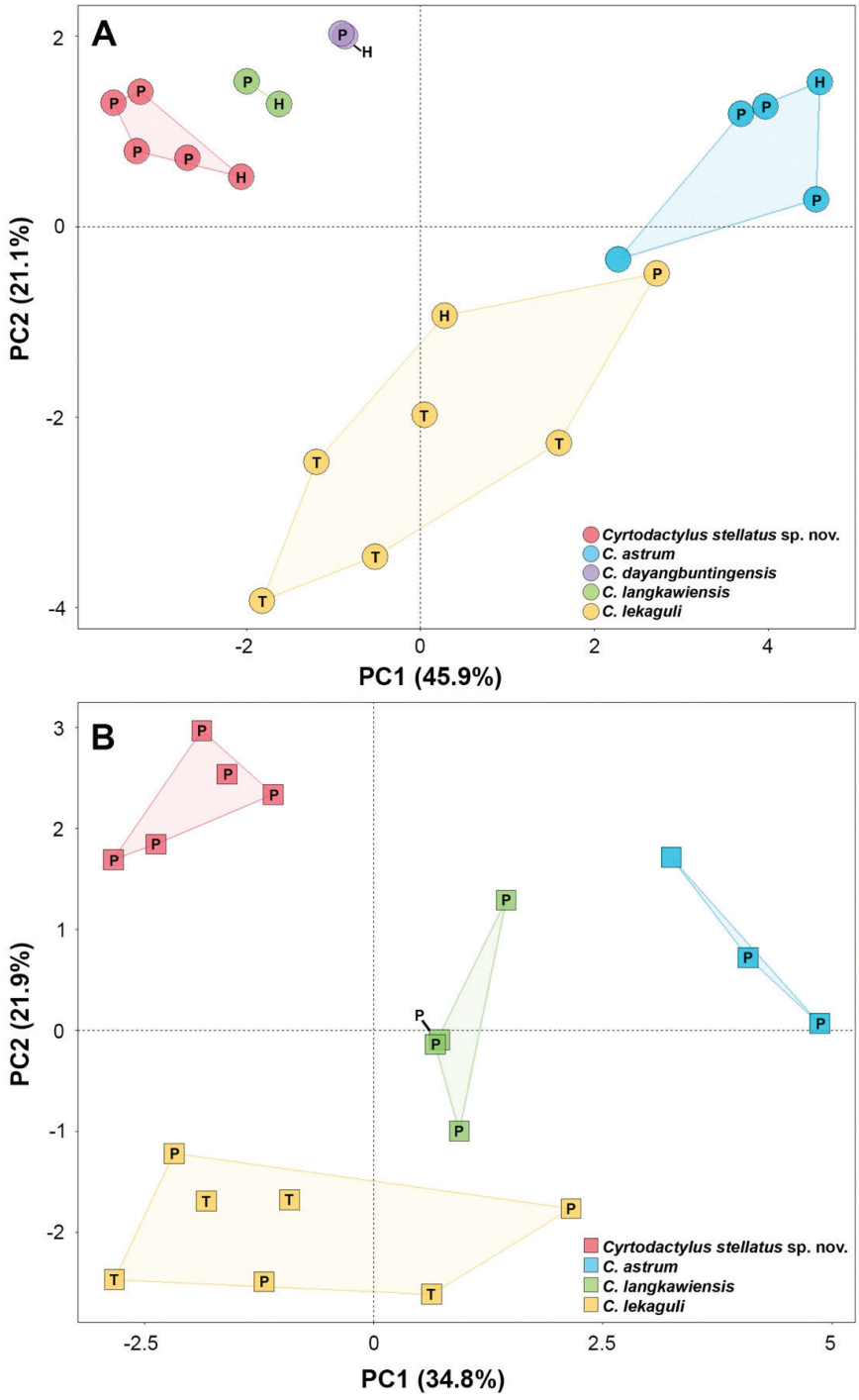

Figure 4. Plots of the first two principal components of *Cyrtodactylus stellatus* sp. nov. and the closely related species in Clade A based on adjusted mensural characters of **A** males and **B** females. The letters in the scatter plots refer to holotype (= H), paratype (= P), and topotype (= T).

from *C. astrum*, *C. langkawiensis* and *C. lekaguli* in nine characters (ANOVA, $p < 0.001$–0.007) except SVL_{adj}, TW_{adj}, AG_{adj}, HL_{adj}, ED_{adj} and EL_{adj} (ANOVA or Kruskal-Wallis test, $p = 0.052$–0.631). Subsequent Tukey's test revealed that the Tarutao Island population was significantly different from *C. astrum* in FL_{adj}, TBL_{adj}, HW_{adj}, HD_{adj}, EE_{adj}, ES_{adj}, and EN_{adj}; *C. langkawiensis* in HW_{adj}, ES_{adj}, EN_{adj}, and IN_{adj}; and *C. lekaguli* in HD_{adj}, IO_{adj}, and IN_{adj}. Summary pairwise results (Tukey's test or Dunn's test) of significant differences in morphological characters for adult males and females of Clade A are shown in Table 5. Additional differences in meristic characters and coloration are discussed in the comparison sections.

Table 4. Summary statistics and factor loadings of the first three principal components (PC) of 15 mensural characters for males and females of *Cyrtodactylus stellatus* sp. nov. and its closely related species including *C. astrum*, *C. dayangbuntingensis*, *C. langkawiensis*, and *C. lekaguli*. Bold texts indicate high loadings.

Characters	Males			Females		
	PC1	PC2	PC3	PC1	PC2	PC3
SVL_{adj}	0.660	-0.284	0.293	0.374	-0.097	-0.127
TW_{adj}	0.436	**0.795**	-0.073	0.380	**0.845**	0.194
FL_{adj}	**0.855**	-0.228	-0.051	0.693	0.111	0.003
TBL_{adj}	**0.951**	0.098	-0.032	**0.881**	0.181	0.102
AG_{adj}	-0.261	**-0.728**	0.364	-0.030	0.157	0.824
HL_{adj}	0.459	-0.508	-0.560	0.532	-0.194	0.537
HW_{adj}	**0.943**	-0.168	0.177	**0.785**	-0.350	-0.197
HD_{adj}	**0.838**	-0.325	0.188	0.526	-0.647	0.170
ED_{adj}	0.552	-0.195	-0.491	0.137	-0.086	0.612
EE_{adj}	**0.829**	-0.171	0.194	**0.755**	-0.410	0.266
ES_{adj}	**0.932**	0.113	0.054	**0.900**	-0.078	-0.271
EN_{adj}	**0.875**	0.246	0.142	**0.922**	0.122	-0.263
IO_{adj}	0.143	**0.850**	0.435	0.361	**0.854**	0.033
EL_{adj}	0.303	**0.770**	-0.417	0.343	0.690	-0.298
IN_{adj}	-0.105	0.093	0.560	-0.089	**0.719**	0.238
Eigenvalue	6.882	3.161	1.587	5.222	3.289	1.835
Percentage of variance	45.879	21.073	10.581	34.813	21.928	12.235
Cumulative proportion	45.879	66.952	77.533	34.813	56.741	68.976

Table 5. Summary pairwise results of statistically significant characters (Tukey's test; $p < 0.05$) from 15 mensural characters for males and females of *Cyrtodactylus stellatus* sp. nov. and closely related species (Clade A). Abbreviations are listed in Table 2. Key: * tested by Dunn's test; M = male; F = female.

		Cyrtodactylus stellatus sp. nov.		*C. astrum*		*C. langkawiensis*	
		M	F	M	F	M	F
Cyrtodactylus stellatus sp. nov.	M	–	–	–	–	–	–
	F	–	–	–	–	–	–
C. astrum	M	SVL, FL, TBL, HL, HW, HD, EE, ES*, EN	–	–	–	–	–
	F	–	FL, TBL, HW, HD, EE, ES, EN	–	–	–	–
C. langkawiensis	M	–	–	–	–	–	–
	F	–	HW, ES, EN, IN	–	HW, IN	–	–
C. lekaguli	M	SVL, TW, FL, HL, HW, HD, EE, ES*, IO, EL	–	TW, FL, TBL, HW, EN, IO, EL	–	–	–
	F	–	HD, IO, IN	–	FL, TBL, HW, ES, EN, IO, EL	–	ES

Taxonomic hypotheses

Cyrtodactylus samples from Tarutao Island, Mueang Satun District, Satun Province differed from its congeners in mtDNA, morphometrics and morphological comparisons. These corroborated lines of evidence provide sufficient support to warrant them specific species status and is described as new below.

Taxonomy

***Cyrtodactylus stellatus* sp. nov.**
http://zoobank.org/F2AF3CB9-F0FE-4749-9785-F57C7CAC021C
Figures 5–11
Stellar Bent-toed Gecko

Holotype. Adult male (ZMKU R 00905, Figs 5–7) collected from Thailand, Satun Province, Mueang Satun District, Tarutao National Park, Tarutao Island, Pha (= cliff) Toe Boo (6°42.185'N; 99°38.895'E; 2 m a.s.l.), on 11 March 2019 by Korkhwan Termprayoon, Anchalee Aowphol, Attapol Rujirawan, Natee Ampai and Siriporn Yodthong.

Paratypes (Figs 8–9). Two adult males (ZMKU R 00906–00907) and two adult females (ZMKU R 00908–00909), same data as holotype. One adult female (ZMKU R 00913) same data as holotype except collected on 12 May 2019. One adult male (ZMKU R 00903) and two adult females (ZMKU R 00899–00900), same data as holotype, except collected on 5 November 2017 by Korkhwan Termprayoon, Attapol Rujirawan, Natee Ampai, and Siriporn Yodthong. One adult male (ZMKU R 00915) collected from Thailand, Satun Province, Mueang Satun District, Tarutao National Park, Tarutao Island, Tarutao Outcrop (6°41.617'N; 99°38.796'E; 3 m a.s.l.) on 12 March 2019 by Korkhwan Termprayoon, Anchalee Aowphol, Attapol Rujirawan, Natee Ampai and Siriporn Yodthong.

Referred specimens. ZMKU R 00901 (immature male) and ZMKU R 00902 (immature female) same data as holotype except collected on 5 November 2017 by Korkhwan Termprayoon, Attapol Rujirawan, Natee Ampai, and Siriporn Yodthong. ZMKU R 00904 (immature male) same data as holotype, except collected on 5 April 2018. ZMKU R 00910–00911 (two immature males) and ZMKU R 00912 (immature female) same data as holotype. ZMKU R 00914 (immature female) same data as holotype except collected on 12 May 2019. ZMKU R 00916 (immature male) and ZMKU R 00917 (juvenile) collected from Thailand, Satun Province, Mueang Satun District, Tarutao National Park, Tarutao Island, Tarutao Outcrop (6°41.617'N; 99°38.796'E; 3 m a.s.l.) on 12 March 2019 by Korkhwan Termprayoon, Anchalee Aowphol, Attapol Rujirawan, Natee Ampai and Siriporn Yodthong.

Diagnosis. *Cyrtodactylus stellatus* sp. nov. can be distinguished from all other species of the *C. pulchellus* group by the combination of the following characters: (1) SVL 86.3–95.9 mm in adult males, 86.6–96.1 mm in adult females; (2) 12–15 supralabial and 10–13 infralabial scales; (3) weak tuberculation on body; (4) no tubercles on ven-

tral surfaces of forelimbs, gular region, or in ventrolateral body folds; (5) 32–47 paravertebral tubercles; (6) 19–23 longitudinal rows of dorsal tubercles; (7) 32–40 rows of ventral scales; (8) 20–23 subdigital lamellae on the fourth toe; (9) 24–29 femoroprecloacal pores in adult males; (10) precloacal pores present in adult females; (11) deep precloacal groove in males; (12) dorsum bearing a scattered pattern of white tubercles; (13) four dark dorsal body bands; (14) 10–12 dark caudal bands on original tail; (15) white caudal bands in adults heavily infused with dark pigmentation; and (16) posterior portion of tail in hatchlings and juveniles white.

Description of holotype. Adult male SVL 94.2 mm; head large, moderate in length (HL/SVL 0.29) and wide (HW/HL 0.61), somewhat flattened (HD/HL 0.38), distinct from neck, and triangular in dorsal profile; lores concave anteriorly, inflated posteriorly; frontal and prefrontal regions deeply concave; canthus rostralis rounded anteriorly; snout elongate (ES/HL 0.39), rounded in dorsal profile, laterally constricted; eye large (ED/HL 0.25); ear opening elliptical, moderate in size (EL/HL 0.09), obliquely oriented; eye to ear distance slightly greater than diameter of eye; rostral rectangular, divided dorsally by an inverted Y-shaped furrow, bordered posteriorly by left and right supranasals and internasal, bordered laterally by first supralabials; external nares bordered anteriorly by rostral, dorsally by a large anterior supranasal, posteriorly by two postnasals, ventrally by first supralabial; 13/14 (left/right) rectangular supralabials extending to just beyond upturn of labial margin, tapering abruptly below midpoint of eye; second supralabial slightly larger than first; 11/11 infralabials tapering in size posteriorly; scales of rostrum and lores slightly raised, larger than granular scales on top of head and occiput, those on posterior portion of canthus rostralis slightly larger; scales on occiput intermixed with small tubercles; large, boney frontal ridges bordering orbit confluent with boney, V-shaped, transverse, parietal ridge; dorsal superciliaries elongate, smooth, largest anteriorly; mental triangular, bordered laterally by first infralabials and posteriorly by left and right, trapezoidal postmentals which contact medially for 50% of their length; one row of slightly enlarged, elongate sublabials extending posteriorly to the seventh (left) and fifth (right) infralabials; small, granular, gular scales grading posteriorly into larger, flat, smooth, imbricate, pectoral and ventral scales.

Body relatively short (AG/SVL 0.46) with well-defined, non-tuberculate, ventrolateral folds; dorsal scales small, granular, interspersed with low, regularly arranged, weakly keeled tubercles, smaller intervening tubercles occasionally present; tubercles extend from occiput to caudal constriction, absent from regenerated portion of tail; tubercles on occiput and nape relatively small, those on body largest; approximately 21 longitudinal rows of tubercles at midbody; 36 paravertebral tubercles; 33 flat imbricate ventral scales between ventrolateral body folds; ventral scales larger than dorsal scales; precloacal scales large, smooth; deep precloacal groove.

Forelimbs moderate in stature, relatively short (FL/SVL 0.16); scales on dorsal surfaces of forelimbs granular intermixed with larger tubercles; scales of ventral surface of forearm flat, subimbricate, tubercles absent; palmar scales small, weakly rounded; digits well-developed, inflected at basal, interphalangeal joints; subdigital lamellae rec-

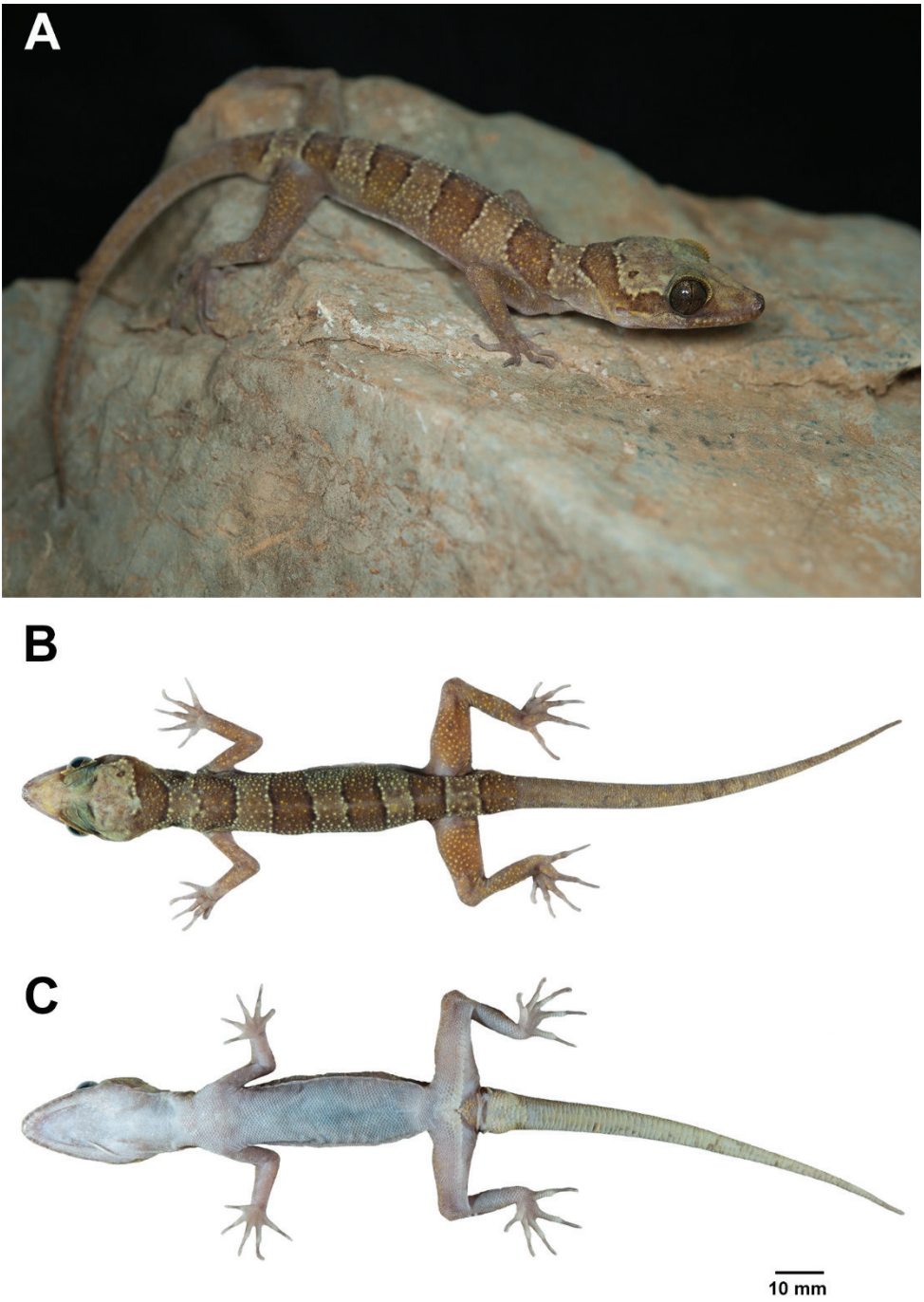

Figure 5. Adult male holotype of *Cyrtodactylus stellatus* sp. nov. (ZMKU R 00905) from Tarutao Island, Satun Province. **A** specimen in life and immediately before preservative: **B** dorsal and **C** ventral views.

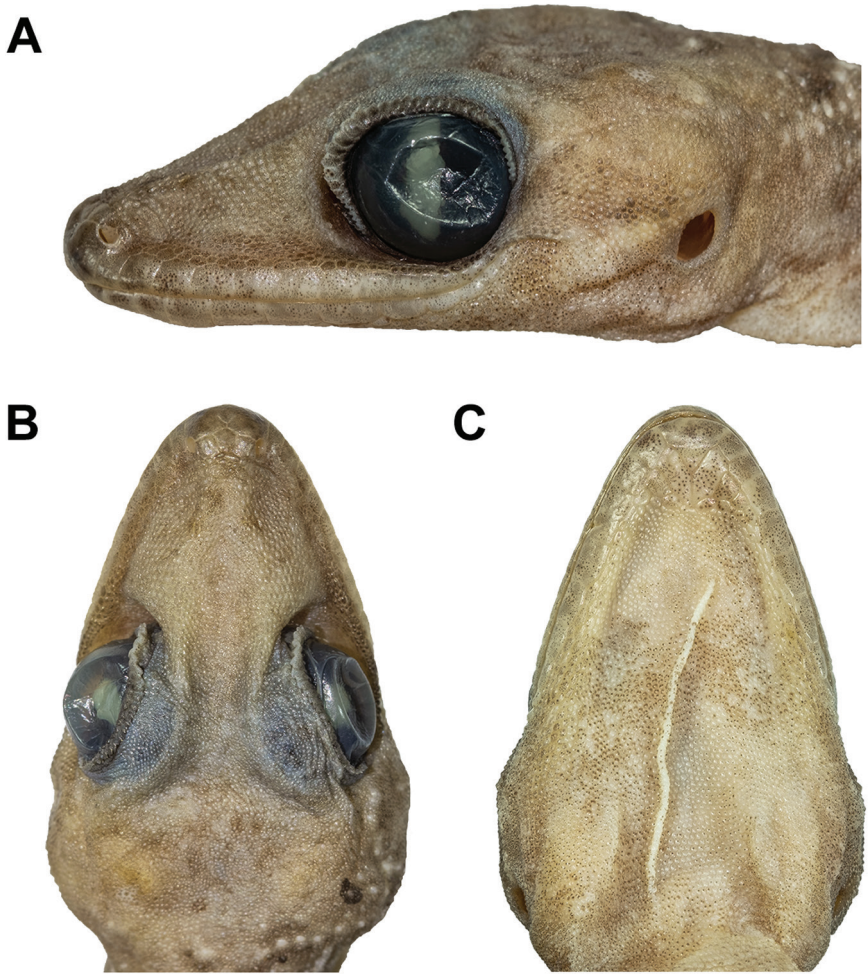

Figure 6. Head of the holotype of *Cyrtodactylus stellatus* sp. nov. (ZMKU R 00905): **A** lateral view of the left side **B** dorsal view, and **C** ventral view.

tangular proximal to joint inflection, only slightly expanded distal to inflection; digits narrower distal to joints; claws well-developed, sheathed by a dorsal and ventral scale; the fifth digit broken on left forearm; hind limbs more robust than forelimbs, moderate in length (TBL/SVL 0.19), larger tubercles on dorsal surface of legs separated by smaller juxtaposed scales; ventral scales of thigh flat, smooth, imbricate, larger than dorsal granular scales; ventral, tibial scales flat, smooth, imbricate; a single row of 34 enlarged femoroprecloacal scales extend nearly from knee to knee through precloacal region where they are continuous with enlarged, pore-bearing precloacal scales; 27 separated pore-bearing femoroprecloacal scales (Fig. 10A), forming an inverted T bearing a deep, precloacal groove; six pore-bearing scales bordering groove (three on each side

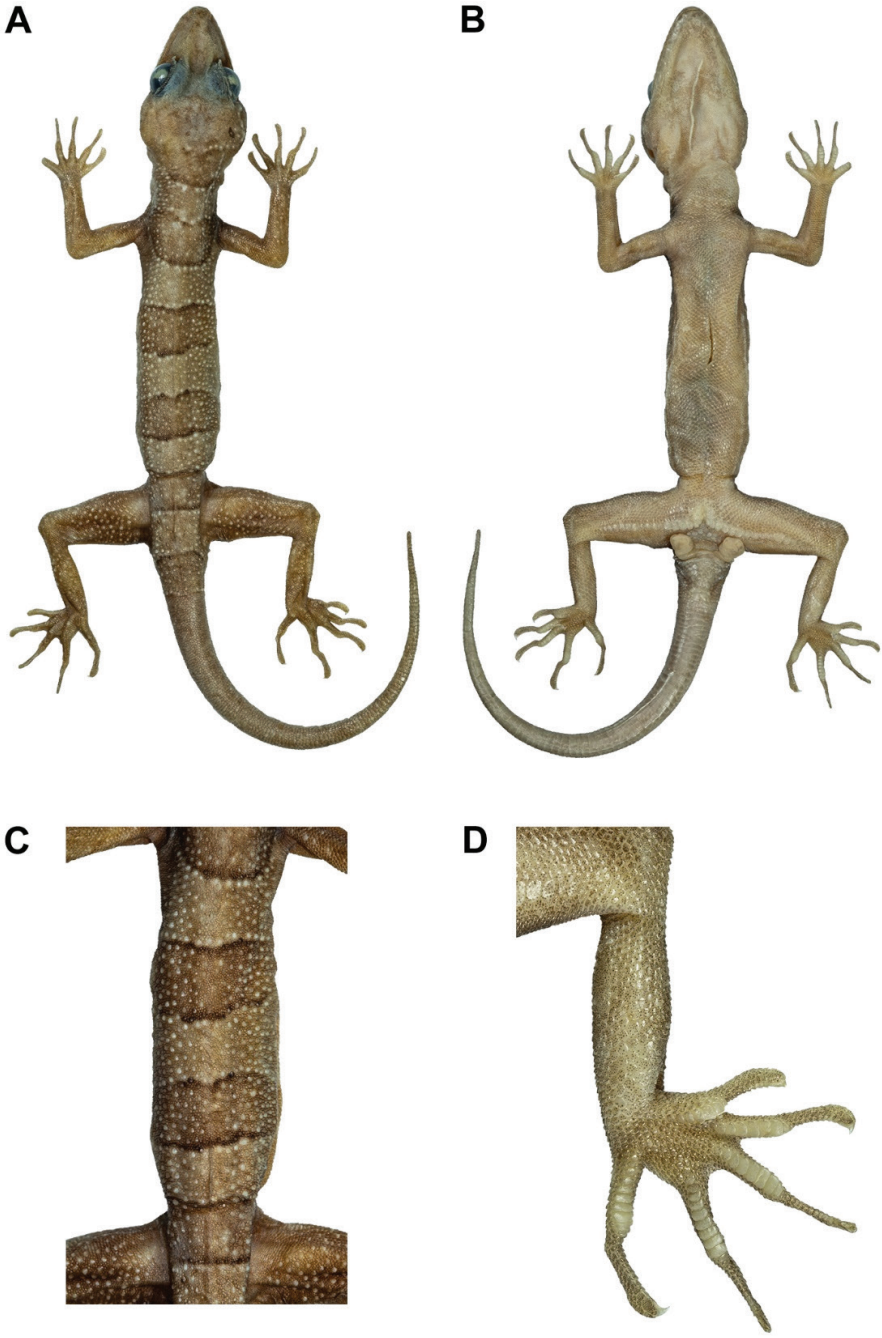

Figure 7. Male holotype of *Cyrtodactylus stellatus* sp. nov. (ZMKU R 00905) in preservation. **A** dorsal and **B** ventral views **C** tuberculation on dorsum, and **D** ventral view of left foot.

Figure 8. Male paratypes of *Cyrtodactylus stellatus* sp. nov. in preservation. **A** dorsal and **B** ventral views; from left to right: ZMKU R 00903, ZMKU R 00906, ZMKU R 00907, and ZMKU R 00915.

of groove); postfemoral scales immediately posterior to enlarged scale row small, nearly granular, forming an abrupt union with postfemoral scales on posteroventral margin of thigh; plantar scales weakly rounded to flat; digits well developed, inflected at basal, interphalangeal joints; subdigital lamellae proximal to joint inflection rectangular, only slightly expanded distal to inflection; digits narrower distal to joints; claws well-developed, sheathed by a dorsal and ventral scale; 21/22 subdigital lamellae on the 4th toe.

Tail 94.8 mm in length, completely regenerated, 9.2 mm in width at base, tapering to a point; regenerated tail covered with small, smooth, rectangular scales dorsally; base of tail bearing hemipenial swellings; one row of 4/4 medium-sized postcloacal tubercles on each hemipenial swelling; postcloacal scales smooth, flat, large, imbricate.

Coloration in life (Fig. 5). Dorsal ground color of head, body, and limbs light-brownish grey; a wide, dark-brown nuchal band bordered anteriorly and posteriorly by thin, creamy-white lines bearing tubercles that extend from the posterior margin of one eye to the posterior margin of other eye; the color of nuchal band and creamy-white lines is faded above left ear opening; four dark-brown body bands between nuchal loop and hind limb insertions that are also bordered anteriorly and posteriorly by thin, creamy-white lines bearing tubercles, first band terminates at shoulders, second and third bands terminate just dorsal of ventrolateral folds, the fourth band terminates at

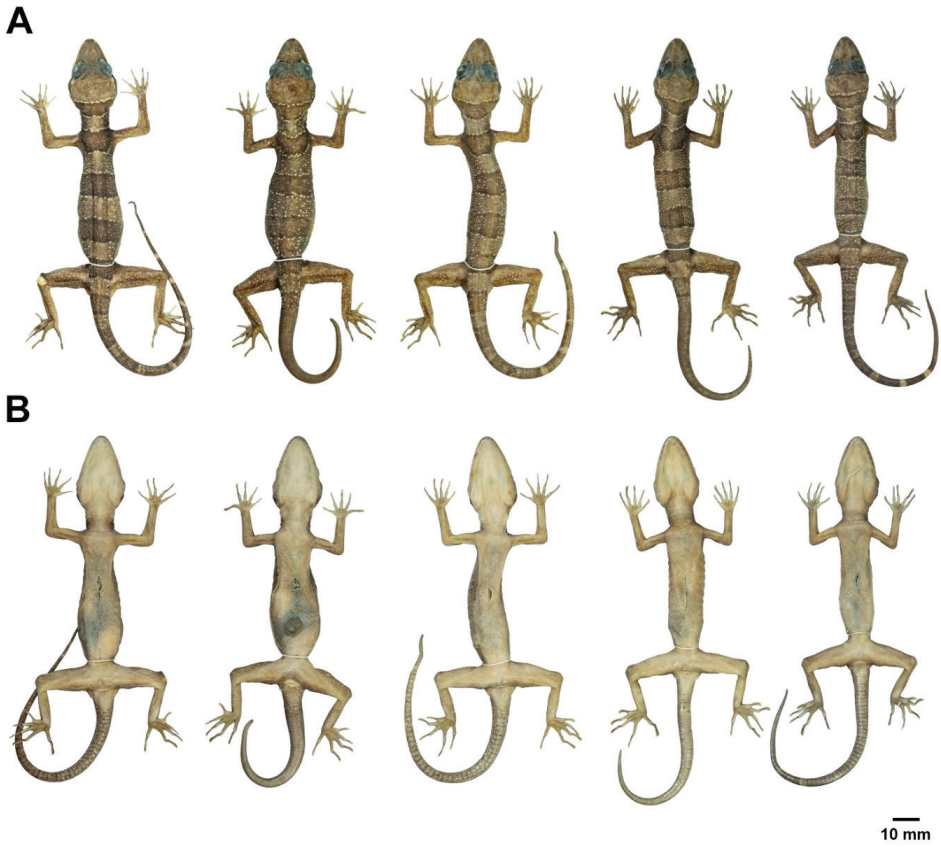

Figure 9. Female paratypes of *Cyrtodactylus stellatus* sp. nov. in preservation. **A** dorsal and **B** ventral views; from left to right: ZMKU R 00899, ZMKU R 00900, ZMKU R 00908, ZMKU R 00909, and ZMKU R 00913.

femurs; dark body bands slightly larger than light-colored interspaces; creamy-white to light-yellow tubercles scattered on dorsal surfaces of nape, body, and limbs; one additional dark-brown band posterior to hind limbs; light-brown regenerated tail, bearing yellowish pigment on some scales; ventral surfaces of head smudged with brown; abdomen and limbs beige, with slightly darker, lateral regions.

Coloration in preservative (Figs 6, 7). The overall color pattern of head, body, limbs, and tail similar to that in life with some fading. Ground color of head, body, limbs, and dorsum light-brown; dark body bands lighter than in life. Colored tuberculation on dorsum fade to off-white. Tan colored on the ventral surface.

Variation. *Cyrtodactylus stellatus* sp. nov. usually varies in coloration and banding pattern (Figs 8–11; Tables 6, 7). All specimens possess a clear dark-brown nuchal band which is less clearly defined in ZMKU R 00903 and the holotype. In adult females, precloacal pores are present but they lack the precloacal groove (Fig. 10B). Four specimens (ZMKU R 00903, ZMKU R 00907, ZMKU R 00911, and ZMKU R 00913) have prominent light-yellow tubercles scattered on the dorsum and limbs. Male paratype (ZMKU R 00907) has continuous pore-bearing femoroprecloacal scales. Original

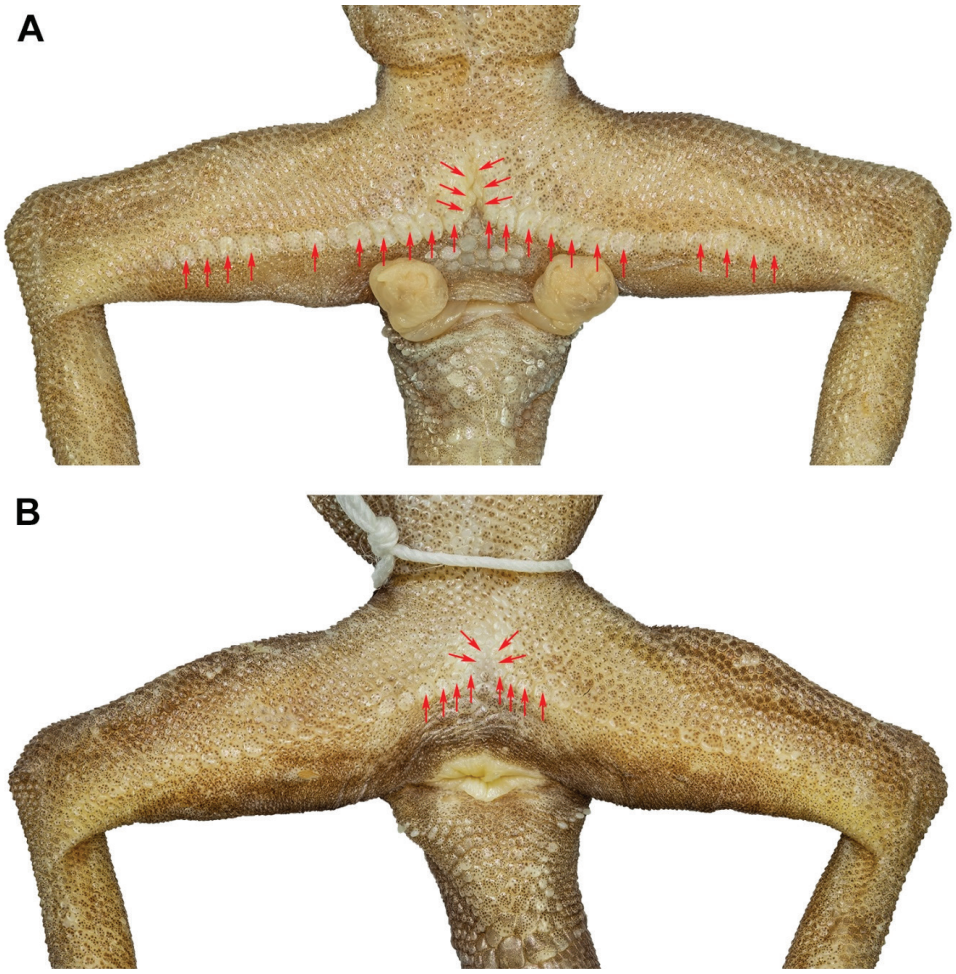

Figure 10. Precloacal region of *Cyrtodactylus stellatus* sp. nov. showing **A** precloacal depression with pore-bearing femoroprecloacal scales in male holotype (ZMKU R 00905), and **B** pore-bearing precloacal scales with lacking depression in female paratype (ZMKU R 00900). Red arrows show pore-bearing scales.

tails (ZMKU R 00899, ZMKU R 00901–00902, ZMKU R 00910, ZMKU R 00912, and ZMKU R 00916) have 10–12 dark caudal bands (Fig. 11A, B), light bands diffused with dark pigment in adults (immaculate in immature and juvenile), subcaudal scales transversely enlarged and shallow caudal furrows. Male paratypes have a single row of 3–4L/2–4R postcloacal tubercles on each hemipenial swelling except ZMKU R 00907 which has two rows of 4/5 on each side. This character in female paratypes is very small, and a single row of 2–4/2–4 on each side at the base of tail.

In life, the juvenile (ZMKU R 00917; SVL 43.1 mm) had a body pattern similar to the adults but with less prominent tuberculation, brownish yellow ground color of body, dark body bands are bordered by yellow lines, some bearing tubercles, the original tail has approximately 10 dark caudal bands, the posterior portion of tail is white, and light caudal bands are immaculate (Fig. 11C).

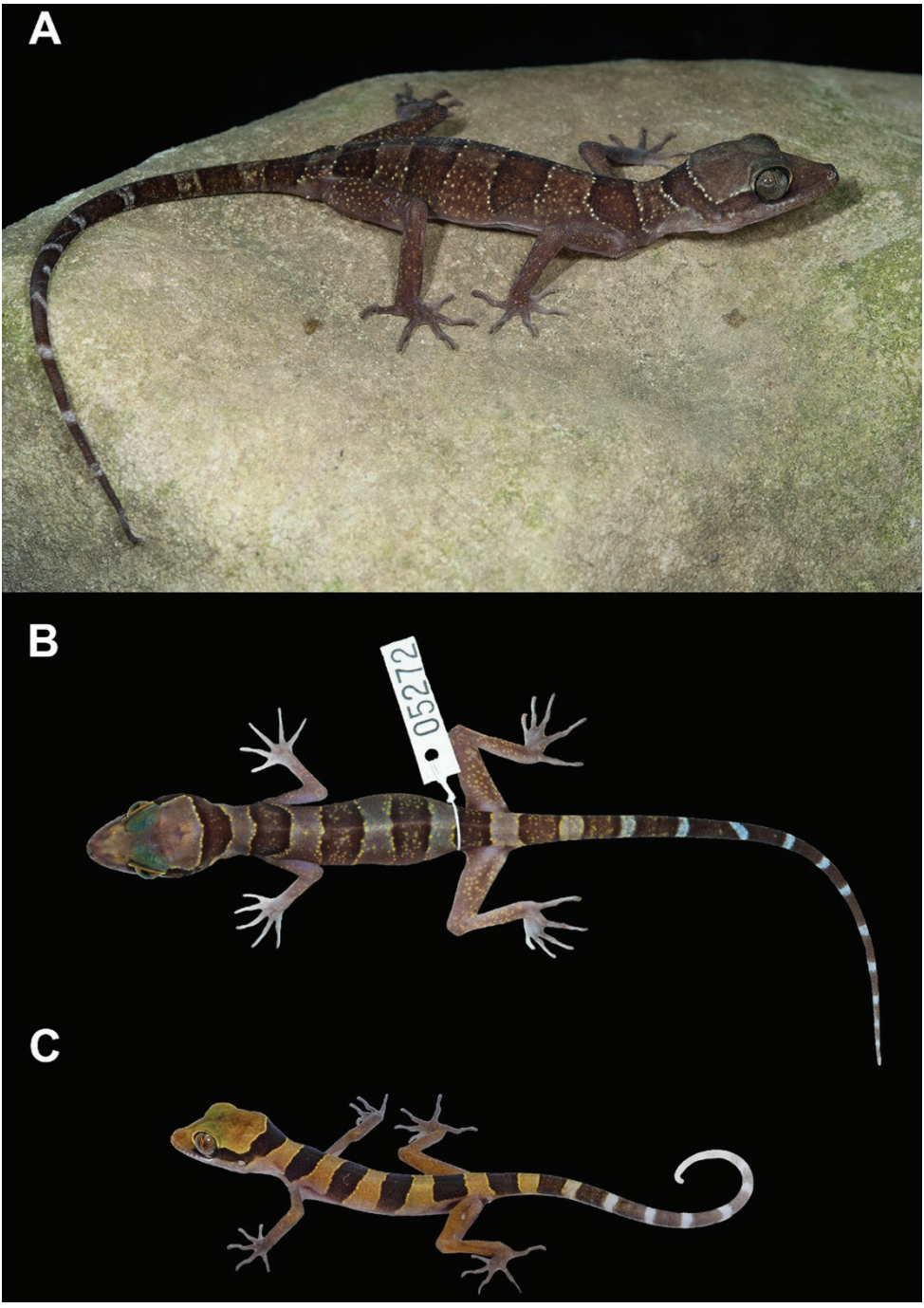

Figure 11. Variation of *Cyrtodactylus stellatus* sp. nov. **A** adult female ZMKU R 00899 having 11 dark caudal bands on the original tail and white caudal bands infused with dark pigmentation **B** immature female ZMKU R 00902 (field number AA 05272) having 12 dark caudal bands on the original tail with immaculate white caudal bands, and **C** juvenile ZMKU R 00917 having light-yellow color on the body and bearing white tail tip.

Table 6. Descriptive measurement (millimeters), meristic (left/right) and color pattern characters of the type series of *Cyrtodactylus stellatus* sp. nov. Key: H = holotype; P = paratype; M = male; F = female; / = data unavailable or unapplicable; b = broken; r = regenerated. Morphological abbreviations are defined in Table 2.

	ZMKU R 00905	ZMKU R 00903	ZMKU R 00906	ZMKU R 00907	ZMKU R 00915	ZMKU R 00899	ZMKU R 00900	ZMKU R 00908	ZMKU R 00909	ZMKU R 00913
	H	P	P	P	P	P	P	P	P	P
Sex	M	M	M	M	M	F	F	F	F	F
SVL	94.2	95.9	94.6	87.9	86.3	96.1	93.6	94.8	90.4	86.6
TL	94.8r	96.8r	92.3r	69.0r	18.5b	124.4	70.5r	107.5r	81.7r	102.3r
TW	9.2	9.7	9.2	8.4	7.5	7.6	9.1	9.1	10.3	7.1
FL	15.4	15.3	15.1	14.4	14.1	14.9	14.5	15.9	15.6	14.8
TBL	18.1	18.3	17.8	17.4	17.6	17.7	17.3	18.1	17.8	16.5
AG	43.3	43.7	43.9	44.4	39.6	46.0	44.5	44.5	45.4	39.9
HL	27.6	26.3	27.0	25.2	24.8	26.5	26.9	27.3	26.4	25.7
HW	16.7	16.3	17.3	15.4	14.7	16.4	16.8	17.2	15.7	15.2
HD	10.4	9.6	10.8	9.2	8.7	10.4	10.2	10.1	9.4	9.2
ED	6.8	6.7	6.7	5.9	5.8	6.4	6.8	6.6	6.6	5.6
EE	7.1	7.6	7.2	6.3	6.2	6.9	7.0	7.0	6.7	6.8
ES	10.8	10.7	10.9	9.8	9.8	10.9	10.8	10.7	10.4	10.1
EN	8.5	8.3	8.3	7.8	7.5	8.2	8.3	8.5	8.1	7.9
IO	5.9	6.2	6.6	5.8	5.5	6.0	6.4	6.1	5.7	6.2
EL	2.4	2.5	2.2	2.0	2.0	2.0	2.8	2.7	2.1	2.3
IN	2.9	3.2	3.5	3.1	3.0	3.8	3.3	3.2	3.2	2.6
SL	13/14	14/13	15/12	13/14	13/12	13/13	13/13	13/12	12/12	13/13
IL	11/11	10/10	11/12	12/12	11/11	11/11	12/11	12/12	10/11	11/11
PVT	36	35	41	38	43	38	40	40	40	47
LRT	21	20	21	19	22	20	21	19	22	22
VS	33	37	36	35	36	37	39	37	37	36
4TL	21/22	21/21	21/21	21/20	23/22	22/22	21/21	22/23	22/20	20/20
FPP in adult males	27	25	24	29	27	/	/	/	/	/
PP in adult females	/	/	/	/	/	15	12	14	11	11
BB	4	4	4	4	4	4	4	4	4	4
DCB	/	/	/	/	/	11	/	/	/	/
Body band/ interspace ratio	1.12	1.20	1.04	1.10	1.68	1.07	1.03	1.23	1.06	0.92
Precloacal groove	Deep	Deep	Deep	Deep	Deep	Absent	Absent	Absent	Absent	Absent
Femoroprecloacal pores continuous	No	No	No	Yes	No	/	/	/	/	/
Tuberculation	Weak	Weak	Weak	Weak	Weak	Weak	Weak	Weak	Weak	Weak
Tubercles on ventral surface of forelimb	No	No	No	No	No	No	No	No	No	No
Tubercles in gular region	No	No	No	No	No	No	No	No	No	No
Ventrolateral fold tuberculate	No	No	No	No	No	No	No	No	No	No
Dorsum bearing scattered pattern of white tubercles	Yes	Yes	Yes	Yes	Yes	Yes	Yes	Yes	Yes	Yes
Hatchlings/ juveniles with white tail tip	/	/	/	/	/	/	/	/	/	/
Adult posterior caudal region white	/	No	/	/	/	No	/	No	/	/
White caudal bands in adults immaculate	/	No	/	/	/	No	/	No	/	No

Distribution. *Cyrtodactylus stellatus* sp. nov. is currently known only from Tarutao Island, Satun Province, Thailand (Figs 1, 12A).

Natural history. All specimens of *C. stellatus* sp. nov. were collected from a karst forest at night (1950–2100 h) with temperatures between 27.1–32.2 °C and relative humidity between 71.4–93.0%. The specimens were found on karst walls, within karst crevices and on nearby karst boulders. Some specimens occurred on tree trunks or

Table 7. Descriptive meristic (left/right) and color pattern characters of the referred specimens of *Cyrtodactylus stellatus* sp. nov. Key: RF = referred specimen; IM-M = immature male; IM-F = immature female; J = juvenile; / = data unavailable or unapplicable. Morphological abbreviations are defined in Table 2.

	ZMKU R 00901	ZMKU R 00902	ZMKU R 00904	ZMKU R 00910	ZMKU R 00911	ZMKU R 00912	ZMKU R 00914	ZMKU R 00916	ZMKU R 00917
	RF	RF	RF	RF	RF	RF	RF	RF	RF
Age	IM-M	IM-F	IM-M	IM-M	IM-M	IM-F	IM-F	IM-M	J
SVL	77.4	68.4	72.5	82.5	81.8	73.8	81.9	79.9	43.1
SL	12/12	13/13	12/12	12/13	14/14	14/14	13/13	13/14	/
IL	10/11	11/12	10/11	11/11	10/12	13/11	10/11	10/11	/
PVT	38	38	32	41	41	41	42	40	/
LRT	20	21	19	22	19	19	22	23	/
VS	34	40	34	37	32	37	38	37	/
4TL	22/21	22/22	21/20	21/21	20/21	23/23	22/21	21/22	/
FFP in adult males	/	/	/	/	/	/	/	/	/
PP in adult females	/	/	/	/	/	/	/	/	/
BB	4	4	4	4	4	4	4	4	4
DCB	11	12	/	11	/	10	/	11	/
Body band/ interspace ratio	1.35	1.36	1.40	1.09	0.99	1.44	1.22	1.39	/
Precloacal groove	/	/	/	/	/	/	/	/	/
Tuberculation	Weak	Weak	Weak	Weak	Weak	Weak	Weak	Weak	Weak
Tubercles on ventral surface of forelimb	No	No	No	No	No	No	No	No	No
Tubercles in gular region	No	No	No	No	No	No	No	No	No
Ventrolateral fold tuberculate	No	No	No	No	No	No	No	No	No
Dorsum bearing scattered pattern of white tubercles	Yes	Yes	Yes	Yes	Yes	Yes	Yes	Yes	No
Hatchlings/juveniles with white tail tip	No	No	No	No	No	No	No	No	Yes
Adult posterior caudal region white	/	/	/	/	/	/	/	/	/
White caudal bands in adults immaculate	/	/	/	/	/	/	/	/	/

vines near the karst formations (Fig. 12). The holotype was found on a karst wall approximately 1 m above the ground within karst forest. Eight specimens (ZMKU R 00900, ZMKU R 00906, ZMKU R 00908, ZMKU R 00911–00912, ZMKU R 00913, and ZMKU R 00915–00916) were found on karst walls from 0.5–3.0 m above the ground. ZMKU R 00907, ZMKU R 00910, and ZMKU R 00914 were found in karst crevices. Three specimens (ZMKU R 00901, ZMKU R 00903, and ZMKU R 00909) were found on karst boulders. Four specimens (ZMKU R 00899, ZMKU R 00902, ZMKU R 00904, and ZMKU R 00917) were perched on vegetation near karst walls or karst boulders.

Two gravid females (ZMKU R 00899–00900) were collected in November 2017 and contained two eggs (externally visible). The juvenile was found on a vine in May 2019. *Cyrtodactylus stellatus* sp. nov. appears to be nocturnal and sympatric with two other gekkonids, *Gehyra mutilata* Wiegmann, 1834 and the diurnal species *Cnemaspis tarutaoensis* Ampai et al., 2019.

Etymology. The specific epithet *stellatus* is Latin word, meaning starry or starred, and refers to scattered pattern of light-colored tubercles on dorsum and limbs. The name corresponds with the sister taxon *C. astrum* that shared similar diagnostic character (scattered light-colored tubercles pattern on dorsum).

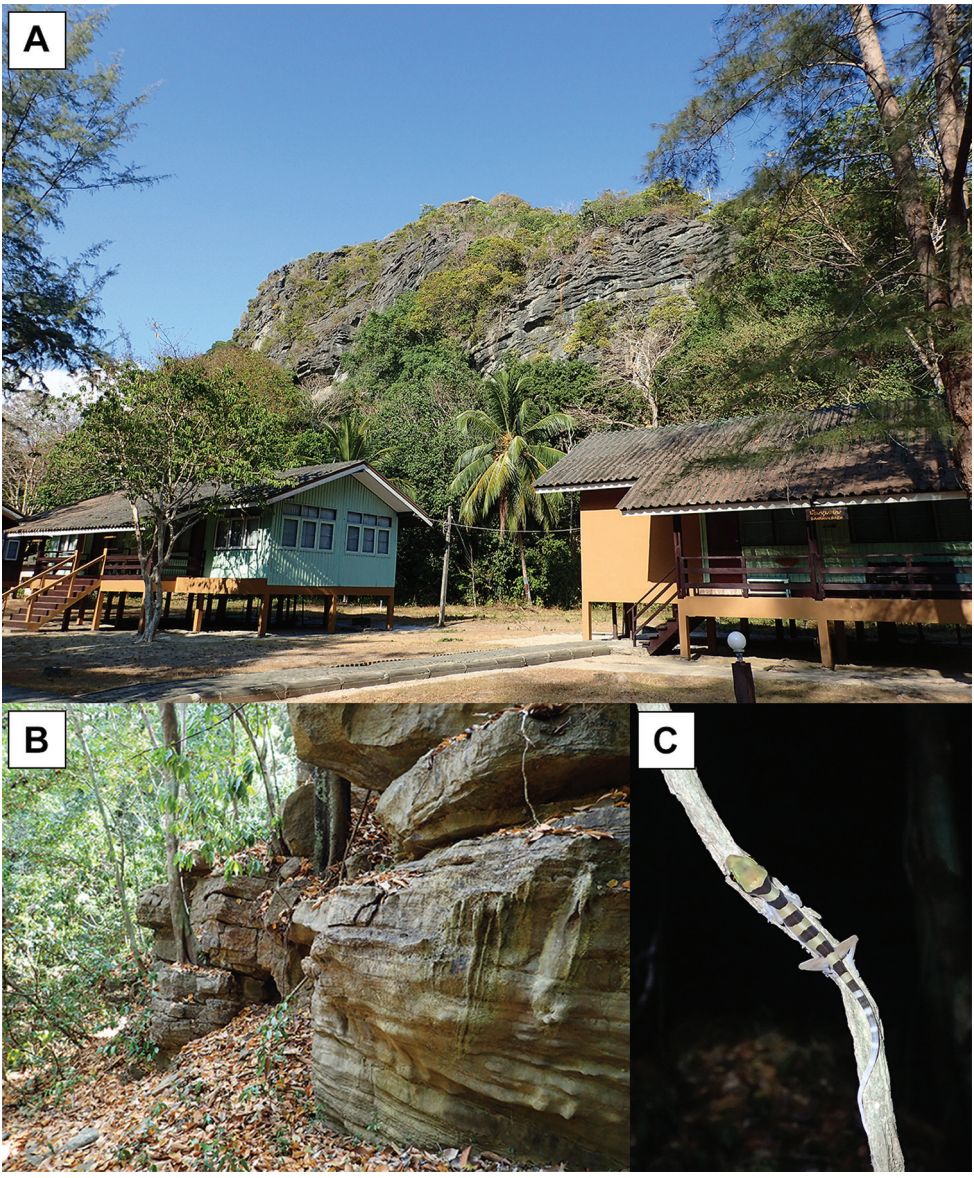

Figure 12. Habitat of *Cyrtodactylus stellatus* sp. nov. at the type locality, Tarutao Island, Satun Province, Thailand. **A** Pha Toe Boo karst formation **B** karst microhabitat structure and **C** vegetation (vine) used by a juvenile in karst habitat.

Comparison. *Cyrtodactylus stellatus* sp. nov. can be distinguished from other species in the *C. pulchellus* group by having a combination of weak tuberculation on the body; no tubercles on ventral surface of forelimbs, gular region, or in ventrolateral body folds; 19–23 longitudinal tubercle rows; 32–40 ventral scales; 20–23 subdigital lamellae on the fourth toe; 24–29 femorprecloacal pores in males; deep precloacal

Table 8. Diagnostic characters of *Cyrtodactylus stellatus* sp. nov. and its related species within the *C. pulchellus* group. W = weak; P = prominent; / = data unavailable. Some information was collected from the following literature (Grismer et al. 2012, 2014, 2016; Quah et al. 2019, Wood et al. 2020, and Termprayoon et al. 2021).

	Clade A					Clade B											
	stellatus sp. nov.	*astrum*	*dayangbuntingensis*	*langkawiensis*	*lekaguli*	*australotitiwangaensis*	*bintangrendah*	*bintangtinggi*	*evanquahi*	*hidupselamanya*	*jelawangensis*	*longgongensis*	*macrotuberculatus*	*pulchellus*	*sharkari*	*timur*	*trilatofasciatus*
Sample size	10	13	3	10	16	12	6	14	3	14	4	4	39	13	1	5	6
Maximum SVL	96.1	108.3	99.0	99.8	108.3	120.1	114.4	111.1	96.0	102.7	119.8	103.1	117.9	114.1	100.1	120.5	122.2
SL	12–15	10–12	12–14	9–12	10–12	9–12	8–12	9–13	9 or 10	9–11	10–12	10 or 11	9–12	11	10–12	9–12	9–13
IL	10–13	9–12	10–11	8–10	9–11	9–13	8 or 10	8–11	9 or 10	8–10	8–10	8–10	9–11	10	8–11	8–11	7–11
PVT	32–47	40–57	35–36	34–44	30–50	37–45	36–44	31–42	31–34	33–43	38–43	36–41	36–42	31	34–38	39–48	34–49
LRT	19–23	20–29	20–22	21–25	20–25	22–30	22–25	21–26	18–23	19–24	23–25	22–25	19–27	22–26	24	21–24	23–27
VS	32–40	31–46	36–39	38–43	30–43	32–40	31–39	36–40	29–33	26–33	31–36	32 or 33	17–28	29–34	41	31–40	33–36
4TL	20–23	20–24	21–23	19–21	20–25	21–25	21–24	21–24	22–23	19–24	21–24	20–23	19–23	21–26	24	21–25	22–27
FPP in adult males	24–29	28–38	26–29	30	30–40	39–45	41–46	37–41	32–36	17–22	36	39–41	28–42	33–39	46	21 or 22	41–46
PP in adult females	11–15	Absent	Absent	Absent	Absent	Absent	Absent	Absent	Absent	Absent	Absent	Absent	Absent	Absent	Absent	Absent	Absent
No. of body bands	4	4	4	4 or 5	4 or 5	3(1) or 4	4	3(1) or 4	6 or 7	4	4	4 or 5	3–4	4	4	4	3
Body band/ interspace ratio	0.92–1.68	0.98–2.07	0.75	0.75–1.00	0.86–2.00	1.00–2.00	1.00–1.25	1.00–1.25	0.82–1.10	1.00–1.25	1.00–1.50	0.50–1.25	0.95–1.74	0.75–1.25	1.75	1.00–1.25	2.00–2.75
DCB	10–12	13 or 14	>7	11–16	12–14	7–8	8 or 9	8–10	9–11	8–10	10	14	7–10	8–10	7	8–10	6–7
Precloacal groove in males	Deep	Deep	Deep	Deep	Deep	Deep	Deep	Deep	Shallow	Deep	Deep	Deep	Deep	Deep	Shallow	Deep	Deep
Femoroprecloacal pores continuous	Both	Yes	Yes	Yes	Yes	Yes	Yes	Yes	Yes	Yes	Yes	Yes	Yes	Yes	Yes	Yes	Yes
Tuberculation	W	W	W	W	W	P	P	P	P	W	P	W	P	P	W	W	P
Tubercles on ventral surface of forelimb	No	No	No	No	No	No	No	No	No	No	Yes	No	Yes	No	No	No	No
Tubercles in gular region	No	No	No	No	No	No	No	No	No	No	No	No	Yes	No	No	No	No
Ventrolateral fold tuberculate	No	No	No	No	No	No	Yes	No	No	No	No	No	Yes	No	No	No	No
Dorsum bearing scattered pattern of white tubercles	Yes	Yes	Yes	No	No	No	No	No	No	No	No	No	No	No	No	No	No
Hatchlings/juveniles with white tail tip	Yes	Yes	Yes	Yes	Yes	No	No	No	Yes	Yes	Yes	/	No	No	/	No	No
Adult posterior caudal region white	No	No	No	No	No	No	No	No	Yes	Yes	No	No	No	No	No	No	No
White caudal bands in adults immaculate	No	No	No	No	No	Yes	Yes	Yes	No	Yes	No	Yes	No	Yes	Yes	Yes	Yes

groove in males; 11–15 precloacal pores in females; scattered pattern of white, cream or light-yellow tubercles on dorsum; 10–12 dark caudal bands on original tail; white caudal bands on original tail infused with dark pigmentation in adults; and juveniles with white tail tip. Additional comparisons between *C. stellatus* sp. nov. and other species in the *C. pulchellus* group are in Table 8.

Based on phylogenetic tree, *C. stellatus* sp. nov. is embedded in Clade A along with *C. astrum, C. dayangbuntingensis, C. langkawiensis*, and *C. lekaguli*. It can be distinguished from all four species by having smaller maximum SVL of 96.1 mm (vs. 108.3 mm in *C. astrum*, 99.0 mm in *C. dayangbuntingensis*, 99.8 mm in *C. langkawiensis*, and 108.3 in *C. lekaguli*); 24–29 femoroprecloacal pores in males (vs. 28–38 in *C. astrum*, 30 in *C. langkawiensis*, and 30–40 in *C. lekaguli*); 11–15 precloacal pores in females (vs. absent in *C. astrum, C. dayangbuntingensis, C. langkawiensis*, and *C. lekaguli*); scattered pattern of white, cream or light-yellow tubercles on dorsum (vs. absent in *C. langkawiensis*, and *C. lekaguli*); the ratio of dark body bands to the light color interspaces 0.92–1.68 (vs. 0.75 in *C. dayangbuntingensis*); 10–12 dark caudal bands (vs. 13 or 14 in *C. astrum*).

Discussion

The discovery of *C. stellatus* sp. nov. brings the total number of species in the *C. pulchellus* group to 17, of which four have been reported from Thailand. This new species is only known from karst habitats on Tarutao Island and seems to have a narrow geographic distribution (endemic to Tarutao Island). Molecular analyses recovered it as the sister taxon to *C. astrum* and is closely related to *C. dayangbuntingensis, C. langkawiensis,* and *C. lekaguli*. Although *C. stellatus* sp. nov. showed a similar morphological pattern to its sister species, morphological analyses and comparisons of meristic characters revealed that this new species is clearly different from its congeners species of *Cyrtodactylus*. Among *Cyrtodactylus*, most useful diagnostic characters are associated with the femoral and precloacal pores (Harvey et al. 2015). These characters are easily detected in males, but those in females are superficial and only found in some species (e.g., *C. marmoratus* Gray, 1831; *C. psarops* Harvey et al., 2015; *C. sworderi* Smith, 1925). We found differences in pore-bearing scales between *C. stellatus* sp. nov. and other species in the *C. pulchellus* group, that proved to be useful in distinguishing among species. Members of the *C. pulchellus* group mostly possess a continuous series of enlarged, pore-bearing femoroprecloacal scales in males, but *C. stellatus* sp. nov. presents a discontinuous row of femoroprecloacal pores except one individual (ZMKU R 00907), which has a continuous series. Moreover, the presence of precloacal pores were found in females of *C. stellatus* sp. nov., which has not been reported in the other species (Grismer et al. 2012; Quah et al. 2019; Wood et al. 2020, Termprayoon et al. 2021).

In addition, we found that the reported sampling localities of *C. lekaguli* (ZMKU R 00720–00723) were incorrectly stated as "Thailand, Changwat Province, Takua Pa District, Phangnga" in previous studies (i.e., Grismer et al. 2016; Quah et al. 2019;

Wood et al. 2020, Termprayoon et al. 2021). Therefore, we corrected the sampling localities to "Thailand, Phang-nga Province, Mueang Phang-nga District" (see Table 1).

The discovery of this new species suggests that undiscovered species of the *C. pulchellus* group may still occur in southern Thailand where there are still numerous unexplored karst areas. Additional surveys are needed to determine the extent of the geographic range of *C. stellatus* sp. nov. and the *C. pulchellus* group in as a whole in the region.

Acknowledgments

This research was supported by the Center of Excellence on Biodiversity (BDC), Office of Higher Education Commission (BDC-PG4-160022). Research protocol was approved by the Institutional Animal Care and Use Committee of Faculty of Science, Kasetsart University (project number ACKU61-SCI-006). KT was supported by a grant from the Faculty of Science, Kasetsart University (50th Anniversary of Faculty of Science). AR and AA were supported by Kasetsart University Research and Development Institute (KURDI), the Department of Zoology, and International SciKU Branding (ISB), Faculty of Science, Kasetsart University. NA was supported by Srinakharinwirot University Research Grant. The Department of National Parks, Wildlife and Plant Conservation, Thailand for providing permission to conduct the research in Tarutao National Park and Khao Banthat Wildlife Sanctuary. Kanchanapan Kamhang (Tarutao National Park) and Bamrungrat Ploydam (Khao Banthat Wildlife Sanctuary) for facilitating the fieldwork. L. Lee Grismer (La Sierra University), Wachara Sanguansombat and Sunchai Makchai (Thailand Natural History Museum) made specimens in their care available for study. Siriporn Yodthong assisted with fieldwork. This paper is contribution number 950 of the Auburn University Museum of Natural History. We thank L. Lee Grismer and Evan S.H. Quah for providing their suggestions, which greatly improved the manuscript.

References

Ampai N, Rujirawan A, Wood PL Jr, Stuart BL, Aowphol A (2019) Morphological and molecular analyses reveal two new insular species of *Cnemaspis* Strauch, 1887 (Squamata, Gekkonidae) from Satun Province, southern Thailand. ZooKeys 858: 127–161. https://doi.org/10.3897/zookeys.858.34297

Chan KO, Grismer LL (2021) Correcting for body size variation in morphometric analysis. bioRxiv 2021.05.17.444580. https://doi.org/10.1101/2021.05.17.444580

Chomdej S, Suwannapoom C, Pawangkhanant P, Pradit W, Nazarov RA, Grismer LL, Poyarkov NA (2020) A new species *Cyrtodactylus* Gray (Squamata: Gekkonidae) from western Thailand and the phylogenetic placement of *C. inthanon* and *C. doisuthep*. Zootaxa 4838(2): 179–209. https://doi.org/10.11646/zootaxa.4838.2.2

Davis HR, Bauer AM, Jackman TR, Nashriq I, Das I (2019) Uncovering karst endemism within Borneo: two new *Cyrtodactylus* species from Sarawak, Malaysia. Zootaxa 4614(2): 331–352. https://doi.org/10.11646/zootaxa.4614.2.4

Gray JE (1827) A synopsis of the genera of saurian reptiles, in which some new genera are introduced, and the others reviewed by actual examination. Philosophical Magazine 2: 54–58. https://doi.org/10.1080/14786442708675620

Gray JE (1831) A synopsis of the species of Class Reptilia. In: Griffith, E. & Pidgeon, E. (Eds), The Animal Kingdom arranged in Conformity with its Organisation, by the Baron Cuvier, with Additional Descriptions of all the Species hitherto named, and of many before noticed. Whittaker, Treacher and Co., London, 1–110.

Grismer LL, Ahmad N (2008) A new insular species of *Cyrtodactylus* (Squamata: Gekkonidae) from the Langkawi Archipelago, Kedah, Peninsular Malaysia. Zootaxa 1924: 53–68. https://doi.org/10.11646/zootaxa.1924.1.3

Grismer LL, Wood PL Jr, Le MD, Quah ES, Grismer JL (2020a) Evolution of habitat preference in 243 species of Bent-toed geckos (Genus *Cyrtodactylus* Gray, 1827) with a discussion of karst habitat conservation. Ecology and Evolution 10(24): 13717–13730. https://doi.org/10.1002/ece3.6961

Grismer LL, Wood PL Jr, Quah ES, Grismer MS, Thura MK, Oaks JR, Lin A (2020b). Two new species of *Cyrtodactylus* Gray, 1827 (Squamata: Gekkonidae) from a karstic archipelago in the Salween Basin of southern Myanmar (Burma). Zootaxa 4718(2): 151–183. https://doi.org/10.11646/zootaxa.4718.2.1

Grismer LL, Chan KO, Oaks JR, Neang T, Sokun L, Murdoch ML, Stuart BL, Grismer JL (2020c). A new insular species of the *Cyrtodactylus intermedius* (Squamata: Gekkonidae) group from Cambodia with a discussion of habitat preference and ecomorphology. Zootaxa 4830(1): 75–102. https://doi.org/10.11646/zootaxa.4830.1.3

Grismer LL, Wood PL Jr, Anuar S, Quah ES, Muin MA, Mohamed M, Chan KO, Sumarli AX, Loredo AI, Heinz HM (2014) The phylogenetic relationships of three new species of the *Cyrtodactylus pulchellus* complex (Squamata: Gekkonidae) from poorly explored regions in northeastern Peninsular Malaysia. Zootaxa 3786(3): 359–381. https://doi.org/10.11646/zootaxa.3786.3.6

Grismer LL, Wood PL Jr, Thura MK, Zin T, Quah ES, Murdoch ML, Grismer MS, Lin A, Kyaw H, Lwin N (2018) Twelve new species of *Cyrtodactylus* Gray (Squamata: Gekkonidae) from isolated limestone habitats in east-central and southern Myanmar demonstrate high localized diversity and unprecedented microendemism. Zoological Journal of the Linnean Society 182(4): 862–959. https://doi.org/10.1093/zoolinnean/zlx057

Grismer LL, Wood PL Jr, Quah ES, Anuar S, Muin MA, Sumontha M, Ahmad N, Bauer AM, Wangkulangkul S, Grismer JL, Pauwels OS (2012) A phylogeny and taxonomy of the Thai-Malay Peninsula Bent-toed Geckos of the *Cyrtodactylus pulchellus* complex (Squamata: Gekkonidae): combined morphological and molecular analyses with descriptions of seven new species. Zootaxa 3520: 1–55. https://doi.org/10.11646/zootaxa.3520.1.1

Grismer LL, Wood PL Jr, Anuar S, Grismer MS, Quah ES, Murdoch ML, Muin MA, Davis HR, Aguilar C, Klabacka R, Cobos AJ, Aowphol A, Site JW Jr (2016) Two new Bent-

toed Geckos of the *Cyrtodactylus pulchellus* complex from Peninsular Malaysia and multiple instances of convergent adaptation to limestone forest ecosystems. Zootaxa 4105(5): 401–429. https://doi.org/10.11646/zootaxa.4105.5.1

Grismer LL, Wood PL Jr, Poyarkov NA, Le MD, Karunarathna S, Chomdej S, Suwannapoom C, Qi S, Liu S, Che J, Quah ES, Kraus F, Oliver PM, Riyanto A, Pauwels OSG, Grismer JL (2021a) Karstic landscapes are foci of species diversity in the world's third-largest vertebrate genus *Cyrtodactylus* Gray, 1827 (Reptilia: Squamata; Gekkonidae). Diversity 13(5): 183. https://doi.org/10.3390/d13050183

Grismer LL, Wood PL Jr, Poyarkov NA, Le MD, Kraus F, Agarwal I, Oliver PM, Nguyen SN, Nguyen TQ, Karunarathna S, Welton LJ, Stuart BL, Luu VQ, Bauer AM, O'Connell KA, Quah ESH, Chan KO, Ziegler T, Ngo H, Nazarov RA, Aowphol A, Chomdej S, Suwannapoom C, Siler CD, Anuar S, Tri NV, Grismer JL (2021b) Phylogenetic partitioning of the third-largest vertebrate genus in the world, *Cyrtodactylus* Gray, 1827 (Reptilia; Squamata; Gekkonidae) and its relevance to taxonomy and conservation. Vertebrate Zoology 71: 101–154. https://doi.org/10.3897/vertebrate-zoology.71.e59307.figure30

Harvey MB, O'Connell KA, Barraza G, Riyanto A, Kurniawan N, Smith EN (2015) Two new species of *Cyrtodactylus* (Squamata: Gekkonidae) from the Southern Bukit Barisan Range of Sumatra and an estimation of their phylogeny. Zootaxa 4020: 495–516. https://doi.org/10.11646/zootaxa.4020.3.5

Huelsenbeck JP, Ronquist F (2001) MRBAYES: Bayesian inference of phylogenetic trees. Bioinformatics 17(8): 754–755. https://doi.org/10.1093/bioinformatics/17.8.754

Kamei RG, Mahony S (2021) A new species of Bent-toed gecko (Squamata: Gekkonidae: *Cyrtodactylus* Gray, 1827) from the Garo Hills, Meghalaya State, north-east India, and discussion of morphological variation for *C. urbanus*. Herpetological Journal 31(3): 177–196. https://doi.org/10.33256/31.3.177196

Kumar S, Stecher G, Li M, Knyaz C, Tamura K (2018) MEGA X: Molecular Evolutionary Genetics Analysis across computing platforms. Molecular Biology and Evolution 35(6): 1547–1549. https://doi.org/10.1093/molbev/msy096

Lanfear R, Frandsen PB, Wright AM, Senfeld T, Calcott B (2016) PartitionFinder 2: new methods for selecting partitioned models of evolution for molecular and morphological phylogenetic analyses. Molecular biology and evolution 34(3): 772–773. https://doi.org/10.1093/molbev/msw260

Lê S, Josse J, Husson F (2008) FactoMineR: An R package for multivariate analysis. Journal of Statistical Software 25(1): 1–18. https://doi.org/10.18637/jss.v025.i01

Liu S, Rao D (2021) A new species of *Cyrtodactylus* Gray, 1827 (Squamata, Gekkonidae) from Yunnan, China. ZooKeys 1021: 109–126. https://doi.org/10.3897/zookeys.1021.60402

Lleonart J, Salat J, Torres GJ (2000) Removing allometric effects of body size in morphological analysis. Journal of Theoretical Biology 205: 85–93. https://doi.org/10.1006/jtbi.2000.2043

Luu VQ, Bonkowski M, Nguyen TQ, Le MD, Schneider N, Ngo HT, Ziegler T (2016) Evolution in karst massifs: Cryptic diversity among bent-toed geckos along the Truong Son Range with descriptions of three new species and one new country record from Laos. Zootaxa 4107(2): 101–140. https://doi.org/10.11646/zootaxa.4107.2.1

Macey JR, Larson A, Ananjeva NB, Papenfuss TJ (1997) Evolutionary shifts in three major structural features of the mitochondrial genome among iguanian lizards. Journal of Molecular Evolution 44(6): 660–674. https://doi.org/10.1007/PL00006190

McCoy MW, Bolker BM, Osenberg CW, Miner BG, Vonesh JR (2006) Size correction: Comparing morphological traits among populations and environments. Oecologia 148: 547–554. https://doi.org/10.1007/s00442-006-0403-6

Miller MA, Pfeiffer W, Schwartz T (2010) Creating the CIPRES Science Gateway for inference of large phylogenetic trees. In: 2010 Gateway Computing Environments Workshop (GCE). 1–8 pp. https://doi.org/10.1109/GCE.2010.5676129

Minh BQ, Nguyen MAT, von Haeseler A (2013) Ultrafast approximation for phylogenetic bootstrap. Molecular Biology and Evolution 30(5): 1188–1195. https://doi.org/10.1093/molbev/mst024

Murdoch ML, Grismer LL, Wood PL Jr, Neang T, Poyarkov NA, Ngo VT, Nazarov RA, Aowphol A, Pauwels OSG, Nguyen HN, Grismer JL (2019) Six new species of the *Cyrtodactylus intermedius* complex (Squamata: Gekkonidae) from the Cardamom Mountains and associated highlands of Southeast Asia. Zootaxa 4554(1): 1–62. https://doi.org/10.11646/zootaxa.4554.1.1

Nazarov RA, Pauwels OSG, Konstantinov EL, Chulisov AS, Orlov NL, Poyarkov NA Jr (2018) A new karst-dwelling bent-toed gecko (Squamata: Gekkonidae: *Cyrtodactylus*) from Xiangkhoang Province, northeastern Laos. Zoological Research 39(3): 202–219. https://doi.org/10.24272/j.issn.2095-8137.2018.010

Neang T, Henson A, Stuart BL (2020) A new species of *Cyrtodactylus* (Squamata, Gekkonidae) from Cambodia's Prey Lang Wildlife Sanctuary. ZooKeys 926: 133–158. https://doi.org/10.3897/zookeys.926.48671

Nielsen SV, Oliver PM (2017) Morphological and genetic evidence for a new karst specialist lizard from New Guinea (*Cyrtodactylus*: Gekkonidae). Royal Society Open Science 4(11): 170781. https://doi.org/10.1098/rsos.170781

Pauwels OS, Nazarov RA, Bobrov VV, Poyarkov NA (2018) Taxonomic status of two populations of Bent-toed Geckos of the *Cyrtodactylus irregularis* complex (Squamata: Gekkonidae) with description of a new species from Nui Chua National Park, southern Vietnam. Zootaxa 4403(2): 307–335. https://doi.org/10.11646/zootaxa.4403.2.5

Purkayastha J, Das M, Bohra SC, Bauer AM, Agarwal I (2020) Another new *Cyrtodactylus* (Squamata: Gekkonidae) from Guwahati, Assam, India. Zootaxa 4732(3): 375–392. https://doi.org/10.11646/zootaxa.4732.3.2

Quah ES, Grismer LL, Wood PL Jr, Sah SAM (2019) The discovery and description of a new species of Bent-toed Gecko of the *Cyrtodactylus pulchellus* complex (Squamata: Gekkonidae) from the Langkawi Archipelago, Kedah, Peninsular Malaysia. Zootaxa 4668(1): 51–75. https://doi.org/10.11646/zootaxa.4668.1.3

R Core Team (2019) R: A language and environment for statistical computing. R Foundation for Statistical Computing, Vienna, Austria. https://www.R-project.org/

Rambaut A, Drummond AJ, Xie D, Baele G, Suchard MA (2018) Posterior summarization in Bayesian phylogenetics using Tracer 1.7. Systematic Biology 67(5): 901–904. https://doi.org/10.1093/sysbio/syy032

Riyanto A, Farajallah A, Hamidy A, Fitriana YS, Munir M, Kurniawan N, Smith EN (2020) Taxonomic evaluation of two similar bent-toed geckos Squamata: Gekkonidae: *Cyrtodactylus* Gray, 1827) from East Java, Indonesia. Zootaxa 4830(1): 186–196. https://doi.org/10.11646/zootaxa.4830.1.8

Reist JD (1985) An empirical evaluation of several univariate methods that adjust for size variation in morphometric data. Canadian Journal of Zoology 63: 1429–1439. https://doi.org/10.1139/z85-213

Ronquist F, Teslenko M, Van Der Mark P, Ayres DL, Darling A, Höhna S, Larget B, Liu L, Suchard MA, Huelsenbeck JP (2012) MrBayes 3.2: efficient Bayesian phylogenetic inference and model choice across a large model space. Systematic Biology 61: 539–542. https://doi.org/10.1093/sysbio/sys029

Smith MA (1925) A new Ground-Gecko (*Gymnodactylus*) from the Malay Peninsula. Journal of the Malayan Branch of the Royal Asiatic Society 3: 87–87. https://www.jstor.org/stable/41560434

Sumontha M, Pauwels OS, Kunya K, Nitikul A, Samphanthamit P, Grismer LL (2012) A new forest-dwelling gecko from Phuket Island, Southern Thailand, related to *Cyrtodactylus macrotuberculatus* (Squamata: Gekkonidae). Zootaxa 3522: 61–72. https://doi.org/10.11646/zootaxa.3522.1.4

Termprayoon K, Rujirawan A, Grismer LL, Wood PL Jr, Aowphol A (2021) Taxonomic reassessment and phylogenetic placement of *Cyrtodactylus phuketensis* (Reptilia, Gekkonidae) based on morphological and molecular evidence. ZooKeys 1040: 91–121. https://doi.org/10.3897/zookeys.1040.65750

Thorpe RS (1975) Quantitative handling of characters useful in snake systematics with particular reference to interspecific variation in the Ringed Snake *Natrix natrix* (L.). Biological Journal of the Linnean Society 7: 27–43. https://doi.org/10.1111/j.1095-8312.1975.tb00732.x

Thorpe RS (1983) A review of the numerical methods for recognized and analysing racial differentiation. In: Felsenstein J (Ed) Numerical Taxonomy. Berlin Heidelberg: Springer, 404–423. https://doi.org/10.1007/978-3-642-69024-2_43

Trifinopoulos J, Nguyen LT, von Haeseler A, Minh BQ (2016) W-IQ-TREE: a fast online phylogenetic tool for maximum likelihood analysis. Nucleic Acids Research 44 (W1): W232–W235. https://doi.org/10.1093/nar/gkw256

Turan C (1999) A note on the examination of morphometric differentiation among fish populations: the truss system. Turkish Journal of Zoology 23: 259–263.

Uetz P, Freed P, Aguilar R, Hošek J (2021) The Reptile Database: http://www.reptile-database.org [accessed 5 August 2021]

Wickham H (2016) ggplot2: Elegant graphics for data analysis. Springer-Verlag, New York. https://doi.org/10.1007/978-3-319-24277-4

Wiegmann AFA (1834) Beiträge zur Zoologie, gesammelt auf einer Reise um die Erde, von Dr. Meyen FJF, M.D.A.D.N. Siebente Abhandlung. Amphibien. Nova Acta Physico-medica Academiae Caesareae Leopoldino-Carolinae Naturae Curiosorum. Halle 17: 183–268. https://www.biodiversitylibrary.org/page/54248370

Wilcox TP, Zwickl DJ, Heath TA, Hillis DM (2002) Phylogenetic relationships of the dwarf boas and a comparison of Bayesian and bootstrap measures of phylogenetic support. Molecular Phylogenetics and Evolution 25: 361–371. https://doi.org/10.1016/S1055-7903(02)00244-0

Wood PL Jr, Heinicke MP, Jackman TR, Bauer AM (2012) Phylogeny of bent-toed geckos (*Cyrtodactylus*) reveals a west to east pattern of diversification. Molecular phylogenetics and evolution 65(3): 992–1003. https://doi.org/10.1016/j.ympev.2012.08.025

Wood PL Jr, Grismer LL, Muin MA, Anuar S, Oaks JR, Sites JW Jr (2020) A new potentially endangered limestone-associated Bent-toed Gecko of the *Cyrtodactylus pulchellus* (Squamata: Gekkonidae) complex from northern Peninsular Malaysia. Zootaxa 4751(3): 437–460.

Appendix I

Specimens examined

Cyrtodactylus astrum: **Peninsular Malaysia**, Perlis, Gua Wang Burma: LSUHC 09928 (female) and LSUHC 100075 (male).

Cyrtodactylus lekaguli: **Thailand**, Trang Province, Na Yong District: ZMKU R 00918, THNHM 017781, THNHM 017784, THNHM 017787, THNHM 017791 (5 males), and ZMKU R 00919, ZMKU R 00921, THNHM 017694, THNHM 017777, THNHM 017788, THNHM 017790 (6 females).

ZooKeys 1070: 135–149 (2021)
doi: 10.3897/zookeys.1070.66598
https://zookeys.pensoft.net

RESEARCH ARTICLE

A peer-reviewed open-access journal
ZooKeys
Launched to accelerate biodiversity research

Mitogenomics of historical type specimens clarifies the taxonomy of Ethiopian *Ptychadena* Boulenger, 1917 (Anura, Ptychadenidae)

Jacobo Reyes-Velasco[1*], Sandra Goutte[1*], Xenia Freilich[2], Stéphane Boissinot[1]

1 *New York University Abu Dhabi, Saadiyat Island, Abu Dhabi, UAE* **2** *Department of Biology, Queens College, City University of New York, Flushing, NY, USA*

Corresponding author: Stéphane Boissinot (stephane.boissinot@nyu.edu)

Academic editor: Angelica Crottini | Received 28 March 2021 | Accepted 7 September 2021 | Published 12 November 2021

http://zoobank.org/5AD4E9EF-055A-48D0-8349-751C4CC68398

Citation: Reyes-Velasco J, Goutte S, Freilich X, Boissinot S (2021) Mitogenomics of historical type specimens clarifies the taxonomy of Ethiopian *Ptychadena* Boulenger, 1917 (Anura, Ptychadenidae). ZooKeys 1070: 135–149. https://doi.org/10.3897/zookeys.1070.66598

Abstract

The taxonomy of the *Ptychadena neumanni* species complex, a radiation of grass frogs inhabiting the Ethiopian highlands, has puzzled scientists for decades because of the morphological resemblance among its members. Whilst molecular phylogenetic methods allowed the discovery of several species in recent years, assigning pre-existing and new names to clades was challenged by the unavailability of molecular data for century-old type specimens. We used Illumina short reads to sequence the mitochondrial DNA of type specimens in this group, as well as ddRAD-seq analyses to resolve taxonomic uncertainties surrounding the *P. neumanni* species complex. The phylogenetic reconstruction revealed recurrent confusion between *Ptychadena erlangeri* (Ahl, 1924) and *P. neumanni* (Ahl, 1924) in the literature. The phylogeny also established that *P. largeni* Perret, 1994 represents a junior synonym of *P. erlangeri* (Ahl, 1924) and distinguished between two small species, *P. nana* Perret, 1994, restricted to the Arussi Plateau, and *P. robeensis* Goutte, Reyes-Velasco, Freilich, Kassie & Boissinot, 2021, which inhabits the Bale Mountains. The phylogenetic analyses of mitochondrial DNA from type specimens also corroborate the validity of seven recently described species within the group. Our study shows how modern molecular tools applied to historical type specimens can help resolve long-standing taxonomic issues in cryptic species complexes.

Keywords

Grass frogs, Historical DNA, *Ptychadena*, taxonomy, type specimens

* These authors contributed equally to this work.

Introduction

In the highlands of Ethiopia, frogs of the genus *Ptychadena* Boulenger, 1917 form a monophyletic radiation known as the *Ptychadena neumanni* species complex (Freilich et al. 2014). The molecular evolution of this group has been studied extensively, establishing it as a model system to study lineage diversification, speciation and biogeography in the region (Mengistu 2012; Freilich et al. 2014, 2016; Smith et al. 2017a; Reyes-Velasco et al. 2018). As in other regions of Africa, species of the genus *Ptychadena* of the Ethiopian highlands are difficult to distinguish from one-another based on morphological features alone (Poynton 1970; Bwong et al. 2009; Dehling and Sinsch 2013). Five *Ptychadena* species from the Ethiopian highlands were originally described based on morphology: *P. neumanni* (Ahl, 1924), *P. erlangeri* (Ahl, 1924), *P. cooperi* (Parker, 1930), *P. nana* Perret, 1980 and *P. wadei* Largen, 2000. A sixth species, *P. largeni*, was described by Perret (1994), but later synonymized with *P. neumanni* by Largen (2001). While some of the original descriptions allow for unambiguous species identification (e.g., *P. cooperi* and *P. harenna* Largen, 1997), assigning names to most of the lineages is challenging because some of the original discriptions do not provide diagnostic characters since the type series contain specimens belonging to different species (see Goutte et al. 2021).

Several authors found substantial morphological variation among populations of *P. neumanni*, which led them to suggest that this taxon consisted of multiple species (Perret 1994; Largen 1997, 2001). Freilich et al. (2014) used mitochondrial and nuclear loci to study the evolutionary history of the group, and their results showed that *P. neumanni* in fact comprised five distinct taxa, which did not form a monophyletic group. The authors refrained from describing the potential new species they identified because they were not able to compare their specimens with the type specimens of previously described species. Instead of providing new names, they assigned numbers to each one of the undescribed taxa they identified with their genetic analyses (i.e., *Ptychadena* cf. *neumanni 1–5*). Smith et al. (2017a) re-analyzed the combined molecular datasets of Mengistu (2012) and Freilich et al. (2014), as well as sequences from 30 new specimens, and recovered the same five highland taxa Freilich et al. (2014) had identified. Smith and colleagues then assigned new or pre-existing taxonomic names to each one of those lineages. However, they did not compare their material to the type specimens of previously described species in their morphological or molecular analyses and it thus remained unclear to which genetic lineage the names *P. neumanni*, *P. erlangeri*, *P. largeni* and *P. nana* should be assigned (Reyes-Velasco et al. 2018).

Recently, Goutte et al. (2021) revised the taxonomy of the group, based on morphology, molecular data, and call analyses and described four new species corresponding to four genetic lineages identified by Freilich et al. (2014) and Reyes-Velasco et al. (2018): *Ptychadena beka* Goutte, Reyes-Velasco, Freilich, Kassie & Boissinot, 2021, *P. delphina* Goutte, Reyes-Velasco, Freilich, Kassie & Boissinot, 2021, *P. doro* Goutte, Reyes-Velasco, Freilich, Kassie & Boissinot, 2021 and *P. robeensis* Goutte, Reyes-Velasco, Freilich, Kassie & Boissinot, 2021.

Table 1. Taxonomic history of the *Ptychadena neumanni* species complex.

Species	Author, year	Largen, 2001	Freilich et al. 2014	Smith et al. 2017	Reyes-Velasco et al. 2018	Goutte et al 2021 & this study
P. neumanni	Ahl, 1924	*P. neumanni* / *P. erlangeri*	*P. erlangeri*	*P. erlangeri*	*P. erlangeri*	*P. neumanni*
P. erlangeri	Ahl, 1924	*P. neumanni* / *P. erlangeri*	*P.* cf. *neumanni 2*	*P. largeni*	*P.* cf. *neumanni 2*	*P. erlangeri*
P. cooperi	Parker, 1930	*P. cooperi*	*P. cooperi*	*P. cooperi*	*P. cooperi*	*P. cooperi*
P. nana	Perret, 1980	*P. nana*	-	-	*P.* cf. *Mt. Gugu*	*P. nana*
P. largeni	Perret, 1994	*P. neumanni*	*P.* cf. *neumanni 2*	*P. largeni*	*P.* cf. *neumanni 2*	*P. erlangeri*
P. harenna	Largen, 1997	*P. harenna*	*P. harenna*	*P. harenna*	*P. harenna*	*P. harenna*
P. levenorum	Smith et al. 2017b	*P. neumanni*	*P.* cf. *neumanni 3*	*P. levenorum*	*P.* cf. *neumanni 3*	*P. levenorum*
P. goweri	Smith et al. 2017b	*P. erlangeri*	*P.* cf. *neumanni 4*	*P. goweri*	*P.* cf. *neumanni 4*	*P. goweri*
P. amharensis	Smith et al. 2017b	*P. neumanni* / *P. erlangeri*	*P.* cf. *neumanni 5*	*P. amharensis*	*P.* cf. *neumanni 5*	*P. amharensis*
P. beka	Goutte et al. 2021	*P. neumanni* / *P. erlangeri*	*P.* cf. *neumanni 1*	*P. neumanni*	*P.* cf. *neumanni 1*	*P. beka*
P. delphina	Goutte et al. 2021	-	*P. erlangeri*	*P. erlangeri*	*P.* cf. *erlangeri Metu*	*P. delphina*
P. doro	Goutte et al. 2021	-	*P. erlangeri*	*P. erlangeri*	*P.* cf. *erlangeri Gecha*	*P. doro*
P. robeensis	Goutte et al. 2021	-	*P. nana*	*P. nana*	*P. nana*	*P. robeensis*

In order to resolve the taxonomy and systematics of the group, we extracted DNA from formalin or spirit-fixed type specimens of the species from which only morphological data was available (*P. erlangeri*, *P. largeni*, *P. nana* and *P. neumanni*) and reconstructed partial mitochondrial genomes. These sequences were included in a molecular phylogeny, along with mitochondrial DNA (mtDNA) from more recently collected material included in Reyes-Velasco et al. (2018) and in recent species descriptions (Fig. 1; Smith et al. 2017b; *P. amharensis* Smith, Noonan & Colston, 2017, *P. goweri* Smith, Noonan & Colston, 2017 and *P. levenorum* Smith, Noonan & Colston, 2017). We compared our mtDNA phylogeny to one obtained from thousands of genome-wide SNPs obtained from ddRAD-seq (Reyes-Velasco et al. 2018) to test for congruence between mitochondrial genetic lineages and species. These analyses allowed the assignment of existing names to genetic lineages and the validation of the three new species described by Smith et al (2017b). Finally, four previously identified lineages were established as new species, which we describe as *P. beka*, *P. delphina*, *P. doro* and *P. robeensis* elsewhere (Goutte et al. 2021).

Material and methods

DNA extraction and sequencing of type specimens

We aimed to extract mtDNA from type specimens for which molecular data was unavailable. The types of *Ptychadena cooperi* and *P. harenna* were not sequenced, as these two species are easily distinguishable morphologically and there is no ambiguity regarding their taxonomic status (Goutte et al. 2021). We obtained authorization from the Museum für Naturkunde Berlin (**ZMB**) and the Museum d'Histoire Naturelle, Genève (**MHNG**) to sample a small amount of muscle or liver tissue from the type

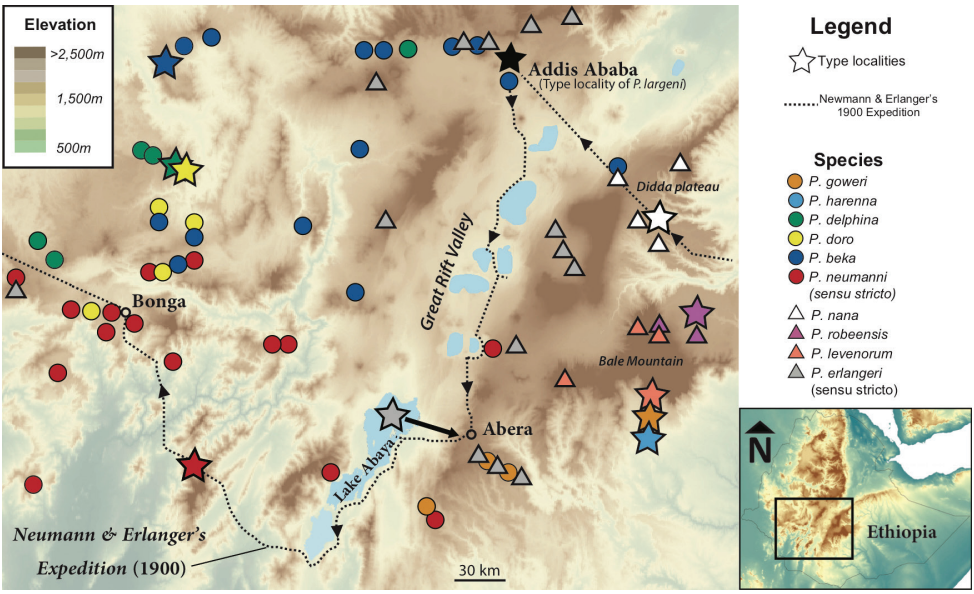

Figure 1. Map of Ethiopia showing localities of individuals in the *Ptychadena neumanni* species complex used in this study. Samples with genetic data are represented by different colored circles (*P. neumanni* species group) or triangles (*P. erlangeri* species group). Stars depict the approximate type localities of *P. neumanni* (red), *P. erlangeri* (grey), and *P. nana* (white). A black star represents Addis Ababa, the type locality of *P. largeni*, a junior synonym of *P. erlangeri.* The approximate route of Oscar Neumann and Carlo von Erlanger's 1900 expedition in Abyssinia, during which the type specimens of all the above species were collected (except for *P. largeni*) is represented by a dashed line. Black arrow indicates the likely correct type locality for *P. erlangeri* as suggested by the authors (see Discussion).

specimens of *Ptychadena neumanni* (lectotype, ZMB 26879; paralectotype, ZMB 57183), *P. erlangeri* (holotype, ZMB 26887), *P. largeni* (paratypes, MHNG 2513-15 & 2513-56) and *P. nana* (holotype, ZMB 26878). Tissue sampling did not result in any major visible damage to the vouchers, as most tissue was taken from pre-existing incisions. Dissecting tools were cleaned with a 10% bleach solution before and after tissue extraction.

Although we could not find information about the mode of preservation used at the time of collection, it is likely that the type specimens had been fixed in formalin or some form of spirit, which renders the extraction of DNA challenging and requires a different protocol than when using fresh tissue. We followed the protocol described by Shedlock et al. (1997). In short, approximately ~5 mg of tissue (muscle or liver) was placed in a 2 mL tube and washed in 1X GTE buffer for four days, changing the buffer daily. The tissue was then incubated for four additional days at 65 °C in a 2 mL tube with 500 µL cell lysis buffer, 100 µL proteinase K, and 20 µL 1 mM DTT (dithiothreitol). Proteinase K was added daily until all the tissue was completely digested. A standard potassium acetate (KOA) DNA precipitation protocol was then followed. A detailed protocol for the DNA extraction is provided in the Suppl. material 1. To

reduce the possibility of contamination, DNA extraction was carried out using new reagents in a marine biology lab that does not work with amphibian samples, and multiple negative controls (using deionized water) were used along the process.

DNA concentration was measured using a high sensitivity kit in a Qubit fluorometer (Life Technologies) and DNA fragment size distribution and concentration was estimated using a Bioanalyzer 7500 high sensitivity DNA chip (Agilent, Santa Clara, CA, USA). A NEBNext FFPE DNA Repair Mix (New England Biolabs) was used to repair damaged bases prior to library preparation, which was carried out with a NEB library preparation kit. The shredding step was skipped because of the fragmented nature of historical DNA. All libraries were pooled and sequenced on an Illumina NextSeq 550 (75 bp paired-end) at the Genome Core Facility of New York University Abu Dhabi, UAE. The FASTx Toolkit (Gordon and Hannon 2010) was used to remove Illumina adaptors and low-quality reads (mean Phred score < 20). The final average read length was 63 bp after trimming (Suppl. material 2). The program *FastQC* (Andrews 2010) was then used to observe if base composition was biased towards the end of the raw reads, which is a common phenomenon resulting from deamination (Dabney et al. 2013) when sequencing older DNA, however this was not observed. Summary statistics describing the sequencing data are available in Suppl. material 2: Table S1. All sequences are deposited in GenBank (MW375737–MW375766; Suppl. material 2: Table S2).

Assembly of mitochondrial genomes

Whole mitochondrial genomes of the type specimens were assembled from the Illumina reads using MITObim (Hahn et al. 2013). MITObim uses an iterative baiting method to generate mitochondrial contigs from short reads. First, a published sequence of the mitochondrial genome of *Ptychadena mascareniensis* (Duméril & Bibron, 1841) (GenBank reference number JX564890) was used as the reference mitogenome, with the default program settings, except for a *k*-mer length of 21. The analysis was then run again using the resulting contigs from the first MITObim run. An additional 21 mitochondrial genomes from fresh samples collected by us of members of the *P. neumanni* species complex were also assembled following the same protocol (Suppl. material 2: Table S2). These samples were sequenced for another project on the genomics of the *Ptychadena neumanni* species group (Hariyani et al. in prep.) following the sampling, tissue handling and DNA extraction protocols of Reyes-Velasco et al. (2018).

Phylogenetic analysis of mtDNA

We reconstructed phylogenetic relationships within the *Ptychadena neumanni* species complex using three different datasets. First, all 13 mitochondrial protein-coding genes and the rRNA 12S and 16S genes were used. No stop codon was found in the protein-coding sequences. We excluded tRNAs because in some cases these were not complete or were difficult to align. Because we did not have the complete mitochondrial genome for all species, we used a subset of genes which was obtained for all species as a second

dataset. This dataset included the 12S and 16S rRNA, as well as the protein-coding gene cytochrome *c* oxidase I (*cox1*). In the last dataset, we included only the rRNA 16S, in order to be able to include as many individuals as possible. Alignments at each gene were performed in MAFFT v. 7 (Katoh and Standley 2013), and other ambiguously aligned regions were removed using the online server G-Blocks (Castresana 2000) with the least stringent options selected. Geneious v. 9.1.6 (Biomatters Ltd., Auckland, NZ) was used to manually trim any remaining poorly aligned regions and to ensure that protein-coding genes were in the correct reading frame. Our final concatenated datasets consisted of 15,708 bp for the dataset that included all genes and 2522 bp for the reduced dataset (12S, 16S and *cox1*).

The best-fit model of nucleotide evolution for each gene was selected using the Bayesian Information Criterion (BIC) in PartitionFinder v. 1.1.1 (Lanfear et al. 2012; Suppl. material 2: Table S3). Data was partitioned by gene and by codon position in protein-coding genes. All genes were concatenated using the program Sequence Matrix (Vaidya et al. 2011) and performed Bayesian phylogenetic inference (BI) in MrBayes v. 3.2.2 (Ronquist et al. 2012) on the CIPRES Science Gateway server (Miller et al. 2010).

For both datasets, the BI analyses consisted of four runs of 10^7 generations, sampling every 1000^{th} generation, with four chains (three heated and one cold). Convergence between the runs was assessed by visually inspecting overlap in likelihood and parameter estimates between the runs, as well as effective sample sizes and potential scale reduction factor (PSRF) value estimates for each run using Tracer v. 1.6 (Rambaut et al. 2014). Individual runs converged by 10^5 generations, based on the PSRF, so the first 25% of each run were discarded as burn-in. The runs were combined, and the resulting tree was visualized in FigTree v. 1.4.2 (Rambaut 2014).

Analyses of ddRAD-seq data

In a previous study (Reyes-Velasco et al. 2018), we sequenced thousands of loci from across the genome of all known lineages of *Ptychadena* inhabiting the Ethiopian highlands (12 putative species, 105 individuals) using double digest restriction-site associated DNA sequencing (ddRAD-seq). Here we briefly describe the methods used as more details were provided in our original article.

Individuals of the *Ptychadena neumanni* species complex were collected in the highlands of Ethiopia between 2011 and 2018. Tissue samples were extracted and stored in RNAlater or 95% ethanol. Genomic DNA was extracted with one of the following methods: with the use of a DNeasy blood and tissue kit (Qiagen, Valencia, CA), with the use of Serapure beads (Rohland and Reich 2012), or by standard potassium acetate extraction. DNA concentration was measured with a Qubit fluorometer (Life Technologies) so that DNA sample concentrations could be standardized. Genomic DNA was then digested with the enzymes SbfI and MspI (Peterson et al. 2012). Barcoded samples were size-selected between 400 and 550 base pairs using a Pippin Prep (Sage Science, Beverly, MA, USA), and attached to unique Illumina

indices (Peterson et al. 2012). Libraries were sequenced on an Illumina HiSeq2500 (100 bp paired-end reads) at the Genome Core Facility of New York University Abu Dhabi, United Arab Emirates.

Ipyrad 0.6.17 (Eaton and Overcast 2020) was used to assemble loci *de novo* and create SNP datasets. After quality filtering, a total of ~158 million sequencing reads were retained, with a mean coverage of about 1.60 million reads, and a mean of ~11,400 RAD-tags per individual. We obtained between 800 and 2918 polymorphic loci and between 28,000–36,000 SNPs (Reyes-Velasco et al. 2018). The best model of evolution for our concatenated ddRAD-seq dataset was estimated with using BIC in PAUP v. 4.0.a151 (Swofford 1993), which showed the GTR + I + G model as the most supported. Maximum likelihood (ML) was implemented in RAxML v. 8 (Stamatakis 2014) to infer evolutionary relationships between populations and species in this group. RAxML was performed with rapid bootstrapping in the CIPRES portal (Miller et al. 2010).

Results

DNA extraction, sequencing and assembly of mtDNA genomes

DNA was successfully extracted from the type specimens of *Ptychadena neumanni*, *P. erlangeri*, *P. largeni* and *P. nana*. After quality filtering, a total of ~1.1 billion reads were retained, with highly variable coverage across individuals (49–359 million reads; Suppl. material 2: Table S1). The complete mitochondrial genome was recovered for five out of the six type specimens and a partial sequence was obtained for the holotype of *P. nana*. The total number of reads from the type specimens that mapped to the reference mitochondrial genome ranged between 802 (*P. nana* holotype) to > 900,000 (*P. erlangeri* holotype; Suppl. material 2: Table S1). We found no correlation between the amount of DNA recovered and the final number of reads for each specimen.

Phylogenetic analysis

As the assignment of species names to genetic lineages was based on mitochondrial sequences, we first verified that the assignment of individuals to genetic lineages using mitochondrial markers was congruent with that obtained using genome-wide loci from ddRAD-seq (Fig. 2). The clustering of 105 individuals based on nuclear SNPs and on mitochondrial sequences was perfectly congruent (Figs 2, 3a, b); thus, we considered that, at least in this particular case, mitochondrial DNA was sufficient to assign samples to the genetic clusters identified by previous authors (Freilich et al. 2014; Smith et al. 2017a; Reyes-Velasco et al. 2018; Goutte et al. 2021).

Our phylogenetic analysis based on three mitochondrial genes (Fig. 3c) recovered 11 mitochondrial clusters corresponding to 11 of the 12 genetic lineages, with high support. The only exception was *P. delphina*, for which mitochondrial sequences did not form a clade (Fig. 3c). The lectotype and paralectotype of *P. neumanni* (ZMB

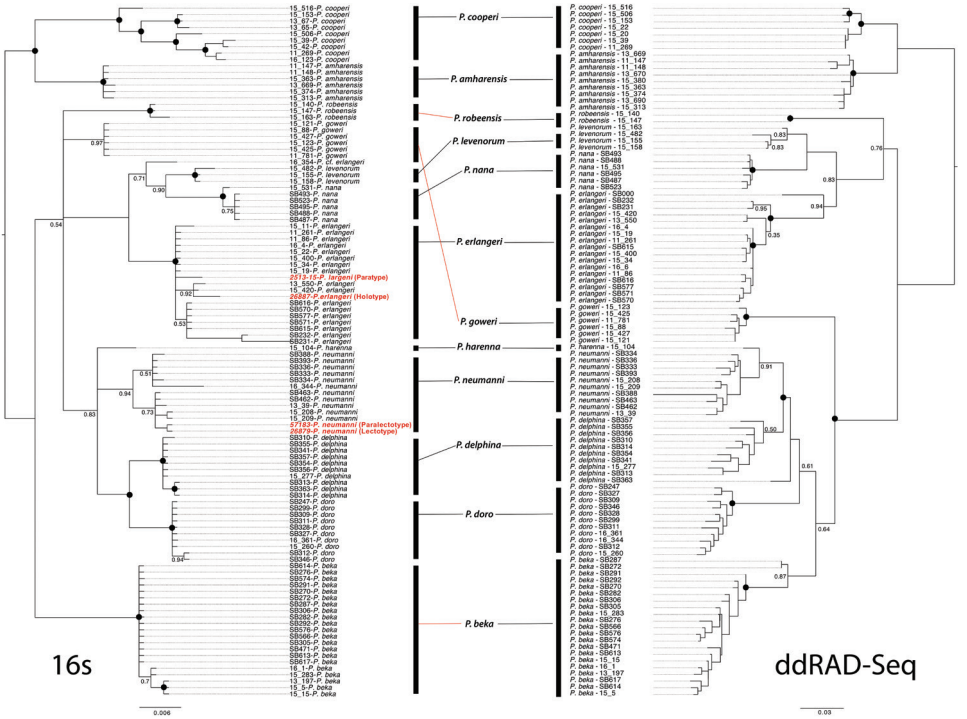

Figure 2. Comparisons of the topologies of the mitochondrial rRNA 16S (left) and ddRAD-seq (right) for members of the *Ptychadena neumanni* species complex. Type specimens are indicated in red in the 16S phylogeny. Red lines indicate clades that differ in their placement between 16S and ddRAD-seq, however, the assignment of individuals to a particular species is identical between datasets. Numbers at nodes represent posterior support (pp), while black dots represent nodes with posterior support of 1.

26879 and ZMB 57183) were nested with strong support (PP = 1) within the clade that had been referred to as *P. erlangeri* by multiple authors (Freilich et al. 2014; Smith et al. 2017a; Reyes-Velasco et al. 2018). The holotype of *P. erlangeri* (ZMB26887) and the paratypes of *P. largeni* (MHNG 2513–15 and 2513–56) all grouped with strong support (PP = 1) with individuals previously assigned to either *P.* cf. *neumanni* 2 (Freilich et al. 2014) or *P. largeni* (Smith et al. 2017a). This result demonstrates that *P. largeni* represents a junior synonym of *P. erlangeri*.

The holotype of *Ptychadena nana* (ZMB26878) did not group with individuals from the Bale Mountains identified as *P. nana* by previous authors (Freilich et al. 2014; Smith et al. 2017a; Reyes-Velasco et al. 2018; Fig. 3c) but instead grouped with individuals from the Arussi Plateau (= Didda Plateau; Fig. 1), which corresponds to the type locality for the species (Perret 1980). The holotypes for the three species described by Smith et al. (2017a), *P. amharensis*, *P. goweri* and *P. levenorum*, clustered with genetic lineages that did not include sequences derived from historical type specimens (Figs 2, 3) and thus constitute valid species. Finally, four lineages did not include any type specimen of species described by Smith et al. (2017a) or prior and the corresponding species were

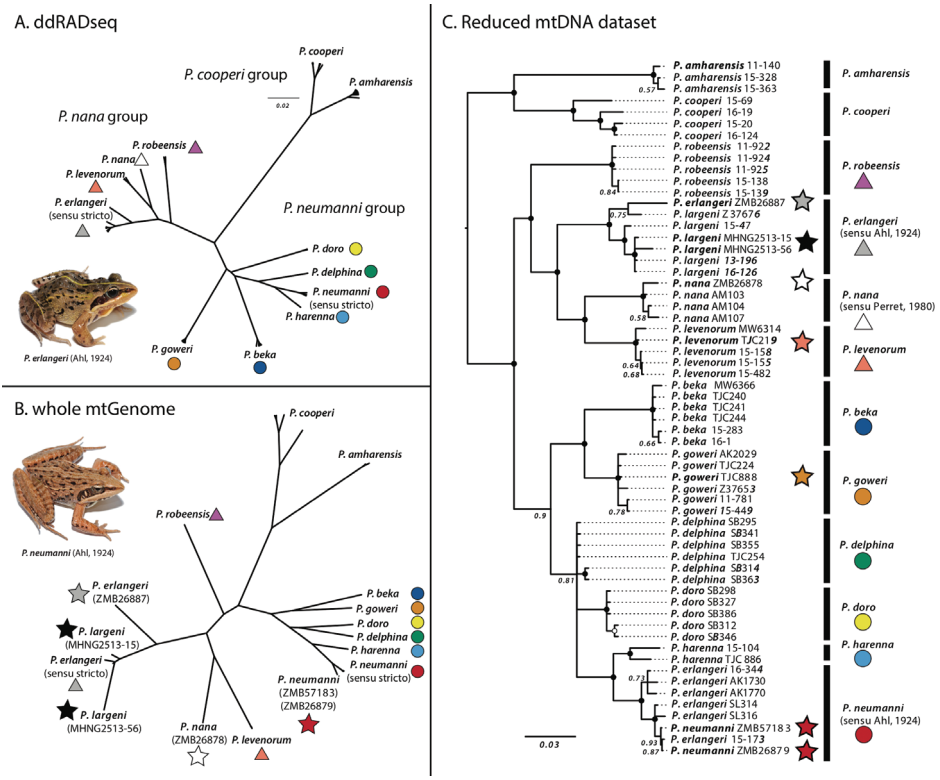

Figure 3. Phylogenetic inference of members of the *Ptychadena neumanni* species complex based on mtDNA and ddRAD-seq data **A** unrooted UPGMA tree of members of the *P. neumanni* species complex based on 2182 SNPs obtained with ddRAD-sequencing **B** unrooted Bayesian phylogenetic inference based on the complete mitochondrial genomes of members of the group **C** bayesian phylogenetic inference based on the concatenated sequences of the 12S and 16S rRNA and *cox1*. Black circles represent nodes with a posterior support of 1. Names in bold indicate type specimens, while stars indicate historical type specimens sequenced here and are color-coded as in Figure 1. Photographs represent members of the *P. neumanni* species complex; *P. erlangeri* (top), *P. neumanni* (bottom).

recently described by Goutte et al. (2021; *P. beka*, *P. delphina*, *P. doro* and *P. robeensis*). Notably, the lineage corresponding to *P. cf. neumanni 1* of Freilich et al. (2014), which was previously suggested to be conspecific with *P. neumanni* by Smith et al. (2017a), was in fact genetically distinct and corresponded to the recently described *P. beka*.

Discussion

In this study, we used historical DNA from century-old type specimens to resolve the convoluted taxonomy of the *Ptychadena neumanni* species complex. Our results established the correspondence between genetic lineages and species originally described on morphological characters only. This allowed us to correct recurrent taxonomic errors

made by multiple authors since the descriptions of the first species of the group, and to define which lineages correspond to new species. In addition, we were able to confirm the validity of some recently described taxa (*P. goweri*, *P. amaharensis*, *P. levenorum*, *P. robeensis*, *P. delphina*, *P. doro* and *P. beka*) and to synonymize others (*P. largeni*). Perret (1994) described *Ptychadena largeni* from specimens of *P. erlangeri* collected by Malcom J. Largen in Addis Ababa. Perret based his diagnosis of *Ptychadena largeni* on the absence of continuous dorsal folds in males and a smaller body size than *P. erlangeri* or *P. neumanni*. However, Largen (1997) casted doubt on the validity of this species and eventually synonymized it with *P. neumanni* (Largen, 2001), even though he had originally assigned those individuals to *P. erlangeri*. Our results confirm that Largen's original identification of the specimens he collected in Addis Ababa was correct and that *P. largeni* is a junior synonym of *P. erlangeri* and not of *P. neumanni*. Confusion in the taxonomy of the *Ptychadena neumanni* complex arose from the difficulty to identify morphologically similar species and the absence of comparison between sequenced and type specimens. To assign species names to populations, multiple authors have relied on geographic localities (Freilich et al. 2014; Smith et al. 2017a; Reyes-Velasco et al. 2018). In many cases, however, type locality data may be insufficient to attribute species names, either because species distribution ranges overlap or because type locality information is unreliable. For example, the holotype of *P. erlangeri* was collected during Oscar Neumann and Carlo von Erlanger's expedition to Abyssinia in 1900; with the type locality indicated as "Lake Abaya" (Ahl 1924). The lake is located at 1200 m a.s.l., which is substantially lower than any other known locality for members of the *P. neumanni* species complex (>1500 m a.s.l.; Largen and Spawls 2010) and seems an unlikely locality for a population of *P. erlangeri*. However, on their way to Lake Abaya, the expedition party spent some time in the village of Abera, which is located at ~2700 m a.s.l. (Neumann 1902). We believe that the holotype of *P. erlangeri* was either collected between Abera and Lake Abaya or at Abera itself, nearby which we have collected *P. erlangeri* (15 km SE; Fig. 1). Confusion emerging from imprecise type localities is inevitable for many specimens collected in such expeditions, which were the main source of scientific collections in past centuries. Systematists should thus take these inconsistencies into account and refer to the physical name-bearing types as the main source of information, rather than type locality data alone. The recent development of methods to sequence DNA from formalin-fixed historical specimens provides a unique opportunity to expand the use of type specimens, and to include them in molecular phylogenetic analyses (Ruane and Austin 2017). In recent years, multiple techniques have been developed to obtain mtDNA from historical museum specimens of amphibians, which has been fundamental in resolving long and convoluted taxonomic questions. These newly developed techniques include target enrichment of mitochondrial DNA (Rancilhac et al. 2020; Scherz et al. 2020) or the use of single-stranded libraries (Lyra et al. 2020; Straube et al. 2021). In the present study, developing capture probes or single-stranded DNA libraries was not needed to obtain enough DNA for sequencing. However, multiple factors might influence DNA preservation (Straube et al. 2021), and additional pre-sequencing preparation steps may be necessary for other

historical specimens. The sequencing of museum material may not always be possible due to DNA damage, because extracting tissues would damage type specimens, the type specimens have been lost, or simply because these methods might be too costly for researchers. Yet, recent technical progress as well as decreased sequencing costs open new opportunities for the use of museum specimens, thus highlighting the importance of museum collections in modern taxonomic research.

Acknowledgements

We thank curators and collection managers from multiple institutions, including Bezawork Afework Bogale and M. Ketema, Natural History Collection, Addis Ababa University, Ethiopia; Jeff Streicher, Natural History Museum, London; Andreas Schmitz, Museum d'Histoire Naturelle, Genève; Mark-Oliver Rödel and Frank Tillack, Museum für Naturkunde Berlin. Multiple undergraduate students and postdoctoral researchers helped with fieldwork. Kyle O'connell provided useful tips for the extraction of DNA from museum material. Yann Bourgeois assisted with the use of MITObim. Yann Bourgeois and Joseph Manthey provided helpful suggestions on an earlier version of this manuscript. We are in debt with Marc Arnoux and Nizar Drou, from the Genome Core Facility and the Bioinformatics group at NYUAD. This research was carried out on the High-Performance Computing resources at New York University Abu Dhabi. We also thank Simon Maddock and Loïs Rancilhac for reviewing an earlier version of this manuscript, which helped improve the article.This project was funded by NYUAD Grant AD180 to SB. The NYUAD Sequencing Core is supported by NYUAD Research Institute grant G1205A to the NYUAD Center for Genomics and Systems Biology.

References

Ahl E (1924) Über eine froschsammlung aus Nordost-Afrika und Arabien. Mitteilungen aus dem Zoologischen museum in Berlin 11: 1–12. https://doi.org/10.1002/mmnz.4830110102

Andrews S (2010) FastQC: A Quality Control Tool for High Throughput Sequence Data. http://www.bioinformatics.babraham.ac.uk/projects/fastqc

Bwong BA, Chira R, Schick S, Veith M, Lötters S (2009) Diversity of Ridged Frogs (Ptychadenidae: *Ptychadena*) in the easternmost remnant of the Guineo-Congolian rain forest: an analysis using morphology, bioacoustics and molecular genetics. Salamandra 45: 129–146.

Castresana J (2000) Selection of conserved blocks from multiple alignments for their use in phylogenetic analysis. Molecular Biology and Evolution 17: 540–552. https://doi.org/10.1093/oxfordjournals.molbev.a026334

Dabney J, Meyer M, Pääbo S (2013) Ancient DNA damage. Cold Spring Harbor Perspectives in Biology 5: 1–9. https://doi.org/10.1101/cshperspect.a012567

Dehling JM, Sinsch U (2013) Diversity of Ridged Frogs (Anura: Ptychadenidae: *Ptychadena* spp.) in wetlands of the upper Nile in Rwanda: Morphological, bioacoustic, and molecu-

lar evidence. Zoologischer Anzeiger - A Journal of Comparative Zoology 253: 143–157. https://doi.org/10.1016/j.jcz.2013.08.005

Duméril AMC, Bibron G (1841) 8 Erpétologie générale, ou, Histoire naturelle complète des reptiles. Librarie Enclyclopedique de Roret, Paris.

Eaton DAR, Overcast I (2020) ipyrad: Interactive assembly and analysis of RADseq datasets. Bioinformatics 36: 2592–2594. https://doi.org/10.1093/bioinformatics/btz966

Freilich X, Tollis M, Boissinot S (2014) Hiding in the highlands: Evolution of a frog species complex of the genus Ptychadena in the Ethiopian highlands. Molecular Phylogenetics and Evolution 71: 157–169. https://doi.org/10.1016/j.ympev.2013.11.015

Freilich X, Anadón JD, Bukala J, Calderon O, Chakraborty R, Boissinot S, Calderon D, Kanellopoulos A, Knap E, Marinos P, Mudasir M, Pirpinas S, Rengifo R, Slovak J, Stauber A, Tirado E, Uquillas I, Velasquez M, Vera E, Wilga A, Evolutionary Genetics - Class of 2013 (2016) Comparative Phylogeography of Ethiopian anurans: impact of the Great Rift Valley and Pleistocene climate change. BMC Evolutionary Biology 16: e206. https://doi.org/10.1186/s12862-016-0774-1

Gordon A, Hannon G (2010) FASTX-Toolkit: FASTQ/A short-reads preprocessing tools. http://hannonlab.cshl.edu/fastx_toolkit

Goutte S, Reyes-Velasco J, Freilich X, Kassie A, Boissinot S (2021) Taxonomic revision of grass frogs (Ptychadenidae, Ptychadena) endemic to the Ethiopian highlands. ZooKeys 1016: 77–141. https://doi.org/10.3897/zookeys.1016.59699

Hahn C, Bachmann L, Chevreux B (2013) Reconstructing mitochondrial genomes directly from genomic next-generation sequencing reads – a baiting and iterative mapping approach. Nucleic Acids Research 41: e129. https://doi.org/10.1093/nar/gkt371

Katoh K, Standley DM (2013) MAFFT Multiple Sequence Alignment Software Version 7: Improvements in Performance and Usability. Molecular Biology and Evolution 30: 772–780. https://doi.org/10.1093/molbev/mst010

Lanfear R, Calcott B, Ho SYW, Guindon S (2012) PartitionFinder: Combined Selection of Partitioning Schemes and Substitution Models for Phylogenetic Analyses. Molecular Biology and Evolution 29: 1695–1701. https://doi.org/10.1093/molbev/mss020

Largen M, Spawls S (2010) Amphibians and Reptiles of Ethiopia and Eritrea. Edition Chimaira / Serpent's Tale NHBD, Frankfurt am Main, 687 pp.

Largen MJ (1997) Two new species of *Ptychadena* Boulenger 1917 (Amphibia Anura Ranidae) from Ethiopia, with observations on other members of the genus recorded from this country and a tentative key for their identification. Tropical Zoology 10: 223–246. https://doi.org/10.1080/03946975.1997.10539339

Largen MJ (2001) Catalogue of the amphibians of Ethiopia, including a key for their identification. Tropical Zoology 14: 307–402. https://doi.org/10.1080/03946975.2001.10531159

Lyra ML, Lourenço ACA, Pinheiro PDP, Pezzuti TL, Baêta D, Barlow A, Hofreiter M, Pombal JP, Haddad CFB, Faivovich F (2020) High-throughput DNA sequencing of museum specimens sheds light on the long-missing species of the *Bokermannohyla claresignata* group (Anura: Hylidae: Cophomantini). Zoological Journal of the Linnean Society 190, 4(2020): 1235–1255.

Mengistu AA (2012) Amphibian diversity, distribution and conservation in the Ethiopian highlands: morphological, molecular and biogeographic investigation on *Leptopelis* and *Ptychadena* (Anura). PhD thesis, University of Basel, Switzerland, 204 pp.

Miller MA, Pfeiffer W, Schwartz T (2010) Creating the CIPRES Science Gateway for inference of large phylogenetic trees. In: 2010 Gateway Computing Environments Workshop (GCE), 1–8. https://doi.org/10.1109/GCE.2010.5676129

Neumann O (1902) From the Somali Coast through Southern Ethiopia to the Sudan. The Geographical Journal 20: 373. https://doi.org/10.2307/1775561

Parker HW (1930) 1. Report on the Amphibia collected by Mr. J. Omer-Cooper in Ethiopia. Proceedings of the Zoological Society of London 100: 1–6. https://doi.org/10.1111/j.1096-3642.1930.tb00961.x

Perret J-L (1980) Sur Quelques *Ptychadena* (Amphibia Ranidae) d'Ethiopie. Monitore Zoologico Italiano. Supplemento 13: 151–168.

Perret J-L (1994) Description de *Ptychadena largeni* sp. nov. (Anura, Ranidae) d'Ethiopie. Bulletin de la Société Neuchâteloise des Sciences Naturelles 117: 67–77.

Peterson BK, Weber JN, Kay EH, Fisher HS, Hoekstra HE (2012) Double Digest RADseq: An Inexpensive Method for De Novo SNP Discovery and Genotyping in Model and Non-Model Species. PLoS ONE 7: e37135. https://doi.org/10.1371/journal.pone.0037135

Poynton JC (1970) Guide to the *Ptychadena* (Amphibia: Ranidae) of the southern third of Africa. Annals of the Natal Museum 20: 365–375.

Rambaut A (2014) FigTree. Institute of Evolutionary Biology, Univ. Edinburgh. http://tree.bio.ed.ac.uk/software/figtree/

Rambaut A, Suchard MA, Xie D, Drummond AJ (2014) Tracer v1.6. http://beast.bio.ed.ac.uk/Tracer

Rancilhac L, Bruy T, Scherz MD, Pereira EA, Preick M, Straube N, Lyra ML, Ohler A, Streicher JW, Andreone F, Crottini A (2020) Target-enriched DNA sequencing from historical type material enables a partial revision of the Madagascar giant stream frogs (genus *Mantidactylus*). Journal of Natural History 54(1–4): 87–118. https://doi.org/10.1080/00222933.2020.1748243

Reyes-Velasco J, Manthey JD, Bourgeois Y, Freilich X, Boissinot S (2018) Revisiting the phylogeography, demography and taxonomy of the frog genus *Ptychadena* in the Ethiopian highlands with the use of genome-wide SNP data. PLoS ONE 13: e0190440. https://doi.org/10.1371/journal.pone.0190440

Rohland N, Reich D (2012) Cost-effective, high-throughput DNA sequencing libraries for multiplexed target capture. Genome Research 22: 939–946. https://doi.org/10.1101/gr.128124.111

Ronquist F, Teslenko M, van der Mark P, Ayres DL, Darling A, Höhna S, Larget B, Liu L, Suchard MA, Huelsenbeck JP (2012) MrBayes 3.2: Efficient Bayesian Phylogenetic Inference and Model Choice Across a Large Model Space. Systematic Biology 61: 539–542. https://doi.org/10.1093/sysbio/sys029

Ruane S, Austin CC (2017) Phylogenomics using formalin-fixed and 100+ year-old intractable natural history specimens. Molecular Ecology Resources 17: 1003–1008. https://doi.org/10.1111/1755-0998.12655

Scherz, MD, Rasolonjatovo SM, Köhler J, Rancilhac L, Rakotoarison A, Raselimanana AP, Ohler A, Preick M, Hofreiter M, Glaw F, Vences M (2020) 'Barcode fishing' for archival DNA from historical type material overcomes taxonomic hurdles, enabling the description

of a new frog species. Scientific reports 10(1): 1–17. https://doi.org/10.1038/s41598-020-75431-9

Shedlock AM, Haygood MG, Pietsch TW, Bentzen P (1997) Enhanced DNA extraction and PCR amplification of mitochondrial genes from formalin-fixed museum specimens. BioTechniques 22: 394–396, 398, 400. https://doi.org/10.2144/97223bm03

Smith ML, Noonan BP, Colston TJ (2017a) The role of climatic and geological events in generating diversity in Ethiopian grass frogs (genus *Ptychadena*). Royal Society Open Science 4: e170021. https://doi.org/10.1098/rsos.170021

Smith ML, Noonan BP, Colston TJ (2017b) Correction to 'The role of climatic and geological events in generating diversity in Ethiopian grass frogs (genus *Ptychadena*)'. Royal Society Open Science 4: e171389. https://doi.org/10.1098/rsos.171389

Straube N, Lyra ML, Paijmans JL, Preick M, Basler N, Penner J, Rödel MO, Westbury MV, Haddad CF, Barlow A, Hofreiter M (2021) Successful application of ancient DNA extraction and library construction protocols to museum wet collection specimens. Molecular Ecology Resources 21: 2299–2315. https://doi.org/10.1111/1755-0998.13433

Stamatakis A (2014) RAxML version 8: a tool for phylogenetic analysis and post-analysis of large phylogenies. Bioinformatics 30: 1312–1313. https://doi.org/10.1093/bioinformatics/btu033

Swofford DL (1993) PAUP: phylogenetic analysis using parsimony. Computer program distributed by the Illinois Natural History Survey, Champaign, Illinois.

Vaidya G, Lohman DJ, Meier R (2011) SequenceMatrix: concatenation software for the fast assembly of multi-gene datasets with character set and codon information. Cladistics 27: 171–180. https://doi.org/10.1111/j.1096-0031.2010.00329.x

Supplementary material 1

Detailed guidelines for the DNA extraction from museum specimens used in this study

Authors: Jacobo Reyes-Velasco, Sandra Goutte, Xenia Freilich, Stéphane Boissinot

Data type: guidelines

Link: https://doi.org/10.3897/zookeys.1070.66598.suppl1

Supplementary material 2

Table S1

Authors: Jacobo Reyes-Velasco, Sandra Goutte, Xenia Freilich, Stéphane Boissinot

Data type: molecular data

Explanation note: Number of raw reads that passed quality filtering, average read length and number of reads that mapped to the mitochondrial genome for the type specimens sequen.

Link: https://doi.org/10.3897/zookeys.1070.66598.suppl2

ZooKeys 1070: 151–164 (2021)
doi: 10.3897/zookeys.1070.73847
https://zookeys.pensoft.net

RESEARCH ARTICLE

A peer-reviewed open-access journal
ZooKeys
Launched to accelerate biodiversity research

New species of the genus *Spio* (Annelida, Spionidae) from the southern and western coasts of Korea

Geon Hyeok Lee[1], Karin Meißner[2], Seong Myeong Yoon[3], Gi-Sik Min[1]

1 *Department of Biological Sciences, Inha University, Incheon 22212, Republic of Korea* **2** *German Centre for Marine Biodiversity Research, Senckenberg am Meer, c/o Universität Hamburg, Martin-Luther-King-Platz 3, D-20146, Hamburg, Germany* **3** *Department of Biology, College of Natural Sciences, Chosun University, Gwangju 61452, Republic of Korea*

Corresponding authors: Seong Myeong Yoon (smyun@chosun.ac.kr), Gi-Sik Min (mingisik@inha.ac.kr)

Academic editor: Greg Rouse | Received 2 September 2021 | Accepted 12 October 2021 | Published 15 November 2021

http://zoobank.org/73661A23-F563-4D58-9A81-E55AB3CFCF45

Citation: Lee GH, Meißner K, Yoon SM, Min G-S (2021) New species of the genus *Spio* (Annelida, Spionidae) from the southern and western coasts of Korea. ZooKeys 1070: 151–164. https://doi.org/10.3897/zookeys.1070.73847

Abstract

A new spionid polychaete, *Spio pigmentata* **sp. nov.**, is described from the southern and western coasts of Korea. This new species differs from its congeners by the combination of the following morphological characteristics: the presence of orange-brown pigmentation on the anterior part of the prostomium, black pigmentation on the peristomium and along the body, U-shaped nuchal organs, a comparatively long extension of metameric dorsal ciliated organs, three pairs of white dots per chaetiger, two to three posterior abranchiate chaetigers, and the presence of tridentate neuropodial hooded hooks. The partial 16S ribosomal DNA (rDNA) and nuclear 18S rDNA sequences of the new species and *Spio* sp. 2 reported by Abe and Sato-Okoshi (2021) from Japan showed high similarity, indicating that these two specimens belong to the same species. A detailed description and illustrations of the new species, together with molecular information, are provided.

Keywords

Korea Strait and Yellow Sea, molecular analysis, morphology, *Spio pigmentata* sp. nov.,taxonomy

Introduction

Spio Fabricius, 1785 is one of the most speciose genera of Spionidae Grube, 1850. It currently comprises 37 species occurring all over the world (Read and Fauchald 2021). *Spio filicornis* (O. F. Müller, 1776), the type species of the genus, has been repeatedly misidentified and eventually regarded as a cosmopolitan species with worldwide distribution (Okuda 1937; Imajima and Hartman 1964; Paik 1975, 1982, 1989). The confusion regarding the taxonomy of this species has been considerable, and it was evident that the identity of *S. filicornis* needed to be stabilized. Against this background, a neotype of the species from the type locality in Greenland was designated by Meißner et al. (2011), with a detailed redescription based on traditional characteristics and additional diagnostic characteristics that had been rarely or only briefly described in previous publications. They examined traditional morphological characteristics such as the shape of the anterior margin of the prostomium, length of the first branchiae, and the beginning, shape, and number of hooded hooks. They also examined additional diagnostic characteristics including the pigmentation of the body, shape of nuchal organs, extension of dorsal ciliated organs, the number and arrangement of white dots (pores of ventral epidermal glands), shape of notopodial postchaetal lamellae in the posteriormost region of the body, and the number of posterior abranchiate chaetigers (see Meißner et al. 2011). Further, molecular information regarding the three gene regions, mitochondrial cytochrome c oxidase subunit 1 (COI), 16S ribosomal DNA (16S rDNA), and the nuclear 18S ribosomal DNA (18S rDNA), also has previously been provided (Meißner et al. 2011). Thus, the re-examination of *Spio* specimens that have been identified as *S. filicornis* is now possible by additional morphological and molecular analyses, and the species can no longer be regarded as a species of worldwide distribution without scientific proof (Meißner et al. 2011).

Six *Spio* species, *S. borealis* Okuda, 1937; *S. filicornis*; *S. kurilensis* Buzhinskaya, 1990; *S. martinensis* Mesnil, 1896; *S.* cf. *pettiboneae* Foster, 1971; *S. picta* Zachs, 1933; and *S. unidentata* Chlebovitsch, 1959, have been recorded in Northeast Asia (Okuda 1937; Imajima and Hartman 1964; Wu et al. 1965; Paik 1975, 1982, 1989; Bick and Meißner 2011; Glasby et al. 2016). Okuda (1937) was the first author to report *S. filicornis* in this region, from Hokkaido Island, Japan. Imajima and Hartman (1964) later identified *Spio* specimens collected from the same area as *S. filicornis*. In Korean waters, Paik (1975, 1982, 1989) first recorded *S. filicornis* that having a prostomium with a rounded margin, a ball-shaped elevation (papillate form) on the posterior part of the prostomium, well-developed first branchiae, and bidentate hooded hooks from chaetiger 12. Characteristics later discussed by Meißner et al. (2011) were neither illustrated nor described in these publications, and hence are unknown for these specimens from Asian waters. Unfortunately, no information on deposition of Paik's (1975, 1982, 1989) specimens had been provided.

In this study, *Spio* specimens newly collected from the southern and western coasts of Korea were examined in detail to determine the species to which they belong. An

illustrated description of the new species is provided together with the partial DNA sequences of three gene regions (COI, 16S rDNA, and 18S rDNA).

Materials and methods

Sampling and morphological observations

Adult specimens examined in the present study were collected from the intertidal zones of the southern and western coasts of Korean waters (Fig. 1) using 500 μm-mesh sieves. The observations were performed for both live and fixed specimens. The live specimens were relaxed in 10% $MgCl_2$ solution, and morphological characteristics were observed under a stereomicroscope (Leica MZ125; Germany). Photographs were taken using a digital camera (Tucsen Dhyana 400DC; Fuzhou Fujian, China) with a capture program (Tucsen Mosaic version 15; Fuzhou Fujian, China). After observation, the specimens were fixed in 4% formaldehyde for morphological analysis, washed, and subsequently transferred to 70% ethanol. For the molecular studies, the specimens were fixed with 95% ethanol. Some formalin-fixed specimens (briefly transferred to distilled water) were stained with methylene green solution to observe the pores of ventral epidermal glands, according to the method of Meißner (2005). The specimens for scanning electron microscopic examination were dehydrated using a t-BuOH freeze dryer (VFD-21S Vacuum Device; Ibaraki, Japan). The specimens were mounted on stubs and coated with gold-palladium and observations were performed using a scanning electron microscope (SU3500; Hitachi, Tokyo, Japan). Type and voucher specimens examined in this study were deposited at the National Institute of Biological Resources, South Korea (NIBR), the Senckenberg Research Institute in Frankfurt, Germany (SMF), and the Zoological Museum Hamburg, Germany (ZMH).

Molecular analysis

Genomic DNA was extracted from the tissues of the palps of five specimens (NIBRIV0000829700–4) using a LaboPass Tissue Mini (Cosmo GENETECH, Seoul, South Korea) according to the manufacturer's protocol. Polymerase chain reaction amplification of the partial DNA sequences of three gene regions (COI, 16S rDNA, and 18S rDNA) was performed using the following primer sets: LCO1490 and HCO709 for COI (Blank et al. 2007), 16Sar and 16Sbr for 16S rDNA (Kessing et al. 1989), and 18E and 18B for 18S rDNA (Mincks et al. 2009). Molecular analyses were performed using the partial sequences aligned using Geneious 8.1.9 (Biomatters, Auckland, New Zealand). The maximum-likelihood tree was constructed based on the concatenated partial sequences of the COI, 16S rRNA, and 18S rRNA gene regions using IQ-TREE with the GTR+F+R3 model with 1000 replicates (Kalyaanamoorthy et al. 2017; Hoang et al. 2018). The obtained DNA sequences were registered in GenBank.

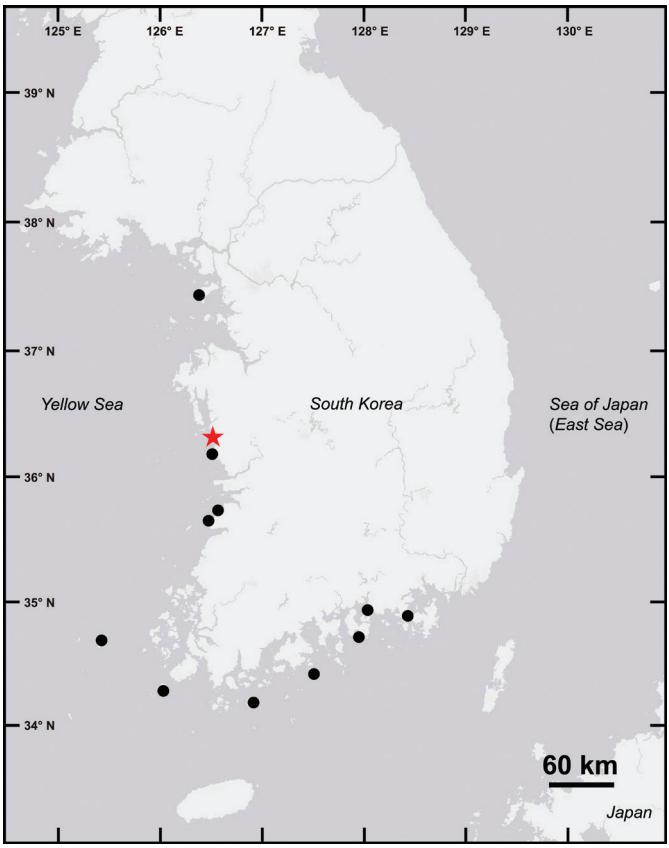

Figure 1. Map of the sampling locations of *Spio pigmentata* sp. nov. in this study. Type locality (red star) and collection locations of other examined specimens (circle).

Results

Systematics

Order Spionida *sensu* Rouse & Fauchald, 1997
Family Spionidae Grube, 1850
Genus *Spio* Fabricius, 1785

***Spio pigmentata* sp. nov.**
http://zoobank.org/C4BA64C6-C570-4D77-A3BC-49722FC36934

Spio filicornis: Paik, 1975: 420, 1982: 808, 1989: 465, fig. 175.
Spio sp. 2: Abe and Sato-Okoshi, 2021: 63, fig. 9L–N.

Material examined. ***Type locality***. Yellow Sea, Korea, 36°15'42.9"N, 126°32'47.9"E, intertidal sand. ***Holotype.*** Complete, without palps, formalin (NIBRIV0000888168) (Fig. 2), 21 Oct. 2020. ***Paratypes.*** Four complete (NIBRIV0000888164–7), three

complete (SMF 30259), two complete (ZMH P-30424), formalin, Yellow Sea, Korea, 37°26'50.0"N 126°22'3.9"E, 13 Jan. 2021, intertidal sand.

Non-type materials. Yellow Sea, Korea, intertidal sand: 27 anterior fragments (af), formalin, 34°18'43"N, 126°1'59"E, 22 Aug. 2017; 1 complete (NIBRIV0000862794), 33 af, formalin, 34°41'22.5"N, 125°25'43.8"E, 16 May. 2018; 71 af, formalin, 35°40'45.2"N, 126°31'26.5"E, 18 Mar. 2018; 14 af, 95% ethanol, 35°38'03.4"N, 126°27'57.2"E, 17 May. 2018; 5 af, 95% ethanol, 35°39'16.4"N, 126°29'26.0"E, 19 Sep. 2020; 4 af, 95% ethanol, 35°35'44.6"N, 126°29'07.9"E, 18 Sep. 2020, 5 complete, formalin, 4 af (NIBRIV0000888159–60), 95% ethanol, 35°35'44.6"N, 126°29'07.9"E, 19 Sep. 2020; 1 af, formalin, 35°40'44.2"N, 126°31'29.7"E, 21 Sep. 2020; 1 af, formalin, same locality as holotype, 21Oct. 2020; 9 complete, 1 af, formalin, same locality as paratypes, 15 Jan 2021. Korea Strait, Korea: 10 af, formalin, 34°28'05.5"N, 127°28'16"E, 26 May. 2017, intertidal sand; 3 complete, 22 af, formalin, 34°11'03.7"N, 126°54'37.5"E, 26 Jul. 2017, intertidal sand; 2 af, 95% ethanol, 34°53'19.9"N, 128°26'41.2"E, 20 Jul 2020, intertidal muddy sand; 5 af, formalin, 35°40'44.2"N, 126°31'29.7"E, 21 Sep. 2020, intertidal sand; 1 af, formalin, 2 complete (NIBRIV0000888162–3), 95% ethanol, 34°55'37.7"N, 128°02'13.3"E, 23 Jun. 2020, muddy sand between gravel and macrophytes; 8 complete, 2 af, formalin, 1 af (NIBRIV0000888161), 95% ethanol, 34°43'45.1"N, 127°57'09.7"E, intertidal sand; 1 af, formalin, 36°13'53.3"N, 126°31'47.2"E, 20 Oct. 2020, intertidal sand; 1 af, formalin, 36°09'41.2"N, 126°31'11.1"E, 20 Oct. 2020, intertidal sand.

Diagnosis. Prostomium broadly rounded, slightly expanded at anterolateral margin, extending to chaetiger 1; nuchal organs with short median and long lateral ciliary bands, lateral bands extending up to transverse ciliated band (tcb) of chaetiger 3. Metameric dorsal ciliated organs double-paired, present from chaetiger 3. Branchiae from chaetiger 1 to almost end of body, length of first pair slightly shorter than that of second pair; branchiae mostly free from notopodial lamellae. White dots present from about chaetiger 3 to the end of the middle body region; three pairs of white dots per chaetiger. Neuropodial hooded hooks tridentate, present from chaetiger 11, uppermost tooth very inconspicuous. Pygidium with thin dorsolateral pair and stout but slightly longer ventral pair of anal cirri.

Description. Holotype complete specimen with 67 chaetigers, about 15.7 mm in length and about 1.0 mm in width (Fig. 2). Other specimens complete with 58–73 chaetigers, 12.0–17.0 mm in length and 0.9–1.2 mm in width.

Prostomium entire and rounded anteriorly, slightly expanded at anterolateral margin, extending to chaetiger 1; prostomium with orange-brown pigmentation on anterior part, middle part of prostomium comparatively broad, posterior part with highly elevated papilla; two pairs of black eyes arranged in trapezoid; anterior pair larger, slightly crescent-shaped or oval, widely spaced; posterior pair smaller, rounded, closely spaced; weak transverse depression between anterior and middle part of prostomium (Figs 3A, B, 6A, 7A). Peristomium separated from prostomium by a narrow furrow (Fig. 7A). Peristomial palps reaching chaetigers 6–9 (Fig. 5A).

Nuchal organs and metameric dorsal ciliated organs distinctly observed in well-preserved and live specimens; nuchal organs U-shaped due to posterior fusion of

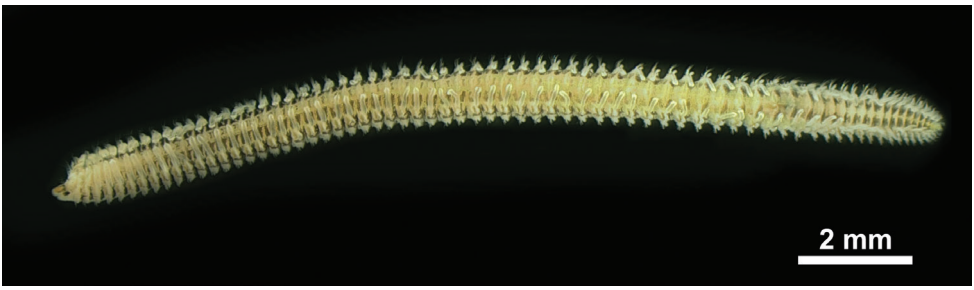

Figure 2. *Spio pigmentata* sp. nov., holotype, palps removed, fixed in formalin, NIBRIV0000888168.

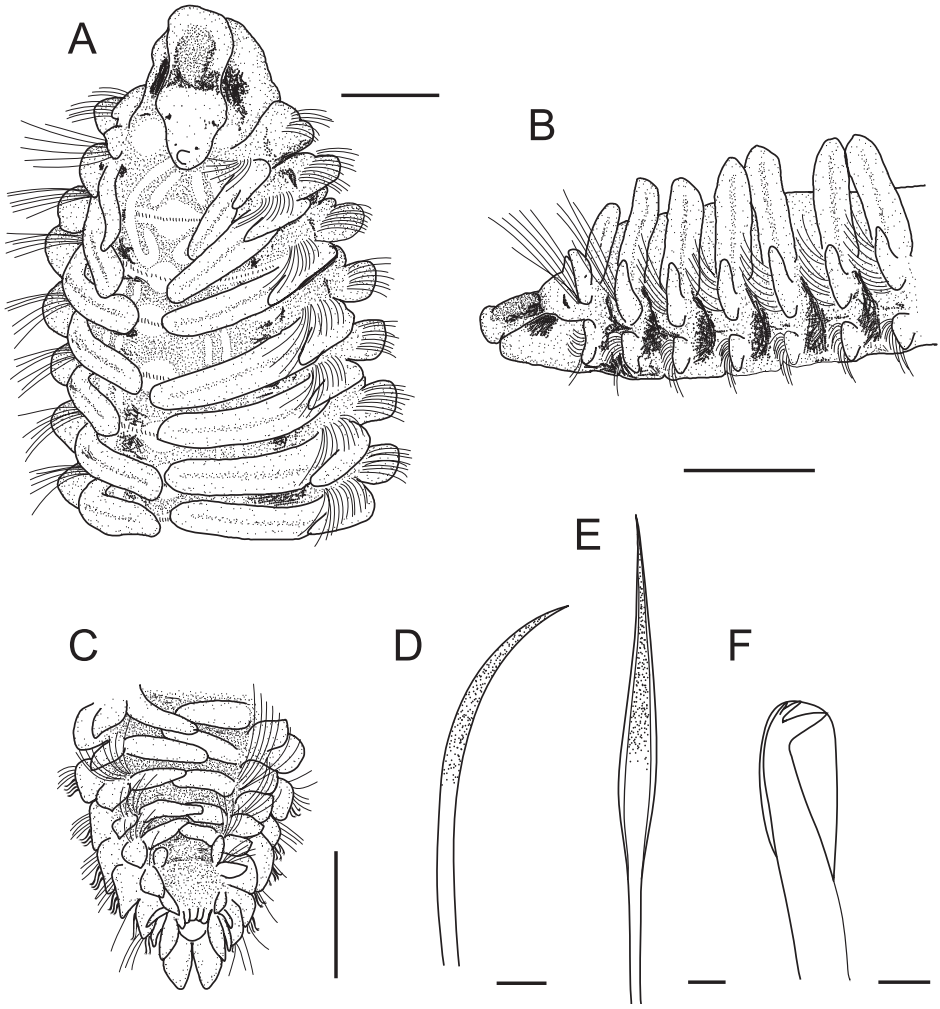

Figure 3. *Spio pigmentata* sp. nov. **A–C** holotype (NIBRIV0000888168) **D–F** paratype (NIBRIV0000888166) **A** anterior end, dorsal view **B** anterior end, lateral view **C** posterior end, dorsal view **D** ventral sabre chaeta from chaetiger 52 **E** anterior neurochaetae from chaetiger 22 **F** neuropodial hooded hook from chaetiger 22. Scale bars: A–C = 0.5 mm, D–F = 20.0 μm.

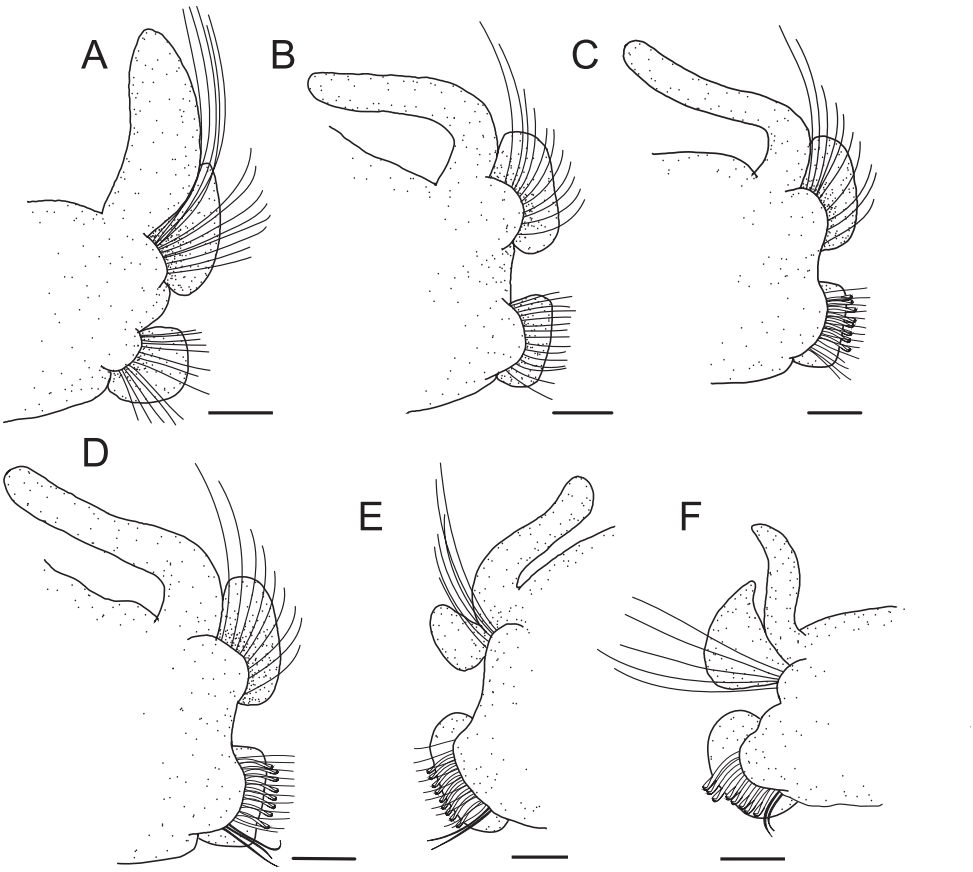

Figure 4. *Spio pigmentata* sp. nov., paratype (NIBRIV0000888166) **A–G** parapodium from chaetiger 1, 10, 21, 22nd last, 11th last, and 7th last, all anterior view. Scale bars: 0.2 mm.

median and lateral ciliated bands, long and recurved on chaetiger 2, and reaching to first transverse ciliated band (tcb) on chaetiger 2 (Figs 3A, 6A, 7A). Metameric dorsal ciliated organs double paired, present from between branchiae 3 and 4 (i.e., after second tcb), extending up to chaetiger 40 in holotype (38–47 in 62–73 chaetiger individuals) (Figs 3A, 5, 6A, 7A). White dots present from chaetiger 3 to chaetiger 50 in holotype (42–52 in 62–73 chaetiger individuals); three pairs of white dots per chaetiger; lateral two pairs closely spaced (Figs 5B, 6B, C, 7B). Intersegmental transverse ciliation absent.

Branchiae present from chaetiger 1 to almost end of body, absent only on last 2 or 3 (rarely 4) chaetigers (Fig. 2); length of first pair of branchiae two-thirds to four-fifths the length of second pair (Fig. 3A, B); comparatively longest and widest branchiae on chaetigers 2–12, becoming thinner and shorter posteriorly; about last 10 branchiae distinctly shorter and thinner; branchiae with cilia on inner and furrow on outer side; branchiae mostly separated from postchaetal notopodial lamellae (Fig. 4). Notopodia on chaetiger 1 slightly shifted dorsally; notopodial postchaetal lamellae almost lanceo-

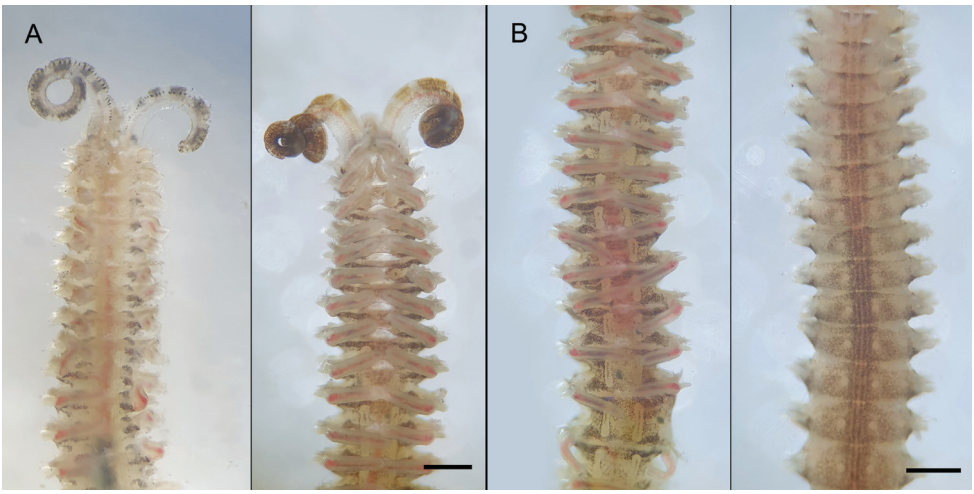

Figure 5. *Spio pigmentata* sp. nov., live specimens in seawater **A** specimens with palps, black-ringed (left) and dark brown (right), dorsal view **B** middle body, double-paired dorsal ciliated organs (left) and ventral white dots (right) views. Scale bars: 0.5 mm.

late (Fig. 4A); from chaetiger 2 lamellae broadly rounded, slightly tapered superiorly (Fig. 4B–D), becoming smaller in middle to posterior chaetigers (Fig. 4F), and larger, subtriangular in about last 17 chaetigers (Fig. 4G). Neuropodial postchaetal lamellae rounded in about first four chaetigers, becoming broader and larger in along anterior and middle chaetigers, largest in posteriormost chaetigers (Fig. 4).

Notopodial chaetae all capillaries; notochaetae in anterior and middle chaetigers arranged in two rows; notochaetae of anterior row with stout sheath, heavily granulated, slightly shorter than chaetae of posterior row, granulation disappearing in middle chaetigers; notochaetae of posterior row thinner, with narrow sheath, non-granulated; additional fascicle of 6–9 very long, thin capillaries without granulations present at superior position, longest in first three chaetigers; notochaetae in posterior chaetigers thin and long, arranged in irregular rows. Neuropodial chaetae with granulated or non-granulated capillaries, hooded hooks, and inferior fascicle of capillaries; capillaries of anterior neuropodia arranged in two rows; neurochaetae of anterior row with distinct sheaths, stout, heavily granulated (Fig. 3E); neurochaetae of posterior row non-granulated, less stout, replaced by 7–9 hooded hooks from chaetiger 11 (rarely 12); neuropodial hooded hooks tridentate, main fang well developed, uppermost tooth inconspicuous (Fig. 3F); inferior fascicle of 2–5 long, thin, non-granulated capillaries from chaetiger 1, replaced by 2–4 (usually 3) stout granulated, ventral sabre chaetae in inferiormost position from about chaetigers 16–19 (rarely 13–15) (Fig. 3D).

Pygidium with two pairs of anal cirri; dorsolateral pair shorter and thinner, comparatively widely spaced, and ventral pair longer, very stout, conical with rounded tip and closely spaced (Fig. 3C).

Pigmentation. Highly variable but conspicuous in live or well-preserved specimens (some specimens without pigmentation). Palps in live specimens with vari-

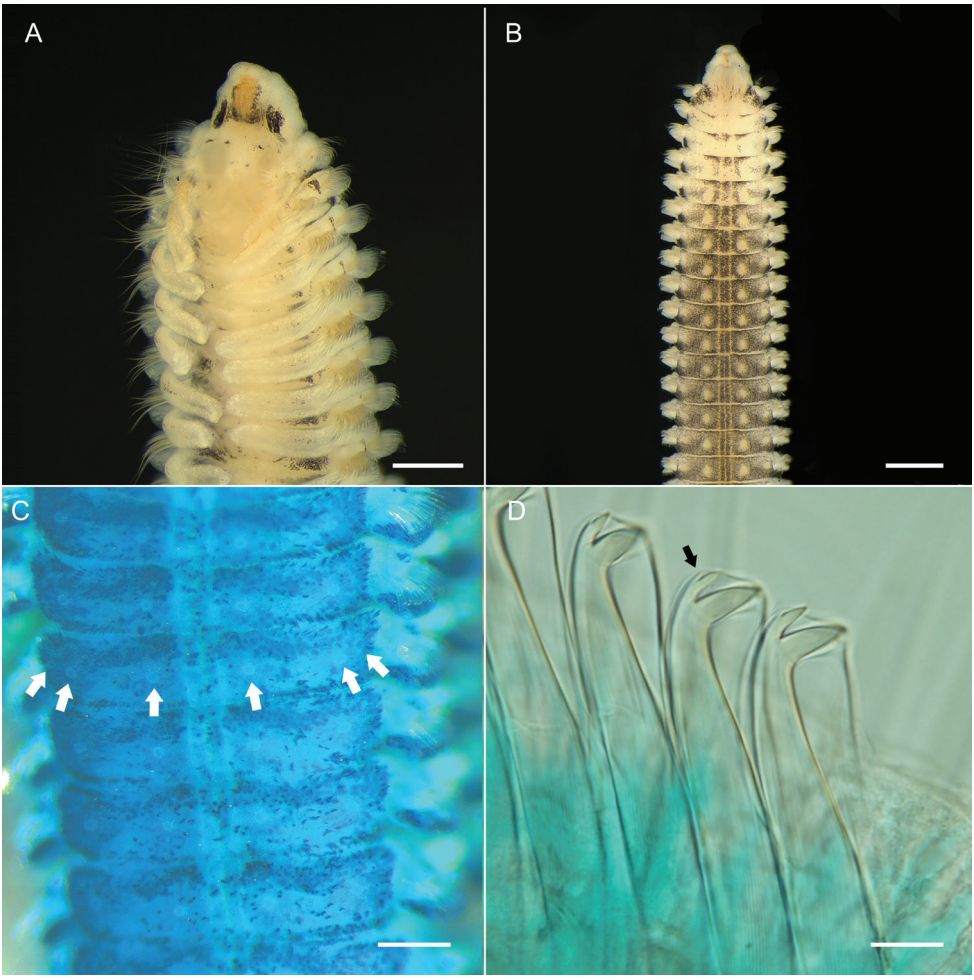

Figure 6. *Spio pigmentata* sp. nov. **A, B** holotype (NIBRIV0000888168), fixed in formalin **C, D** paratype (NIBRIV0000888167), fixed in formalin **A** anterior end, dorsal view **B** anterior end, ventral view **C** methyl green staining pattern of anterior end, ventral view, white dots (arrows) **D** neuropodial hooded hooks from chaetiger 15, inconspicuous uppermost tooth (arrow). Scale bars: 0.5 mm **(A–C)**; 20.0 µm **D**.

able pigmentation, about 6–15 light to dark brown spots or black ringed appearance (Fig. 5A, B); pigmentation fades in formalin- and ethanol-fixed specimens, but light brown pigmentation along the food groove remains. Well-preserved specimens with orange-brown and black pigmentation as follows: medial part of prostomium with orange-brown pigmentation, often faded in formalin- and ethanol-fixed specimens; prostomium with black pigmentation on the anterior to transverse depression margin of the prostomium, dorsal side of the peristomium next to the prostomium; black pigmented patches in front of, and in particular, behind tcb dorsolaterally in about the first six chaetigers in holotype (Fig. 6A), and some specimens with distinct patches (Fig. 5B). If black pigmented patches are distinct on the ventral side, white dots (pores of ventral glands) are clearly visible (Figs 5D, 6B).

Methyl green staining pattern (MGSP). The anterior part of the prostomium and peristomium, margins of branchiae and postchaetal lamellae, and anal cirri were intensively stained. Transfer of stained specimens to distilled water for approximately 10 min, resulted in white dots being visible against the bluish background on the ventral side (Fig. 6C). Three pairs of dots were visible on chaetiger 3 to end of middle body region; lateral two pairs closely spaced, easily confused as one pair.

Biology. In the present study, the specimens were found mostly in intertidal zones of fine sand, rarely muddy sand, and sometimes a mixture of gravel and macrophytes (*Zostera marina*). According to Abe and Sato-Okoshi (2021), planktonic larvae of *Spio* sp. 2 with two rows of black melanophore spots on each side of the dorsum from chaetiger 1 onward, linked by band-shaped medial black pigmentation from chaetiger 4 or 5 are found in Sasuhama and Onagawa Bay between April and August (see cited publication for further details). Adult specimens were collected from muddy sand sediments of shallow waters in Sasuhama, Japan (Abe and Sato-Okoshi 2021).

Etymology. The specific name, pigmentata, originates from the Latin word pigmentum, meaning "pigment" This name refers to the new species having conspicuous black pigmentation on the body.

Distribution. Along the southern and western coasts of Korea; Sasuhama and Onagawa Bay, north-eastern Japan.

Genetics

Three DNA gene regions (COI, 16S rDNA, and 18S rDNA) from five specimens (NIBRIV0000888159–63) of the new species were determined. The lengths of each gene sequence were up to 683 bp for COI, 479 bp for 16S rDNA, and 1761 bp for 18S rDNA. The newly determined sequences have been registered in GenBank under the accession numbers MZ661756–60 (COI), MZ663825–29 (16S rDNA), and MZ663820–22 (18S rDNA). The intra-specific genetic distances between the five specimens were 0.2–1.1% for COI (666 bp) and 0.0–0.3% for the 16S rDNA (390 bp); no variation was detected with respect to the 18S rDNA (1645 bp). Pairwise genetic distances were calculated between new species and other currently available *Spio* species–*S. arndti* Meißner, Bick & Bastrop, 2011; *S. blakei*; *S. filicornis*; *S. symphyta* Meißner, Bick & Bastrop, 2011; and *Spio* sp. 2–mined from GenBank for comparison (Meißner and Götting 2015; Meißner et al. 2011; Abe and Sato-Okoshi 2021). The interspecific genetic distances between the new species and other *Spio* species were 17.2–22.6% for COI (536 bp), 5.4–17.9% for the 16S rDNA (487 bp), and 0.1–3.5% (1756 bp) for the 18S rDNA. The 16S (LC595766) and 18S rDNA (LC545924) sequences of *Spio* sp. 2 reported by Abe and Sato-Okoshi, 2021 from Japan showed 99.8% (16S: 461/462 bp) and 100.0% (18S: 1760/1760 bp) similarity with *S. pigmentata* sp. nov., indicating that these two specimens are the same species. A phylogenetic tree was constructed based on the concatenated partial gene sequences of COI (525 bp), the 16S rDNA (454 bp), and

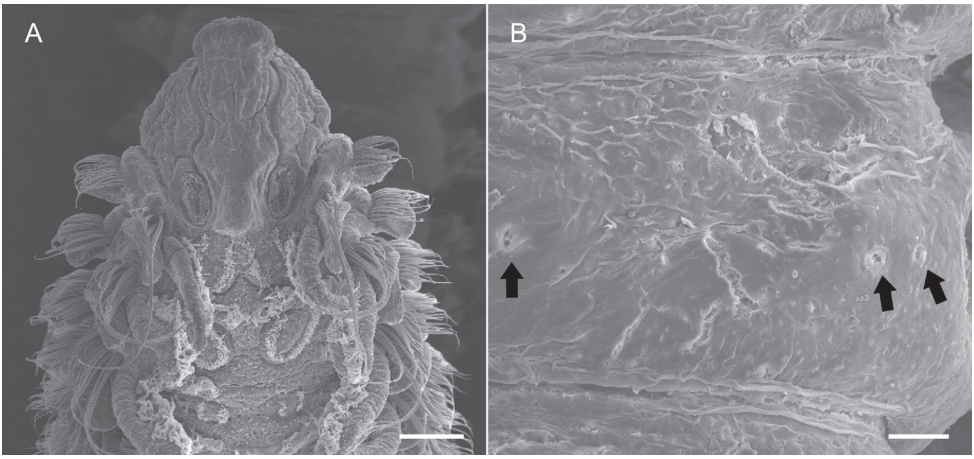

Figure 7. *Spio pigmentata* sp. nov., paratype (NIBRIV0000888165). **A** anterior end, dorsal view, palps removed **B** right half of middle chaetiger, ventral surface, gland openings (arrows). wScale bars: 0.2 mm **A**; 40.0 μm **B**.

Table 1. GenBank accession numbers of sequences used for phylogenetic analysis.

Species	Type locality	GenBank accession number			Data source
		COI	16S	18S	
Spio pigmentata sp. nov.	Korea	MZ661760	MZ663829	MZ663822	Present study
Spio arndti	Baltic Sea	FR823429	FR823439	FR823434	Meißner et al. 2011
Spio symphyta	North Sea	FR823427	FR823437	FR823432	"
Spio filicornis	West Greenland	FR823425	FR823435	FR823430	"
Spio blakei	Australia	KP636501	KP636502	KP636507	Meißner and Götting 2015
Scolelepis (*Scolelepis*) *daphoinos*	China	MW509617	MW494645	MW494652	Lee and Min 2021

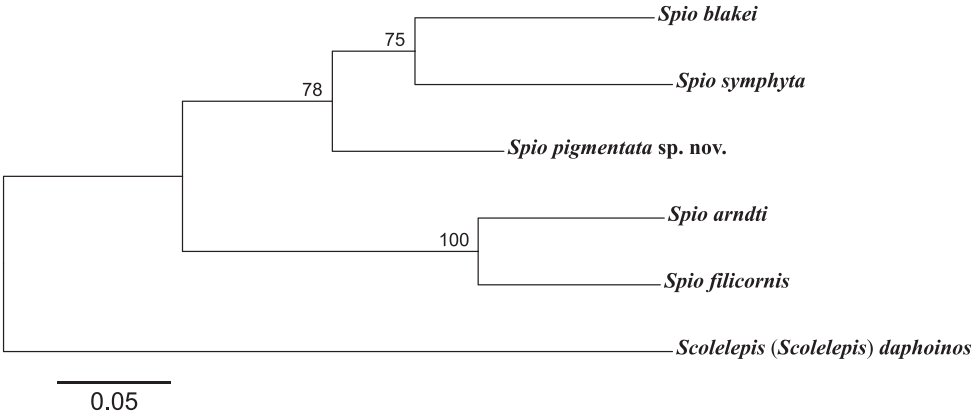

Figure 8. Maximum likelihood (ML) tree for 1,381 bp inferred from combined partial mitochondrial COI, 16S rDNA, and nuclear 18S rDNA from six spionid polychaetes. Numbers above the branch indicate ML bootstrap values from 1000 replication. The sequence of *Scolelepis* (*Scolelepis*) *daphoinos* was used for outgroup rooting.

the 18S rDNA (394 bp), using maximum likelihood analyses (Fig. 8). The sequence of *Scolelepis* (*Scolelepis*) *daphoinos* Zhou, Ji & Li, 2009 was used as an outgroup taxon (Lee and Min 2021). The GenBank accession numbers are listed in Table 1. Phylogenetic analysis showed that two monophyletic clades were formed in *Spio*. The new species was present in a clade with *S. blakei* and *S. symphyta.*

Discussion

Morphological examination of *Spio* specimens from the southern and western coasts of Korea, combined with the molecular analysis of three gene regions from newly collected materials, revealed the presence of a previously undescribed species of *Spio*, *S. pigmentata* sp. nov. The new species agrees well with Paik's (1975, 1982, 1989) description of *S. filicornis* with respect to most diagnostic features and only differs in the dentation of hooded hooks (see above). The morphological examination in this study showed that the uppermost tooth in the tridentate hooks is very inconspicuous (e.g., new species in the present study and *S. symphyta* in Meißner et al. 2011). This can easily lead to erroneous conclusions. We suggest that the undescribed species newly collected during this study and the species previously known as *S. filicornis* by Paik's (1975, 1982, 1989) from Korean waters are the same.

The new species is morphologically very similar to *S. blakei* Maciolek, 1990 from Australia in having the following characteristics: the length of first branchiae, the shape of nuchal organs, extension of dorsal ciliated organs, shape of hooded hooks, the number of abranchiate chaetigers, and the shape of the anal cirri (Meißner and Gotting 2015). However, the new species can be distinguished from *S. blakei* by the presence of three pairs of white dots per chaetiger instead of two pairs and having 7–9 tridentate hooded hooks instead of 4–5 (Meißner and Götting 2015). In the Far East of the temperate region, the new species and *S. picta* from the Kuril Islands share tridentate hooded hooks. The new species, however, differs from *S. picta* by the presence of orange-brown and black pigmentation instead of only light to dark brown, the shape of its nuchal organs (U-shaped vs straight), the number of hooded hooks (7–9 vs 8–13), and the fusion of notopodial postchaetal lamellae (mostly separated vs completely fused in the anterior and middle regions) (Bick and Meißner 2011).

According to the results of the molecular studies, the species was already recorded in Japan and published as unidentified *Spio* sp. 2 by Abe and Sato-Okoshi (2021). The known distribution of *S. pigmentata* sp. nov. ranges from the Korea Strait and the Yellow Sea of Korea to northeastern Japan.

The phylogenetic tree resulting from the analysis of molecular data revealed that *S. pigmentata* sp. nov. formed a clade with *S. blakei* and *S. symphyta* (Fig. 8). The morphological characteristics also imply a close relationship of these species. These three *Spio* species share U-shaped nuchal organs, and the two species that form a second clade (*S. arndti* and *S. filicornis*) share almost straight nuchal organs. Despite the high species diversity of the genus, the available DNA data are very poor. Further studies based on

detailed morphological and molecular information of *Spio* species are needed to reveal additional information on their genetic relationships.

The identity of *Spio* species described in Northeast Asia should be verified based on both morphological and genetic studies (see Meißner et al. 2011). For example, the description of the specimens from China identified as *S. martinensis* showed morphological differences in the shape of the apical tooth of neuropodial hooded hooks and the number of posterior abranchiate chaetigers with the specimen from the type locality in France (Wu et al. 1965; Lavesque et al. 2015), and hence might be doubtful. Unfortunately, the DNA information of specimens from China and France is still unknown. Further studies are needed to resolve these and related problems.

Acknowledgements

This study was supported by the research funds from the National Institute of Biological Resources (NIBR), funded by the Ministry of Environment (MOE) of the Republic of Korea (NIBR 201902204). This study was also supported by the Korea National Park Service and Inha University.

References

Abe H, Sato-Okoshi W (2021) Molecular identification and larval morphology of spionid polychaetes (Annelida, Spionidae) from northeastern Japan. ZooKeys 1015:1–86. https://doi.org/10.3897/zookeys.1015.54387

Bick A, Meißner K (2011) Redescription of four species of *Spio* and *Microspio* (Polychaeta, Spionidae) from the Kuril Islands and Peter the Great Bay, northwest Pacific. Zootaxa 2968: 39–56. https://doi.org/10.11646/zootaxa.2968.1.3

Blank M, Laine A, Jürss K, Bastrop R (2008) Molecular identification key based on PCR/RFLP for three polychaete sibling species of the genus *Marenzelleria*, and the species' current distribution in the Baltic Sea. Helgoland Marine Research 62: 129–141. https://doi.org/10.1007/s10152-007-0081-8

Hoang DT, Chernomor O, Haeseler A, Minh BQ, Vinh LS (2018) UFBoot2: improving the ultrafast bootstrap approximation. Molecular Biology and Evolution 35: 518–522. https://doi.org/10.1093/molbev/msx281

Imajima M, Hartman O (1964) The polychaetous annelids of Japan. I–II. Allan Hancock Foundation Occasional Papers 26: 1–452.

Kalyaanamoorthy S, Minh BQ, Wong TKF, von Haeseler A, Jermiin LS (2017) ModelFinder: fast model selection for accurate phylogenetic estimates. Nature Methods 14: 587–589. https://doi.org/10.1038/nmeth.4285

Kessing B, Croom H, Martin A, McIntosh C, Owen McMillian W, Palumbi S (1989) The Simple Fool's Guide to PCR. Department of Zoology, University of Hawaii, Honolulu, 47 pp.

Lavesque N, Bonifácio P, Meißner K, Blanchet H, Gouillieux B, Dubois S, Bachelet G (2015) New records of *Spio symphyta* and *Spio martinensis* ('Polychaeta': Canalipalpata: Spionidae) from Arcachon Bay (France), NE Atlantic. Marine Biodiversity 45: 77–86. https://doi.org/10.1007/s12526-014-0230-7

Lee GH, Min G (2021) First Record of *Scolelepis* (*Scolelepis*) *daphoinos* (Annelida: Polychaeta: Spionidae) in South Korea. Animal Systematics, Evolution and Diversity 37: 229–234.

Maciolek NJ (1990) A redescription of some species belonging to the genera *Spio* and *Microspio* (Polychaeta: Annelida) and descriptions of three new species from the northwestern Atlantic Ocean. Journal of Natural History 24: 1109–1141. https://doi.org/10.1080/00222939000770701

Mincks SL, Dyal PL, Paterson GLJ, Smith CR, Glover AG (2009) A new species of *Aurospio* (Polychaeta, Spionidae) from the Antarctic shelf, with analysis of its ecology, reproductive biology and evolutionary history. Marine Ecology 30: 181–197. https://doi.org/10.1111/j.1439-0485.2008.00265.x

Meißner K (2005). Revision of the genus *Spiophanes* (Polychaeta: Spionidae); with new synonymies, new records and descriptions of new species. Zoosystematics and Evolution 81(1): 3–66. https://doi.org/10.1002/mmnz.200310001

Meißner K, Bick A, Bastrop R (2011) On the identity of *Spio filicornis* (O.F. Müller, 1776)– with the designation of a neotype, and the description of two new species from the North East Atlantic Ocean based on morphological and genetic studies. Zootaxa 2815: 1–27. https://doi.org/10.11646/zootaxa.2815.1.1.1

Meißner K, Götting M (2015) Spionidae (Annelida: 'Polychaeta': Canalipalpata) from Lizard Island, Great Barrier Reef, Australia: the genera *Malacoceros*, *Scolelepis*, *Spio*, *Microspio*, and *Spiophanes*. Zootaxa 4019: 378–413. https://doi.org/10.11646/zootaxa.4019.1.15

Okuda S (1937) Spioniform polychaetes from Japan. Journal of the Faculty of Science, Hokkaido Imperial University, Series 6 (Zoology) 5: 217–254.

Paik EI (1975) The polychaetous annelids in Korea (III). Research Bulletin of the Hyosung Women's University 17: 409–438.

Paik EI (1982) [Taxonomic studies on polychaetous annelids in Korea]. Research Bulletin of the Hyosung Women's University 24: 745–913. [in Korean]

Paik EI (1989) [Illustrated Encyclopedia of Fauna and Flora of Korea, Vol. 32]. Ministry of Education Press, Seoul, 452–468. [in Korean]

Read G, Fauchald K, (Ed.) (2021) World Polychaeta Database. *Spio* Fabricius, 1785. World Register of Marine Species. http://www.marinespecies.org/aphia.php?p=taxdetails&id=129625 [Accessed on: 2021-08-03]

Wu BL, Chen M, Sun RP (1965) On the occurrence of a spionid worm, *Spio martinensis* Mesnil in the Yellow Sea, with notes on its larval development. Oceanologia et Limnologia Sinica 7: 25–31. [in Chinese with English abstract] http://en.cnki.com.cn/Article_en/CJFDTotal-HYFZ196501001.htm